



**UiT** The Arctic University of Norway

Faculty of Biosciences, Fishery, and Economics

# **Life on Air: On the Physiological Basis of Atmospheric Methane Oxidizing Bacteria**

Tilman Schmider

A dissertation for the degree of Philosophiae Doctor, March 2024

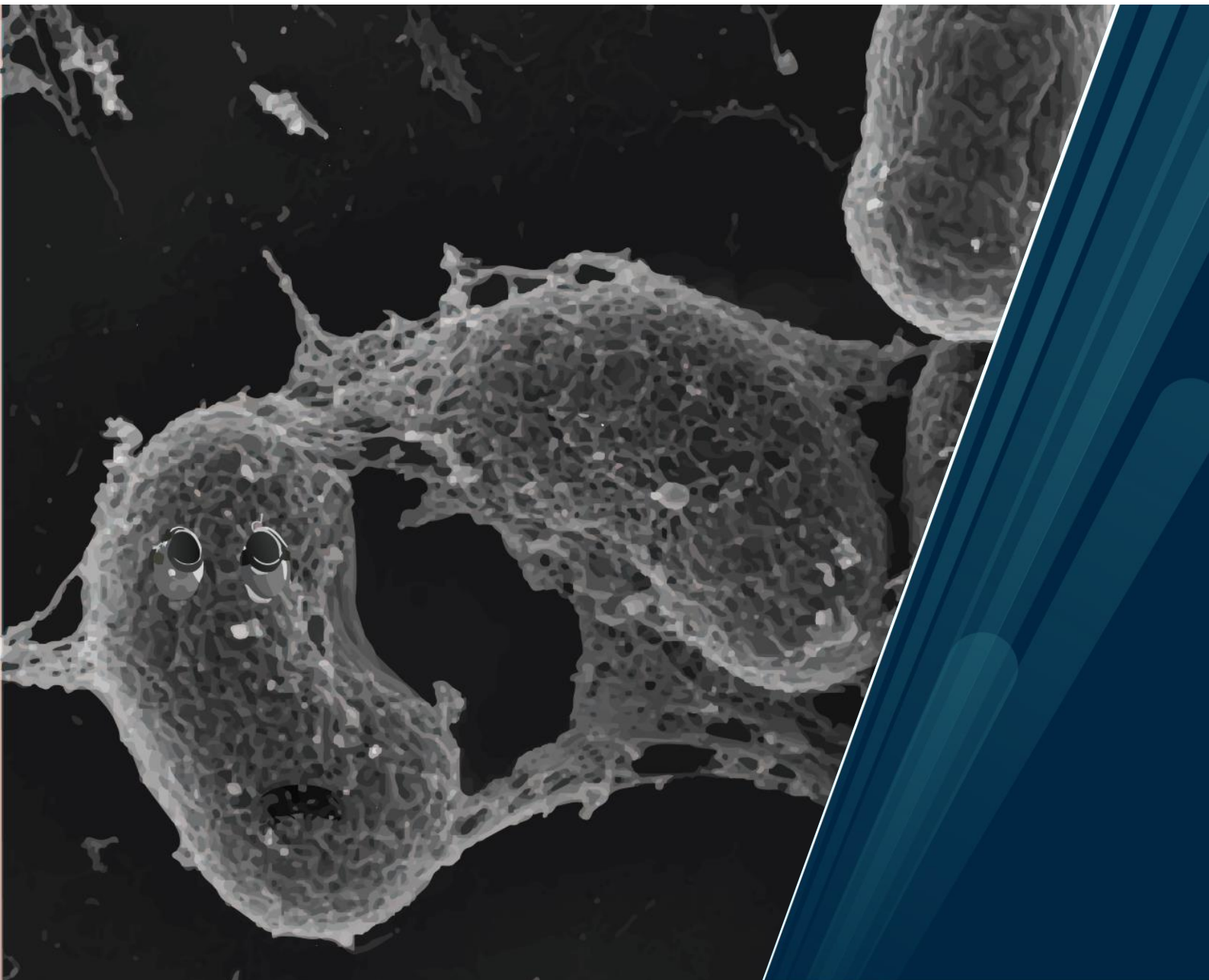




# Table of Contents

Acknowledgements .....	5
Abstract .....	7
List of papers .....	8
Abbreviations .....	9
1 Introduction .....	11
1.1 Atmospheric methane .....	11
1.2 Methanotrophs .....	12
1.3 Why study atmMOB and the biological sink of atmospheric CH <sub>4</sub> ?.....	13
1.4 Atmospheric methane oxidizing bacteria .....	14
1.5 Ecology and phylogeny of atmospheric methane oxidizing bacteria .....	14
1.6 Physiology of atmospheric methane oxidizing bacteria .....	17
1.6.1 (i) Oligotrophs .....	17
1.6.2 (ii) Flush feeders.....	21
1.6.3 (iii) Facultative CH <sub>4</sub> oxidizers.....	22
1.6.4 (iv) Ammonia oxidizers .....	22
1.7 Main objectives.....	23
1.8 Secondary objective.....	24
1.9 The methanotrophic strains .....	24
1.9.1 <i>Methylocystaceae</i> .....	24
1.9.2 <i>Methylocapsa</i> .....	26
1.10 Aerobic methane oxidation .....	28
1.10.1 Activation of CH <sub>4</sub> .....	28
1.10.2 Methanol oxidation .....	29
1.10.3 Formaldehyde oxidation.....	30

1.10.4	Assimilation of carbon via the glycine cleavage system and the serine cycle ...	34
1.11	Oxidation of atmospheric hydrogen and carbon monoxide.....	35
1.12	N <sub>2</sub> -fixation by methanotrophs.....	36
2	Material and Methods.....	38
2.1	Filter cultivation .....	38
2.2	Oxidation of atmospheric trace gases and energy yield estimation.....	39
2.2.1	Quantification of cells in filter cultures.....	40
2.2.2	Cellular dry mass estimation and carbon content.....	41
2.3	N <sub>2</sub> fixation on air by atmMOB .....	41
2.4	AtmMOB adjustments to growth on air .....	42
2.5	Global distribution of atmMOB .....	45
3	Results .....	46
3.1	Paper 1: Simultaneous Oxidation of Atmospheric Methane, Carbon Monoxide, and Hydrogen for Bacterial Growth.....	46
3.2	Paper 2: Physiological Basis for Atmospheric Methane Oxidation and Methanotrophic Growth on Air .....	47
3.2.1	Colony formation, trace gas oxidation, and cellular energy yield during growth on air .....	47
3.2.2	Comparative proteomics .....	48
3.2.3	Specific affinity .....	49
3.2.4	Growth on nitrogen from air .....	49
3.2.5	Conclusions .....	50
3.3	Global distrubtion of atmMOB.....	51
4	Discussion .....	52
4.1	Physiological strategies of atmMOB to oxidize atmospheric CH <sub>4</sub> .....	52
4.2	Ecology and phylogeny of atmMOB.....	55
4.3	Metabolic potential of atmMOB for biotechnology .....	56

5	References .....	58
	Publications .....	72

## Acknowledgements

Before I was allowed to work in the laboratories of UiT, I had to join a course about health, safety, environmental matters, and emergency preparedness. During this course, the lecture stated that “*my leader is the most important person in my life*” which is, especially for a German, a delicate statement. Of course, he was referring to my PI and Supervisor Alex. Even though I do not fully agree with the statement, amongst others, because my partner in life Andrea might read the acknowledgement, there is definitely a grain of truth if referred to the work life of a PhD candidate. When I first met Alex during my masters in Vienna, thinking I was talking to another master student (guess the fresh ocean air does not only conserve cod), I had no idea of his plans to recruit Andrea as postdoc for his research group in Tromsø. But with Andrea as arctic soil enthusiast and me as good and planless partner, it was quickly settled that I would end up in Tromsø. Luckily, I did not regret the decision at all. Alex, you did a great job not only scientifically but also socially as PI and supervisor, which, unfortunately, does not seem to be the default in science. Many thanks for that!

My original PhD topic addressed the methanotrophic community of a pingo system in Svalbard. As the pandemic rendered the sampling on Svalbard impossible, I was forced to change the PhD topic and focus on methanotrophic pure cultures that appear to grow on air. This change significantly minimized the risk of drowning in a dark, muddy pond or being assimilated by a polar bear. Also, it gave me the opportunity to continue the research on these fascinating bacteria, that was started by the group under Mette’s leadership. Thus, Mette and Alex, many thanks that you enabled this unique opportunity.

Even though these fascinating bacteria I focused on can grow on air, they want to be wined and dined. Due to their special nature they demand to be grown on filters when fed with air which requires a lot of work. As Anne Grethe prepared most of the countless filter cultures that I have burned during my PhD and helped me a lot in general, a big thanks to you Anne Grethe.

If one starts to work at a new workplace, it is always helpful to have a person around that knows the lab, the infrastructure, and the right people. It is especially helpful if the person is as nice and willing to help as Bente. Bente, thank you for your help whenever it was needed.

Next, I want to thank my office mate Yin, all members of the CECO and the Microplants group which I am part of, and all co-authors contributing to the publications. It is nice to work in an environment mainly driven by curiosity as major motivation. You made my time as PhD really enjoyable!

Natürlich will ich auch meiner Familie, die mich in meinem bisherigen Werdegang immer unterstützt hat, danken. Phrasen wie diese erscheinen mir immer etwas leer, darum versuche ich es auf den Punkt zu bringen: Eintauschen will ich euch nicht.

And of course, I want to thank Andrea. I guess the lecturer confused Alex with you.

For those that I have not mentioned by name or forgotten, even though they have earned my thanks, many thanks and please excuse me. I am writing this section at the very end of my thesis. Most likely, your name was sacrificed to the submission deadline.

## Abstract

Atmospheric methane oxidizing bacteria (atmMOB) constitute the only known biological sink for atmospheric methane (CH<sub>4</sub>). By oxidizing the potent greenhouse gas CH<sub>4</sub> at its atmospheric concentration, they mitigate global warming. Despite the discovery of atmMOB in soils worldwide, the research on atmMOB stagnated as methanotrophs, that oxidize atmospheric CH<sub>4</sub> enduringly, have escaped isolation for decades. In 2019, the isolation of an atmMOB *Methylocapsa gorgona*, capable of growing “on air” (i.e., with air as sole carbon and energy source), eventually succeeded. Building on this atmMOB isolate, the physiological strategies and metabolic traits enabling methanotrophic growth on air have been investigated during this PhD thesis. To do so, a set of methods, specifically designed for bacterial cultures growing on filters that float on medium, has been established, comprising trace gas oxidation experiments, cell quantification, comparative proteomics, and <sup>15</sup>N-based isotopic labelling. Besides *M. gorgona*, the capability of five additional methanotrophic species to grow on air and their physiological strategies were investigated. In total, four of the six methanotrophic species, including three outside the canonical atmMOB group USC $\alpha$ , could grow on air, quadrupling the number of known atmMOB in pure culture. Additionally, the atmMOB were found to cover their nitrogen requirements from air. A combination of three physiological characteristics was identified as basis of the atmMOB to grow on air: A mixotrophic lifestyle, as all species oxidized atmospheric hydrogen (H<sub>2</sub>) and/or carbon monoxide (CO) in addition to CH<sub>4</sub>; energy requirements for growth below the energy value previously assumed necessary for cellular maintenance; and high apparent specific affinities for CH<sub>4</sub>. On a metabolic level, the atmMOB decreased investments in biosynthesis while increasing investments in trace gas oxidation during growth on air. As a first comprehensive work on atmMOB in pure culture, this thesis reveals strategies of atmMOB to grow on air, challenging previous notions of energy constraints for aerobic growth and the phylogeny of atmMOB. The findings suggest that the atmosphere supports larger atmMOB populations than assumed, indicating that their global distribution and impact on the global carbon cycle have been underestimated. Also, their role in mitigating global warming might be more important as they consume the indirect greenhouse gases H<sub>2</sub> and CO in addition to CH<sub>4</sub>. The atmMOB pure cultures and the methods developed in this thesis, are promising steppingstones to model the interaction between rising atmospheric CH<sub>4</sub> levels, global warming, and the biological sink for atmospheric CH<sub>4</sub>, and to evaluate the potential of atmMOB for the biofiltration of low-CH<sub>4</sub> emissions and other biotechnological applications.

# List of papers

## Paper 1:

### **Simultaneous Oxidation of Atmospheric Methane, Carbon Monoxide and Hydrogen for Bacterial Growth**

Alexander Tøsdal Tveit, Tilman Schmider, Anne Grethe Hestnes, Matteus Lindgren, Alena Didriksen and Mette Marianne

Microorganisms 2021, 9, 153. <https://doi.org/10.3390/microorganisms9010153>

## Paper 2:

### **Physiological Basis for Atmospheric Methane Oxidation and Methanotrophic Growth on Air**

Tilman Schmider, Anne Grethe Hestnes, Julia Brzykcy, Hannes Schmidt, Arno Schintlmeister, Benjamin R. K. Roller, Ezequiel Jesús Teran, Andrea Söllinger, Oliver Schmidt, Martin F. Polz, Andreas Richter, Mette M. Svenning, Alexander T. Tveit

Manuscript accepted in Nature Communications

## Abbreviations

$\alpha_A^0$	–	specific apparent affinity
ANME	–	anaerobic methane oxidizing archaea
AtmMOB	–	atmospheric methane oxidizing bacteria
ATP	–	adenosine triphosphate
c	–	gas concentration
CH <sub>2</sub> O	–	formaldehyde
CH <sub>3</sub> OH	–	methanol
CH <sub>4</sub>	–	methane
C-mol	–	carbon mol
CO	–	carbon monoxide
CO <sub>2</sub>	–	carbon dioxide
CODH	–	carbon monoxide dehydrogenase
D <sub>2</sub> O	–	deuterium oxide/heavy water
EMP	–	Earth Microbiome Project
Fae	–	formaldehyde-activating enzyme
Fch	–	formate-tetrahydrofolate ligase
Fdh	–	formate dehydrogenase
Fold	–	methylene-H <sub>4</sub> F dehydrogenase/methylene-H <sub>4</sub> F cyclohydrolase
GCS	–	glycine cleavage system
H <sub>2</sub> O	–	water
H <sub>4</sub> F	–	tetrahydrofolate
H <sub>4</sub> MPT	–	tetrahydromethanopterin
HCOO <sup>-</sup>	–	formate
Hhy	–	NiFe group 1h hydrogenase
kJ	–	kilojoule
K <sub>m</sub>	–	half saturation constant
K <sub>m(app)</sub>	–	apparent half saturation constant
LEL	–	lower explosive level
MDH	–	methanol dehydrogenase
MMO	–	methane monooxygenase
MOB	–	aerobic methane oxidizing bacteria
MtdA	–	methylene-H <sub>4</sub> F/ methylene-H <sub>4</sub> MPT dehydrogenase
MtdB	–	methylene-H <sub>4</sub> MPT dehydrogenase
N <sub>2</sub>	–	dinitrogen
NanoSIMS	–	secondary ion mass spectrometry
NH <sub>3</sub>	–	ammonia
Nif	–	molybdenum-iron nitrogenase
O <sub>2</sub>	–	dioxgen
OAA	–	oxaloacetate
OH	–	hydroxyl radicals
PBS	–	phosphate saline buffer
PHB	–	poly-β-hydroxybutyrate
pMMO	–	particulate methane monooxygenase
ppb	–	parts per billion
ppm	–	parts per million

<b>PPQ</b>	–	pyrroloquinoline quinone
<b>sMMO</b>	–	soluble methane monooxygenase
<b>SMR</b>	–	suspended microchannel resonator
<b>USC<math>\alpha</math></b>	–	upland soil cluster alpha
<b>USC<math>\gamma</math></b>	–	upland soil cluster gamma
<b>v</b>	–	oxidation rate
<b>V<sub>max</sub></b>	–	maximal oxidation rate
<b>V<sub>max(app)</sub></b>	–	apparent maximal oxidation rate

# 1 Introduction

## 1.1 Atmospheric methane

Despite low atmospheric concentrations, methane ( $\text{CH}_4$ ) is a greenhouse gas with a strong impact on climate change. Over a time horizon of 100 years, its global warming potential is estimated to be 30 times higher than carbon dioxide ( $\text{CO}_2$ ). On a 20-year timescale, the global warming potential of  $\text{CH}_4$  surpasses the potential of  $\text{CO}_2$  80 times<sup>1,2</sup>. This time dependent change in the global warming potential of  $\text{CH}_4$  derives from its short atmospheric lifetime of ca. 12 years<sup>3</sup>.  $\text{CH}_4$  is responsible for about 20% of the global warming induced by long-lived greenhouse gases. Since pre-industrial times, the atmospheric concentration of  $\text{CH}_4$  has increased by 150% to  $1911.81 \pm 0.59$  parts per billion (ppb) in 2022<sup>1,4,5</sup> (Fig.1).

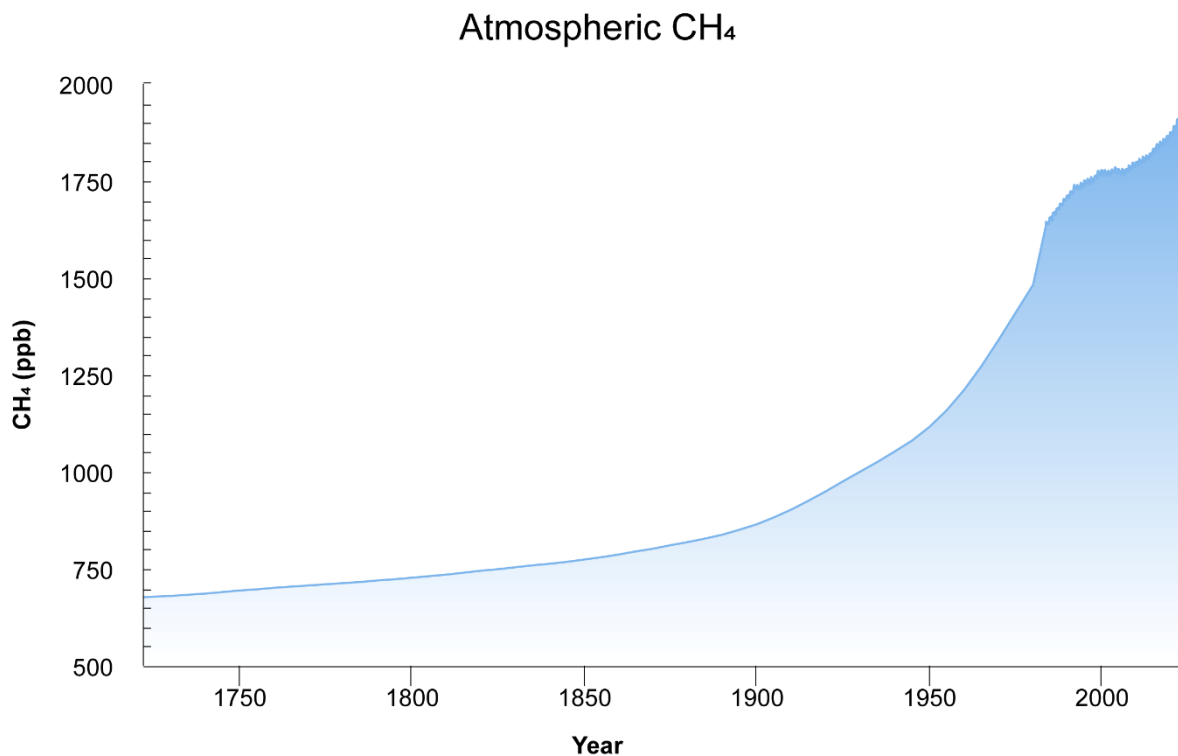


Figure 1. Atmospheric  $\text{CH}_4$  concentration in ppb since 1750 (<https://www.methanelevels.org/>).

$\text{CH}_4$  sources that cause the increasing atmospheric concentrations can be broadly categorized into pyrogenic, thermogenic, and biogenic groups<sup>6</sup>. Pyrogenic  $\text{CH}_4$  originates from the partial combustion of fossil fuels and biofuels and of biomass and soil carbon during wildfires. Thermogenic  $\text{CH}_4$  has been formed over millions of years through geological processes. It seeps from the subsurface to the atmosphere via mud volcanos, marine seeps, terrestrial seeps or

through exploitation of fossil fuels<sup>6</sup>. For a long time, strictly anaerobic microorganisms belonging to the domain of Archaea (methanogens) have been considered as the only considerable biogenic CH<sub>4</sub> source. However, a study demonstrated the generation of CH<sub>4</sub> by aquatic and terrestrial cyanobacteria under light, dark, oxic, and anoxic conditions, linking CH<sub>4</sub> production to phototrophic primary production<sup>7</sup>. In 2022, a study reported CH<sub>4</sub> formation in metabolic active organism triggered by free iron and reactive oxygen species, implying that all living cells possess the potential to generate CH<sub>4</sub><sup>8</sup>. Still, the major sources of biogenic CH<sub>4</sub> are inhabited by methanogens and comprise a wide range of anoxic anthropogenic and natural ecosystems, ranging from rice paddies, digestive systems of ruminants, organic waste deposits, and oxygen-poor freshwater reservoirs to wetlands, oceans, and termites<sup>6,7</sup>. The major sink of atmospheric CH<sub>4</sub> is the chemical oxidation of CH<sub>4</sub> by hydroxyl radicals (OH) in troposphere and stratosphere accounting for approximately 95% of the loss<sup>6,9,10</sup>. The remaining 5% of the estimated loss is caused by methanotrophic bacteria that constitute the sole biological sink of atmospheric CH<sub>4</sub>.

## 1.2 Methanotrophs

Methanotrophs, that utilize CH<sub>4</sub> as energy and carbon source, are the only known biological CH<sub>4</sub> sink<sup>11,12</sup>. They comprise a phylogenetically diverse group of anaerobic and aerobic prokaryotes that oxidize CH<sub>4</sub> to CO<sub>2</sub> and play a major role in the global CH<sub>4</sub> cycle as they mitigate CH<sub>4</sub> emissions before reaching the atmosphere. It is estimated that methanotrophs mitigate 500 – 798 Tg CH<sub>4</sub> per year<sup>9,13</sup>. In anoxic environments, anaerobic CH<sub>4</sub> oxidizing archaea (ANME) oxidize CH<sub>4</sub> by coupling the oxidation to the reduction of the electron acceptors sulfate, nitrate, iron, or manganese. In addition, methanotrophic bacteria of the candidate phylum NC10 oxidize CH<sub>4</sub> in anoxic environments using an intra-aerobic pathway that generates oxygen (O<sub>2</sub>) from nitrite<sup>14–18</sup>. In oxic environments, aerobic methane oxidizing bacteria (MOB) oxidize CH<sub>4</sub> with O<sub>2</sub> to CO<sub>2</sub>. Atmospheric methane oxidizing bacteria (atmMOB), a subgroup of MOB, constitute the above-mentioned biological sink for atmospheric CH<sub>4</sub> as they can oxidize CH<sub>4</sub> at its atmospheric concentration. The defining characteristic of MOB is the methane monooxygenase (MMO) that catalyzes the oxidation of CH<sub>4</sub> to methanol. Depending on their major pathway of carbon fixation, aerobic methanotrophs have been divided into three groups: Type I methanotrophs, mainly dominated by

*Gammaproteobacteria*, fix carbon via the ribulose monophosphate pathway. Type II methanotrophs use the serine pathway for carbon fixation and belong to the class of *Alphaproteobacteria*<sup>19</sup>. Some Type II methanotrophs within the family *Beijerinckiaceae* also encode the Calvin-Benson-Bassham Cycle although the functional role of the cycle in these methanotrophs remains unclear<sup>20</sup>. Type III methanotrophs fix carbon via the Calvin-Benson-Bassham Cycle and belong to the *Verrucomicrobia*<sup>21</sup>. However, the finding of methanotrophs within the *Actinobacteria* that fix carbon also via the ribulose monophosphate pathway renders the classification based on carbon fixation pathways as outdated<sup>22</sup>. Additionally, a recent study suggests that aerobic methanotrophs might also be represented within the *Gemmatimonadota*<sup>23</sup>. Thus, the classification of aerobic methanotrophs into *types* should be only considered as synonym for the phylogenetic groups<sup>19</sup> and needs to be updated according to the latest scientific progress.

### **1.3 Why study atmMOB and the biological sink of atmospheric CH<sub>4</sub>?**

Since 2007, after a brief period of stability, the atmospheric CH<sub>4</sub> concentration started to increase rapidly<sup>3</sup> (Fig. 1). This increase has been linked to several causes: The declining OH concentration in the atmosphere that weakens the major atmospheric CH<sub>4</sub> sink, the increase of anthropogenic CH<sub>4</sub> emissions from agricultural and fossil fuel sources, and the increasing microbial CH<sub>4</sub> production in wetlands. The increasing microbial production suggests that current increases in the atmospheric CH<sub>4</sub> concentration are also driven by microbial feedback responses to global warming<sup>24-26</sup>. In contrast to the declining chemical sink for atmospheric CH<sub>4</sub>, the biological sink has the potential to grow with increasing concentrations of atmospheric CH<sub>4</sub>. As the biological sink is within reach of management practices, its natural potential might be maximized to increase the removal of atmospheric CH<sub>4</sub><sup>27</sup>. Additionally, atmMOB might be promising biocatalyst for the biofiltration of CH<sub>4</sub> emissions<sup>28</sup>. However, the ecology, phylogeny, and especially the physiology of atmMOB is subject to major uncertainties caused by a historical lack of atmMOB in pure culture. These uncertainties have therefore prevented efficient management of the biological sink; understanding and predicting feedback responses by atmMOB to increasing concentrations of atmospheric CH<sub>4</sub>; and the utilization of atmMOB for the biofiltration of emissions containing CH<sub>4</sub>. Thus, a better understanding of atmMOB

might, in light of the climate crisis, offer a toolset to mitigate CH<sub>4</sub> emissions, convert mitigated CH<sub>4</sub> emissions efficiently into valuable carbon compounds, and cope with increasing atmospheric concentrations of CH<sub>4</sub>.

## **1.4 Atmospheric methane oxidizing bacteria**

Despite the discovery of aerobic methanotrophy by Kaserer and Söhngen in the early 20<sup>th</sup> century, the first indication of atmospheric CH<sub>4</sub> oxidation was reported in 1982<sup>29</sup>. In that study, swamp soils were shown to emit CH<sub>4</sub> when waterlogged, but consume atmospheric CH<sub>4</sub> when dry. The discovery of biphasic CH<sub>4</sub> oxidation kinetics of soils by Bender and Conrad in 1992<sup>30</sup>, was another early indication of the existence of atmMOB. They discovered that soils exposed to low and high CH<sub>4</sub> concentrations show different kinetic properties. At low CH<sub>4</sub> concentrations, they measured high affinity activities and low maximal methane oxidation rates ( $V_{max}$ ). Exposing the same soil to high CH<sub>4</sub> concentrations led to low affinity activities and high  $V_{max}$ . They concluded that methanotrophs only cultivatable at high CH<sub>4</sub> concentrations (in literature also referred to as canonical or conventional methanotrophs) are responsible for the low affinity activity. The high affinity, however, was assigned to either an unknown group of methanotrophs or an activity of the “canonical” methanotrophs that had escaped discovery<sup>31</sup>. Either way, as the investigated soils, in contrast to autoclaved controls, showed oxidation activity at CH<sub>4</sub> mixing ratios of 1700 ppb, another evidence was supplied that methanotrophic bacteria can act as sink for atmospheric CH<sub>4</sub>. Since the discovery of the biphasic CH<sub>4</sub> oxidation kinetics, two major, yet partially unanswered questions have shaped the research in the scientific field: Which methanotrophs are responsible for the oxidation of atmospheric CH<sub>4</sub> and how can these methanotrophs survive and grow with the apparent energy limitations inherent to the oxidation of the low atmospheric CH<sub>4</sub> concentrations?

## **1.5 Ecology and phylogeny of atmospheric methane oxidizing bacteria**

Atmospheric CH<sub>4</sub> oxidation has been mainly linked to aerobic and dry soils that are often referred to as “upland soils”. In these soils, atmMOB oxidize CH<sub>4</sub> that diffuses from the overlying atmosphere into the soil<sup>32</sup>. Examples for soil ecosystems in which net uptake of

atmospheric CH<sub>4</sub> has been measured are manifold, including forest soils<sup>33,34</sup>, tropical soils<sup>35</sup>, grasslands and meadows<sup>36</sup>, landfill cover soils<sup>37</sup>, deserts<sup>38</sup>, heathlands<sup>39</sup>, dryland rice soils<sup>40,41</sup>, tundra soils<sup>42,43</sup>, and dry swamp soils<sup>29</sup>. However, also caves<sup>44</sup> and the surfaces of plants like birches, spruces<sup>45</sup>, and mosses<sup>46</sup> can represent sinks for atmospheric CH<sub>4</sub>. Studies, that coupled the *pmoA* gene of MOB (encodes the β subunit of the particulate methane monooxygenase) as functional marker to isotope or fluorescence labeling, assigned the oxidation of atmospheric CH<sub>4</sub> in upland soils to the activity of two clades within the *Alpha*- and *Gammaproteobacteria*, the upland soil cluster alpha (USCα) and the upland soil cluster gamma (USCγ)<sup>47-49</sup>. Besides the abundance of USCα and USCγ, the *pmoA* of representatives within *Methylocystaceae*, *Beijerinckaceae*, *Methylococcaceae*, *Crenotrichaceae* and cluster 1 – 5, have been found in environments with net CH<sub>4</sub> uptake<sup>33,50,51</sup>.

As summarized by Dunfield<sup>32</sup> and Kolb<sup>33</sup>, different environmental factors affect methanotrophic communities and the biological sink for atmospheric CH<sub>4</sub> in soils. These factors comprise, among others, temperature, diffusivity, water content, pH, nitrogen availability, and anthropogenic disturbances. It is important to keep in mind that these factors should not only be considered isolated but that their interactions modify their individual impact<sup>52,53</sup>.

King et al. concluded from CH<sub>4</sub> oxidation rates of forest soils and methanotrophic communities at different temperatures and different CH<sub>4</sub> concentrations, that temperature has a rather weak effect on the uptake of atmospheric CH<sub>4</sub> by the methanotrophic community<sup>54</sup>. According to the study, this low response to temperature changes by methanotrophs is caused by the limited diffusion of CH<sub>4</sub> into the soil at atmospheric CH<sub>4</sub> concentrations as methanotrophs exposed to high CH<sub>4</sub> concentrations showed a strong response to temperature change<sup>54</sup>. The diffusion limitation at atmospheric CH<sub>4</sub> concentrations is also reflected by a gradient of decreasing CH<sub>4</sub> observed in soils (e.g., Whalen et al. 1992<sup>55</sup>) as rapid diffusion of CH<sub>4</sub> from the atmosphere should not result in a gradient. A study modelling the uptake of atmospheric methane by soils between the years 1900 and 2100, also identified diffusion as a major factor driving atmospheric CH<sub>4</sub> oxidation but in addition pointed out that temperature became an important factor for the increasing methanotrophic rates in soils<sup>56</sup>. Increasing temperature can stimulate or suppress CH<sub>4</sub> oxidation as it influences the enzyme activity<sup>52</sup>. However, the effect of temperature on growth, the physiological state of atmMOB cells, and the CH<sub>4</sub> oxidation rate has never been studied directly as isolates of atmMOB were unavailable. Besides direct impacts on CH<sub>4</sub>

oxidation, temperature can change soil moisture, and thus cause water stress that decreases CH<sub>4</sub> oxidation or improve gas diffusion that increases CH<sub>4</sub> oxidation<sup>57</sup>. The diffusion of CH<sub>4</sub> in water is 10 000 times slower than in air<sup>32,55</sup>. Thus, the water content is a critical factor impacting CH<sub>4</sub> diffusion, CH<sub>4</sub> availability, and eventually oxidation rates by atmMOB at atmospheric CH<sub>4</sub> concentrations.

The pH does not seem to have a large effect on the oxidation of atmospheric CH<sub>4</sub> by soils as oxidation has been detected in wide range of soils with different pH<sup>33</sup>. However, major shifts in pH can lead to a loss of CH<sub>4</sub> oxidation activity<sup>33,58</sup>. Furthermore, pH is a main driver of the methanotrophic community composition in environments representing atmospheric CH<sub>4</sub> sinks as it influences the abundance of USC $\alpha$  and USC $\gamma$ <sup>33,47,50,59,60</sup>. USC $\alpha$  members are more likely to be abundant in acidic environments while members of the USC $\gamma$  are abundant in alkaline environments, a trend also observed for “conventional” methanotrophs within the *Alpha*- and *Gammaproteobacteria*<sup>61</sup>.

Since the beginning of industrialization, the anthropogenic release of reactive nitrogen has more than doubled the nitrogen input into global ecosystems<sup>62</sup>. The increased input is mainly caused by fertilizer usage, combustion of fossil fuels, and industrial activities. Reactive nitrogen is also emitted to the atmosphere causing an increased nitrogen deposition to surfaces and thus impacts terrestrial and marine ecosystems globally by modifying the biogeochemical nitrogen cycle<sup>63,64</sup>. Amongst others, consequences of nitrogen deposition on ecosystems are fertilization, acidification, and accumulation of excess nutrients<sup>63,65</sup>. How the increased nitrogen input and availability of reactive nitrogen in general influences the biological sink for atmospheric CH<sub>4</sub> sink is unclear<sup>66</sup>. Often, nitrogen fertilization inhibits atmospheric CH<sub>4</sub> oxidation<sup>67,68</sup>, but also stimulatory effects of nitrogen fertilization have been reported<sup>69,70</sup>. Overall, the impact of nitrogen on CH<sub>4</sub> oxidation seems to depend on the diversity and activity of methanotrophic community, the type and amount of the reactive nitrogen, and the exposure time to the nitrogen fertilizer<sup>69,71,72</sup>. In contrast to the extensively studied effect of increased reactive nitrogen on the biological sink for atmospheric CH<sub>4</sub>, the effect of nitrogen limitation on atmMOB and the sink is unknown as a lack of atmMOB in pure culture has prevented research<sup>66</sup>. Besides changes in the nitrogen input, other anthropogenic activities impact the biological sink for atmospheric CH<sub>4</sub><sup>73</sup>. For example, the conversion of ecosystems to agricultural sites disturbs the uptake of atmospheric CH<sub>4</sub> as agriculture practices can, among others, cause limitation of gas diffusion,

water stress, soil compaction, disruption of the soil structure, and increased bulk density<sup>73-75</sup>. Additionally, agrochemicals, logging, and soil acidification can decrease atmospheric CH<sub>4</sub> oxidation<sup>76-79</sup>.

## 1.6 Physiology of atmospheric methane oxidizing bacteria

Dunfield<sup>32</sup> summarized four potential strategies of atmMOB that might enable survival and growth with the apparent energy limitations inherent to the oxidation of the low atmospheric CH<sub>4</sub> concentrations in air:

- (i) atmMOB are oligotrophs that manage to grow and survive on atmospheric CH<sub>4</sub> alone.
- (ii) atmMOB are flush feeders that feed on CH<sub>4</sub> generated in deeper soil layers in addition to atmospheric CH<sub>4</sub>.
- (iii) atmMOB grow on substrates in addition to atmospheric CH<sub>4</sub>.
- (iv) atmMOB grow on other substrates than atmospheric CH<sub>4</sub> and the CH<sub>4</sub> is co-oxidized in a process that does not yield energy.

### 1.6.1 (i) Oligotrophs

Conrad reviewed<sup>80</sup> the theoretical constraints for microorganisms oxidizing CH<sub>4</sub>, hydrogen (H<sub>2</sub>), and carbon monoxide (CO) as substrate for their energy metabolism. Traces of all three gases are present in the atmosphere at mixing ratios of 1919 ppb for CH<sub>4</sub> (August 2023 [https://gml.noaa.gov/ccgg/trends\\_ch4/](https://gml.noaa.gov/ccgg/trends_ch4/)), 530 ppb for H<sub>2</sub>, and 90 ppb for CO<sup>81,82</sup>. The Gibbs free energy resulting from the oxidation of mentioned gases at atmospheric concentrations add up to -797 kJ mol<sup>-1</sup> (assuming a CH<sub>4</sub> concentration of 1750 ppb), -199 kJ mol<sup>-1</sup>, and -235 kJ, respectively. Therefore, the low atmospheric partial pressure of the gases does not constrain microorganisms thermodynamically. Rather, according to Conrad<sup>80</sup>, the constraints are of kinetic nature. The oxidation of low gas concentration needs to proceed quick enough to generate sufficient energy for cellular maintenance and growth. Assuming Michaelis-Menten kinetics, this can be explained based on the following equation:

$$v = c \times \frac{V_{\max(app)}}{K_{m(app)}} \quad (I)$$

In which  $v$  is the oxidation rate,  $c$  the gas concentration,  $V_{\max(app)}$  the apparent maximal oxidation rate of the cell, and  $K_{m(app)}$  the apparent half saturation constant of the cell. In general, the half saturation constant ( $K_m$ ) (half saturation constant for an enzyme) displays the gas concentration at which the enzymes involved in the oxidation processes are half-saturated. Hence, the constant provides information about binding affinity of enzyme and substrate. The higher the binding affinity, the tighter the enzyme binds the substrate. The  $K_m$  is defined as dissociation constant and thus, a low  $K_m$  translates into a high affinity and vice versa. On a cellular level the apparent affinity  $K_{m(app)}$  (half saturation constant of a cell) needs to be coupled to a sufficiently high  $V_{\max(app)}$  (which can be achieved by a high number of enzymes per cell) to meet cellular maintenance energy requirements at atmospheric gas concentrations. Thus, the apparent specific affinity that puts  $V_{\max(app)}$  and  $K_{m(app)}$  into relation seems to be a valid measure of oligotrophy, while the high apparent affinity as measure is ambiguous since it doesn't give information about the oxidation rate and eventually the corresponding energy yield (Fig.2). The apparent specific affinity is defined as:

$$a_A^0 = \frac{V_{\max(app)}}{K_{m(app)}} \quad (II)$$

and represents the initial slope of a Michaelis-Menten hyperbolic curve and the pseudo first-order rate constant<sup>83</sup>. It directly indicates reaction rates at low substrate concentrations catalyzed by microorganisms<sup>84</sup>. Since the oxidation rate  $v$  equals the product of ambient gas concentration  $c$  and specific affinity  $a_A^0$  (equation I), a high apparent specific affinity is necessary to meet cellular maintenance energy requirements at atmospheric  $CH_4$  concentrations. In a study by Tijhuis et al.<sup>85</sup>, stating that maintenance energy is mainly influenced by temperature, the average microbial maintenance energy is estimated to be 4.5 kJ per C-mol biomass per hour at 25° C. The value is in so far important as it is the basic premise for later theoretical assumptions on how methanotrophs live on atmospheric  $CH_4$  concentrations by Conrad<sup>80</sup>.

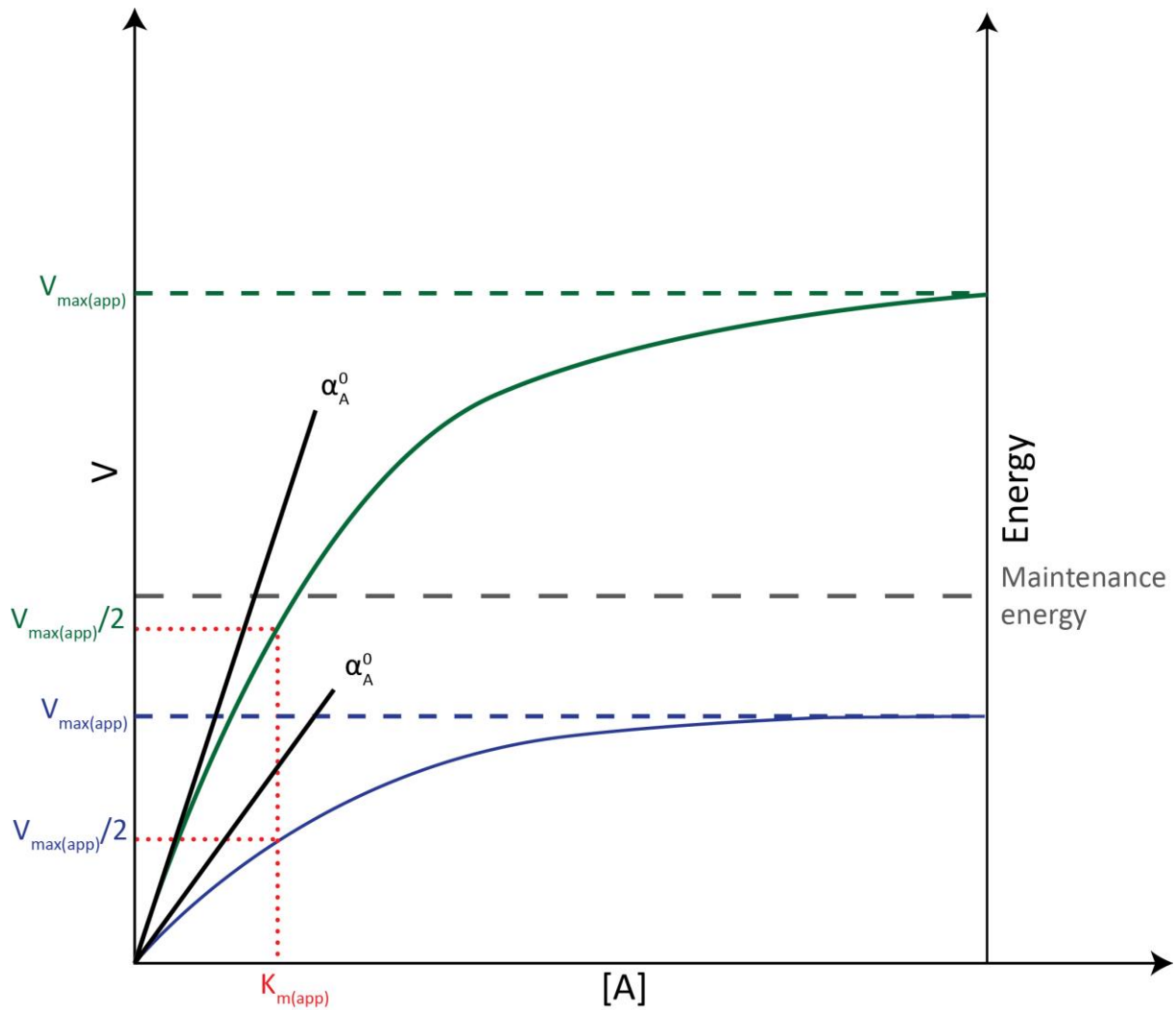


Figure 2: Two different Michaelis Menten hyperbolic curves with the same  $K_{m(app)}$  but different  $V_{max(app)}$  to illustrate  $\alpha_A^0$  and the related energy yield. [A] substrate concentration (e.g.  $CH_4$ ). The  $K_{m(app)}$  is defined as the substrate concentration at which  $V_{max(app)}$  is half ( $V_{max(app)}/2$ ).

The lack of pure cultures has prevented evaluation of the theory that atmMOB are oligotrophs capable of growing on atmospheric  $CH_4$  alone. However, the theory that atmMOB are oligotrophs capable of growing on atmospheric  $CH_4$  alone is supported by low apparent half saturation constants ( $K_{m(app)} < 0.1 \mu M$ ) found in upland soils (Fig. 3).

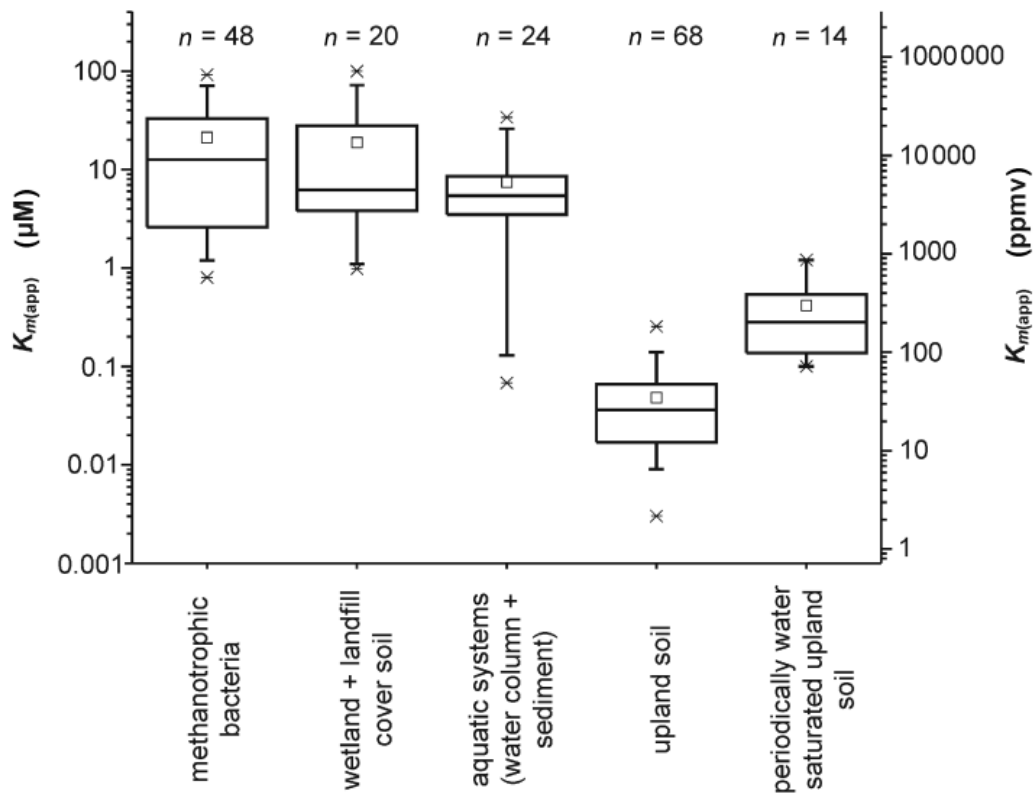


Figure 3. Box plot of  $K_{m(\text{app})}$  values for methane oxidation in pure cultures of methanotrophic bacteria and in different ecosystems. The upper and lower box lines represent the 25th and 75th percentile values (= 50% of all values). The horizontal line in the box represents the 50th percentile (median) and the square symbol the mean. Error bars denote the 5th and 95th percentiles and asterisks the upper and lower limits<sup>86</sup>.

Until now, the only energy yield estimations for atmMOB at atmospheric  $\text{CH}_4$  are derived from environmental studies. For example, a study<sup>87</sup> estimated the  $\text{CH}_4$  oxidation rate by the MOB community in forest soils partly dominated by USC $\alpha$ . There, the rate was assessed by combining qPCR-based quantification of MOB and their  $\text{CH}_4$  oxidation, amounting  $540 - 800 \times 10^{-18} \text{ mol CH}_4 \text{ cell}^{-1} \text{ hour}^{-1}$ . The value is more than 10 times higher than the oxidation rate needed ( $40 \times 10^{-18} \text{ mol CH}_4 \text{ cell}^{-1} \text{ hour}^{-1}$ ) to supply the above-mentioned maintenance energy (4.5 kJ per C-mol biomass per hour). Thus, the study supports the theory that atmMOB are oligotrophs, i.e., being able to survive and grow on atmospheric  $\text{CH}_4$  alone. However, the authors revoked this energy estimation in later study stating that the qPCR-based approach likely overestimated the cell-specific  $\text{CH}_4$  oxidation rates. In the later study, the authors reported atmospheric  $\text{CH}_4$  oxidation rates of  $1 - 14 \times 10^{-18} \text{ mol CH}_4 \text{ cell}^{-1} \text{ hour}^{-1}$  in forests soils<sup>88</sup>.

### 1.6.2 (ii) Flush feeders

The second theoretical strategy described by Dunfield<sup>32</sup> implies that atmMOBs are flush feeders. They feed on CH<sub>4</sub> periodically generated in deeper soil layers in addition to atmospheric CH<sub>4</sub>. The CH<sub>4</sub> concentration in soil layers can be elevated during periods with increased soil water content (e.g. after rainfall) as the high soil water content restricts O<sub>2</sub> diffusion. The decreased O<sub>2</sub> tension creates suitable conditions for methanogens to generate CH<sub>4</sub>. The resulting increased CH<sub>4</sub> concentration stimulates “conventional” methanotrophs to oxidize CH<sub>4</sub>. After the CH<sub>4</sub> concentration has decreased to an atmospheric level, methanotrophs oxidize atmospheric CH<sub>4</sub> until they transition into an inactive state. Indications of flush feeding were, for example, observed in alpine tundra soils that were first exposed to H<sub>2</sub> and CO<sub>2</sub> to induce hydrogenotrophic CH<sub>4</sub> generation<sup>88</sup>. After the CH<sub>4</sub> concentration fell back to atmospheric, the atmospheric CH<sub>4</sub> oxidation rates of these soils were three times higher than of soils serving as controls. A study targeting the methanotrophic community in paddy soils provided first evidence for flush feeding as “conventional” methanotrophs abundant in the paddy soils regained the ability to oxidize atmospheric CH<sub>4</sub> for several days after being exposed to high CH<sub>4</sub> concentrations<sup>89</sup>. Additionally, it was shown that a *Methylocystis* strain oxidized atmospheric CH<sub>4</sub> for three months after being cultivated under a 10% CH<sub>4</sub> atmosphere<sup>90</sup>. A potential process underlying flush feeding is the accumulation of storage compounds that allows MOB to stay active for a certain period of starvation. Presumably, during exposure to increased CH<sub>4</sub> concentrations, methanotrophs build up storage compounds such as poly-β-hydroxybutyrate (PHB) or glycogen. These storage compounds can later be used as reducing equivalents and are together with the oxidation of atmospheric CH<sub>4</sub> sufficient to meet cellular growth and maintenance requirements. Several studies reported storage compound accumulation in methanotrophs and determined different reasons for the accumulation. PHB can be accumulated if reducing energy is excessive<sup>91</sup>, but also induced stress and nutrient- and nitrogen-limitation seem to trigger PHB accumulation<sup>89,92</sup>. Pure culture-based studies reported PHB accumulation ranging between 7 – 68% of the total dry weight in *Methylocystis* and *Methylosinus* cells<sup>92,93</sup>. In line with that, a recent study on the gammaproteobacterial methanotroph *Methylobacter tundripaludum* SV96 demonstrated accumulation of glycogen at high temperatures<sup>94</sup>. While these data demonstrate that storage compounds are utilized by methanotrophs, there is still no direct evidence that such compounds play a role in the growth of MOB at atmospheric CH<sub>4</sub> concentrations.

### 1.6.3 (iii) Facultative CH<sub>4</sub> oxidizers

The third theory on how atmMOB grow, assumes that they are facultative methanotrophs, i.e. in addition to atmospheric CH<sub>4</sub>, the organisms can utilize other substrates<sup>32</sup>. By showing that “conventional” methanotrophic *Methylocella* species can grow on the multicarbon compounds acetate, pyruvate, succinate, malate, and ethanol, the conjecture that the single carbon intermediates of aerobic CH<sub>4</sub> oxidation, methanol, formaldehyde, and formate, are the only potential energy source, was proven wrong<sup>95</sup>. Additionally, members of the genera *Methylocystis* and *Methylocapsa* were shown to grow on acetate and/or ethanol<sup>96-99</sup>. Further, a representative of the genus *Methylocystis* has been shown to oxidize H<sub>2</sub> in addition to CH<sub>4</sub> as energy source<sup>100</sup>. *Methylocapsa* gorgona MG08, central to this thesis as it represents the first methanotroph in pure culture found to grow with air as the only substrate, encodes not only a NiFe group 1h hydrogenase (Hhy) but also a MuCo class 1 carbon monoxide dehydrogenase (CODH)<sup>101</sup>. Thus, it carries the potential to gain additional energy through the oxidation of H<sub>2</sub> and carbon monoxide (CO). The same study revealed the genomic potential to use these gases in several other members of the genera *Methylocapsa*, *Methylocystis*, and *Methylosinus*. However, whether the oxidation of mentioned gases at atmospheric trace concentrations contribute to the energy conservation by atmMOB remained unclear at that point.

### 1.6.4 (iv) Ammonia oxidizers

The last theory proposed by Dunfield<sup>32</sup> to explain atmospheric CH<sub>4</sub> oxidation is based on ammonia-oxidizing bacteria. The key enzyme of ammonia oxidation, the ammonia monooxygenase, and the methane monooxygenase are very likely to share the same evolutionary origin<sup>102,103</sup>. The two enzymes have been found to oxidize ammonia (NH<sub>3</sub>) and CH<sub>4</sub> as both compounds are structurally analogous. However, there is no proof that the resulting toxic methanol can be further utilized by ammonia oxidizers<sup>104</sup>. Nonetheless, ammonia oxidizers might contribute to atmospheric CH<sub>4</sub> oxidation by co-oxidizing CH<sub>4</sub> instead of NH<sub>3</sub>, but their impact on atmospheric CH<sub>4</sub> oxidation seems to be neglectable<sup>32</sup>.

## 1.7 Main objectives

My PhD thesis builds up on the study “Widespread soil bacterium that oxidizes atmospheric methane” by Tveit et al.<sup>101</sup> that was published in 2019. The study reports the isolation and an initial characterization of *Methylocapsa gorgona* MG08, the first known atmMOB able to grow with air as sole energy and carbon source, and the first member of the USC $\alpha$  in pure culture. The lack of atmMOB in pure culture has prevented the assessment of the above-mentioned potential strategies that enable growth on atmospheric CH<sub>4</sub> concentrations for many years. By finally having atmMOB in pure culture, my PhD thesis aimed at deciphering the physiological strategies of *M. gorgona* MG08 that enable its growth on air. Additionally, in growth tests prior to my project, it has been shown that not only *M. gorgona* MG08, but also five additional methanotrophic strains within the three different genera *Methylocapsa*, *Methylocystis*, and *Methylosinus*, all belonging to *Alphaproteobacteria*, form colonies when cultivated on filters floating on medium and with air as the only source of energy and carbon. These five strains are *Methylocapsa acidiphila* B2, *Methylocapsa aurea* KYG, *Methylocapsa palsarum* NE2, *Methylocystis rosea* SV97, and *Methylosinus trichosporium* OB3b. These strains, as well as *M. gorgona* MG08, encode functional complexes for the oxidation of H<sub>2</sub> and/or CO (Fig. 4) and thus the potential to oxidize these two gases in addition to CH<sub>4</sub>. The physiology underlying colony formation of these methanotrophic strains is likely based on one or more of the three theoretical strategies described in detail in the previous chapter (see section 1.6): (i) AtmMOB as “Oligotrophs” that grow with methane as the sole carbon and energy source; (ii) AtmMOB as “Flush feeders”; (iii) AtmMOB as “Facultative oxidizers” of additional atmospheric gases. By investigating the six different methanotrophic strains and their physiological strategies to live on air, the PhD aimed to answer the following questions which represent my main objectives:

- What is the physiological basis for atmospheric CH<sub>4</sub> oxidation?
- Do the methanotrophic strains oxidize the atmospheric trace gases H<sub>2</sub> and CO in addition to CH<sub>4</sub>?
- What is the energy yield per cell during oxidation of trace gases in air?
- Do the metabolic strategies of atmMOB vary between strains?
- Is atmospheric CH<sub>4</sub> oxidation geographically and phylogenetically more widespread than previously thought?

## 1.8 Secondary objective

In addition to my main objectives a secondary objective is based on the fact that the six strains encode all genes required for dinitrogen (N<sub>2</sub>) fixation<sup>101</sup> (Fig. 4) and show growth on nitrogen-free medium<sup>101,105–109</sup> when cultivated at high concentrations of CH<sub>4</sub> implying N<sub>2</sub> fixation by the strains. Additionally, growth experiments with four of the MOB strains cultivated on filters while being exposed to air as sole substrate and nitrogen source resulted in colony formation indicating that the strains might be able to fix N<sub>2</sub> when grown with air as their only source of carbon, energy, and nitrogen. If true, the N<sub>2</sub> fixation could provide a crucial advantage for life in oligotrophic soils and atmMOB would not only play an important role in the carbon cycle as atmospheric CH<sub>4</sub> sink but also impact the nitrogen cycle and serve as potential nitrogen source in nitrogen limited environments. However, N<sub>2</sub> fixation is presumably too costly<sup>110</sup> for atmMOB if the theoretical energy assumptions by Conrad<sup>80</sup> hold true. In addition to the energy costs for N<sub>2</sub>-fixation, the nitrogenase, the key enzyme involved in the N<sub>2</sub> fixation process, is very O<sub>2</sub> sensitive. Given the fact that some of the mentioned strains only seem to fixate N<sub>2</sub> under reduced O<sub>2</sub> tension, N<sub>2</sub>-fixation of the strains while being exposed to air seems to be rather unlikely. However, based on the observation of colony formation on nitrogen-free medium and air as sole substrate, the PhD targeted the following question representing my secondary objective:

- Do the atmMOB strains fix N<sub>2</sub> during growth with air as sole carbon, energy, and nitrogen source?

## 1.9 The methanotrophic strains

The following section comprises a description of the methanotrophic strains that were screened for their ability to grow with air as sole carbon and energy source during this PhD thesis.

### 1.9.1 *Methylocystaceae*

Two of the strains that show colony formation when grown on filters exposed to air, namely *Methylosinus trichosporium* OB3b and *Methylocystis rosea* SV97, belong to the family *Methylocystaceae* within the class *Alphaproteobacteria*. As reviewed by Dedysh and Knief<sup>19</sup>, methanotrophs within this family of gram-negative bacteria fix carbon via the serine pathway.

*Methylosinus trichosporium* OB3b, one of the most extensively studied methanotrophs, is an exospore forming, mesophilic, motile, rod-shaped microorganism with the capability to fixate  $N_2$ <sup>105,111</sup>. Depending on the copper availability it expresses either soluble methane monooxygenases (sMMO) or particulate methane monooxygenases (pMMO) (see section 1.10 below). Under N-limited growth conditions, the cells can accumulate up to 55,5% PHB<sup>112,113</sup>. Besides the functional complex for pMMO and a nitrogenase, it also encodes all subunits of a Hhy hydrogenase and an incomplete CODH complex<sup>101</sup> (Fig. 4).

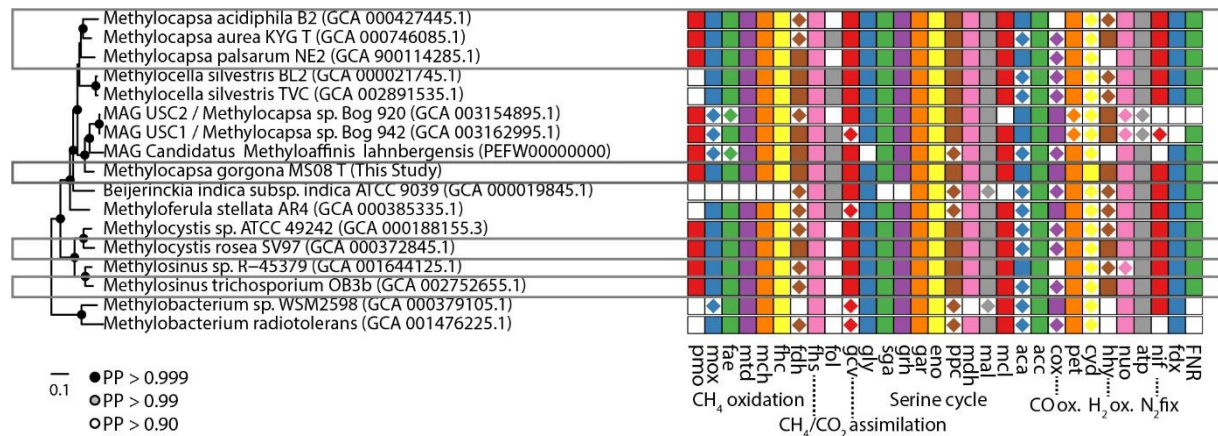


Figure 4. Phylogeny of the six respective methanotrophic strains *M. acidiphila* B2, *M. aurea* KYG, *M. palsarum* NE2, *M. gorgona* MG08, *M. rosea* SV97, and *M. trichosporium* OB3b based on 34 marker genes, and the presence/absence of functional complexes encoded in the genome of the respective strains. The methanotrophic strains are highlighted by the grey box. Presence of a complete complex is indicated by a solid square. Complexes that are incomplete are indicated by an embedded diamond. Abbreviations for functional complexes: aca, carbonic anhydrase; acc, acetyl-CoA carboxylase; atp, ATP synthase; cox, carbon monoxide dehydrogenase; cyd, terminal c cytochrome oxidase; eno, enolase; fae, formaldehyde activating enzyme; fdh, formate dehydrogenase; fdx, ferredoxin, 2Fe-2S; fhc, formyltransferase/hydrolase complex; fhs, formate-tetrahydrofolate ligase; FNR, ferredoxin-NADP+ oxidoreductase; fol, bifunctional 5,10-methylene-tetrahydrofolate dehydrogenase, and 5,10-methylene-tetrahydrofolate cyclohydrolase; gck, 2-glycerate kinase; gcv, glycine cleavage complex; gly, serine hydroxymethyltransferase; hhy, [NiFe] hydrogenase; hpr, hydroxypyruvate reductase; mch, methenyl tetrahydromethanopterin cyclohydrolase; mcl, malyl-CoA lyase; mdh, malate dehydrogenase; mtd, NAD(P)-dependent methylene tetrahydromethanopterin dehydrogenase; mtk, malate thiokinase; mxa, methanol dehydrogenase; nif, nitrogenase; nuo, NADH-quinone oxidoreductase; pet, ubiquinol-cytochrome reductase; pmo, particulate methane mono-oxygenase; ppc, phosphoenolpyruvate carboxylase; and sga, serine-glyoxylate aminotransferase<sup>101</sup>.

*Methylocystis rosea* SV97 is a non-motile, rod-shaped, 1.1–2.5 mm long and 0.8–1.1 mm wide, mesophilic methanotroph<sup>106</sup> (Fig. 5). It was isolated from a wetland soil showing minor  $CH_4$  emissions near Ny-Ålesund, Svalbard, Norway. It grows at temperatures ranging from 5 to 37°C and a pH from 5.5 to 9.0. Like *M. trichosporium* OB3b, it accumulates PHB, fixes  $N_2$  and encodes complete pMMO, nitrogenase, and Hhy complexes, and an incomplete CODH complex (Fig. 4).

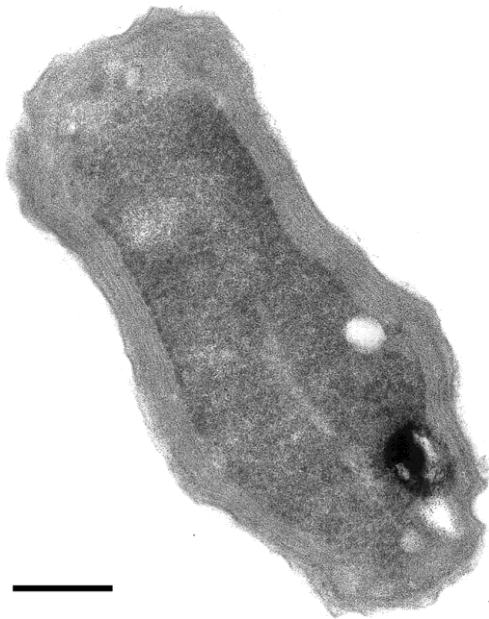


Figure 5. Transmission electron micrograph of a cell of *Methylocystis rosea* SV97 showing the type II intracytoplasmic membranes aligned with the periphery of the cell and inclusions (white spot). Bar, 200 nm.<sup>106</sup>

### 1.9.2 *Methylocapsa*

*Methylocapsa acidiphila* B2, *Methylocapsa aurea* KYG, *Methylocapsa palsarum* NE2, and *Methylocapsa gorgona* MG08 comprise, except the recently isolated *Methylocapsa polymorpha*<sup>114,115</sup>, all the so far isolated species of the genus *Methylocapsa* and they all form colonies when incubated with air as the only carbon and energy source. The genus belongs to the family *Beijerinckiaceae* within the *Alphaproteobacteria*. Methanotrophic members of the family *Beijerinckiaceae* are gram-negative, moderately acidophilic, and use the serine pathway for carbon assimilation<sup>19</sup>.

*Methylocapsa acidiphila* B2 is a non-motile, curved coccoid shaped strain. The cells are 0.5 – 0.8  $\mu\text{m}$  wide and 0.8 – 1.2  $\mu\text{m}$  long. It grows within a temperature range of 10 – 30  $^{\circ}\text{C}$  and a pH range of 4.2 – 7.2. It fixes  $\text{N}_2$ <sup>107</sup>, accumulates PHB, possesses a full pMMO and nitrogenase complex, an incomplete Hhy complex and completely lacks the functional complex for CO oxidation<sup>101</sup> (Fig. 4).

*Methylocapsa aurea* KYG was isolated from a soil sample collected from under a small ephemeral brook in a forest near Marburg, Germany. The cells are non-motile, slightly curved rods, 0.7 – 1.2  $\mu\text{m}$  wide and 1.8 – 3.1  $\mu\text{m}$  long (Fig. 6). *M. aurea* KYG can fix  $\text{N}_2$  under reduced

O<sub>2</sub> tension. It grows at temperatures ranging from 2 – 33 °C<sup>108</sup> and a pH of 5.2 and can accumulate PHB. Its genome encodes complete complexes for a pMMO, a nitrogenase, and a Hhy. The CODH complex is incomplete.

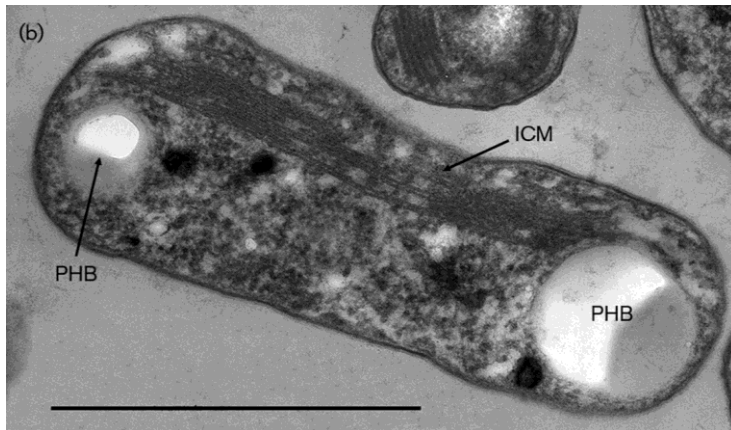


Figure 6. Electron micrograph of an ultrathin section of a methane-grown cell of strain KYG. ICM, Intracytoplasmic membrane; PHB, poly-β-hydroxybutyrate. Bar, 1 μm.<sup>108</sup>

*Methylocapsa palsarum* NE2 was isolated from a wet moss collected at a collapsed palsa site in northern Norway<sup>109</sup>. It is non-motile and forms slightly curved, 1.0 – 1.2 μm wide and 1.6 – 2.4 μm long rods (Fig. 7). It grows within a range of 6 to 32 °C and a pH range of 4.1 – 8.0. *M. palsarum* NE2 can fix N<sub>2</sub> under reduced O<sub>2</sub> tension. The strain encodes complete complexes of pMMO, and nitrogenase. The CODH complex is incomplete and it does not carry genes encoding for Hhy.

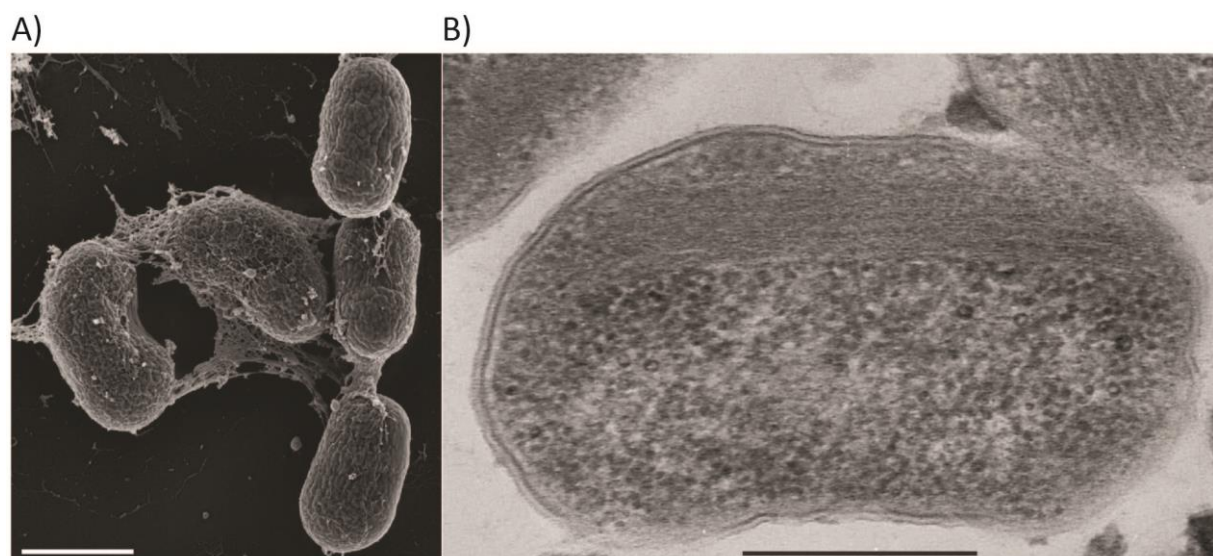


Figure 7. A) Scanning electron micrograph of *Methylocapsa palsarum* NE2 cells. B) Electron micrograph of an ultrathin section of *Methylocapsa palsarum* NE2 cells. Bars, A) 1 μm. B) 0.5 μm.<sup>109</sup>

*Methylocapsa gorgona* MG08 was isolated from cover soil sampled in a ditch at a retired subarctic landfill in northern Norway<sup>101</sup>. *M. gorgona* MG08 cells are non-motile, thick rods that are 0.6 – 0.8  $\mu\text{m}$  wide and 0.8 – 1.5  $\mu\text{m}$  long (Fig. 8). It grows within a range of 7 – 37 °C and a pH of 6 – 7.5. It can fix  $\text{N}_2$  and encodes complete complexes for pMMO, nitrogenase, Hhy, and CODH.

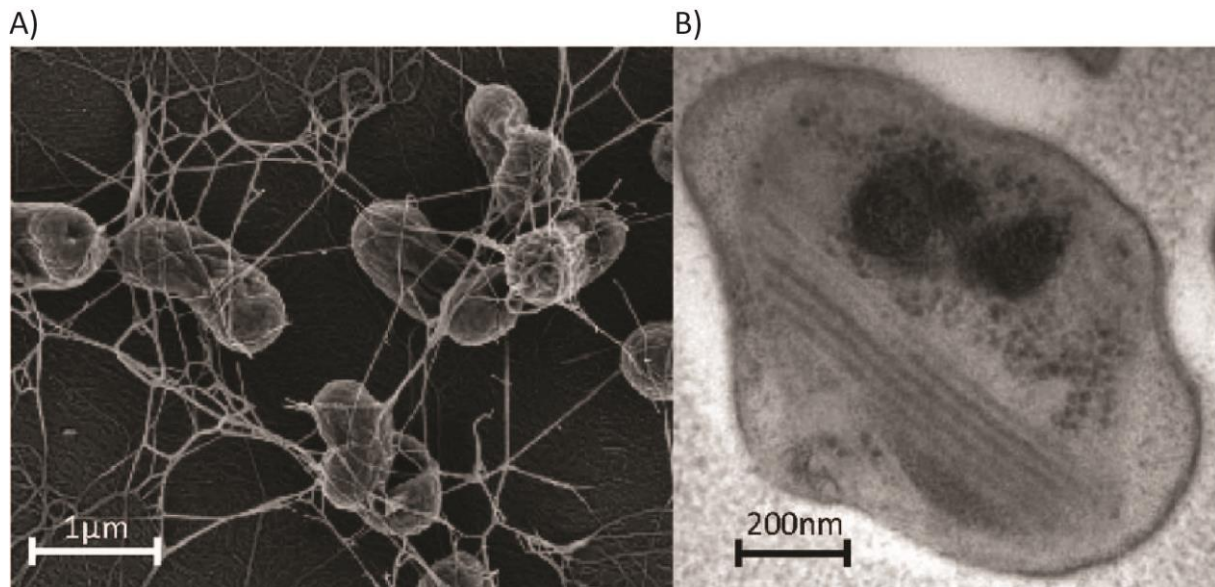


Figure 8. A) Scanning electron micrograph of *M. gorgona* MG08 cells. B) Transmission electron micrograph of a *M. gorgona* MG08 cell showing intracytoplasmic membranes and inclusions that resemble PHB granules.<sup>101</sup>

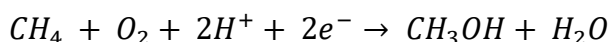
## 1.10 Aerobic methane oxidation

### 1.10.1 Activation of $\text{CH}_4$

Aerobic methanotrophs oxidize  $\text{CH}_4$  to  $\text{CO}_2$  using  $\text{O}_2$  as electron acceptor<sup>11</sup>. The first step of the oxidation is the activation and the conversion of  $\text{CH}_4$  to methanol by the methane monooxygenase (MMO). Two forms of MMOs are known. The soluble methane monooxygenase (sMMO) that occurs in the cytoplasm of methanotrophs and the particulate methane monooxygenase (pMMO) which is bound to intracellular membranes<sup>116</sup>. In contrast to the sMMO, the pMMO is found in almost all methanotrophs<sup>117</sup>. The sMMO, an enzyme consisting of a hydroxylase, a reductase, and a regulatory protein, employs a diiron cluster as catalytic site<sup>118</sup>. The pMMO, comprises the three subunits PmoA, PmoB, and PmoC that are organized in a trimer of PmoA, PmoB, and PmoC protomers, and requires copper for its activity<sup>119,120</sup>. As enzyme preparation techniques for structural analysis caused structural

changes and decreasing activity of the pMMO, the location and composition of its active site is still uncertain. Recent attempts to reconstitute the pMMO on nanodiscs to mimic the cellular environment of the pMMO restored its activity and revealed its structure in a lipid (membrane like) environment substantially revising the view of the pMMO<sup>120</sup>.

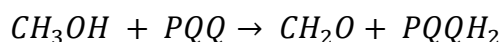
For the oxidation of CH<sub>4</sub> to methanol (CH<sub>3</sub>OH), the MMOs need CH<sub>4</sub>, O<sub>2</sub>, and a reductant (Fig. 9) to reduce the excess oxygen atom of O<sub>2</sub> to water:



NADH/H<sup>+</sup> acts as the reductant for the sMMO. In case of the pMMO, hydroquinone derivatives, NADH, methanol, succinate, and H<sub>2</sub> have been identified as electron donor *in vitro*<sup>121–123</sup>, but how the electrons are transferred to the catalytic center of the pMMO is still unclear.

### 1.10.2 Methanol oxidation

The next step during the oxidation of CH<sub>4</sub> to CO<sub>2</sub> is the oxidation of the intermediate methanol to formaldehyde (CH<sub>2</sub>O) (Fig. 9):



The reaction is catalyzed by a periplasmic, pyrroloquinoline quinone (PQQ) linked methanol dehydrogenase (MDH), a heterotetrameric enzyme consisting of two large and two small subunits<sup>124</sup>. The catalytic center can either contain a calcium (Ca<sup>2+</sup>) or a lanthanide (Ln<sup>3+</sup>) ion<sup>125,126</sup>. The MDH oxidizes methanol by reducing the prosthetic PQQ to the corresponding quinol and subsequently a two-step electron transfer to cytochrome c completes the oxidation. This oxidation step is accompanied by the generation of a proton gradient. The protons are retained in the cytoplasm while the electrons are transferred via cytochromes through a cytoplasmic membrane to a terminal oxidase. There, oxygen accepts the electrons and consumes protons from the cytoplasm. The electron transfer from MDH to oxygen is thought to operate several proton translocation segments<sup>117</sup>. Additionally, MDHs are known to oxidize methanol to formate (HCOO<sup>-</sup>), but with a considerably lower conversion rate and substrate affinity<sup>124</sup>.

### 1.10.3 Formaldehyde oxidation

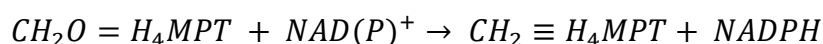
The formaldehyde that results from the oxidation of methanol is transported to the cytoplasm (Fig. 9). There, it can be utilized in two different ways as described by Trotsenko and Murrell<sup>117</sup>. Either it is oxidized via formate to CO<sub>2</sub>, or it can be assimilated via two different pathways, the Quayle ribulose monophosphate pathway (RuMP) or the serine cycle. As the methanotrophs, emphasized on in this work, apply the serine cycle for formaldehyde assimilation and tetrahydromethanopterin- (H<sub>4</sub>MPT) and tetrahydrofolate- (H<sub>4</sub>F) dependent routes for formaldehyde oxidation, only these pathways are described in the following. It is assumed that the H<sub>4</sub>MPT-dependent pathway is the major catabolic route for formaldehyde oxidation<sup>127</sup>, while the enzymes involved in the H<sub>4</sub>F-dependent route mainly seem to maintain a high level of intermediates to feed the assimilatory serine cycle<sup>128</sup>.

The first step of the H<sub>4</sub>MPT-dependent formaldehyde oxidation is the condensation of formaldehyde and H<sub>4</sub>MPT to methylene-H<sub>4</sub>MPT:



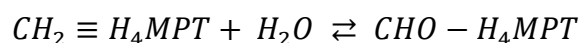
This condensation either occurs spontaneously or can be catalyzed by a methylene-H<sub>4</sub>MPT-specific formaldehyde-activating enzyme (Fae)<sup>128-130</sup>.

The second step is the oxidation of methylene-H<sub>4</sub>MPT to methenyl-H<sub>4</sub>MPT:

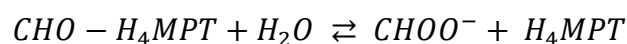


The methylene-H<sub>4</sub>MPT can be oxidized by the methylene-H<sub>4</sub>MPT dehydrogenase MtdA, that also catalyzes the reversible dehydrogenation of methylene-H<sub>4</sub>F, or the methylene-H<sub>4</sub>MPT-specific dehydrogenase MtdB<sup>131,132</sup>. The oxidation of methylene-H<sub>4</sub>MPT to methenyl-H<sub>4</sub>MPT by MtdA and MtdB is exergonic and thus, proceeds essentially irreversible. This plus the Fae activity supports an efficient and quantitative conversion of formaldehyde via the H<sub>4</sub>MPT-dependent route<sup>128</sup>.

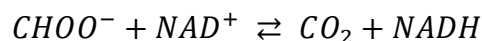
Next, the methenyl-H<sub>4</sub>MPT cyclohydrolase Mch hydrolyzes methenyl-H<sub>4</sub>MPT to formyl-H<sub>4</sub>MPT<sup>133</sup>:



Then, the formyltransferase/hydrolase complex Fhc converts formyl-H<sub>4</sub>MPT to formate (CHOO<sup>-</sup>)<sup>134</sup>.



Finally, the resulting formate is oxidized to CO<sub>2</sub>:

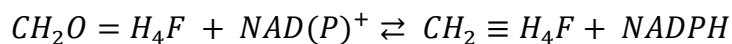


A NAD<sup>+</sup>-dependent formate dehydrogenase (Fdh) is involved in this last step of the CH<sub>4</sub> oxidation (Fig. 9). Fdhs have been considered to catalyze the oxidation of formate to CO<sub>2</sub> nearly irreversible<sup>135</sup>. However, it has been shown that certain Fdhs reduce CO<sub>2</sub> to formate as well<sup>136</sup>, and thus represent a potential entry point of CO<sub>2</sub> for carbon assimilation in non-phototrophic organisms.

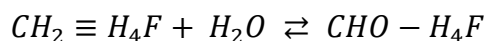
The H<sub>4</sub>F-dependent oxidation of formaldehyde to CO<sub>2</sub> (Fig. 9), that is thought to primarily feed the assimilatory serine cycle, operates in the oxidative or reductive direction depending on the requirements of the cell, as its reactions are fully reversible<sup>117,128,137</sup>. The condensation of the reactive formaldehyde and H<sub>4</sub>F proceeds spontaneously:



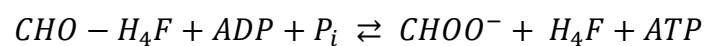
The methylene-H<sub>4</sub>F can either enter the glycine cleavage/synthesis (GCS) system that synthesizes glycine out of methylene-H<sub>4</sub>F, NADH, NH<sub>3</sub>, and CO<sub>2</sub><sup>138</sup>, the serine cycle for further assimilation, or it can be oxidized. The oxidation is catalyzed by a MtdA or a bifunctional methylene-H<sub>4</sub>F dehydrogenase/methylene-H<sub>4</sub>F cyclohydrolase (FolD) to methenyl-H<sub>4</sub>F:



During the next step of the oxidation, the resulting methenyl-H<sub>4</sub>F is hydrolyzed to formyl-H<sub>4</sub>F by a FolD or a methenyl-H<sub>4</sub>F cyclohydrolase (Fch):



The formyl- $H_4F$  is then oxidized to formate by a formate-tetrahydrofolate ligase (Fhs). The reaction is coupled to the formation of adenosine triphosphate (ATP)<sup>139</sup>:



In general, the dehydrogenases that take part in the oxidation from  $CH_4$  to  $CO_2$  are coupled to the energy conservation, while the oxidases are usually not energy conserving<sup>140</sup>. In total,  $CH_4$  oxidation yields six electrons usable for aerobic respiration, carbon fixation, or the activation of  $CH_4$ <sup>119</sup>.

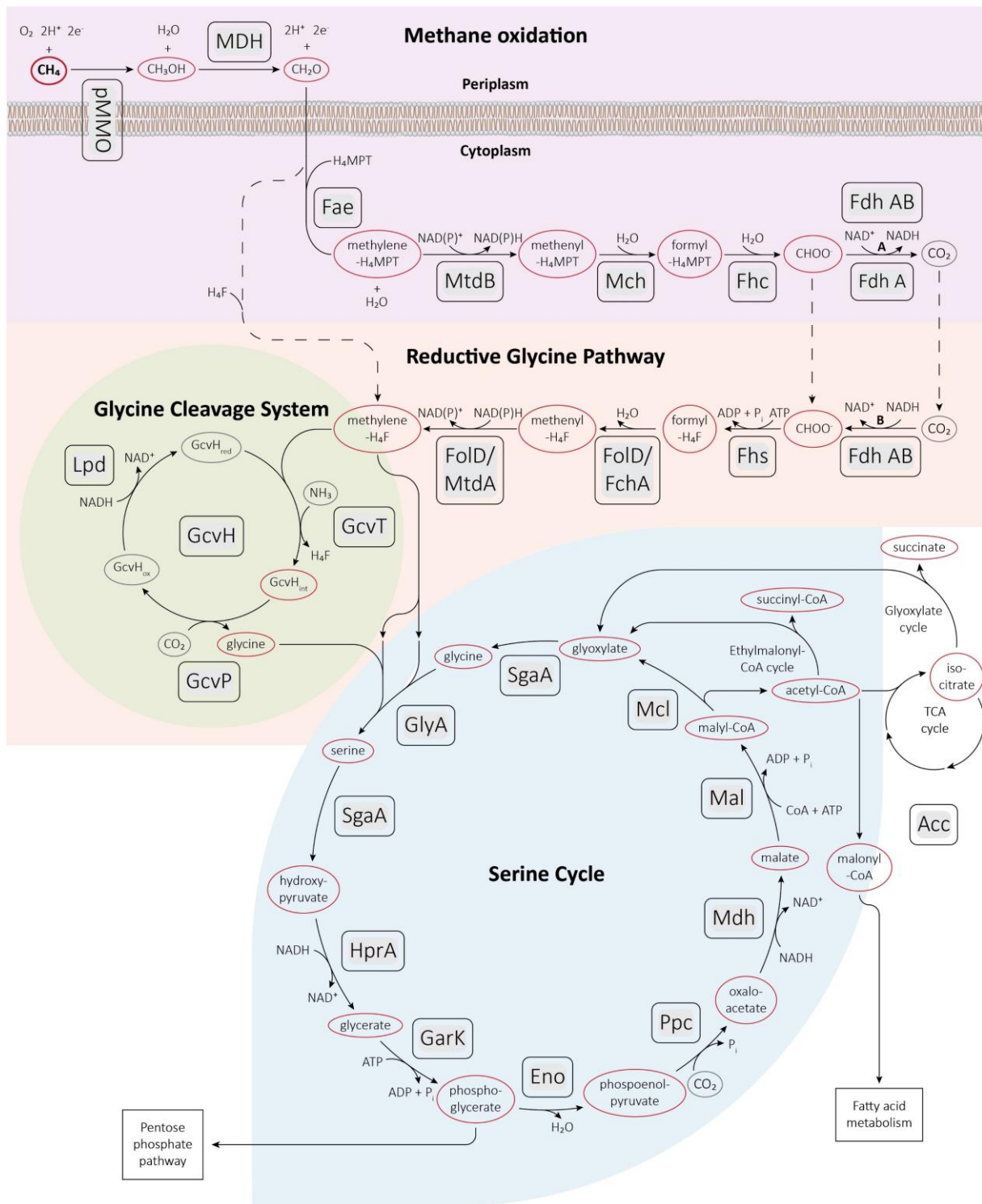


Figure 9. pMMO – particulate methane monooxygenase, MDH – methanol dehydrogenase (Mox) and putative lanthanide-dependent methanol dehydrogenase (XoxF), Hhy – [NiFe] group 1h hydrogenase, CODH – [MuCO] class I carbon monoxide dehydrogenase, Fae – formaldehyde activating enzyme, MtdB – NAD(P)-dependent methylene-tetrahydromethanopterin dehydrogenase, Mch – methenyl-tetrahydromethanopterin cyclohydrolase, Fhc – formyltransferase/hydrolase, Fdh A – NAD-dependent formate-dehydrogenase, Fdh AB – molybdopterin binding reversible formate dehydrogenase/ $\text{CO}_2$  reductase, Fhs – formate-tetrahydrofolate ligase, FolD – bifunctional 5,10-methylene-tetrahydrofolate dehydrogenase/ 5,10-methenyl-tetrahydrofolate cyclohydrolase, FchA – methenyltetrahydrofolate cyclohydrolase, MtdA – NADP-dependent methylenetetrahydrofolate dehydrogenase, GcvH – glycine cleavage system H protein, GcvT – aminomethyltransferase, GcvP - glycine dehydrogenase, Lpd

– dihydrolipoyl dehydrogenase, GlyA – serine hydroxymethyltransferase, SgaA – Serine-glyoxylate aminotransferase, HprA – glycerate dehydrogenase, GarK – 2-glycerate kinase, Eno – enolase, Ppc – phosphoenolpyruvate carboxylase, Mdh – malate dehydrogenase, Mal – malate-CoA ligase, Mcl – L-malyl-CoA lyase, Acc – Acetyl-CoA carboxylase, NAD<sup>+</sup> – nicotinamide adenine dinucleotide, NADP<sup>+</sup> – nicotinamide adenine dinucleotide phosphate, ATP – adenosine triphosphate.

#### 1.10.4 Assimilation of carbon via the glycine cleavage system and the serine cycle

As mentioned above, the formaldehyde that results from the oxidation of CH<sub>4</sub> and methanol can spontaneously condense with H<sub>4</sub>F to methylene-H<sub>4</sub>F and then enter the glycine cleavage system (GCS) or the serine cycle (Fig. 9). Alternatively, the formaldehyde is oxidized via the H<sub>4</sub>MPT-mediated route to formate. The formate is then reduced via the H<sub>4</sub>F-mediated route to methylene-H<sub>4</sub>F before entering the GCS or the serine cycle. Studies involving *Methylobacterium extorquens* AM1 have demonstrated that mutants defective in any of the three enzymes involved in the H<sub>4</sub>F mediated formaldehyde oxidation could not grow on methanol implying that this pathway plays an important role in carbon assimilation<sup>139,141</sup>. Later, it was shown that the reductive pathway via formate to methylene-H<sub>4</sub>F and not the spontaneous condensation of formaldehyde and H<sub>4</sub>F represents the major assimilatory flux<sup>142</sup>. Another possibility to assimilate carbon is the reduction of CO<sub>2</sub> to formate by a reversible Fdh and the further reduction to methylene-H<sub>4</sub>F<sup>143</sup>.

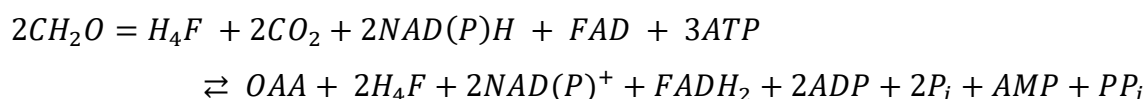
The GCS consists of four loosely associated enzymes and converts the methylene-H<sub>4</sub>F, NH<sub>3</sub>, CO<sub>2</sub>, and NADH, to glycine, H<sub>4</sub>F and NAD<sup>+</sup>:



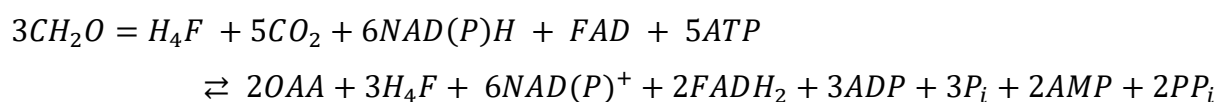
The conversion of formate and CO<sub>2</sub> to the C<sub>2</sub>-amino acid glycine is referred to as the core module of the reductive glycine pathway<sup>144</sup> (Fig. 9).

Next in carbon assimilation is the serine cycle (Fig. 9). As summarized by Anthony<sup>145,146</sup>, the serine cycle differs from other formaldehyde assimilation pathways as its intermediates are carboxylic acids and amino acids instead of carbohydrates. It drives the conversion of the C<sub>1</sub> compound formaldehyde to C<sub>3</sub> and C<sub>4</sub> intermediates and thereby provides precursors for further biosynthesis. Two molecules of formaldehyde and two of glycine result in two molecules of phosphoglycerate. One phosphoglycerate is assimilated while the other is carboxylated to phosphoenolpyruvate and further converted via oxaloacetate to malyl-CoA. The malyl-CoA is

cleaved to glyoxylate and acetyl-CoA. The glyoxylate is converted to glycine, while there are two different variants of the serine cycle to oxidize the acetyl-CoA to glyoxylate<sup>145,146</sup>. One variant involves the glyoxylate cycle (encoded by the *Methylocapsa* strains) to oxidize acetyl-CoA to glyoxylate, the other variant involves the ethylmalonyl-CoA cycle for the oxidation (encoded by the *Methylocystis rosea* SV97). The energy and carbon balances of both variants normalized to the production of oxaloacetate (OAA)<sup>146</sup> are:



for the glyoxylate cycle based serine cycle, and:



for the ethylmalonyl-CoA cycle.

## 1.11 Oxidation of atmospheric hydrogen and carbon monoxide

Besides CH<sub>4</sub>, the most abundant atmospheric trace gases that represent potential energy sources for microorganisms are H<sub>2</sub> and CO with average atmospheric concentrations of 530, and 90 ppb<sup>81,119</sup>, respectively. As reviewed by Greening and Grinter<sup>93</sup>, hydrogenotrophic and carboxydrotrophic microorganisms, that oxidize atmospheric concentrations of H<sub>2</sub> and CO, respectively, are assumed to grow heterotrophically while they oxidize H<sub>2</sub> and CO to cover their cellular maintenance energy to persist periods of starvation enabling long-term survival<sup>147-149</sup>. To do so, these microorganisms have evolved enzymes with high affinities that are reflected in K<sub>m(app)</sub> values smaller than 150 nM for the respective gases<sup>119</sup>. The high affinity oxidation of H<sub>2</sub> and CO is attributed to [NiFe] hydrogenases within different and distantly related groups, named Hhy, Huc, Hyo, and Hyl and molybdenum-dependent carbon monoxide dehydrogenases (CODH), respectively<sup>119</sup>. Both enzymes are metalloenzymes consisting of multiple subunits. All known high affinity hydrogenases comprise two subunits, a small and a large one. In Hhy, the hydrogenase encoded in some of the six investigated methanotrophic strains, the two subunits are arranged in a protomer. Two of these protomers dimerize to the final hydrogenase<sup>150</sup>. The high affinity CODH consist of three subunits, a small, a medium, and a

large subunit organized in a trimer. Two trimers dimerize to form the enzyme<sup>119,150,151</sup>. Both of high affinity enzymes seem to be anchored at the cytoplasmic side of the inner membrane<sup>152–154</sup>. Until recently, the measurements describing the high affinity oxidation of H<sub>2</sub> and CO were solely based on whole cell kinetics. However, in 2023, a Huc hydrogenase (K<sub>m</sub> = 129 nM) was successfully isolated, and its kinetics characterized<sup>155</sup>. The electrons from the oxidation of H<sub>2</sub> are thought or, in case of the isolated hydrogenase, shown to be directly transferred into the respiratory chain<sup>119,155</sup>:



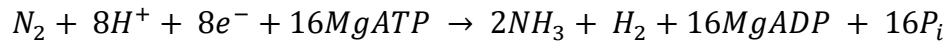
The same applies to the electrons from the oxidation of CO with H<sub>2</sub>O to CO<sub>2</sub>:



## 1.12 N<sub>2</sub>-fixation by methanotrophs

The ability of MOB to fix N<sub>2</sub> has been confirmed for representatives within *Alpha*- and *Gammaproteobacteria*, and *Verrucomicrobiota*<sup>156,157</sup>. Complete structural genes (*nifHDK*) for the molybdenum-dependent isozyme of the nitrogenase, the enzyme that catalyzes the biological reduction of N<sub>2</sub> to ammonia (NH<sub>3</sub>), have been found in 98% of the methanotrophs within the *Alphaproteobacteria* and in 89% within the *Gammaproteobacteria*, suggesting that MOB play an important role in N<sub>2</sub>-fixation<sup>158–160</sup>. As methanotrophs require approximately 0.25 mole nitrogen per mole carbon assimilated, their nitrogen requirements are relatively high<sup>69,145</sup>. Thus, the ability to fix N<sub>2</sub> seems to be a necessity to prevent cellular nitrogen limitations in oligotrophic environments. To fix N<sub>2</sub>, MOB need to overcome two major obstacles, the irreversible inactivation of the nitrogenase by oxygen and the high energy requirements of the fixation of N<sub>2</sub><sup>161</sup>. Especially during the oxidation of atmospheric CH<sub>4</sub> by atmMOB, these obstacles seem to be problematic as atmMOB are exposed to high O<sub>2</sub> tensions while facing an apparent energy limitation. In free-living diazotrophs (N<sub>2</sub>-fixing microorganisms), heterocysts, aggregation of individual bacteria, and a high respiratory activity can create a nearly anoxic environment to protect the nitrogenase from inactivation by O<sub>2</sub><sup>162–164</sup>. Besides, a conformational protection, during which the nitrogenase forms a reversible state that is oxygen-tolerant but inactive, enables survival of nitrogenases during oxygen stress<sup>165</sup>. The high energy

requirements to break the N-N triple bond of N<sub>2</sub> that represents one of the strongest bonds in nature and the further reduction to ammonia is reflected by the optimal stoichiometry of the reaction<sup>160,166,167</sup>:



All six strains investigated within this thesis encode a molybdenum-iron nitrogenase (Nif)<sup>101,168</sup>. This nitrogenase is a two component metalloprotein that consists of an iron (Fe) and a molybdenum iron (MoFe) protein. The Fe protein is a homodimeric ATPase and the obligate reductase of the nitrogenase that couples ATP hydrolysis to the electron transfer to the MoFe protein<sup>160,166</sup>. The MoFe protein is a  $\alpha_2\beta_2$  tetramer with two metalloclusters and a MoFe cofactor being the active site where N<sub>2</sub> is bound and reduced<sup>166</sup>. During N<sub>2</sub> fixation the MoFe protein undergoes various reduced states that are required to bind and reduce N<sub>2</sub>. The binding of N<sub>2</sub> and the reduction of the triple bond follows a reductive elimination reaction that is associated with the evolution of H<sub>2</sub><sup>169</sup>.

## 2 Material and Methods

### 2.1 Filter cultivation

Key to grow atmMOB with air as sole carbon and energy source (hereafter referred to as growth “on air”) was the cultivation of cells on polycarbonate filters that float on a defined, carbon-free medium (hereafter “filter cultivation”) (Fig. 10, 11, 12.1). This method is based on filter cultivation techniques that were originally invented to isolate “uncultivable” microorganisms by simulating natural environments<sup>170,171</sup>. A major advantage of filter cultivation over conventional cultivation techniques using liquid media is the superior mass transfer of gases to the cells, as the cells are only surrounded by a thin boundary layer of medium (Fig. 10). This enables diffusion of atmospheric trace gases to the cells quick enough to support growth, while media is supplied. Further, the cells that are immobilized on the supporting filter cannot escaped detection. Thus, growth of cells leading to colony formation can be observed using microscopy (Fig. 10).

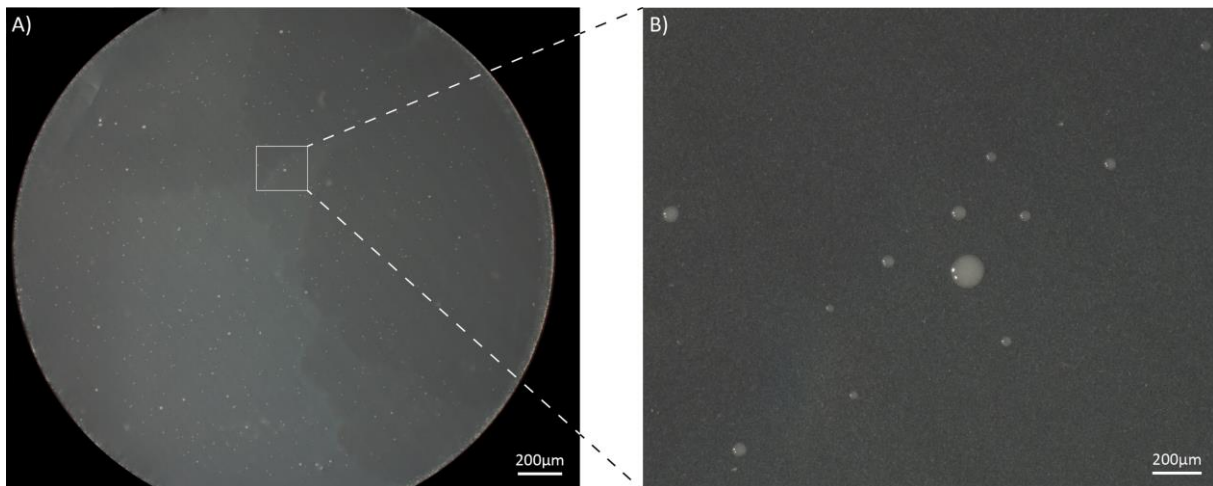


Figure 10. A) Light microscopic image of a *Methylocapsa gorgona* MG08 culture on a polycarbonate filter after a 12-month incubation period on a carbon- and nitrogen-free growth medium. B) Magnified image section of the filter colony shown in A). Single colonies of cells coated by thin boundary layer.

To create filter cultures, the methanotrophic strains were cultivated in a serum bottle using liquid medium and high CH<sub>4</sub> concentrations and used as inoculum (Fig. 12.1). A fraction of this inoculum was filtered on polycarbonate filter supported by a glass fiber filter using a filtration manifold (Fig. 12.1) and applying vacuum. During this step, the inoculum was rinsed in the manifold cylinder with a suitable washing solution (e.g., growth medium). After the filtration, the thinly populated filter (Fig. 12.1) was moved on growth medium in a petri dish. The petri

dish enabled aeration and by that constant substrate supply while keeping the filter culture sterile. Because of the slow growth of atmMOB on air, filter cultures needed to be incubated for several months to form colonies big enough to confirm growth and to accumulate sufficient biomass for further experiments (Fig. 12).

## **2.2 Oxidation of atmospheric trace gases and energy yield estimation**

The oxidation of atmospheric  $\text{CH}_4$ ,  $\text{H}_2$ , and  $\text{CO}$  and the estimation of the energy yield from the oxidation of these gases were assessed by conducting oxidation experiments. Therefore, filter cultures were moved to glass bottles containing a defined volume of growth medium. The bottles were sealed airtight with suitable caps (Fig. 12.2). By purging the headspace of the glass bottles with synthetic air containing 400 ppm  $\text{CO}_2$  and adding  $\text{CH}_4$ ,  $\text{H}_2$ , and  $\text{CO}$  manually using a gas syringe, a defined headspace was created (Fig. 12.2). To assess the oxidation rates, the filter cultures were incubated at a constant temperature and the change of the  $\text{CH}_4$ ,  $\text{H}_2$ , and  $\text{CO}$  in the headspace over time was measured via gas chromatography. For each measurement, the gas from the headspace was sampled using a gas tight syringe. In addition, the pressure in the headspace was measured using a manometer. By knowing the gas volume and the gas pressure in the bottle headspace, the temperature during incubation, and the relative concentration of the respective gas species, the mass of each trace gas at the different sampling timepoints was calculated via the ideal gas law. As the low trace gas concentrations were rate-limiting (reflected by an oxidation rate proportional to the concentration of the trace gas), pseudo first order kinetics for the oxidation of atmospheric  $\text{CH}_4$ ,  $\text{H}_2$ , and  $\text{CO}$  were assumed. By knowing the change in mass of the gases over time, the reaction rate constant could be calculated using the integrated rate law for first order reactions. By knowing the reaction rate constant, the oxidation rates of the respective gases by the filter cultures at atmospheric concentrations could be calculated. To determine the oxidation rates per cell, the number of cells within the filter cultures was quantified (see section 2.2.1). Under consideration of the Gibbs free energy changes for the oxidation of the respective gases at atmospheric concentrations and the cellular oxidation rates, the energy yield per cell was calculated. To compare the energy yield from substrate consumption and thus the energy sufficient for maintenance and growth of different microbial species, the energy yield per cell was normalized to dry mass carbon and hour (kJ C-

$\text{mol}^{-1} \text{h}^{-1}$ ). This was achieved by considering the carbon content (see section 2.2.2), the cellular dry weight, and the cellular energy yield during trace gas oxidation of the respective species.

### 2.2.1 Quantification of cells in filter cultures

The quantification of the cell numbers in filter cultures is challenging due to the formation of multilayered colonies during growth (Fig. 11). This prevents direct quantification of cell numbers on the filter via microscopy. As consequence, two different approaches were employed to quantify cell numbers of filter cultures for the publications included in this thesis.

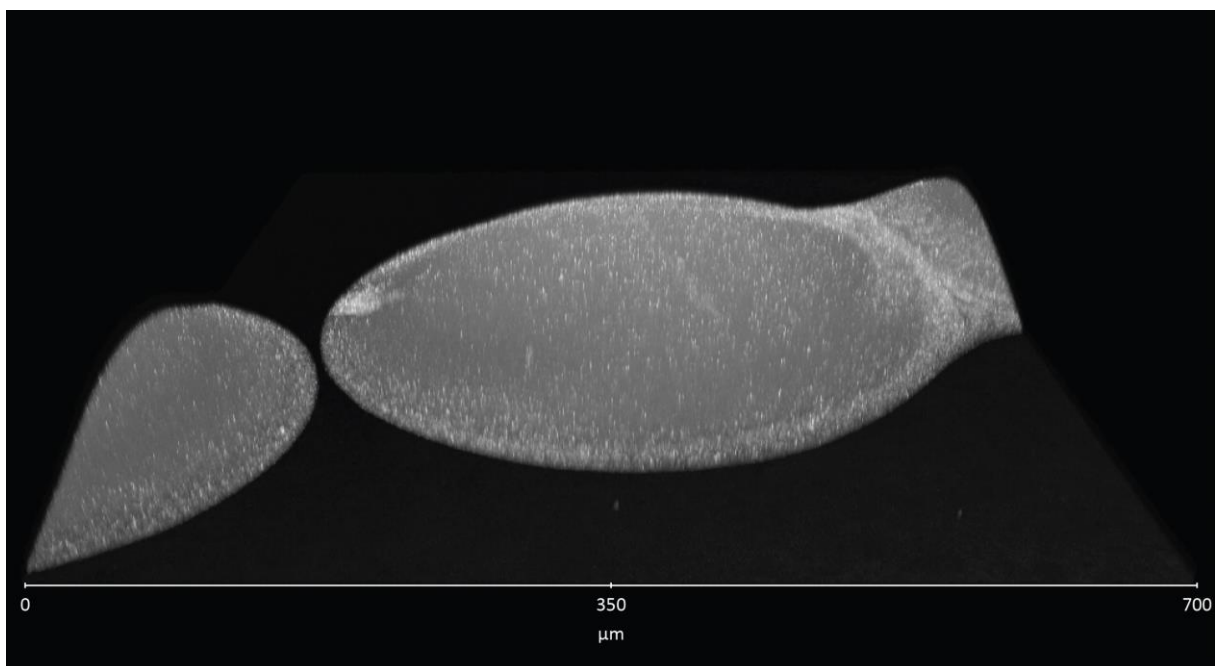


Figure 11. Stacked confocal images of SYBR green II stained *Methylocapsa palsarum* NE2 cells in colonies after long-term incubation on air.

For paper 1, the cell numbers were determined by comparing the DNA mass of filter cultures to the DNA masses of known cell numbers from liquid cultures of the same species. For paper 2, cells on the filters were stained using a fluorescent nucleic acid stain, washed from the filters, and collected in tubes. The collected and stained cells were counted using flow cytometry (Fig. 12.2).

### **2.2.2 Cellular dry mass estimation and carbon content**

As for the cell quantification, the cellular dry mass of the methanotrophic strains was determined differently for both papers. For paper 1, the cell concentration of a liquid culture was determined via microscopy. A defined amount of this liquid culture with known cell concentration was pelleted in a tube via centrifugation and the supernatant discarded. The resulting pellet was dried in an oven and weighed. The cellular dry weight was calculated by dividing the weight of the dry pellet by the number of cells pelleted. For paper 2, the cellular dry weight was determined by measuring single-cell buoyant mass distributions of cells from filter cultures in H<sub>2</sub>O-based and deuterium oxide (D<sub>2</sub>O)-based solutions of phosphate saline buffer (PBS) using a suspended microchannel resonator (SMR)<sup>172-174</sup>. The SMR is basically a “balance” that consist of a vibrating microcantilever with an internal microfluidic channel. The SMR oscillates at a frequency proportional to its mass. When a cell, that is transported by a solution of known density, passes through the channel, the resonance frequency of the cantilever changes by an amount proportional to the cells buoyant mass<sup>173</sup>. To determine the cellular dry mass, buoyant mass measurements in two fluids of differing densities (H<sub>2</sub>O-based and D<sub>2</sub>O-based solutions of PBS) were required<sup>174</sup>.

To determine the cellular carbon content, the methanotrophic strains were grown in stirred-tank bioreactors to receive sufficient biomass. The harvested biomass was washed to remove the growth medium and lyophilized. The cellular carbon content of the methanotrophic strains was determined using an elemental analyzer coupled to an isotope ratio mass-spectrometer.

### **2.3 N<sub>2</sub> fixation by atmMOB**

To evaluate if the methanotrophic strains can fix N<sub>2</sub> during growth on air, filter cultures were incubated with air as sole carbon, energy, and nitrogen source. After accumulation of sufficient biomass, the filter cultures were incubated in sealed bottles with air and trace concentration of CH<sub>4</sub>, H<sub>2</sub>, and CO as mentioned (see section 2.2). Additionally, a known amount of <sup>15</sup>N<sub>2</sub> was added to the bottle headspace. The rationale is that growing cells capable of fixing N<sub>2</sub>, enrich <sup>15</sup>N isotopes in their biomass. These enriched <sup>15</sup>N isotopes can be detected using mass spectrometry. As growth on air by atmMOB is very slow, long incubation times for cellular <sup>15</sup>N enrichment were needed. Therefore, filter cultures of atmMOB were kept under a <sup>15</sup>N<sub>2</sub>

headspace for two months. After, cells were harvested by washing from filters and lyophilized. The relative  $^{15}\text{N}$  to  $^{14}\text{N}$  ratio of the cellular biomass was detected using Nanoscale secondary ion mass spectrometry (NanoSIMS) (Fig. 12.3). During NanoSIMS an primary cesium ion beam erodes the surface of a sample releasing atoms and molecular fragments. A fraction of these secondary particles is ionized. The secondary ions are characteristics of the sample region eroded and can be manipulated with ion optics. Therefore, the secondary ions can be directed to a mass spectrometer where the ions are measured<sup>175</sup>. Based on that, a quantitative atomic mass image of the analyzed sample region can be created. The NanoSIMS couples microscopy and isotopic analysis at high mass resolution and spatial resolution down to 50nm<sup>176</sup>. This enabled the detection of low  $^{15}\text{N}$  enrichments in single atmMOB cells while only little biomass was required for analysis.

## **2.4 AtmMOB adjustments to growth on air**

To assess the metabolic adjustments of atmMOB during growth on air, comparative proteomics experiments were performed. As proteins carry out a majority of cellular functions and are closely related to the phenotype of cells, comparative proteomics is a universal approach to unravel the differences between two cellular states with respect to the molecular mechanisms involved in various processes<sup>177</sup>. During these experiments, the proteome of an atmMOB strain incubated at elevated  $\text{CH}_4$  concentrations was compared to the proteome of the same strain at atmospheric  $\text{CH}_4$  concentrations (Fig. 12.4). The comparison of these two physiological states enabled to investigate the allocation of cellular investments into biological processes relevant for growth on air and thus, to some extent, how the atmMOB species manage to grow on air. Filter cultures grown with air as sole carbon and energy source grow very slowly and accumulate only little amounts of biomass. Thus, to minimize loss of biomass, the filter cultures were washed from the filter, collected (Fig. 12.2), and concentrated by lyophilization. For the identification and the relative quantification of proteins, proteins were extracted from the biomass and then digested to peptides using the enzyme trypsin. The resulting peptides were separated via liquid chromatography and analyzed using tandem mass spectrometry. The resulting peptide spectra were compared to a strain specific protein library. If a peptide spectrum matched the spectrum of a specific amino acid sequence predicted from the protein library, the match was counted as peptide spectrum match and the peptide was assigned to the

matching protein. Based on this approach for identification and quantification, the protein abundances of the two different treatments could be compared enabling the identification of major protein allocation, and thus metabolic adjustments, during growth on air.

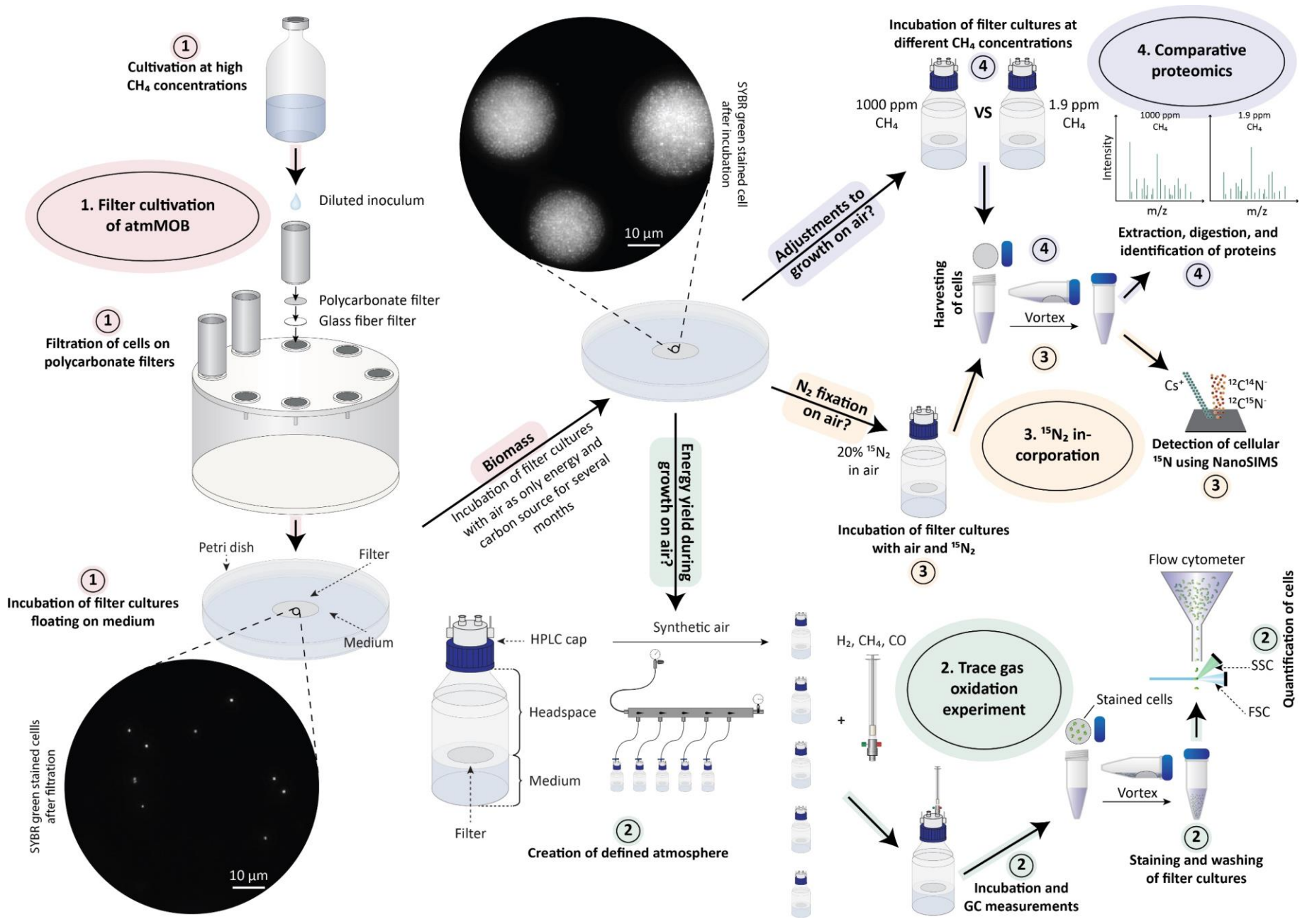


Figure 12. Simplified overview of the most important methods and workflows used and established during the PhD to answer the research questions investigated. ① Basic cultivation steps to create filter cultures with sufficient biomass for further analysis. ② Simplified steps performed for the estimation of energy yields from the oxidation of the three trace gases CH<sub>4</sub>, CO, and H<sub>2</sub> in air. ③ Simplified steps performed to test N<sub>2</sub> fixation of atmMOB exposed to air. ④ Simplified steps performed to determine the adjustments by atmMOB to growth on air via comparative proteomics.

## 2.5 Global distribution of atmMOB

To outline their global distribution, the environments atmMOB are found in, and eventually to gain a first impression of the ecological relevance of atmMOB, the publicly available 16S rRNA gene fragment collection of the Earth Microbiome Project (EMP) was screened for the atmMOB species investigated in this thesis as previously described<sup>94</sup>. The EMP is a large-scale collaborative project employing standardized collection, curation, and analysis of environmental samples<sup>178–180</sup>. Sample processing, sequencing, and core amplicon data analysis were performed by the EMP ([www.earthmicrobiome.org](http://www.earthmicrobiome.org)), and all amplicon sequence data and metadata have been made public through the EMP data portal ([qiita.microbio.me/emp](http://qiita.microbio.me/emp)). To obtain putative atmMOB 16S rRNA gene fragments, all EMP 16S rRNA gene fragments with >98.5% sequence identity to the 16S rRNA genes of *M. gorgona*, *M. aurea*, *M. palsarum*, and *M. rosea* were selected via BLASTN search<sup>181</sup>. In total, all the 23, 813 EMP samples from the three EMP datasets (`emp_deblur_90bp.qc_filtered.biom`, `emp_deblur_100bp.qc_filtered`, `emp_deblur_150bp.qc_filtered.biom`) that include sample location coordinates, representing 1294 unique geographic locations, were screened for the presence and abundance of the four atmMOB. R<sup>182</sup> (version 4.1.3) was used to analyze the environmental distribution and relative abundances of *M. gorgona*, *M. aurea*, *M. palsarum*, and *M. rosea* like 16S rRNA gene fragments and to graphically display the results (Rstudio version 2022.02.2+485). This was done using the R packages tidyverse version 1.3.1 (<https://cran.r-project.org/web/packages/tidyverse/>), maps version 3.4.0 (<https://cran.r-project.org/web/packages/maps/>), and mapdata version 2.3.0 (<https://cran.r-project.org/web/packages/mapdata/>).

## 3 Results

### 3.1 Paper 1: Simultaneous Oxidation of Atmospheric Methane, Carbon Monoxide, and Hydrogen for Bacterial Growth

This study builds upon the previously reported findings that *M. gorgona* MG08, the first member of the USCα in pure culture, can grow on air by oxidizing atmospheric CH<sub>4</sub> concentrations. In addition to a pMMO, *M. gorgona* MG08 encodes a [NiFe] group 1 high affinity respiratory hydrogenase (Hhy) and a [MoCu] class I respiratory carbon monoxide dehydrogenase<sup>101</sup>. Based on this, the capability of *M. gorgona* MG08 filter cultures to oxidize the trace gases H<sub>2</sub> and CO at their atmospheric concentrations, in addition to atmospheric CH<sub>4</sub>, was tested. The major finding of the study was the simultaneous oxidation of atmospheric CH<sub>4</sub>, H<sub>2</sub>, and CO to sub-atmospheric concentrations by *M. gorgona* MG08 during growth on air. This demonstrated that a mixotrophic lifestyle, based on the three most abundant trace gases in the atmosphere that represent energy sources, enables *M. gorgona* MG08 to grow on air. Furthermore, it was shown that the oxidation of atmospheric CH<sub>4</sub> does not depend on the oxidation of H<sub>2</sub> and CO, while the oxidation of H<sub>2</sub> and CO proceed without the presence of CH<sub>4</sub>. Based on the trace gas oxidation rates measured for *M. gorgona* MG08, the study reports the first energy yield estimates for an atmMOB pure culture during growth on air, namely 0.38 kJ C-mol<sup>-1</sup> h<sup>-1</sup>. This value, that represents an estimate for growth, is approximately 7.5 times lower than the basic premise assumed necessary for cellular maintenance stated in literature (2.8 kJ C-mol<sup>-1</sup> h<sup>-1</sup> at 20°C)<sup>80</sup>. However, the butyl rubber stoppers, used to seal the incubation bottles, emitted trace amounts of CO, and caused minor trace gases diffusion during the oxidation experiments. This might have impacted the accuracy of the estimations. Nevertheless, based on the study's findings, it was concluded that a metabolic flexibility enabling the mixotrophic oxidation of atmospheric CH<sub>4</sub>, H<sub>2</sub>, and CO and low energy requirements allow *M. gorgona* MG08 to grow on air.

### 3.2 Paper 2: Physiological Basis for Atmospheric Methane Oxidation and Methanotrophic Growth on Air

This study is based on two major questions that have remained partially unanswered since the discovery of atmospheric CH<sub>4</sub> oxidation by methanotrophs: Which methanotrophs are responsible for the oxidation of atmospheric CH<sub>4</sub>? How can these organisms survive and grow despite the apparent energetic limitations inherent to the oxidation of the low atmospheric CH<sub>4</sub> concentrations? Besides the oxidation of atmospheric CH<sub>4</sub> by methanotrophs assigned to the proteobacterial USC $\alpha$  and USC $\gamma$ , the presence of “conventional” methanotrophs in soils being net sinks for atmospheric CH<sub>4</sub> indicated that members of the genera *Methylocapsa*, *Methylosinus*, and *Methylocystis* might also contribute to atmospheric CH<sub>4</sub> oxidation. Therefore, the alphaproteobacterial, methanotrophic strains *Methylocystis rosea* SV97, *Methylosinus trichosporium* OB3b, *Methylocapsa acidiphila* B2, *Methylocapsa aurea* KYG, *Methylocapsa palsarum* NE2, in addition to *M. gorgona* MG08, and the gammaproteobacterial, methanotrophic strains *Methylobacter tundripaludum* SV96 were screened for their ability to grow with air as sole energy and carbon source. Further, by estimating the energy yield of atmMOB during growth on air via oxidation experiments, using comparative proteomics to investigate proteome allocations, and determining the  $a_A^0$  for CH<sub>4</sub> during growth on air, the physiological basis of atmMOB was outlined. As the effect of nitrogen limitation on atmMOB has never been investigated, the ability of atmMOB to grow on nitrogen sources available in air was evaluated.

#### 3.2.1 Colony formation, trace gas oxidation, and cellular energy yield during growth on air

Filter cultures of *M. rosea* SV97, *M. trichosporium* OB3b, *M. acidiphila* B2, *M. aurea* KYG, *M. palsarum* NE2, and *M. gorgona* MG08 formed colonies during incubation with air as sole energy and carbon source, while no colonies were formed by *M. tundripaludum* SV96 (thus, *M. tundripaludum* was not further investigated). Additionally, filter cultures of *M. gorgona* MG08 exposed to synthetic air without trace gases did not form colonies. During trace gas oxidation experiments, filter cultures of *M. rosea* SV97, *M. aurea* KYG, *M. palsarum* NE2, and *M. gorgona* MG08, incubated on air for six- and 12-months, enduringly oxidized atmospheric concentration of CH<sub>4</sub>, H<sub>2</sub> and/or CO with strain specific oxidation patterns, while

filter cultures of *M. trichosporium* OB3b and *M. acidiphila* B2 were inactive. The absence of colony formation by *M. gorgona* MG08 in synthetic, trace gas free air and the enduring trace gas oxidation by *M. rosea* SV97, *M. aurea* KYG, *M. palsarum* NE2, and *M. gorgona* MG08 confirmed that these strains can live and grow with air as the sole energy and carbon source. Furthermore, the oxidation experiments revealed mixotrophy by all four strains, showed substantial metabolic differences between the strains, and demonstrated that the enduring oxidation of atmospheric CH<sub>4</sub> is not restricted to members of the USC $\alpha$  and USC $\gamma$ .

The energy yield estimates from the oxidation of trace gases in air ranged from 0.38 to 0.71 kJ C-mol<sup>-1</sup> h<sup>-1</sup>, values 3.9 – 7.4 times lower than the reported average energy requirements for cellular maintenance in aerobic bacteria (2.8 kJ C-mol<sup>-1</sup> h<sup>-1</sup> at 20°C). This contradicted and revised the basic maintenance energy premise for atmMOB.

### 3.2.2 Comparative proteomics

To investigate the metabolic adjustments of *M. gorgona* MG08, *M. rosea* SV97, and *M. palsarum* NE2 during growth on air, the proteome allocation by filter cultures of the respective strains exposed to atmospheric CH<sub>4</sub> were compared to the proteome allocation to filter cultures exposed to 1000 ppm CH<sub>4</sub>. This revealed major proteome shifts related to their core metabolism including transcription, translation, growth, energy metabolism, and amino acid and carbohydrate transport as adjustments during growth on air. In depth analysis of the abundance of proteins involved in trace gas oxidation demonstrated distinct metabolic strategies to oxidize trace gases. While *M. palsarum* NE2 allocated protein investments to CH<sub>4</sub> oxidation, *M. gorgona* MG08 and *M. rosea* SV97 increased investments in H<sub>2</sub> and CO oxidation during growth on air. This implied that the strains allocated resources to increase their  $\alpha_A^0$  for the respective trace gases as adjustments to grow on air as well as niche differentiation. Additionally, investments into carbon assimilation via the serine cycle and into the electron transport chain were decreased by all three strains during growth on air compared to the 1000 ppm CH<sub>4</sub> treatment. Overall, the three strains increased the expression of enzymes for the oxidation of at least one trace gas to maximize uptake rates and energy yield during growth on air, while investments in energy conservation and energy-intensive carbon assimilation were decreased.

### 3.2.3 Specific affinity

To test if atmMOB have a high specific affinity ( $a_A^0$ ) for CH<sub>4</sub> (expressed by the fraction  $V_{\max(\text{app})}$  and  $K_{m(\text{app})}$ ) and thus the capacity to efficiently oxidize CH<sub>4</sub> at low concentrations, the  $a_A^0$  of *M. palsarum* NE2 and *M. gorgona* MG08 when grown on air were measured. Additionally, it was tested if the increased investments in pMMO by *M. palsarum* NE2 and the decreased investments by *M. gorgona* MG08 at atmospheric CH<sub>4</sub> concentrations (see section 3.2.2) translate into a higher and lower  $a_A^0$  for CH<sub>4</sub>, respectively. The  $K_{m(\text{app})}$  of *M. gorgona* MG08 was 48.54 nM CH<sub>4</sub> and the  $V_{\max(\text{app})}$   $4.91 \times 10^{-8}$  nmol cell<sup>-1</sup> h<sup>-1</sup> resulting in a  $a_A^0$  of  $1.01 \times 10^{-9}$  L cell<sup>-1</sup> h<sup>-1</sup>. The  $K_{m(\text{app})}$  of 48.54 nM CH<sub>4</sub> was the first observation of a  $K_{m(\text{app})}$  by a methanotroph in pure culture similar to the low  $K_{m(\text{app})}$  values of upland soils demonstrating a high apparent affinity for CH<sub>4</sub>. The  $K_{m(\text{app})}$  of *M. palsarum* NE2 was 402.08 nM CH<sub>4</sub> and the  $V_{\max(\text{app})}$   $133 \times 10^{-8}$  nmol cell<sup>-1</sup> h<sup>-1</sup> resulting in a  $a_A^0$  of  $3.30 \times 10^{-9}$  L cell<sup>-1</sup> h<sup>-1</sup>. This high  $a_A^0$  suggested that the upregulation of the pMMO at atmospheric CH<sub>4</sub> concentrations in *M. palsarum* NE2 led to a higher CH<sub>4</sub> oxidation capacity compared to *M. gorgona* MG08, which downregulated its pMMO. The results demonstrated that the two atmMOB have a significantly higher  $a_A^0$  for CH<sub>4</sub> than most methanotrophs in pure culture. Additionally, the results demonstrated that a high affinity for CH<sub>4</sub> (expressed by a low  $K_{m(\text{app})}$ ) is not a prerequisite for methanotrophic growth on air, as *M. palsarum* NE2, despite having an eight times higher  $K_{m(\text{app})}$ , oxidized atmospheric CH<sub>4</sub> quicker than *M. gorgona* MG08. Thus, it was concluded that the  $a_A^0$  is the better model to determine the efficiency of atmospheric CH<sub>4</sub> utilization by atmMOB.

### 3.2.4 Growth on nitrogen from air

As the atmMOB, *M. gorgona* MG08, *M. palsarum* NE2, *M. rosea* SV97, and *M. aurea* KYG encode all genes required for N<sub>2</sub> fixation and grow on nitrogen-free medium at high CH<sub>4</sub> concentrations, the potential of the four strains to grow with air as sole nitrogen, carbon, and energy source was tested. Filter cultures of all strains formed colonies on air without bioavailable nitrogen source in the medium, suggesting that all strains covered their nitrogen requirements either by N<sub>2</sub> fixation and/or utilization of reactive nitrogen in air. NanoSIMS-based <sup>15</sup>N<sub>2</sub> fixation experiments resulted in cellular <sup>15</sup>N enrichments higher than theoretically possible from the <sup>15</sup>N<sub>2</sub> gas used during the experiments. This pointed to reactive nitrogen contamination of the <sup>15</sup>N<sub>2</sub>, despite purity test of the gas prior to the experiment resulting in

contamination levels below detection limit. Therefore, N<sub>2</sub> fixation during growth on air could not be confirmed. However, based on the growth on nitrogen-free medium and the NanoSIMS experiments, it was concluded that atmMOB can cover their nitrogen requirements for growth, like energy and carbon, from air.

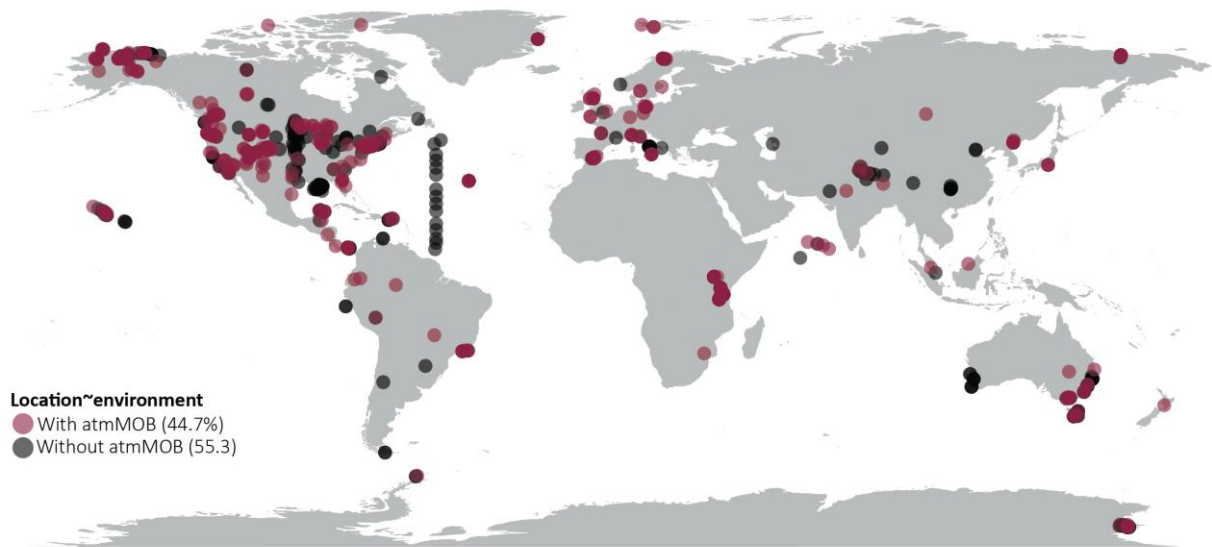
### 3.2.5 Conclusions

Major conclusions drawn from the study:

- Growth on air and enduring oxidation of atmospheric CH<sub>4</sub> is not restricted to members of the clades USC $\alpha$  and  $\gamma$ , but more widespread than previously assumed.
- Former liquid culture-based cultivation approaches underestimated the potential of methanotrophic pure cultures to oxidize atmospheric CH<sub>4</sub>.
- The strain specific oxidation patterns and the estimations of the  $a_A^0$  for CH<sub>4</sub> demonstrate that both the mixotrophic oxidation of atmospheric trace gases and a high  $a_A^0$  for CH<sub>4</sub> are key to obtain sufficient energy for growth on air.
- Energy requirements for growth of atmMOB are substantially lower than the maintenance energy value used as basic premise for the theory that atmMOB have an oligotrophic lifestyle.
- atmMOB can grow on air by decreasing investments in enzymes involved in energy-intensive processes combined with increasing investments in enzymes for the oxidation of trace gases.
- Differing expression patterns of enzymes for trace gas oxidation and the strain-specific trace gas oxidation patterns indicate that a diverse metabolic repertoire has evolved to enable life on air.
- atmMOB cover not only their energy and carbon but also their nitrogen requirements from the atmosphere.

### 3.3 Global distribution of atmMOB

A



B

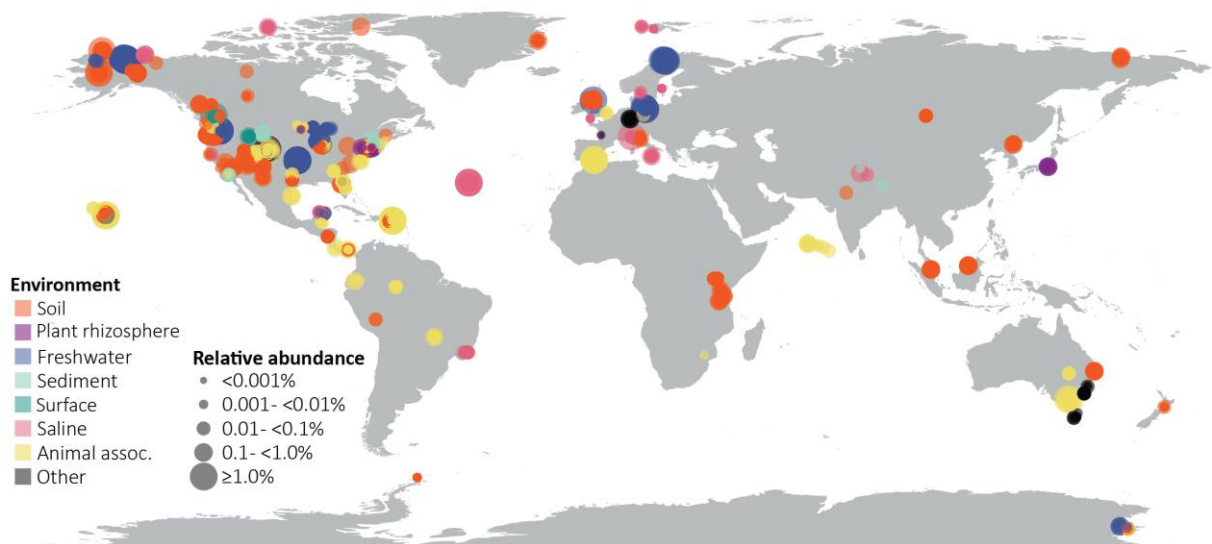


Figure 13. **A)** All geographically unique sample locations and environments accessible in the EMP database and the presence of 16S rRNA gene fragments from putative atmMOB closely related to *M. gorgona*, *M. aurea*, *M. palsarum*, and *M. rosea* within these locations and environments (indicated in red). **B)** Presence and relative abundance of 16S rRNA gene fragments from putative atmMOB closely related to *M. gorgona*, *M. aurea*, *M. palsarum*, and *M. rosea* in EMP samples derived from various environments.

The blast search of the three EMP databases identified 16S rRNA gene fragments of putative atmMOB closely related to *M. gorgona*, *M. aurea*, *M. palsarum*, and *M. rosea* in 44.7% of all geographically unique sample locations within various climate zones (Figure 13A). The 16S rRNA gene fragments of putative atmMOB were present in non-saline samples from soil, plant

rhizosphere, freshwater, sediments, surfaces (dust, house dust, freshwater biofilms), but also in saline and animal associated samples with abundances ranging from less than 0.001% to more than 1% (Figure 13B).

## 4 Discussion

The following discussion aims to put the results reported in paper 1 and 2 into a broader scientific context. A thorough discussion of the individual results can be found in the respective papers.

### 4.1 Physiological strategies of atmMOB to oxidize atmospheric CH<sub>4</sub>

The finding that “conventional” MOB can temporarily gain the ability to oxidize atmospheric CH<sub>4</sub> after exposure to high CH<sub>4</sub> concentrations<sup>41,90</sup> demonstrated that flush feeding (ii) (see section 1.6.2) enables a variety of MOB to oxidize atmospheric CH<sub>4</sub> for short periods until becoming inactive. However, the discovery of the atmospheric CH<sub>4</sub> oxidation by *M. gorgona* MG08 and its genomic potential to oxidize H<sub>2</sub> and CO in 2019<sup>101</sup> suggested that a second physiological strategy to oxidize atmospheric CH<sub>4</sub> besides flush feeding exists. The simultaneous oxidation of CH<sub>4</sub>, H<sub>2</sub>, and CO at their atmospheric trace gas concentration by *M. gorgona* MG08, reported in Paper 1 of this thesis, proofed its metabolic flexibility and mixotrophic nature. This confirmed the hypothetical strategy summarized by Dunfield<sup>32</sup> that facultative methanotrophs (iii) are responsible for oxidation of atmospheric CH<sub>4</sub>, as *M. gorgona* MG08 consumes other substrates in addition to CH<sub>4</sub>. However, even though the genetic potential to assimilate CO<sub>2</sub> using the reductive glycine pathway (see section 1.10.4) is given, it is unclear if *M. gorgona* MG08 can grow on H<sub>2</sub> and CO in absence of CH<sub>4</sub>. Also, the mixotrophy based on trace gases in air differs from the substrates previously assumed to support survival (e.g., intermediates of aerobic CH<sub>4</sub> oxidation or multi carbon compounds like acetate or ethanol) (see section 1.6.3) and enables *M. gorgona* MG08 to utilize the atmosphere as constant and sole source of energy and carbon for growth. Additionally, Paper 1 reported first indications that the energy yield necessary to support cellular maintenance of atmMOB is significantly lower than

assumed in literature<sup>80,85</sup>. This was especially intriguing as the low energy yields from the oxidation of trace gases in air seemed even sufficient for growth. The mixotrophy based on trace gases and these low energy requirements were further investigated in Paper 2 by screening six additional MOB species for their ability to grow with air as sole energy and carbon source. As result, the list of known atmMOB in pure culture able to grow on air was extended by *M. rosea* SV97, *M. palsarum* NE2, and *M. aurea* KYG. Like *M. gorgona* MG08, the three other species also consume atmospheric H<sub>2</sub> and/or CO in addition to CH<sub>4</sub> suggesting that mixotrophy on trace gases might be a common physiological trait of atmMOB able to grow on air. The strongly improved methodology to estimated energy yields from the oxidation of trace gases in air applied in Paper 2 resulted in energy values within the same range of the energy value reported in Paper 1. Thus, not only *M. gorgona* MG08 but also *M. rosea* SV97, *M. palsarum* NE2, and *M. aurea* KYG show energy requirements for growth far below the energy value stated in literature, strongly suggesting that the energy assumed necessary for cellular maintenance of atmMOB has been overestimated. A major problem with this maintenance energy value in literature used to describe the theoretical constraints for microbes utilizing trace gases<sup>80</sup> is that it is not derived from experiments involving atmMOB. It represents the average maintenance energy estimated for a wide range of aerobic and anaerobic microorganisms at different temperatures. The main conclusion of the study reporting this energy value is the correlation of maintenance energy and temperature and not the value itself. Even the authors of the study refer to the energy value as “*first approximation*”<sup>85</sup>. However, due to the absence of atmMOB pure cultures and thus, the possibility to study their energy requirements, the maintenance energy value was used as anchor point to theorize the constrains of microbes utilizing trace gases<sup>80</sup>. Despite their theoretical nature, these constraints that, amongst others, led to the assumption that atmMOB need a high affinity for CH<sub>4</sub> (K<sub>m</sub> of 1 pM to 100 nM) for cellular maintenance, were accepted. As consequence, the research field’s perspective on how atmMOB survive on air was restricted. For example, a study reported atmospheric CH<sub>4</sub> oxidation rates of the methanotrophic communities in beech and spruce forest soils ranging between 1 x 10<sup>-18</sup> and 14 x 10<sup>-18</sup> mol CH<sub>4</sub> cell<sup>-1</sup> h<sup>-1</sup>. These values are in the range of the CH<sub>4</sub> oxidation rates measured in Paper 2 (2 x 10<sup>-18</sup> to 7.3 x 10<sup>-18</sup> mol CH<sub>4</sub> cell<sup>-1</sup> h<sup>-1</sup>) and too low to meet the maintenance energy value in literature. Instead of questioning the maintenance energy value, the authors of the study concluded that the oxidation rates are “...*lower than required for maintenance of methanotrophic biomass...*” and that methanotrophs of the “...*USCa might*

rely on additional carbon sources to conserve enough energy for cell maintenance and growth”<sup>88</sup>. Another example is, as criticized by Dunfield, that the term “‘high-affinity oxidizer’ is frequently used interchangeably with ‘atmospheric methane oxidizer’...”<sup>32</sup>. The specific affinity measurements conducted in Paper 2, demonstrated that a high affinity for CH<sub>4</sub> does not necessarily reflect the capability to efficiently oxidize atmospheric CH<sub>4</sub> concentrations. *M. gorgona* MG08 exhibited a high apparent affinity for CH<sub>4</sub> that is within the range of the values theorized for the hypothesis that atmMOB are oligotrophs (see section 1.6.1). However, it oxidized atmospheric CH<sub>4</sub> significantly slower than *M. palsarum* NE2, which exhibited a lower apparent affinity. Taken together, the findings of Paper 1 and 2 strongly suggest to step away from the theorized maintenance energy and affinity assumptions for atmMOB.

The hypothesis that atmMOB are oligotrophs (see section 1.6.1) that can sustain cellular maintenance and growth by only oxidizing atmospheric CH<sub>4</sub> has not been investigated yet. However, considering the low energy values estimated for the four atmMOB studied in Paper 1 and 2 and the predictions that atmospheric CH<sub>4</sub> represents the major energy source for all four strains during growth on air, as shown in Paper 2, it seems likely that atmMOB can live on atmospheric CH<sub>4</sub> as sole energy source.

As the first assessment of the physiological strategies enabling atmMOB in pure culture to grow on air, the findings reported in Paper 1 and 2 revise our understanding of the energy limitation for aerobic growth with major implications for the research field. Considering the omnipresence of atmospheric trace gases, the low energy requirements of atmMOB, and their ability to utilize air as sole carbon and energy source, these organisms could grow in a wide range of surface environments. Additionally, the low energy requirements suggest that the atmosphere as energy source can support the growth of a significantly larger atmMOB population than previously assumed<sup>80</sup>. If true, a higher amount of CH<sub>4</sub> and CO<sub>2</sub> could be sequestered in atmMOB (see section 1.10.4 for carbon assimilation) increasing their impact on the global carbon cycle. Furthermore, if the trace gas based mixotrophy is a common trait of atmMOB, their role in greenhouse gas mitigation, besides the oxidation of atmospheric CH<sub>4</sub>, could even be of greater importance as H<sub>2</sub> and CO represent indirect greenhouse gases that deplete the atmospheric OH pool (see section 1.1). Especially the ability to efficiently oxidize H<sub>2</sub> might become valuable since a hydrogen-based economy as part of the industrial decarbonization could lead to increased H<sub>2</sub> emissions<sup>183,184</sup>.

## 4.2 Ecology and phylogeny of atmMOB

Based on the results of Paper 2, the growth on air and the enduring oxidation of atmospheric CH<sub>4</sub> is not restricted to members of the clades USC $\alpha$  and  $\gamma$ , but more widespread than previously assumed. The applied filter cultivation has proven as a suitable tool to assess the capability of MOB to utilize atmospheric trace gases and revealed that the atmMOB *M. palsarum* NE2, *M. rosea* SV97, and *M. aurea* KYG formerly considered as “conventional” methanotrophs can grow on air. Neither their 16S rRNA (see Paper 2) nor their *pmoA* genes<sup>101</sup> cluster within the USC $\alpha$ . This represents a valuable addition to the ecological understanding of atmMOB. On one hand, the diversity of MOB capable to enduringly oxidize atmospheric CH<sub>4</sub> has been underestimated, on the other, a broader range of *pmoA* gene sequences might be indicative for the potential to oxidize atmospheric CH<sub>4</sub>. To get a first impression of the ecological relevance of the atmMOB investigated in Paper 2, their global distribution and abundance based on 16S rRNA gene fragments was investigated using EMP databases (see section 2.5 and 3.3). This screening suggested that close relatives of *M. gorgona* MG08, *M. palsarum* NE2, *M. rosea* SV97, and *M. aurea* KYG and thus putative atmMOB are widespread over various climate zones (Fig. 13A) and inhabit not only uplands soils, plants, and caves but are highly abundant in various environments (Fig. 13B). If true, the range of environments contributing to atmospheric CH<sub>4</sub> uptake would be more comprehensive than previously thought as well as the role of atmMOB in carbon cycling and CH<sub>4</sub> mitigation. However, the screening approach used for the global distribution is based on databases containing short 16S rRNA gene fragment sequences (90, 100, and 150 bp). Therefore, the resolution of the results is limited and should be treated with caution as high similarity in 16S rRNA gene fragments does not necessarily translate into the capability to oxidize atmospheric CH<sub>4</sub>. To get more reliable results the methodology should base on datasets combining long 16S rRNA sequences and the *pmoA* as functional markers. Nevertheless, the finding in Paper 2 that the atmMOB can utilize the atmosphere as nitrogen source, in addition to carbon and energy, renders the widespread distribution of atmMOB more plausible. Yet, it remains unclear whether the four atmMOB strains can meet their nitrogen requirements by the fixation of N<sub>2</sub> or the assimilation of reactive nitrogen species in the atmosphere or both.

With the rapidly increasing atmospheric CH<sub>4</sub> concentrations and the ongoing depletion of the chemical sink for atmospheric CH<sub>4</sub>, (see section 1.1 and 1.3) the importance of the biological sink might increase. However, to investigate and model the response of the biological sink to

the increasing atmospheric CH<sub>4</sub> concentrations and the associated increase in substrate availability, it is crucial to further investigate the diversity and abundance of atmMOB across various environments. Additionally, the impact of other environmental factors on atmMOB (see section 1.5), especially in the context of global warming, needs to be scrutinized. Furthermore, gaining a deeper understanding of how anthropogenic activities, such as practices in agriculture, affect atmMOB is essential to successfully manage or maybe even restore biological sinks for atmospheric CH<sub>4</sub>. The four atmMOB pure cultures, along with the methods established throughout this PhD to research them, might be promising steppingstones to do so.

### 4.3 Metabolic potential of atmMOB for biotechnology

Despite the mixotrophy based on trace gases by all four atmMOB that are capable to grow with air as sole energy and carbon source, their metabolic adjustments to grow on air differ. This is illustrated by the repeatedly measured strain-specific trace gas oxidation patterns reported in Paper 1 and 2. These oxidation patterns were further investigated in Paper 2 that describes the proteome adjustments of atmMOB to grow on air. The results demonstrate that the investigated strains allocated resources to enzymes for the oxidation of trace gases differently. *M. palsarum* NE2 allocated resources towards CH<sub>4</sub> oxidation when grown on air, while *M. gorgona* MG08 and *M. rosea* SV97 allocated resources towards H<sub>2</sub> and CO or H<sub>2</sub> oxidation, respectively. This suggests that the three strains increase their specific affinities for the respective gases on air to maximize trace gas oxidation. The measurements of the specific affinities for CH<sub>4</sub> in Paper 2 are in line with the observed enzyme allocation and show that *M. palsarum* NE2 has the highest specific affinity for CH<sub>4</sub> measured so far. As the specific affinity indicates reaction rates at low substrate concentrations<sup>84</sup>, *M. palsarum* NE2 might be an ideal candidate for the biofiltration of emissions containing very low CH<sub>4</sub> concentrations. In contrast to *M. palsarum* NE2, *M. gorgona* MG08 and *M. rosea* SV97 increased their resource allocation towards CH<sub>4</sub> oxidation at “high” CH<sub>4</sub> concentrations (1000 ppm) suggesting high CH<sub>4</sub> oxidation rates at elevated CH<sub>4</sub> concentrations. The enzymatic variability between the strains could enable efficient biofiltration of emission containing a wide range CH<sub>4</sub> concentrations (0.00019 – 5%). This potential for biofiltration of low CH<sub>4</sub> emissions might be of great value as more than 55% of the anthropogenic CH<sub>4</sub> emissions contain CH<sub>4</sub> concentrations below the lower explosive level (LEL) (5% CH<sub>4</sub> in air)<sup>28,185</sup> and thus cannot be combusted for energy recovery. Additionally,

based on its short half-life, the mitigation of CH<sub>4</sub> is considered to be an effective strategy to achieve substantial near-term temperature benefits and to rapidly decelerate global warming<sup>186,187</sup>. Besides the potential of atmMOB to mitigate CH<sub>4</sub> below the LEL, the three strains investigated in detail can utilize the indirect greenhouse gases H<sub>2</sub> and/or CO at atmospheric concentrations. This metabolic flexibility plus their ability to fix CO<sub>2</sub> (see section 1.10.4) might qualify them to efficiently utilize waste gases that contain only minor amounts of CH<sub>4</sub>, H<sub>2</sub>, or CO as feedstock for biomass production. Thus, atmMOB offer the potential to couple the mitigation of greenhouse gases to the production of compounds with relevance in industry. Examples for methanotrophy-based compounds are, amongst others, byproducts of their metabolism such as methanol or formaldehyde, lipids that could be used as fuel, PHA as precursor for bioplastics, and protein-rich food for humans or animals<sup>13</sup>. In addition, the oligotrophy of the atmMOB, enabling growth with minimal nutrient supply, and their ability to utilize the atmosphere as nitrogen source promises low cultivation costs. Furthermore, by having atmMOB in pure culture, genetic engineering approaches might even optimize their metabolic traits suitable for applications in biotechnology. Overall, especially with regards to the climate crisis, atmMOB appear to offer metabolic traits that could greatly contribute to sustainability.

## 5 References

1. IPCC. Climate Change 2014: Synthesis Report. Contribution of Working Groups I, II and III to the Fifth Assessment Report of the Intergovernmental Panel on Climate Change. Core Writing Team, R.K. Pachauri and L.A. Meyer (2014). doi:10.1017/CBO9781107415324.004.
2. Intergovernmental Panel on Climate Change. The Earth's Energy Budget, Climate Feedbacks and Climate Sensitivity. in Climate Change 2021 – The Physical Science Basis 923–1054 (Cambridge University Press, 2023). doi:10.1017/9781009157896.009.
3. Mar, K. A., Unger, C., Walderdorff, L. & Butler, T. Beyond CO<sub>2</sub> equivalence: The impacts of methane on climate, ecosystems, and health. *Environ Sci Policy* **134**, 127–136 (2022).
4. Reay, D. S., Smith, P., Christensen, T. R., James, R. H. & Clark, H. Methane and Global Environmental Change. *Annu Rev Environ Resour* **43**, 165–192 (2018).
5. Lan, X., K.W. Thoning & E.J. Dlugokencky. Trends in globally-averaged CH<sub>4</sub>, N<sub>2</sub>O, and SF<sub>6</sub> determined from NOAA Global Monitoring Laboratory measurements. Trends in globally-averaged CH<sub>4</sub>, N<sub>2</sub>O, and SF<sub>6</sub> determined from NOAA Global Monitoring Laboratory measurements (2023) doi:https://doi.org/10.15138/P8XG-AA10.
6. Kirschke, S. et al. Three decades of global methane sources and sinks. *Nature Geoscience* vol. 6 813–823 Preprint at <https://doi.org/10.1038/ngeo1955> (2013).
7. Bižić, M. et al. Aquatic and terrestrial cyanobacteria produce methane. *Sci Adv* **6**, eaax5343 (2020).
8. Ernst, L. et al. Methane formation driven by reactive oxygen species across all living organisms. *Nature* 2022 603:7901 **603**, 482–487 (2022).
9. Saunio, M. et al. The Global Methane Budget 2000–2017. *Earth Syst Sci Data* **12**, 1561–1623 (2020).
10. Ehhalt, D. H. The atmospheric cycle of methane. *Tellus* **26**, 58–70 (1974).
11. Hanson, R. S. & Hanson, T. E. Methanotrophic Bacteria. *MICROBIOLOGICAL REVIEWS* vol. 60 <https://www.ncbi.nlm.nih.gov/pmc/articles/PMC239451/pdf/600439.pdf> (1996).
12. McGlynn, S. E. Energy Metabolism during Anaerobic Methane Oxidation in ANME Archaea. *Microbes Environ* **32**, 5–13 (2017).
13. Guerrero-Cruz, S. et al. Methanotrophs: Discoveries, Environmental Relevance, and a Perspective on Current and Future Applications. *Frontiers in Microbiology* vol. 12 Preprint at <https://doi.org/10.3389/fmicb.2021.678057> (2021).

14. Valentine, D. L. Biogeochemistry and microbial ecology of methane oxidation in anoxic environments: A review. *Antonie van Leeuwenhoek, International Journal of General and Molecular Microbiology* **81**, 271–282 (2002).
15. Ettwig, K. F. et al. Nitrite-driven anaerobic methane oxidation by oxygenic bacteria. *Nature* **464**, 543–548 (2010).
16. Ettwig, K. F. et al. Archaea catalyze iron-dependent anaerobic oxidation of methane. *Proc Natl Acad Sci U S A* **113**, 12792–12796 (2016).
17. Haroon, M. F. et al. Anaerobic oxidation of methane coupled to nitrate reduction in a novel archaeal lineage. *Nature* **500**, 567–570 (2013).
18. Leu, A. O. et al. Anaerobic methane oxidation coupled to manganese reduction by members of the Methanoperedenaceae. *ISME Journal* **14**, 1030–1041 (2020).
19. Knief, C. Diversity and Habitat Preferences of Cultivated and Uncultivated Aerobic Methanotrophic Bacteria Evaluated Based on *pmoA* as Molecular Marker. *Front Microbiol* **6**, (2015).
20. Hakobyan, A. & Liesack, W. Unexpected metabolic versatility among type II methanotrophs in the Alphaproteobacteria. *Biol Chem* **401**, 1469–1477 (2020).
21. Khadem, A. F. et al. Autotrophic methanotrophy in verrucomicrobia: *Methylacidiphilum fumariolicum solv* uses the calvin-benson-bassham cycle for Carbon Dioxide Fixation. *J Bacteriol* **193**, 4438–4446 (2011).
22. van Spanning, R. J. M. et al. Methanotrophy by a *Mycobacterium* species that dominates a cave microbial ecosystem. *Nat Microbiol* **7**, 2089–2100 (2022).
23. Bay, S. K. et al. Trace gas oxidizers are widespread and active members of soil microbial communities. *Nat Microbiol* **6**, 246–256 (2021).
24. Rigby, M. et al. Role of atmospheric oxidation in recent methane growth. *Proceedings of the National Academy of Sciences* **114**, 5373–5377 (2017).
25. Jackson, R. B. et al. Increasing anthropogenic methane emissions arise equally from agricultural and fossil fuel sources. *Environmental Research Letters* **15**, 071002 (2020).
26. Peng, S. et al. Wetland emission and atmospheric sink changes explain methane growth in 2020. *Nature* **612**, 477–482 (2022).
27. Tate, K. R. Soil methane oxidation and land-use change – from process to mitigation. *Soil Biol Biochem* **80**, 260–272 (2015).
28. La, H., Hettiaratchi, J. P. A., Achari, G. & Dunfield, P. F. Biofiltration of methane. *Bioresour Technol* **268**, 759–772 (2018).

29. Harriss, R. C., Sebacher, D. I. & Day, F. P. Methane flux in the Great Dismal Swamp. *Nature* **297**, 673–674 (1982).
30. Bender, M. & Conrad, R. Kinetics of CH<sub>4</sub> oxidation in oxic soils exposed to ambient air or high CH<sub>4</sub> mixing ratios. *FEMS Microbiol Ecol* **10**, 261–269 (1992).
31. Bender, M. & Conrad, R. Kinetics of CH<sub>4</sub> Oxidation in Oxic Soils Exposed to Ambient Air or High CH<sub>4</sub> Mixing Ratios. *Microbiology Ecology* vol. 101 <https://academic.oup.com/femsec/article/10/4/261/477403> (1992).
32. Dunfield, P. F. The soil methane sink. in *Greenhouse gas sinks* 152–170 (CABI, UK, 2007). doi:10.1079/9781845931896.0152.
33. Kolb, S. The quest for atmospheric methane oxidizers in forest soils. *Environ Microbiol Rep* **1**, 336–346 (2009).
34. Täumer, J. et al. Divergent drivers of the microbial methane sink in temperate forest and grassland soils. *Glob Chang Biol* **27**, 929–940 (2021).
35. Seiler, W., Conrad, R. & Scharffe, D. Field studies of methane emission from termite nests into the atmosphere and measurements of methane uptake by tropical soils. *J Atmos Chem* **1**, 171–186 (1984).
36. Liu, Y. et al. Atmospheric methane oxidation is affected by grassland type and grazing and negatively correlated to total soil respiration in arid and semiarid grasslands in Inner Mongolia. *Soil Biol Biochem* **173**, (2022).
37. Bogner, J., Spokas, K., Burton, E., Sweeney, R. & Corona, V. Landfills as atmospheric methane sources and sinks. *Chemosphere* **31**, 4119–4130 (1995).
38. Striegl, R. G., McConnaughey, T. A., Thorstenson, D. C., Weeks, E. P. & Woodward, J. C. Consumption of atmospheric methane by desert soils. *Nature* **357**, 145–147 (1992).
39. Kruse, C. W. & Iversen, N. Effect of plant succession, ploughing, and fertilization on the microbiological oxidation of atmospheric methane in a heathland soil. *FEMS Microbiol Ecol* **18**, 121–128 (1995).
40. Singh, S., Singh, J. S. & Kashyap, A. K. Methane consumption by soils of dryland rice agriculture: Influence of varieties and N-fertilization. *Chemosphere* **38**, 175–189 (1999).
41. Cai, Y., Zheng, Y., Bodelier, P. L. E., Conrad, R. & Jia, Z. Conventional methanotrophs are responsible for atmospheric methane oxidation in paddy soils. *Nat Commun* **7**, 11728 (2016).
42. Whalen, S. C. & Reeburgh, W. S. Consumption of atmospheric methane by tundra soils. *Nature* **346**, 160–162 (1990).

43. Yun, H. et al. Consumption of atmospheric methane by the Qinghai-Tibet Plateau alpine steppe ecosystem. *Cryosphere* **12**, 2803–2819 (2018).
44. Webster, K. D., Mirza, A., Deli, J. M., Sauer, P. E. & Schimmelmann, A. Consumption of atmospheric methane in a limestone cave in Indiana, USA. *Chem Geol* **443**, 1–9 (2016).
45. Sundqvist, E., Crill, P., Milder, M., Vestin, P. & Lindroth, A. Atmospheric methane removal by boreal plants. *Geophys Res Lett* **39**, (2012).
46. Liebner, S. et al. Methane oxidation associated with submerged brown mosses reduces methane emissions from Siberian polygonal tundra. *Journal of Ecology* **99**, 914–922 (2011).
47. Knief, C., Lipski, A. & Dunfield, P. F. Diversity and Activity of Methanotrophic Bacteria in Different Upland Soils. *Appl Environ Microbiol* **69**, 6703–6714 (2003).
48. Holmes, A. J. et al. Characterization of Methanotrophic Bacterial Populations in Soils Showing Atmospheric Methane Uptake. *Appl Environ Microbiol* **65**, 3312–3318 (1999).
49. Pratscher, J., Vollmers, J., Wiegand, S., Dumont, M. G. & Kaster, A. Unravelling the Identity, Metabolic Potential and Global Biogeography of the Atmospheric Methane-Oxidizing Upland Soil Cluster  $\alpha$ . *Environ Microbiol* **20**, 1016–1029 (2018).
50. Cheng, X.-Y. et al. USC  $\gamma$  Dominated Community Composition and Cooccurrence Network of Methanotrophs and Bacteria in Subterranean Karst Caves. *Microbiol Spectr* (2021) doi:10.1128/SPECTRUM.00820-21.
51. Täumer, J. et al. Linking transcriptional dynamics of CH<sub>4</sub>-cycling grassland soil microbiomes to seasonal gas fluxes. *ISME J* **16**, 1788–1797 (2022).
52. Rafalska, A., Walkiewicz, A., Osborne, B., Klumpp, K. & Bieganowski, A. Variation in methane uptake by grassland soils in the context of climate change – A review of effects and mechanisms. *Science of the Total Environment* vol. 871 Preprint at <https://doi.org/10.1016/j.scitotenv.2023.162127> (2023).
53. Wang, Y. et al. Precipitation determines the magnitude and direction of interannual responses of soil respiration to experimental warming. *Plant Soil* **458**, 75–91 (2021).
54. King, G. M. & Adamsen, A. P. S. Effects of Temperature on Methane Consumption in a Forest Soil and in Pure Cultures of the Methanotroph *Methylomonas rubra*. *Appl Environ Microbiol* **58**, 2758–2763 (1992).
55. Whalen, Stephen C., Reeburgh, William S. & Barber, Valerie A. Oxidation of methane in boreal forest soils: a comparison of seven measures. *Biogeochemistry* **16**, (1992).

56. Murguia-Flores, F., Ganesan, A. L., Arndt, S. & Hornibrook, E. R. C. Global Uptake of Atmospheric Methane by Soil From 1900 to 2100. *Global Biogeochem Cycles* **35**, (2021).
57. Von Fischer, J. C., Butters, G., Duchateau, P. C., Thelwell, R. J. & Siller, R. In situ measures of methanotroph activity in upland soils: A reaction-diffusion model and field observation of water stress. *J Geophys Res Biogeosci* **114**, (2009).
58. Amaral, J. A., Ren, T. & Knowles, R. Atmospheric Methane Consumption by Forest Soils and Extracted Bacteria at Different PH Values. *APPLIED AND ENVIRONMENTAL MICROBIOLOGY* vol. 64 (1998).
59. Kou, Y. et al. Deterministic processes dominate soil methanotrophic community assembly in grassland soils. *Geoderma* **359**, (2020).
60. Cai, Y., Zhou, X., Shi, L. & Jia, Z. Atmospheric Methane Oxidizers Are Dominated by Upland Soil Cluster Alpha in 20 Forest Soils of China. *Microb Ecol* **80**, 859–871 (2020).
61. Zhao, J., Cai, Y. & Jia, Z. The pH-based ecological coherence of active canonical methanotrophs in paddy soils. *Biogeosciences* **17**, 1451–1462 (2020).
62. Fowler, D. et al. The global nitrogen cycle in the Twentyfirst century. *Philosophical Transactions of the Royal Society B: Biological Sciences* **368**, (2013).
63. Kanakidou, M. et al. Past, Present, and Future Atmospheric Nitrogen Deposition. (2016) doi:10.1175/JAS-D-15-0278.s1.
64. Galloway, J. N. et al. Transformation of the Nitrogen Cycle: Recent Trends, Questions, and Potential Solutions. *Science* (1979) **320**, 889–892 (2008).
65. Driscoll, C. T. et al. Nitrogen pollution in the northeastern United States: Sources, effects, and management options. *BioScience* vol. 53 Preprint at [https://doi.org/10.1641/0006-3568\(2003\)053\[0357:NPITNU\]2.0.CO;2](https://doi.org/10.1641/0006-3568(2003)053[0357:NPITNU]2.0.CO;2) (2003).
66. Bodelier, P. L. E. & Steenbergh, A. K. Interactions between methane and the nitrogen cycle in light of climate change. *Current Opinion in Environmental Sustainability* vols 9–10 26–36 Preprint at <https://doi.org/10.1016/j.cosust.2014.07.004> (2014).
67. Steudler, P. A., Bowden, R. D., Melillo, J. M. & Aber, J. D. Influence of nitrogen fertilization on methane uptake in temperate forest soils. *Nature* **341**, 314–316 (1989).
68. Gullledge, J. & Schimel, J. P. Low-Concentration Kinetics of Atmospheric CH<sub>4</sub> Oxidation in Soil and Mechanism of NH<sub>4</sub><sup>+</sup> Inhibition. *Appl Environ Microbiol* **64**, 4291–4298 (1998).
69. Bodelier, P. L. E. & Laanbroek, H. J. Nitrogen as a regulatory factor of methane oxidation in soils and sediments. *FEMS Microbiology Ecology* vol. 47 265–277 Preprint at [https://doi.org/10.1016/S0168-6496\(03\)00304-0](https://doi.org/10.1016/S0168-6496(03)00304-0) (2004).

70. Mohanty, S. R., Bodelier, P. L. E., Floris, V. & Conrad, R. Differential effects of nitrogenous fertilizers on methane-consuming microbes in rice field and forest soils. *Appl Environ Microbiol* **72**, 1346–1354 (2006).
71. Dam, B., Dam, S., Kim, Y. & Liesack, W. Ammonium induces differential expression of methane and nitrogen metabolism-related genes in *Methylocystis* sp. strain SC2. *Environ Microbiol* **16**, 3115–3127 (2014).
72. Bodelier, P. L. E. & Steenbergh, A. K. Interactions between Methane and Nitrogen Cycling: Current Metagenomic Studies and Future Trends. in.
73. Shukla, P. N., Pandey, K. D. & Mishra, V. K. Environmental determinants of soil methane oxidation and methanotrophs. *Crit Rev Environ Sci Technol* **43**, 1945–2011 (2013).
74. Keller, M., Mitre, M. E. & Stallard, R. F. Consumption of atmospheric methane in soils of central Panama: Effects of agricultural development. *Global Biogeochem Cycles* **4**, 21–27 (1990).
75. Knief, C. et al. Diversity of methanotrophic bacteria in tropical upland soils under different land uses. *Appl Environ Microbiol* **71**, 3826–3831 (2005).
76. Priemé, A. & Ekelund, F. Five pesticides decreased oxidation of atmospheric methane in a forest soil. *Soil Biol Biochem* **33**, 831–835 (2001).
77. Boeckx, P., Van Cleemput, O. & Meyer, T. The influence of land use and pesticides on methane oxidation in some Belgian soils. *Biol Fertil Soils* **27**, 293–298 (1998).
78. Yashiro, Y., Kadir, W. R., Okuda, T. & Koizumi, H. The effects of logging on soil greenhouse gas (CO<sub>2</sub>, CH<sub>4</sub>, N<sub>2</sub>O) flux in a tropical rain forest, Peninsular Malaysia. *Agric For Meteorol* **148**, 799–806 (2008).
79. Nanba, K. & King, G. M. Response of Atmospheric Methane Consumption by Maine Forest Soils to Exogenous Aluminum Salts †. *APPLIED AND ENVIRONMENTAL MICROBIOLOGY* vol. 66 <https://journals.asm.org/journal/aem> (2000).
80. Conrad, R. Soil microorganisms oxidizing atmospheric trace gases (CH<sub>4</sub>, CO, H<sub>2</sub>, NO). *Indian J Microbiol* **39**, 193–203 (1999).
81. Novelli, P. C. et al. Molecular hydrogen in the troposphere: Global distribution and budget. *Journal of Geophysical Research: Atmospheres* **104**, 30427–30444 (1999).
82. Novelli, P. C., Masarie, K. A. & Lang, P. M. Distributions and recent changes of carbon monoxide in the lower troposphere. *Journal of Geophysical Research Atmospheres* **103**, 19015–19033 (1998).

83. Dunfield, P. F. & Conrad, R. Starvation Alters the Apparent Half-Saturation Constant for Methane in the Type II Methanotroph *Methylocystis* Strain LR1. *Appl Environ Microbiol* **66**, 4136–4138 (2000).
84. Button, D. K. Kinetics of nutrient-limited transport and microbial growth. *Microbiological Reviews* vol. 49 270–297 Preprint at <https://doi.org/10.1128/membr.49.3.270-297.1985> (1985).
85. Tijhuis, L., Van Loosdrecht, M. C. M. & Heijnen, J. J. A thermodynamically based correlation for maintenance gibbs energy requirements in aerobic and anaerobic chemotrophic growth. *Biotechnol Bioeng* **42**, 509–519 (1993).
86. Knief, C., Kolb, S., Bodelier, P. L. E., Lipski, A. & Dunfield, P. F. The active methanotrophic community in hydromorphic soils changes in response to changing methane concentration. *Environ Microbiol* **8**, 321–333 (2006).
87. Kolb, S., Knief, C., Dunfield, P. F. & Conrad, R. Abundance and activity of uncultured methanotrophic bacteria involved in the consumption of atmospheric methane in two forest soils. *Environ Microbiol* **7**, 1150–1161 (2005).
88. Degelmann, D. M., Borcken, W., Drake, H. L. & Kolb, S. Different Atmospheric Methane-Oxidizing Communities in European Beech and Norway Spruce Soils. *Appl Environ Microbiol* **76**, 3228–3235 (2010).
89. Cai, Y., Zheng, Y., Bodelier, P. L. E., Conrad, R. & Jia, Z. Conventional methanotrophs are responsible for atmospheric methane oxidation in paddy soils. *Nat Commun* **7**, (2016).
90. Knief, C. & Dunfield, P. F. Response and adaptation of different methanotrophic bacteria to low methane mixing ratios. *Environ Microbiol* **7**, 1307–1317 (2005).
91. Sipkema, E. M., de Koning, W., Ganzeveld, K. J., Janssen, D. B. & Beenackers, A. A. C. M. NADH-regulated metabolic model for growth of *Methylosinus trichosporium* OB3b. Model presentation, parameter estimation, and model validation. *Biotechnol Prog* **16**, 176–188 (2000).
92. Asenjo, J. A. & Suk, J. S. Microbial Conversion of Methane into poly- $\beta$ -hydroxybutyrate (PHB): Growth and intracellular product accumulation in a type II methanotroph. *Journal of Fermentation Technology* **64**, 271–278 (1986).
93. López, J. C., Arnáiz, E., Merchán, L., Lebrero, R. & Muñoz, R. Biogas-based polyhydroxyalkanoates production by *Methylocystis hirsuta*: A step further in anaerobic digestion biorefineries. *Chemical Engineering Journal* **333**, 529–536 (2018).
94. Tveit, A. T. et al. Thermal acclimation of methanotrophs from the genus *Methylobacter*. *The ISME Journal* 2023 1–12 (2023) doi:10.1038/s41396-023-01363-7.
95. Dedysh, S. N., Knief, C. & Dunfield, P. F. *Methylocella* species are facultatively methanotrophic. *J Bacteriol* **187**, 4665–4670 (2005).

96. Belova, S. E. et al. Acetate utilization as a survival strategy of peat-inhabiting *Methylocystis* spp. *Environ Microbiol Rep* **3**, 36–46 (2011).
97. Bordel, S. et al. Genome scale metabolic modeling reveals the metabolic potential of three Type II methanotrophs of the genus *Methylocystis*. *Metab Eng* **54**, 191–199 (2019).
98. Dedysh, S. N. & Dunfield, P. F. Facultative and obligate methanotrophs: How to identify and differentiate Them. in *Methods in Enzymology* vol. 495 31–44 (Academic Press Inc., 2011).
99. Im, J., Lee, S. W., Yoon, S., Dispirito, A. A. & Semrau, J. D. Characterization of a novel facultative *Methylocystis* species capable of growth on methane, acetate and ethanol. *Environ Microbiol Rep* **3**, 174–181 (2011).
100. Hakobyan, A., Zhu, J., Glatter, T., Paczia, N. & Liesack, W. Hydrogen utilization by *Methylocystis* sp. strain SC2 expands the known metabolic versatility of type IIa methanotrophs. *Metab Eng* **61**, 181–196 (2020).
101. Tveit, A. T. et al. Widespread soil bacterium that oxidizes atmospheric methane. *Proceedings of the National Academy of Sciences* **116**, 8515–8524 (2019).
102. Holmes, A. J., Costello, A., Lidstrom, M. E. & Murrell, J. C. Evidence that participate methane monooxygenase and ammonia monooxygenase may be evolutionarily related. *FEMS Microbiol Lett* **132**, 203–208 (2006).
103. Tavormina, P. L., Orphan, V. J., Kalyuzhnaya, M. G., Jetten, M. S. M. & Klotz, M. G. A novel family of functional operons encoding methane/ammonia monooxygenase-related proteins in gammaproteobacterial methanotrophs. *Environ Microbiol Rep* **3**, 91–100 (2011).
104. Su, Y. C., Sathyamoorthy, S. & Chandran, K. Bioaugmented methanol production using ammonia oxidizing bacteria in a continuous flow process. *Bioresour Technol* **279**, 101–107 (2019).
105. Murrell, J. C. & Dalton, H. Nitrogen Fixation in Obligate Methanotrophs. *Microbiology (N Y)* **129**, 3481–3486 (1983).
106. Warttinen, I., Hestnes, A. G., McDonald, I. R. & Svenning, M. M. *Methylocystis rosea* sp. nov., a novel methanotrophic bacterium from Arctic wetland soil, Svalbard, Norway (78° N). *Int J Syst Evol Microbiol* **56**, 541–547 (2006).
107. Dedysh, S. N. et al. *Methylocapsa acidiphila* gen. nov., sp. nov., a novel methane-oxidizing and dinitrogen-fixing acidophilic bacterium from Sphagnum bog. *Int J Syst Evol Microbiol* **52**, 251–261 (2002).
108. Dunfield, P. F., Belova, S. E., Vorob'ev, A. V., Cornish, S. L. & Dedysh, S. N. *Methylocapsa aurea* sp. nov., a facultative methanotroph possessing a particulate methane monooxygenase, and emended description of the genus *Methylocapsa*. *Int J Syst Evol Microbiol* **60**, 2659–2664 (2010).

109. Dedysh, S. N. et al. *Methylocapsa palsarum* sp. nov., a methanotroph isolated from a subArctic discontinuous permafrost ecosystem. *Int J Syst Evol Microbiol* **65**, 3618–3624 (2015).
110. Inomura, K., Bragg, J. & Follows, M. J. A quantitative analysis of the direct and indirect costs of nitrogen fixation: a model based on *Azotobacter vinelandii*. *The ISME Journal* 2017 11:1 **11**, 166–175 (2016).
111. Whittenbury, R. & Wilkinson, J. F. Enrichment, Isolation and Some Properties of Methane-utilizing Bacteria. *J Gen Microbiol* **61**, 205–218 (1970).
112. Singh, R., Ryu, J. & Kim, S. W. An Overview on Methanotrophs and the Role of *Methylosinus trichosporium* OB3b for Biotechnological Applications. *Biotechnology and Bioprocess Engineering* 2022 **27**, 1–14 (2022).
113. Zhang, T., Zhou, J., Wang, X. & Zhang, Y. Poly- $\beta$ -hydroxybutyrate Production by *Methylosinus trichosporium* OB3b at Different Gas-phase Conditions. *Iran J Biotechnol* **17**, 10–16 (2019).
114. Belova, S. E. et al. *Methylocapsa polymorpha* sp. nov., a Novel Dinitrogen-Fixing Methanotroph from a Subarctic Wetland. *Microbiology (N Y)* **92**, S107–S113 (2023).
115. Danilova, O. V. et al. One Step Closer to Enigmatic USC $\alpha$  Methanotrophs: Isolation of a *Methylocapsa*-like Bacterium from a Subarctic Soil. *Microorganisms* **11**, (2023).
116. Strong, P. J., Xie, S. & Clarke, W. P. Methane as a resource: Can the methanotrophs add value? *Environ Sci Technol* **49**, 4001–4018 (2015).
117. Trotsenko, Y. A. & Murrell, J. C. Metabolic Aspects of Aerobic Obligate Methanotrophy\*. *Adv Appl Microbiol* **63**, 183–229 (2008).
118. Semrau, J. D., Dispirito, A. A. & Yoon, S. Methanotrophs and copper. *FEMS Microbiol Rev* **34**, 496–531 (2010).
119. Greening, C. & Grinter, R. Microbial oxidation of atmospheric trace gases. *Nat Rev Microbiol* **20**, 513–528 (2022).
120. Koo, C. W., Tucci, F. J., He, Y. & Rosenzweig, A. C. Recovery of particulate methane monooxygenase structure and activity in a lipid bilayer. *Science (1979)* (2022) doi:10.1126/SCIENCE.ABM3282.
121. Baba, T. & Miyaji, A. Catalysis and the Mechanism of Methane Conversion to Chemicals: C-C and C-O Bonds Formation Using Heterogeneous, Homogenous, and Biological Catalysts. *Catalysis and the Mechanism of Methane Conversion to Chemicals: C-C and C-O Bonds Formation Using Heterogeneous, Homogenous, and Biological Catalysts* (Springer Singapore, 2020). doi:10.1007/978-981-15-4132-2.

122. Miyaji, A., Nitta, M. & Baba, T. Influence of copper ions removal from membrane-bound form of particulate methane monooxygenase from *Methylosinus trichosporium* OB3b on its activity for methane hydroxylation. *J Biotechnol* **306**, 100001 (2019).
123. Shiemke, A. K., Cook, S. A., Miley, T. & Singleton, P. Detergent solubilization of membrane-bound methane monooxygenase requires plastoquinol analogs as electron donors. *Arch Biochem Biophys* **321**, 421–428 (1995).
124. Keltjens, J. T., Pol, A., Reimann, J. & Op Den Camp, H. J. M. PQQ-dependent methanol dehydrogenases: Rare-earth elements make a difference. *Appl Microbiol Biotechnol* **98**, 6163–6183 (2014).
125. Anthony, C. The quinoprotein dehydrogenases for methanol and glucose. *Arch Biochem Biophys* **428**, 2–9 (2004).
126. Chistoserdova, L. Lanthanides: New life metals? *World J Microbiol Biotechnol* **32**, 1–7 (2016).
127. Marx, C. J., Chistoserdova, L. & Lidstrom, M. E. Formaldehyde-detoxifying role of the tetrahydromethanopterin-linked pathway in *Methylobacterium extorquens* AM1. *J Bacteriol* **185**, 7160–7168 (2003).
128. Vorholt, J. A. Cofactor-dependent pathways of formaldehyde oxidation in methylophilic bacteria. *Arch Microbiol* **178**, 239–249 (2002).
129. Kallen, R. G. & Jencks, W. P. The Mechanism of the Condensation of Formaldehyde with Tetrahydrofolic Acid. *Journal of Biological Chemistry* **241**, 5851–5863 (1966).
130. Vorholt, J. A., Marx, C. J., Lidstrom, M. E. & Thauer, R. K. Novel Formaldehyde-Activating Enzyme in *Methylobacterium Extorquens* AM1 Required for Growth on Methanol. *JOURNAL OF BACTERIOLOGY* vol. 182 <https://journals.asm.org/journal/jb> (2000).
131. Vorholt, J. A., Chistoserdova, L., Lidstrom, M. E. & Thauer, R. K. The NADP-dependent methylene tetrahydromethanopterin dehydrogenase in *Methylobacterium extorquens* AM1. *J Bacteriol* **180**, 5351–5356 (1998).
132. Hagemeyer, C. H., Chistoserdova, L., Lidstrom, M. E., Thauer, R. K. & Vorholt, J. A. Characterization of a second methylene tetrahydromethanopterin dehydrogenase from *Methylobacterium extorquens* AM1. *Eur J Biochem* **267**, 3762–3769 (2000).
133. Pomper, B. K., Vorholt, J. A., Chistoserdova, L., Lidstrom, M. E. & Thauer, R. K. A methenyl tetrahydromethanopterin cyclohydrolase and a methenyl tetrahydrofolate cyclohydrolase in *Methylobacterium extorquens* AM1. *Eur J Biochem* **261**, 475–480 (1999).

134. Pomper, B. K., Saurel, O., Milon, A. & Vorholt, J. A. Generation of formate by the formyltransferase/hydrolase complex (Fhc) from *Methylobacterium extorquens* AM1. *FEBS Lett* **523**, 133–137 (2002).
135. Moon, M., Park, G. W., Lee, J., Lee, J.-S. & Min, K. Recent progress in formate dehydrogenase (FDH) as a non-photosynthetic CO<sub>2</sub> utilizing enzyme: A short review. *Journal of CO<sub>2</sub> Utilization* **42**, 101353 (2020).
136. Hartmann, T. & Leimkühler, S. The oxygen-tolerant and NAD<sup>+</sup>-dependent formate dehydrogenase from *Rhodobacter capsulatus* is able to catalyze the reduction of CO<sub>2</sub> to formate. *FEBS J* **280**, 6083–6096 (2013).
137. Maden, B. E. H. Tetrahydrofolate and Tetrahydromethanopterin Compared: Functionally Distinct Carriers in C<sub>1</sub> Metabolism. *Biochem. J* vol. 350 (2000).
138. Kikuchi, G., Motokawa, Y., Yoshida, T. & Hiraga, K. Glycine cleavage system: reaction mechanism, physiological significance, and hyperglycinemia. *Proceedings of the Japan Academy, Series B* **84**, 246–263 (2008).
139. Marx, C. J., Laukel, M., Vorholt, J. A. & Lidstrom, M. E. Purification of the Formate-Tetrahydrofolate Ligase from *Methylobacterium extorquens* AM1 and Demonstration of Its Requirement for Methylo-trophic Growth. *J Bacteriol* **185**, 7169–7175 (2003).
140. Lidstrom, M. E. Aerobic Methylo-trophic Prokaryotes. *The Prokaryotes* 618–634 (2006) doi:10.1007/0-387-30742-7\_20.
141. Marx, C. J. & Lidstrom, M. E. Development of an insertional expression vector system for *Methylobacterium extorquens* AM1 and generation of null mutants lacking *mtdA* and/or *fch*. *Microbiology (N Y)* **150**, 9–19 (2004).
142. Crowther, G. J., Kosály, G. & Lidstrom, M. E. Formate as the Main Branch Point for Methylo-trophic Metabolism in *Methylobacterium extorquens* AM1. *J Bacteriol* **190**, 5057–5062 (2008).
143. Sánchez-Andrea, I. et al. The reductive glycine pathway allows autotrophic growth of *Desulfovibrio desulfuricans*. *Nat Commun* **11**, (2020).
144. Claassens, N. J. Reductive Glycine Pathway: A Versatile Route for One-Carbon Biotech. *Trends Biotechnol* **39**, 327–329 (2021).
145. Anthony, C. *The Biochemistry of Methylo-trophs*. (Academic Press, 1982).
146. Anthony, C. How Half a Century of Research was Required to Understand Bacterial Growth on C<sub>1</sub> and C<sub>2</sub> Compounds; the Story of the Serine Cycle and the Ethylmalonyl-CoA Pathway. <https://doi.org/10.3184/003685011X13044430633960> **94**, 109–137 (2011).

147. Cordero, P. R. F. et al. Atmospheric carbon monoxide oxidation is a widespread mechanism supporting microbial survival. *The ISME Journal* 2019 13:11 **13**, 2868–2881 (2019).
148. Islam, Z. F. et al. Two Chloroflexi classes independently evolved the ability to persist on atmospheric hydrogen and carbon monoxide. *The ISME Journal* 2019 13:7 **13**, 1801–1813 (2019).
149. Greening, C., Berney, M., Hards, K., Cook, G. M. & Conrad, R. A soil actinobacterium scavenges atmospheric H<sub>2</sub> using two membrane-associated, oxygen-dependent [NiFe] hydrogenases. *Proc Natl Acad Sci U S A* **111**, 4257–4261 (2014).
150. Schäfer, C. et al. Structure of an Actinobacterial-Type [NiFe]-Hydrogenase Reveals Insight into O<sub>2</sub>-Tolerant H<sub>2</sub> Oxidation. *Structure* **24**, 285–292 (2016).
151. Dobbek, H., Gremer, L., Kiefersauer, R., Huber, R. & Meyer, O. Catalysis at a dinuclear [CuSMo(=O)OH] cluster in a CO dehydrogenase resolved at 1.1-Å resolution. *Proc Natl Acad Sci U S A* **99**, 15971–15976 (2002).
152. Greening, C., Berney, M., Hards, K., Cook, G. M. & Conrad, R. A soil actinobacterium scavenges atmospheric H<sub>2</sub> using two membrane-associated, oxygen-dependent [NiFe] hydrogenases. *Proceedings of the National Academy of Sciences* **111**, 4257–4261 (2014).
153. Cordero, P. R. F. et al. Two uptake hydrogenases differentially interact with the aerobic respiratory chain during mycobacterial growth and persistence. *Journal of Biological Chemistry* **294**, 18980–18991 (2019).
154. Rohde, M., Mayer, F. & Meyer, O. Immunocytochemical localization of carbon monoxide oxidase in *Pseudomonas carboxydovorans*. The enzyme is attached to the inner aspect of the cytoplasmic membrane. *Journal of Biological Chemistry* **259**, 14788–14792 (1984).
155. Grinter, R. et al. Structural basis for bacterial energy extraction from atmospheric hydrogen. *Nature* 2023 615:7952 **615**, 541–547 (2023).
156. Auman, A. J., Speake, C. C. & Lidstrom, M. E. nifH Sequences and Nitrogen Fixation in Type I and Type II Methanotrophs. *Appl Environ Microbiol* **67**, 4009–4016 (2001).
157. Khadem, A. F., Pol, A., Jetten, M. S. M. & Op den Camp, H. J. M. Nitrogen fixation by the verrucomicrobial methanotroph ‘*Methylacidiphilum fumariolicum*’ SolV. *Microbiology (N Y)* **156**, 1052–1059 (2010).
158. Hara, S. et al. In Vivo Evidence of Single <sup>13</sup>C and <sup>15</sup>N Isotope-Labeled Methanotrophic Nitrogen-Fixing Bacterial Cells in Rice Roots. *mBio* **13**, (2022).
159. Raymond, J., Siefert, J. L., Staples, C. R. & Blankenship, R. E. The Natural History of Nitrogen Fixation. *Mol Biol Evol* **21**, 541–554 (2004).

160. Seefeldt, L. C. et al. Reduction of Substrates by Nitrogenases. *Chemical Reviews* vol. 120 5082–5106 Preprint at <https://doi.org/10.1021/acs.chemrev.9b00556> (2020).
161. Poole, R. K. & Hill, S. Respiratory Protection of Nitrogenase Activity in *Azotobacter vinelandii* —Roles of the Terminal Oxidases. *Biosci Rep* **17**, 303–317 (1997).
162. Gallon, J. R. Reconciling the incompatible: N<sub>2</sub> fixation And O<sub>2</sub>. *New Phytologist* **122**, 571–609 (1992).
163. Gebhardt, C., Turner, G. L., Gibson, A. H., Dreyfus, B. L. & Bergersen, F. J. Nitrogen-fixing Growth in Continuous Culture of a Strain of *Rhizobium* sp. Isolated from Stem Nodules on *Sesbania rostrata*. *Microbiology (N Y)* **130**, 843–848 (1984).
164. Fay, P. Oxygen Relations of Nitrogen Fixation in Cyanobacteria. *MICROBIOLOGICAL REVIEWS* vol. 56 <https://journals.asm.org/journal/mr> (1992).
165. Schlesier, J., Rohde, M., Gerhardt, S. & Einsle, O. A Conformational Switch Triggers Nitrogenase Protection from Oxygen Damage by Shethna Protein II (FeSII). *J Am Chem Soc* **138**, 239–247 (2016).
166. Threatt, S. D. & Rees, D. C. Biological nitrogen fixation in theory, practice, and reality: a perspective on the molybdenum nitrogenase system. *FEBS Letters* vol. 597 45–58 Preprint at <https://doi.org/10.1002/1873-3468.14534> (2023).
167. Kalescky, R., Kraka, E. & Cremer, D. Identification of the strongest bonds in chemistry. in *Journal of Physical Chemistry A* vol. 117 8981–8995 (2013).
168. Roberts, G. P., Macneil, T., Macneil, D. & Brill, W. J. Regulation and Characterization of Protein Products Coded by the Nif (Nitrogen Fixation) Genes of *Klebsiella Pneumoniae*. *JOURNAL OF BACTERIOLOGY* <https://journals.asm.org/journal/jb> (1978).
169. Lukoyanov, D. et al. Reductive Elimination of H<sub>2</sub> Activates Nitrogenase to Reduce the N≡N Triple Bond: Characterization of the E<sub>4</sub>(4H) Janus Intermediate in Wild-Type Enzyme. *J Am Chem Soc* **138**, 10674–10683 (2016).
170. Ferrari, B. C., Binnerup, S. J. & Gillings, M. Microcolony cultivation on a soil substrate membrane system selects for previously uncultured soil bacteria. *Appl Environ Microbiol* **71**, 8714–8720 (2005).
171. Svenning, M. M., Warttinen, I., Hestnes, A. G. & Binnerup, S. J. Isolation of methane oxidising bacteria from soil by use of a soil substrate membrane system. *FEMS Microbiol Ecol* **44**, 347–354 (2003).
172. Burg, T. P. et al. Weighing of biomolecules, single cells and single nanoparticles in fluid. *Nature* **446**, 1066–1069 (2007).
173. Grover, W. H. et al. Measuring single-cell density. *Proceedings of the National Academy of Sciences* **108**, 10992–10996 (2011).

174. Feijó Delgado, F. et al. Intracellular Water Exchange for Measuring the Dry Mass, Water Mass and Changes in Chemical Composition of Living Cells. *PLoS One* **8**, e67590 (2013).
175. Lechene, C. et al. High-Resolution Quantitative Imaging of Mammalian and Bacterial Cells Using Stable Isotope Mass Spectrometry. <http://jbiol.com/content/5/6/20> (2006).
176. Herrmann, A. M. et al. Nano-scale secondary ion mass spectrometry - A new analytical tool in biogeochemistry and soil ecology: A review article. *Soil Biol Biochem* **39**, 1835–1850 (2007).
177. Deracinois, B., Flahaut, C., Duban-Deweere, S. & Karamanos, Y. Comparative and quantitative global proteomics approaches: An overview. *Proteomes* vol. 1 180–218 Preprint at <https://doi.org/10.3390/proteomes1030180> (2013).
178. Thompson, L. R. et al. A communal catalogue reveals Earth’s multiscale microbial diversity. *Nature* **551**, 457–463 (2017).
179. Gilbert, J. A., Jansson, J. K. & Knight, R. The Earth Microbiome project: Successes and aspirations. *BMC Biology* vol. 12 Preprint at <https://doi.org/10.1186/s12915-014-0069-1> (2014).
180. Gilbert, J. A. et al. Meeting Report: The Terabase Metagenomics Workshop and the Vision of an Earth Microbiome Project. *Stand Genomic Sci* **3**, 243–248 (2010).
181. Camacho, C. et al. BLAST+: Architecture and applications. *BMC Bioinformatics* **10**, (2009).
182. R Core Team. R: A Language and Environment for Statistical Computing. Preprint at <https://www.R-project.org/> (2022).
183. Ocko, I. B. & Hamburg, S. P. Climate consequences of hydrogen emissions. *Atmos Chem Phys* **22**, 9349–9368 (2022).
184. Dincer, I. Hydrogen 1.0: A new age. *International Journal of Hydrogen Energy* vol. 48 16143–16147 Preprint at <https://doi.org/10.1016/j.ijhydene.2023.01.124> (2023).
185. Avalos Ramirez, A., García-Aguilar, B. P., Jones, J. P. & Heitz, M. Improvement of methane biofiltration by the addition of non-ionic surfactants to biofilters packed with inert materials. *Process Biochemistry* **47**, 76–82 (2012).
186. Smith, S. J. et al. Impact of methane and black carbon mitigation on forcing and temperature: a multi-model scenario analysis. *Clim Change* **163**, 1427–1442 (2020).
187. Ocko, I. B. et al. Acting rapidly to deploy readily available methane mitigation measures by sector can immediately slow global warming. *Environmental Research Letters* **16**, (2021).

## **Publications**

# Paper 1



## Article

# Simultaneous Oxidation of Atmospheric Methane, Carbon Monoxide and Hydrogen for Bacterial Growth

Alexander Tøsdal Tveit <sup>1,\*</sup>,<sup>†</sup> , Tilman Schmider <sup>1,†</sup>, Anne Grethe Hestnes <sup>1</sup>, Matteus Lindgren <sup>2</sup>, Alena Didriksen <sup>1</sup> and Mette Marianne Svenning <sup>1</sup>

<sup>1</sup> Department of Arctic and Marine Biology, UiT, The Arctic University of Norway, 9037 Tromsø, Norway; tilman.schmider@uit.no (T.S.); anne.hestnes@uit.no (A.G.H.); alena.didriksen@uit.no (A.D.); mette.svenning@uit.no (M.M.S.)

<sup>2</sup> CAGE—Centre for Arctic Gas Hydrate, Environment and Climate, Department of Geosciences, UiT, The Arctic University of Norway, 9010 Tromsø, Norway; matteus.lindgren@uit.no

\* Correspondence: alexander.t.tveit@uit.no

† These authors contributed equally to this work.

**Abstract:** The second largest sink for atmospheric methane (CH<sub>4</sub>) is atmospheric methane oxidizing-bacteria (atmMOB). How atmMOB are able to sustain life on the low CH<sub>4</sub> concentrations in air is unknown. Here, we show that during growth, with air as its only source for energy and carbon, the recently isolated atmospheric methane-oxidizer *Methylocapsa gorgona* MG08 (USC $\alpha$ ) oxidizes three atmospheric energy sources: CH<sub>4</sub>, carbon monoxide (CO), and hydrogen (H<sub>2</sub>) to support growth. The cell-specific CH<sub>4</sub> oxidation rate of *M. gorgona* MG08 was estimated at  $\sim 0.7 \times 10^{-18}$  mol cell<sup>-1</sup> h<sup>-1</sup>, which, together with the oxidation of CO and H<sub>2</sub>, supplies 0.38 kJ Cmol<sup>-1</sup> h<sup>-1</sup> during growth in air. This is seven times lower than previously assumed necessary to support bacterial maintenance. We conclude that atmospheric methane-oxidation is supported by a metabolic flexibility that enables the simultaneous harvest of CH<sub>4</sub>, H<sub>2</sub> and CO from air, but the key characteristic of atmospheric CH<sub>4</sub> oxidizing bacteria might be very low energy requirements.

**Keywords:** methane; carbon monoxide; hydrogen; energy; growth; atmospheric trace gases



**Citation:** Tveit, A.T.; Schmider, T.; Hestnes, A.G.; Lindgren, M.; Didriksen, A.; Svenning, M.M. Simultaneous Oxidation of Atmospheric Methane, Carbon Monoxide and Hydrogen for Bacterial Growth. *Microorganisms* **2021**, *9*, 153. <https://doi.org/10.3390/microorganisms9010153>

Received: 1 December 2020

Accepted: 7 January 2021

Published: 12 January 2021

**Publisher's Note:** MDPI stays neutral with regard to jurisdictional claims in published maps and institutional affiliations.



**Copyright:** © 2021 by the authors. Licensee MDPI, Basel, Switzerland. This article is an open access article distributed under the terms and conditions of the Creative Commons Attribution (CC BY) license (<https://creativecommons.org/licenses/by/4.0/>).

## 1. Introduction

Atmospheric methane-oxidizing bacteria (atmMOB) remove 9–47 Tg methane (CH<sub>4</sub>) from the atmosphere annually [1]. The most common hypothesis for explaining how these bacteria can sustain life by oxidizing atmospheric CH<sub>4</sub> is the “high affinity” model, in which a special form of particulate CH<sub>4</sub> monooxygenase allows atmMOB to oxidize the low atmospheric CH<sub>4</sub> concentrations at a high rate [2]. Other hypotheses include the utilization of alternative energy sources or a high specific affinity ( $V_{\max(\text{app})}/K_{m(\text{app})}$ ) [3,4]. AtmMOB are found globally in soils [4] and belong to the two phylogenetic clusters USC $\alpha$  (Alphaproteobacteria) and USC $\gamma$  (Gammaproteobacteria) [5]. The lack of pure cultures from USC $\alpha$  and USC $\gamma$  has prevented studies of the energy metabolism of atmMOB [3]. Conventional methane oxidizing bacteria (MOB) are expected to oxidize around  $0.2\text{--}17 \times 10^{-18}$  mol CH<sub>4</sub> cell<sup>-1</sup> h<sup>-1</sup> at atmospheric CH<sub>4</sub> concentrations at 25 °C, but such rates have been considered too low to provide sufficient energy for growth [6]. Thus, atmMOB were expected to either utilize alternative energy sources or have high affinities for CH<sub>4</sub> [3]. The latter is supported by observations reporting apparent high affinity CH<sub>4</sub> oxidation by microbial communities in oxic soils [7]. Additionally, oxidation rates of  $800 \times 10^{-18}$  mol CH<sub>4</sub> cell<sup>-1</sup> h<sup>-1</sup> were measured in forest soils, far surpassing the cell-specific activity of  $40 \times 10^{-18}$  mol CH<sub>4</sub> cell<sup>-1</sup> h<sup>-1</sup> assumed to be necessary to support minimum cell maintenance requirements [6,8]. At 20 °C, these minimum requirements would demand an energy supply of 2.8 kJ Cmol h<sup>-1</sup>. It is assumed that the high forest soil rates at atmospheric CH<sub>4</sub> concentrations are achieved by the combination of methane

monoxygenases (MMO) with very low half-saturation constants ( $K_m$ ) and high cellular abundances of these enzymes.

The recently described USC $\alpha$  atmMOB species *Methylocapsa gorgona* MG08 has the highest specific affinity ( $V_{\max(\text{app})}/K_{m(\text{app})}$ ) for CH<sub>4</sub> of all tested MOB at  $195 \times 10^{-12}$  L·cell<sup>-1</sup>·h<sup>-1</sup>. However, this translates into a cell-specific CH<sub>4</sub> oxidation rate of only  $10 \times 10^{-18}$  mol CH<sub>4</sub> cell<sup>-1</sup> h<sup>-1</sup> at atmospheric CH<sub>4</sub> concentration [4], seemingly too low to support cellular maintenance [6]. Nevertheless, *M. gorgona* MG08 is able to grow at atmospheric (1.87 p.p.m.v.) CH<sub>4</sub> concentrations [4]. It also carries a [NiFe] group 1 h high-affinity respiratory hydrogenase (*hhyL* and *hhyS*) and a [MoCu] class I respiratory carbon monoxide dehydrogenase, similar to those identified in atmospheric carbon monoxide (CO) and hydrogen (H<sub>2</sub>)-oxidizing microorganisms [4,9–12]. Recent studies have identified the utilization of atmospheric CO and H<sub>2</sub> as energy sources for growth and survival in bacteria [9,11–13], and as support for bacterial primary production in Antarctic and Arctic environments [10,14]. Atmospheric CH<sub>4</sub> concentrations are currently 1.87 p.p.m.v. [15], while the concentrations of atmospheric CO and H<sub>2</sub> are lower. CO concentrations vary, with estimates for uninhabited areas around 0.1 p.p.m.v., while urban areas contain higher concentrations, often above 0.2 p.p.m.v. [16–19]. Atmospheric H<sub>2</sub> concentrations are stable at approximately 0.53 p.p.m.v. [20]. Many MOB carry genes for carbon monoxide and hydrogen oxidation [4], and recently it has been shown that the thermoacidophilic *Methylococcus thermophilus* SolV can oxidize sub-atmospheric H<sub>2</sub> with a high-affinity, membrane-associated [NiFe] hydrogenase [21], while the strain *Methylocystis* sp. SC2 oxidizes hydrogen at higher concentrations [22]. However, the oxidation of atmospheric CO and H<sub>2</sub> to support growth has never been demonstrated for *M. gorgona* MG08 or any other MOB. We have studied how the atmospheric CH<sub>4</sub> oxidizer *M. gorgona* MG08, in pure culture, harvests energy from the atmosphere for growth.

## 2. Materials and Methods

### 2.1. Cultivation

A young stationary culture of *M. gorgona* MG08 was prepared as follows. A 20 mL culture (1:10 (NMS:MilliQ) in diluted liquid nitrate mineral salts (NMS) medium (pH 6.8) (DSMZ medium 921) without EDTA) with a headspace of 20% CH<sub>4</sub> in air (20 mL 100% CH<sub>4</sub> mixed with 80 mL of air) was incubated for 12 days, reaching several days (2–4) into the stationary phase. Inoculum from this culture was precultured in 1:10 (NMS:MilliQ) diluted liquid nitrate mineral salts (NMS) medium (pH 6.8) (DSMZ medium 921) without EDTA under a headspace atmosphere of ~20 p.p.m.v. CH<sub>4</sub> in air for two weeks. The headspace was created by injecting 20  $\mu$ L of 100% CH<sub>4</sub> into the 100 mL ambient air headspace of 120 mL serum bottles containing 20 mL medium, sealed with a butyl rubber stopper and crimp cap. This was used as a start culture for colony growth on filters. The cell concentration in the suspension was determined by fluorescence microscopy after filtration on Anodisc filters (Whatman 6809-6022, Merck, Darmstadt, Germany) and 1000 $\times$  SYBRgreen I (Molecular probes S-7567, ThermoFisher, Waltham, MA, USA) staining as previously described [4]. For staining, filters were transferred (bacteria side up) on top of 200  $\mu$ L droplets of 1000 $\times$  SYBRgreen and incubated for 10 minutes. In the next step, filters were washed twice by transferring them onto 1 mL milliQ water and then air-dried. The whole procedure was performed at room temperature and in the dark. A fresh-made anti-fading solution consisting of 0.1% p-phenylenediamine dihydrochloride in 1:1 glycerol and PBS (phosphate buffered saline pH 7.2) was used for mounting the filters on slides with cover slips.

From the start cultures, the required volume and cell density needed to achieve a cell density of ~20 cells per 63 $\times$  photo area, for a total of ~1  $\times$  10<sup>6</sup> cells per filter, was selected for filter cultivation. For the transfer of cells onto the 47 mm polycarbonate filter, an autoclaved Millipore vacuum filter holder system (cat no XX1004700, Merck, Darmstadt, Germany) with 300 mL glass funnels was used. Firstly, a GF/C filter (Whatman 1822-047, Merck, Darmstadt, Germany) was added as support filter. A polycarbonate filter

(Whatman, Nucleopore 111106, Merck, Darmstadt, Germany) was then added and the funnel was clamped on top. Even distributions of cells on the filters were obtained by pouring 100 mL of autoclaved milliQ-water into the funnel before mixing in 0.1 mL of the start culture cell suspension and applying vacuum. The funnel walls were rinsed twice with 15 mL sterile water during suction. The polycarbonate filters were then transferred into 250 mL bottles (DURAN, Merck, Darmstadt, Germany) in a Holten LaminAir bench and left floating on 50 mL of 1:10 (NMS:MilliQ) diluted liquid NMS medium (pH 6.8) without EDTA. Finally, the bottles were covered with gas permeable parafilm (Merck, Darmstadt, Germany). These bottles were incubated in a ventilated room at 20 °C in darkness for nine months (experiment 1) or 4.5 months (experiment 2), after which the gas uptake experiments were initiated. In Experiment 1, an additional inspection of a filter was performed after eight months. This included a visual inspection and counting of 60 colonies on two different filters to show that the number of generations in almost all growing colonies had surpassed seven (64 cells), indicating that the filters had sufficient biomass to initiate gas uptake experiments.

## 2.2. Temperature Selection

All cultivations and experiments were carried out at 20 °C. This temperature was chosen as it is in the middle of the optimum temperature range for growth (~15–~27 °C) of *M. gorgona* MG08 and was the temperature at which previous experiments were carried out [4].

## 2.3. Gas Uptake and Leakage Experiments

Three experiments were carried out: two gas uptake experiments that included controls and one control experiment. Experiment 1 consisted of 53 × 120 mL bottles, some containing cultures of *M. gorgona* MG08 on filters floating on liquid media. Experiment 2 consisted of 15 bottles. The control experiment consisted of 18 bottles.

In all experiments, the bottles contained 50 mL of 1/10 diluted NMS medium without EDTA. All gases used were of the highest available quality (6.0) (all gases were supplied by AGA). For the first gas uptake experiment, a total of 7 different setups (A–G) of five replicates each were created: A–E contained filters with *M. gorgona* MG08 cells, and F and G did not contain *M. gorgona* MG08 cells. (A) five bottles with 2–4 p.p.m.v. CH<sub>4</sub>, 2–4 p.p.m.v. H<sub>2</sub> and 2–4 p.p.m.v. CO in synthetic air. (B) five bottles with 2–4 p.p.m.v. H<sub>2</sub> and 2–4 p.p.m.v. CO in synthetic air; (C) five bottles with 2–4 p.p.m.v. CH<sub>4</sub> in synthetic air. (D) five bottles with an atmosphere of ambient air (compressed outdoor air); (E) five bottles with synthetic air. (F) five bottles with 2–4 p.p.m.v. CH<sub>4</sub>, 2–4 p.p.m.v. H<sub>2</sub> and 2–4 p.p.m.v. CO in synthetic air. (G) five bottles with ambient air atmosphere.

For the second gas uptake experiment, one condition included cells; five bottles with ~4 p.p.m.v. CH<sub>4</sub>, ~4 p.p.m.v. H<sub>2</sub> and ~4 p.p.m.v. CO in synthetic air. Two conditions included sterile filters; five bottles with ~4 p.p.m.v. CH<sub>4</sub>, ~4 p.p.m.v. H<sub>2</sub> and ~4 p.p.m.v. CO in synthetic air and five bottles with synthetic air atmospheres.

The control experiment to determine gas leakages (18 bottles) included six different types of liquids and headspace compositions: (A) 50 mL MilliQ water and 200 mL headspace of pure helium. (B) Sterile floating polycarbonate filter on 50 mL of 1/10 diluted NMS medium without EDTA and 200 mL headspace with 2–5 p.p.m.v. CH<sub>4</sub>, H<sub>2</sub>, CO in synthetic air. (C) 50 mL of milliQ water and synthetic air. (D) 50 mL of 1/10 diluted NMS medium without EDTA and 2–5 p.p.m.v. CH<sub>4</sub>, H<sub>2</sub>, CO in synthetic air. (E) 50 mL of milliQ water and 2–5 p.p.m.v. CH<sub>4</sub>, H<sub>2</sub>, CO in synthetic air. (F) Empty glass bottle with 250 mL of 2–5 p.p.m.v. CH<sub>4</sub>, H<sub>2</sub>, CO in synthetic air.

To create the mentioned atmospheres, the bottles were sealed with halogenated bromobutyl rubber stoppers (DURAN, Merck, Darmstadt, Germany) and plastic screw caps under a sterile bench. Before usage, the rubber stoppers had been boiled ten times and then autoclaved. The sealed bottles were flushed for 15 min with ambient, high quality synthetic air (N<sub>2</sub>: 78%, O<sub>2</sub>: 21%, CO<sub>2</sub>: 400 p.p.m.v.) or pure helium by using a gassing manifold

connected to sterile single-use needles. The final pressure in the bottles was adjusted to one bar absolute pressure. Afterwards, 1 mL of additional respective gases (CH<sub>4</sub>, CO and H<sub>2</sub>) was added by using a gas tight syringe (VICI AG International, Schenkon, Switzerland) to create the required atmospheres. To prevent contamination, each gassing step was carried out by interconnecting a sterile 0.2 µm cellulose acetate filter (VWR Collection, Lutterworth, UK) between needle and hose or syringe.

The prepared bottles were incubated at 20 °C for 57 days in the first experiment. The headspace concentrations of CH<sub>4</sub>, CO and H<sub>2</sub> were measured the day after preparing the headspace atmospheres and after 7, 17 and 57 days. In the second experiment, the incubation lasted 145 h. In the control experiment, the incubations lasted 6, 54 or 70 days.

For combined measurements of CH<sub>4</sub>, CO and H<sub>2</sub>, 1 mL headspace gas was sampled with a gastight GC syringe (VICI AG International, Schenkon, Switzerland). The contained gas was injected manually into a gas chromatograph (ThermoScientific Trace 1310 with column TG-BOND Msieve 5A, ThermoFisher, Waltham, MA, USA). Detection was achieved by using a PDD detector. A high-quality gas containing 5 p.p.m.v. H<sub>2</sub>, 5 p.p.m.v. CH<sub>4</sub>, and 5 p.p.m.v. CO in N<sub>2</sub> served as standard. To create standard curves, 2 × 0.1 mL, 2 × 0.5 mL, and 2 × 1 mL of the mentioned standard were injected on every measurement day. Bottle gas concentrations were calculated using the standard curve. Masses were calculated by applying the ideal gas law and adjusted for changes in bottle pressure due to gas removal.

#### 2.4. Cell Quantification

Due to several layers of cells forming colonies on the filters after 9 months and 57 days of incubation, the number of cells on four filters per condition A–E in the gas uptake experiment could not be estimated reliably by cell counts. Instead, cell numbers were estimated using DNA extractions and comparison to a standard of DNA extraction yields for known cell numbers of *M. gorgona* MG08 on polycarbonate filters. Cells for a standard were prepared as follows. A 20 mL culture (1:10 (NMS:MilliQ) diluted liquid nitrate mineral salts (NMS) medium (pH 6.8) (DSMZ medium 921) without EDTA) with a headspace of 20% CH<sub>4</sub> in air (20 mL 100% CH<sub>4</sub> mixed with 80 mL of air) was incubated for 12 days, reaching several days (2–4) into the stationary phase. The culture was then exposed to atmospheric concentrations of CH<sub>4</sub> for one additional day during which the number of cells in the culture was estimated using cell counts. Then, the cells were filtered out and the filters were prepared for extractions. With this approach, our aim was to extract DNA from cells in a slow growth state where the cells do not contain multiple partial genomes. Filters for the standard and those from the experiment incubation were cut into 12 pieces and put into 2 mL safelock tubes, after which DNA was extracted from the filters using DNA IQ™ Casework Pro Kit for Maxwell® 16 following the manufacturer's instructions. In brief, we crushed the 12 filter pieces with a metal bead in a tissue lyser (Qiagen, Hilden, Germany) six times, 30 s each, applying liquid nitrogen prior to the first and between each round in the tissue lyser. Prior to extraction, the crushed pieces were spun down. After, 400 µL of extraction buffer containing proteinase K and thioglycerol followed by 400 µL lysis buffer was added. Then, the mixture was transferred into a cartridge of the Maxwell 16 system and processed. DNA extracts were quantified using Qubit (dsDNA HS Assay, Thermo Fisher, Waltham, MA, USA). Cell numbers on filters from the experiment were subsequently determined by comparing the extract yields per filter to those of the standard, converting the values from nanograms of DNA to cell numbers.

#### 2.5. Contamination Tests and Microscopy

In addition to the start of the pre-incubation and after eight months, we inspected filters by fluorescence microscopy at the beginning and end of the first gas uptake experiment. At the end of the experiment, one filter from each of the five treatments was used for contamination tests and fluorescence microscopy. For the second gas uptake experiment, we inspected filters at the beginning and end of the pre-incubation after 4.5 months, in addition to contamination tests after the experiment. Preparation for fluorescence mi-

croscopy was carried out as described for the pre-incubation above. Contamination tests were carried out by cutting filters in pieces and placing them on TGYA plates for 15 days. TGYA plates contained 5 g tryptone, 2.5 g of yeast extract, 1 g of glucose, and 20 g of agar per 1 L of water. Presence and growth of heterotrophic microorganisms was then evaluated by visual inspection. The contamination tests were negative and cell sizes and cell shapes were the same as prior to the experiment, confirming the purity of the culture.

## 2.6. Plotting and Statistics

All plotting was performed using the R [23] package ggplot2 [24].

## 2.7. Cell-Specific Oxidation Rates and Free Energy Yield Calculations

Oxidation rates were estimated by first order rate kinetics models. We log transformed the concentrations over time and fitted linear regression models to the transformed plots. The slope of the linear models corresponds to the rate constants. By multiplying the respective rate constant by the atmospheric concentrations of CH<sub>4</sub>, H<sub>2</sub> and CO, we obtained the rates of oxidation at atmospheric gas concentrations. The fit of the linear models was evaluated and considered to have satisfactory coefficients of determination, giving the following values:  $R^2 - \text{CH}_4 = 0.93$ ,  $R^2 - \text{H}_2 = 0.82$ ,  $R^2 - \text{CO} = 0.68$  (Experiment 1), and  $R^2 - \text{CH}_4 = 0.99$ ,  $R^2 - \text{H}_2 = 0.99$ ,  $R^2 - \text{CO} = 0.99$  (Experiment 2). The oxidation rates of H<sub>2</sub> and CO were subsequently corrected by adjusting for the abiotic gas leakages. Due to the first order rate kinetics nature of the CO ( $R^2$  of linear models = 0.77,  $n = 5$ ) and H<sub>2</sub> ( $R^2$  of linear models = 0.99,  $n = 5$ ) leakages, their respective rate constants were estimated the same way as for the oxidation rates. The rate constants for the biological H<sub>2</sub> and CO oxidation were subsequently adjusted by subtracting or adding the rate constants of the leaks of H<sub>2</sub> (leakage out of the bottle) and CO (leakage into), respectively. For each condition A, B, C, D and E, cell numbers on three filters were estimated. Cell-specific oxidation rates were subsequently calculated by dividing the estimated oxidation rates by the corresponding cell numbers.

The expected maintenance requirements at 20 °C were calculated according to Tjihuis et al. [8]. The Gibbs free energy changes ( $\Delta_r G$ ) were calculated for the following reactions and Gibbs free energies of formation  $\Delta G_f^\circ$  (kJ/mol), assuming atmospheric concentrations and 20 °C: [CH<sub>4</sub> + 2O<sub>2</sub> → CO<sub>2</sub> + 2H<sub>2</sub>O]; [2CO + O<sub>2</sub> → 2CO<sub>2</sub>]; [2H<sub>2</sub> + O<sub>2</sub> → 2H<sub>2</sub>O]. CO: −137.16 kJ/mol, O<sub>2</sub>: 0 kJ/mol, CO<sub>2</sub>: −394.39 kJ/mol, H<sub>2</sub>: 0 kJ/mol, H<sub>2</sub>O: −237.13 kJ/mol, CH<sub>4</sub>: −50.6 kJ/mol. From the oxidation rates and free energy change of the reactions, we could estimate the amount of energy obtained per mol of biomass carbon per hour, applying the dry weight and carbon content of *M. gorgona* MG08 (see below) as previously shown [2,6]. All calculations, raw data and literature data needed for input in the calculations are provided in a detailed format. The data and calculations are provided as excel formulas that can be intuitively followed and inspected. These can serve as a template for those wishing to repeat our calculations for similar experiments and compare those to our data (See Supplementary dataset Table S1, tabs “Experiment 1”, “Experiment 2”, “Gibbs\_free\_energy” and “Maintenance\_energy”).

## 2.8. Estimating Cell Dry Weight

In order to estimate the dry weight of *M. gorgona* MG08, we cultivated 10 × 10 mL of *M. gorgona* MG08 culture as described for a young stationary culture in the cultivation section above. This provided ten replicates from which 1 mL was used for cell counts and 9 mL for drying overnight at 110 °C. Based on this, we calculated that the weight of one *M. gorgona* MG08 cell is  $8.8 \times 10^{-14}$  g dry weight per cell (SD =  $3.1 \times 10^{-14}$ ). We assume that half of the cell consists of carbon [2]. This weight and size (length 1.2 μm and width 0.7 μm) makes *M. gorgona* MG08 the lightest known Alphaproteobacteria MOB, compared to previously weighed strains [2]. While the size of *M. gorgona* MG08 cells do not change when growing with air as its energy and carbon source, compared to higher CH<sub>4</sub> concentrations (it retains its size of length ~1.2 μm and width ~0.7 μm), we acknowledge

that the content, density and thus dry weight of the cells growing in air may differ from that of *M. gorgona* MG08 cultivated at high CH<sub>4</sub> concentrations. Such differences could affect the estimates of kJ Cmol h<sup>-1</sup>. However, due to the low biomass, we were not able to estimate cell weights from filters cultivated in air.

### 3. Results and Discussion

Cells of *M. gorgona* MG08 were pre-incubated on filters under an atmosphere of ambient air (~1.84 p.p.m.v. CH<sub>4</sub>, ~0.39 p.p.m.v. CO and ~0.7 p.p.m.v. H<sub>2</sub>) for eight months. The filters floated on diluted mineral medium within bottles to enable optimal gas transfer. After four months, a subset of the cells had developed into microcolonies of more than 100 cells (Figure 1), while some cells had not divided. Visual inspection and counting showed that the number of generations in the majority of the colonies had surpassed seven (64 cells) (Figure 1C), matching previous observations [4]. Studies have shown that up to three generations can be supported by intracellular storages [4,25,26], confirming that the eight-month pre-incubation was sufficient to ensure growth with carbon and energy harvested solely from air. After nine months of pre-incubation, the filter-containing glass bottles were sealed with rubber stoppers before defined headspace atmospheres were created (Figure 2).

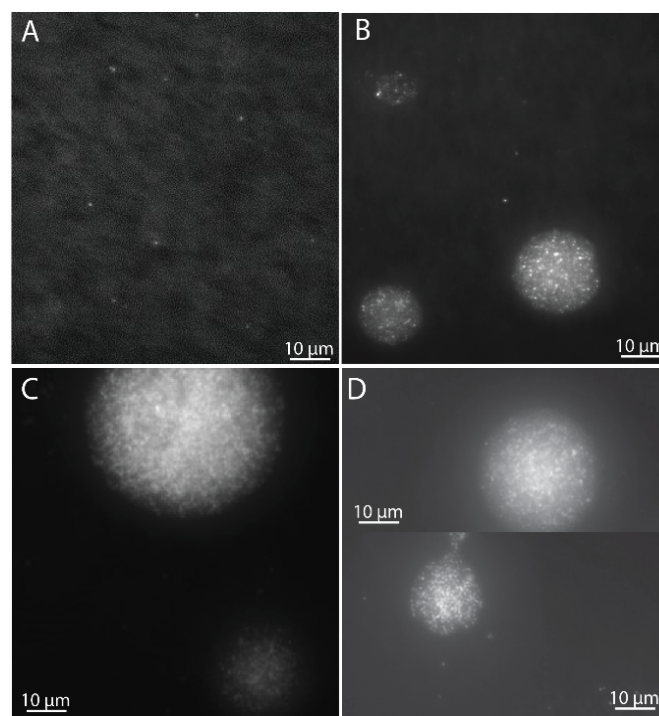


**Figure 1.** Microcolony growth of *M. gorgona* MG08 at different times during pre-incubation and gas uptake experiments. (A) Cells after filtration on polycarbonate filters, prior to incubation. (B) Microcolonies after 4 months of pre-incubation under ambient air. (C) Microcolonies after 8 months of pre-incubation under ambient air. (D) Microcolonies after 9 months of pre-incubation under ambient air and 57 days of gas uptake experiment incubation under synthetic air ((D), upper panel), and synthetic air + 2–4 p.p.m.v. CH<sub>4</sub>, CO and H<sub>2</sub> ((D), lower panel). For fixation, the filters were transferred to fresh-made 2% paraformaldehyde in 1× PBS in the refrigerator overnight. For staining, filters were transferred (side with bacteria up) on top of 200 μL droplets of 1000× SYBRgreen I (10× dilution of the stock concentration provided by Thermo Fisher Scientific, Invitrogen, Molecular probes) and incubated for 10 min, washed, and air dried.

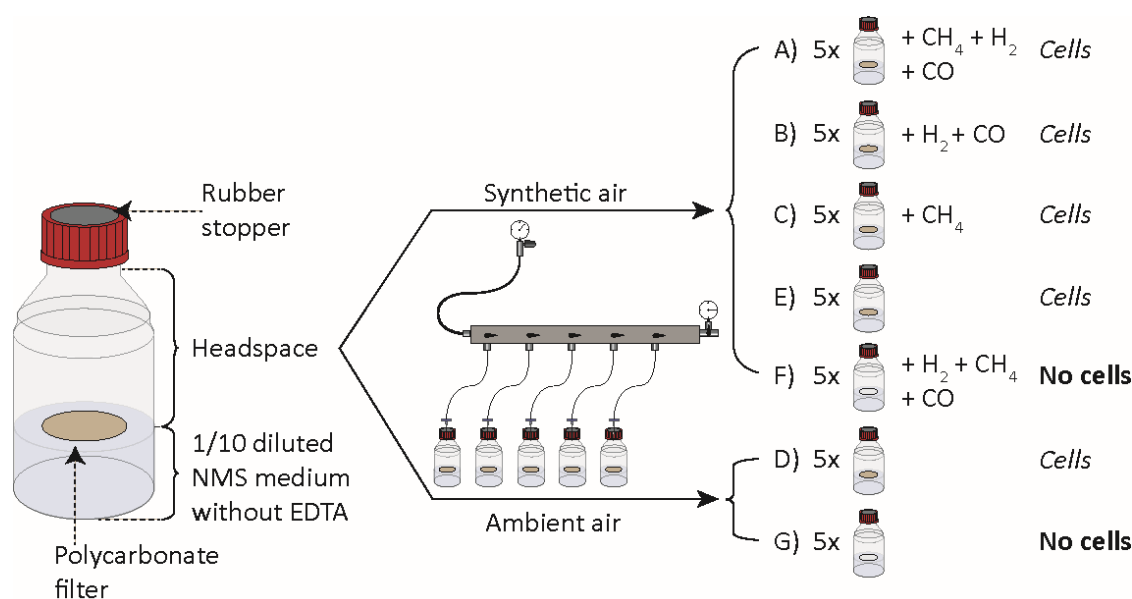


**Figure 2.** Experimental setup for experiment 1 to determine gas uptake by *M. gorgona* MG08. NMS: Nitrate mineral salts. Synthetic air containing less than 0.2 p.p.m.v. of CH<sub>4</sub>, CO and H<sub>2</sub>. Ambient air containing 1.84 p.p.m.v. CH<sub>4</sub>, 0.4 p.p.m.v. CO and 0.7 p.p.m.v. H<sub>2</sub>. All injections of CH<sub>4</sub>, CO and H<sub>2</sub> resulted in a final concentration between 2 and 4 p.p.m.v of the respective gas.

In a 57-day experiment, we could show that *M. gorgona* MG08 is able to oxidize ambient air to sub-atmospheric concentrations of CH<sub>4</sub> and H<sub>2</sub> (Figure 3). In several of the incubations, CH<sub>4</sub> and H<sub>2</sub> concentrations reached below atmospheric levels already after 7 days, while CO concentrations did not decrease below ~0.45 p.p.m.v., which is close to the atmospheric levels in urban areas [16–19] and similar to the average ambient air concentrations measured in the laboratory (0.39 p.p.m.v.). Furthermore, the CH<sub>4</sub> oxidation rates did not depend on the CO and H<sub>2</sub> concentrations (Figure 3A,C,D), while CO and H<sub>2</sub> oxidation proceeded without the presence of CH<sub>4</sub> (Figure 3B).

The stabilization of the CO concentrations around 0.45 p.p.m.v. in bottles with *M. gorgona* MG08 cells, irrespective of the start concentrations, was unexpected (Figure 3A,B,D,E). In the cell-free controls, we observed increasing CO concentrations, reaching 2 p.p.m.v. during 57 days of incubation (Figure 3F,G), suggesting these observations to be due to an abiotic CO source. To identify the CO source, we measured CO, H<sub>2</sub> and CH<sub>4</sub> in several cell-free controls, including empty bottles (Figure 4). CO accumulation was detected in these liquid-free bottles, and even in headspaces exposed to only glass and rubber stoppers. Thus, we concluded that CO was released from the rubber stoppers, meaning that the stabilization of CO concentrations at ~0.45 p.p.m.v. in the presence of *M. gorgona* MG08 was a confirmation of continuous CO oxidation at near ambient air concentrations of ~0.45 p.p.m.v. The decreasing or increasing CH<sub>4</sub> and H<sub>2</sub> concentrations in abiotic controls (Figure 3F,G and Figure 4A–F), on the other hand, could be explained by leakage during long incubation times, as previously observed [27,28]. In addition to the fact that such long-term leakages have been observed previously, the rationale for this conclusion is that the concentrations inside the bottles always increased when the outside concentrations were higher, and decreased when the outside concentrations were lower.

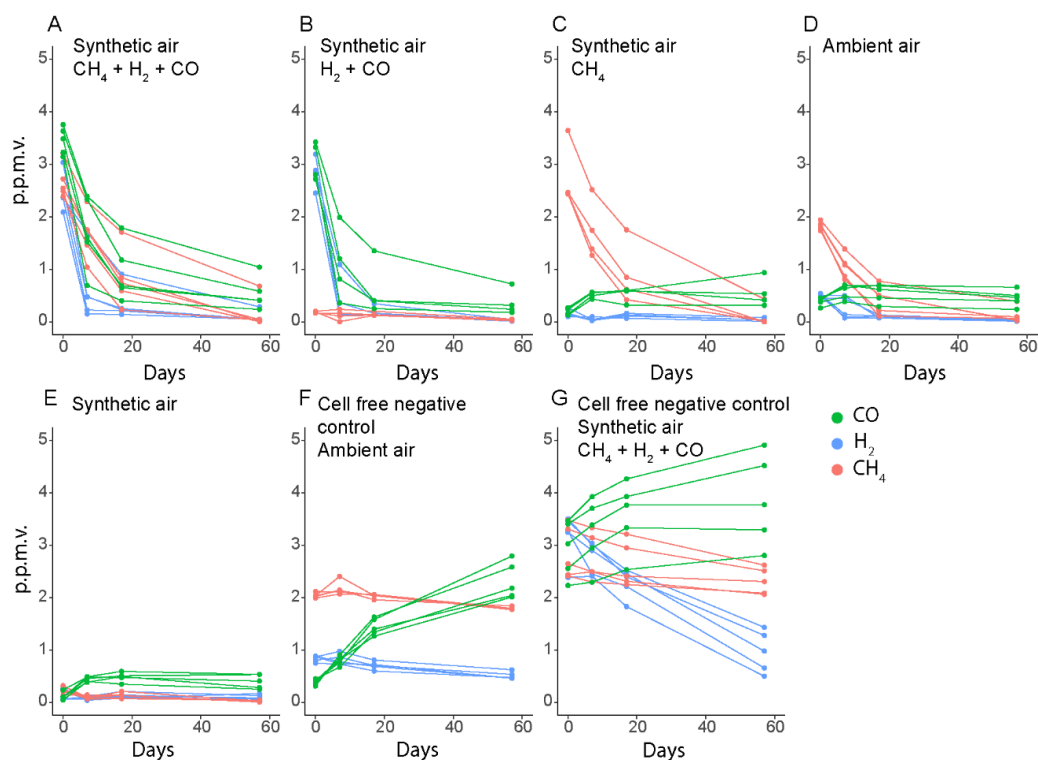


**Figure 3.** Oxidation of CH<sub>4</sub>, CO, and H<sub>2</sub> by *M. gorgona* MG08. (A–E) contained polycarbonate filters with *M. gorgona* MG08 floating on nitrate mineral salts medium. (F,G) contained sterile filters. The lower H<sub>2</sub> concentrations at the start of the ambient air incubations with cells (D) compared to those without cells (F) are due to leaving prepared bottles overnight before measuring the first time point T<sub>0</sub>, allowing some oxidation to already occur. All gases used were of the highest commercially available quality, 6.0 (99.9999% purity). The multiple data points in each color represent different biological replicates from the same condition. Synthetic air contained less than 0.2 p.p.m.v. of CH<sub>4</sub>, CO and H<sub>2</sub>.

#### Cell-Specific Oxidation Rates and Energy Yield

In order to estimate the CH<sub>4</sub>, CO and H<sub>2</sub> uptake rates by *M. gorgona* MG08 at atmospheric concentrations, we tested and confirmed that the rate change of CH<sub>4</sub> uptake fulfilled the assumptions of first order rate kinetics (linear regression through the natural logarithm (LN) of rates over time  $R^2 = 0.93$ ,  $n = 15$ ). As microcolonies contained more than one layer of cells, filter cell counts were not possible. Instead, we performed DNA extractions and cell quantification with a DNA to cell count standard for a subset of the incubation bottles, showing that all but one floating filter contained between 38.1 and 68 million cells (Table S1). Based on these estimates, we calculated the cellular CH<sub>4</sub> oxidation rates at atmospheric CH<sub>4</sub> concentrations to  $0.7\text{--}2.8 \times 10^{-18}$  mol cell<sup>-1</sup> h<sup>-1</sup> at 20 °C ( $n = 9$ ). Similarly, the H<sub>2</sub> and CO oxidation rates at atmospheric concentrations (average H<sub>2</sub> linear model  $R^2 = 0.82$ ,  $n = 10$ , CO  $R^2 = 0.68$ ,  $n = 10$ ) were estimated to be  $0.17\text{--}0.36$  and  $0.20\text{--}0.34 \times 10^{-18}$  mol cell<sup>-1</sup> h<sup>-1</sup>, respectively ( $n = 6$ ). These rates were corrected for the leakage and release of H<sub>2</sub> and CO, respectively. The CH<sub>4</sub> oxidation rates reflect the lower end of the atmospheric oxidation rates estimated for conventional MOB, which range from  $0.2$  to  $17 \times 10^{-18}$  mol cell<sup>-1</sup> h<sup>-1</sup> at 25 °C [6]. However, the rates of conventional MOB forming the basis for these estimates were measured at high CH<sub>4</sub> concentrations and thus do not necessarily represent the rates that would be obtained at atmospheric conditions.

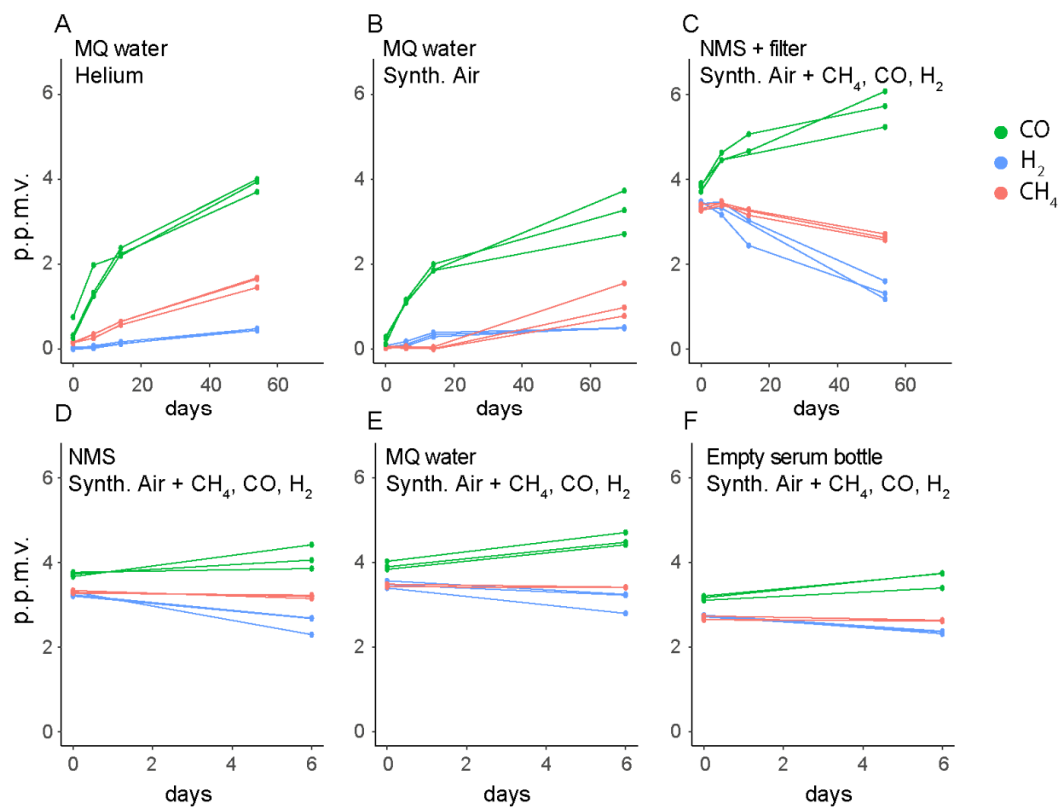


**Figure 4.** Gas leakage and other abiotic gas sources. (A,B) Long incubations of cell-free controls were performed to identify signs of CO and CH<sub>4</sub> leakage or release into or out of the bottles. (C–F) Short incubations of cell-free controls were considered sufficient to identify the same patterns of gas leakage and accumulation irrespective of bottle liquid and headspace composition. MQ: MilliQ. Synth. Air: Synthetic air. NMS: nitrate mineral salts. The multiple data points in each color represent different biological replicates from the same condition. Synthetic air contained less than 0.2 p.p.m.v. of CH<sub>4</sub>, CO and H<sub>2</sub>.

Based on the specific affinity estimated from oxidation rates at higher than atmospheric concentrations, the expected cell-specific CH<sub>4</sub> oxidation rate at atmospheric concentrations can be calculated [2]. From the oxidation rates measured at concentrations between 823 p.p.m.v. and 6% [4], we found that *M. gorgona* MG08 would have a cell specific CH<sub>4</sub> oxidation rate of  $10 \times 10^{-18}$  mol cell<sup>-1</sup> h<sup>-1</sup> when growing at atmospheric concentrations. However, these estimates are more than five times higher than the actual rate measurements at atmospheric concentrations provided in our current study. Thus, *M. gorgona* MG08 may not sustain the same catalytic properties or amount of particulate methane monooxygenase (pMMO) enzymes per cell during growth in air. At concentrations between 823 p.p.m.v. and 6%, we estimated the  $K_{m(\text{app})}$  of *M. gorgona* MG08 to be 4.905 [4], similar to that of various, presumed low affinity, MOB [2]. Although this indicated that *M. gorgona* MG08 has a low affinity for CH<sub>4</sub>, the dependency of  $K_{m(\text{app})}$  on the  $V_{\text{max}}$  prevents us from determining the exact affinity unless we perform comparative kinetic experiments for purified enzymes from several MOB strains, or compare the CH<sub>4</sub> oxidation rates and pMMO concentrations of several different MOB. Thus, it seems plausible that life at atmospheric CH<sub>4</sub> concentrations can be sustained by low affinity enzymes, but it is still uncertain whether this is the case.

The energy yields per mol of CH<sub>4</sub>, CO and H<sub>2</sub> under the provided experimental conditions (ambient air at 20 °C) were approximately −814, −522 and −472 kJ/mol, respectively, assuming the following reactions: [CH<sub>4</sub> + 2O<sub>2</sub> → 2H<sub>2</sub>O + CO<sub>2</sub>], [2CO + O<sub>2</sub> → 2CO<sub>2</sub>], [2H<sub>2</sub> + O<sub>2</sub> → 2H<sub>2</sub>O]. Based on the measured rates, we find that *M. gorgona* MG08 is able to conserve approximately 0.47 kJ Cmol h<sup>-1</sup> from the combined oxidation of CH<sub>4</sub>, H<sub>2</sub> and CO

during growth in air at 20 °C (see data and full calculation in Table S1). This calculation implements our dry weight estimates for *M. gorgona* MG08 (Table S1). Interestingly, these estimates show that *M. gorgona* MG08 cells (length ~1.2 µm and width ~0.7 µm) are three times lighter ( $0.88 \times 10^{-13}$  gDW cell<sup>-1</sup>) than the lightest reported MOB [2]. The mass of a cell could affect its energy budget, as more energy might be needed to supply maintenance in a heavier cell, leaving less for growth. Additionally, a heavier cell might require more energy for growth. Thus, the low weight of *M. gorgona* MG08 may reflect a strategy to reduce energy costs for growth. In contrast to our findings, the previously reported soil CH<sub>4</sub> oxidation rates of  $800 \times 10^{-18}$  mol cell<sup>-1</sup> h<sup>-1</sup> [6] would provide 179 kJ Cmol h<sup>-1</sup>. In order to examine this contradiction and test the validity of our data, we repeated parts of our experiment (condition with 5 p.p.m.v. of each gas CH<sub>4</sub>, H<sub>2</sub> and CO) with shorter pre-incubation (4.5 months) to minimize growth stagnation and the possibility for the accumulation of dead cells on the floating filters.

Furthermore, we shortened the gas uptake experiment to less than one week of incubation to prevent gas leakage effects on rate estimates. This new setup provided highly precise estimates of CH<sub>4</sub>, H<sub>2</sub> and CO uptake rates (Figure 5), which confirmed their first order nature (linear regression through LN of rates over time; CH<sub>4</sub>  $R^2 = 0.99$ ,  $n = 5$ ; H<sub>2</sub>  $R^2 = 0.99$ ; CO  $R^2 = 0.99$ ). Within this timeframe, the leakage of H<sub>2</sub> and CH<sub>4</sub> was negligible (Figure 5B,C), but the release of CO from the rubber stoppers occurred and was corrected for. Interestingly, similar but slightly lower cellular oxidation rates at atmospheric gas concentrations were estimated. The CH<sub>4</sub> uptake ranged from 0.32 to  $1.3 \times 10^{-18}$  mol cell<sup>-1</sup> h<sup>-1</sup>, the H<sub>2</sub> uptake from 0.63 to  $2.1 \times 10^{-18}$  mol cell<sup>-1</sup> h<sup>-1</sup>, and the CO uptake from 0.24 to  $0.69 \times 10^{-18}$  mol cell<sup>-1</sup> h<sup>-1</sup> at 20 °C. We suspect the differences were due to the higher accuracy of the uptake rates, and higher cell number estimates (average  $9.54 \times 10^7$ ; Table S1), despite shorter incubation time (4.5 months). The number of initial cells that form colonies on the filters may vary between experiments, possibly due to small differences in the physiological state of the inoculum. This, and the possibility that colonies of a certain size reach a growth stagnation phase due to limiting concentrations of CH<sub>4</sub>, H<sub>2</sub> and CO around the colony, can explain how additional pre-incubation time in the first experiment did not lead to higher cell numbers per filter than in the second experiment.

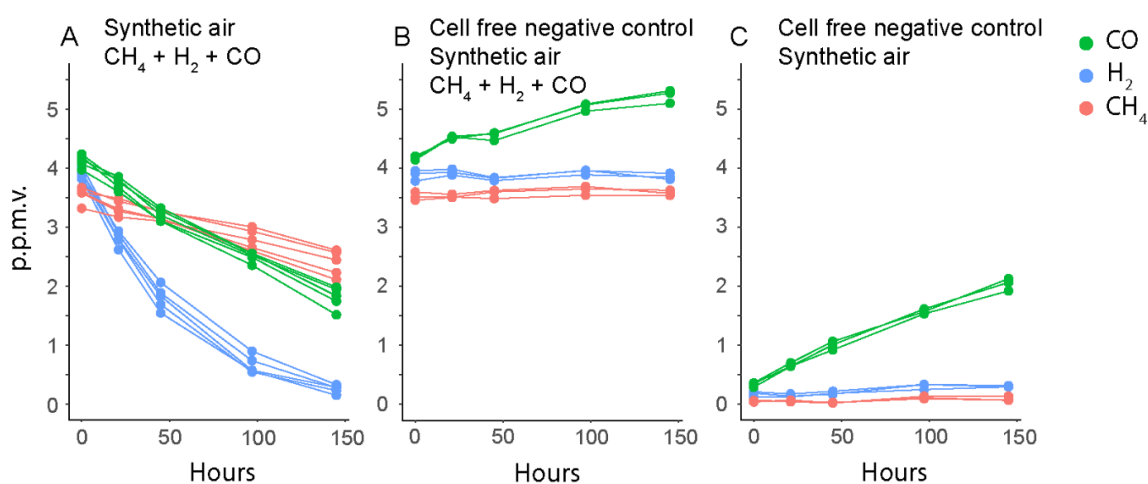


**Figure 5.** Oxidation of CH<sub>4</sub>, CO, and H<sub>2</sub> by *M. gorgona* MG08. (A) filters with *M. gorgona* MG08 floating on nitrate mineral salts medium. (B,C) sterile filters floating on nitrate mineral salts medium. All gases used were of the highest commercially available quality, 6.0 (99.9999% purity). The multiple data points in each color represent different biological replicates from the same condition.

With these new numbers, we find that *M. gorgona* MG08 is able to conserve approximately 0.38 kJ Cmol h<sup>-1</sup> (close to the 0.48 kJ Cmol h<sup>-1</sup> estimated from the first experiment) during growth in air at 20 °C (Table S1). This is more than seven times lower

than the estimated average maintenance requirement of a bacterial population at 20 °C (2.8 kJ Cmol h<sup>-1</sup>) [8]. However, this amount of energy is apparently sufficient to sustain the growth of *M. gorgona* MG08. Thus, we question whether the average maintenance requirement of bacteria [8] appropriately describes the constraints for growth on atmospheric trace gases by *M. gorgona* MG08 and other atmMOB.

With our numbers, the 2.8 kJ Cmol h<sup>-1</sup> minimum requirement mentioned above could be achieved if approximately 14 million out of the ~100 million cells on a filter were active [8]. Alternatively, if cell density and thus weight (cell sizes do not seem to vary with CH<sub>4</sub> concentration) were lower during growth in air, an energy yield of 2.8 kJ Cmol h<sup>-1</sup> or higher, could be achieved. The reason is that the same amount of energy would be distributed on less cellular mass than assumed for our empirical estimate of 0.38 kJ Cmol h<sup>-1</sup>. Regardless, the rates of *M. gorgona* MG08 are substantially lower than those in high upland soils, where CH<sub>4</sub> oxidation rates of up to 800 × 10<sup>-18</sup> mol cell<sup>-1</sup> h<sup>-1</sup>, almost 500 times faster than *M. gorgona* MG08, were measured. However, these were based on soil cell numbers estimated from DNA extractions and *pmoA* qPCR [6]. Thus, the numbers have possibly been underestimated, as DNA extractions from soils may provide less than 100% yields, qPCR quantification can be inhibited by soil-derived impurities in the DNA extract, and primer mismatches can result in an underrepresentation of copy numbers. Methanogenic archaea and acetogenic bacteria were recently found to require much less maintenance energy (0.2 kJ Cmol h<sup>-1</sup>) than previously believed (9.8 kJ Cmol h<sup>-1</sup>) [29]. According to the authors, the low maintenance energy was based on the low growth rates of these organisms, a feature that had not previously been taken into account. If true, low maintenance requirements at low growth rates could also explain how *M. gorgona* MG08 can sustain its slow growth at a limited energy budget.

We conclude that *M. gorgona* MG08 oxidizes the atmospheric trace gases CH<sub>4</sub>, CO and H<sub>2</sub> to harvest energy for growth in air. The ability of *M. gorgona* MG08 to grow using air as its only source of energy and carbon relies not only on this metabolic flexibility, but also on its low energy requirements. Our findings suggest that a high CH<sub>4</sub> affinity is not a prerequisite to live on atmospheric CH<sub>4</sub>.

**Supplementary Materials:** The following are available online at <https://www.mdpi.com/2076-2607/9/1/153/s1>, Table S1: Supplementary data and calculations.

**Author Contributions:** A.T.T. conceived the study with input from T.S., M.M.S. and A.G.H. A.G.H. and M.M.S. established methods for filter cultivation and performed strain cultivation with input from A.T.T. T.S., M.L. and A.T.T. established methods for gas uptake experiments. T.S. performed gas uptake experiments with assistance from M.L. A.D. established and performed method for cell quantification. A.T.T. and T.S. analyzed the data. A.T.T. wrote the manuscript with input from all authors. All authors have read and agreed to the published version of the manuscript.

**Funding:** This study was funded by the Research Council of Norway FRIPRO Mobility Grant Project Time and Energy (251027/RU) to ATT, co-funded by ERC under Marie Curie Grant 606895, and Tromsø Research Foundation starting grant project Cells in the Cold (16\_SG\_ATT) to ATT.

**Conflicts of Interest:** The authors declare that the research was conducted in the absence of any commercial or financial relationships that could be construed as a potential conflict of interest.

## References

1. Van Amstel, A. Methane. A review. *J. Integr. Environ. Sci.* **2012**, *9*, 5–30. [CrossRef]
2. Knief, C.; Dunfield, P.F. Response and adaptation of different methanotrophic bacteria to low methane mixing ratios. *Environ. Microbiol.* **2005**, *7*, 1307–1317. [CrossRef] [PubMed]
3. Dunfield, P.F. *The Soil Methane Sink. Greenhouse Gas. Sinks*; Reay, D.S., Hewitt, C.N., Smith, K.A., Grace, J., Eds.; CABI: Wallingford, UK, 2007; pp. 152–170.
4. Tveit, A.T.; Hestnes, A.G.; Robinson, S.L.; Schintlmeister, A.; Dedysh, S.N.; Jehmlich, N.; Von Bergen, M.; Herbold, C.; Wagner, M.; Richter, A.; et al. Widespread soil bacterium that oxidizes atmospheric methane. *Proc. Natl. Acad. Sci. USA* **2019**, *116*, 8515–8524. [CrossRef] [PubMed]
5. Knief, C. Diversity and habitat preferences of cultivated and uncultivated aerobic methanotrophic bacteria evaluated based on *pmoA* as molecular marker. *Front. Microbiol.* **2015**, *6*. [CrossRef]

6. Kolb, S.; Knief, C.; Dunfield, P.F.; Conrad, R. Abundance and activity of uncultured methanotrophic bacteria involved in the consumption of atmospheric methane in two forest soils. *Environ. Microbiol.* **2005**, *7*, 1150–1161. [[CrossRef](#)]
7. Bender, M.; Conrad, R. Kinetics of CH<sub>4</sub> oxidation in oxic soils exposed to ambient air or high CH<sub>4</sub> mixing ratios. *FEMS Microbiol. Lett.* **1992**, *101*, 261–270. [[CrossRef](#)]
8. Tijhuis, L.; Van Loosdrecht, M.C.M.; Heijnen, J.J. A thermodynamically based correlation for maintenance gibbs energy requirements in aerobic and anaerobic chemotrophic growth. *Biotechnol. Bioeng.* **1993**, *42*, 509–519. [[CrossRef](#)]
9. Cordero, P.R.F.; Bayly, K.; Leung, P.M.; Huang, C.; Islam, Z.F.; Schittenhelm, R.B.; King, G.M.; Greening, C. Atmospheric carbon monoxide oxidation is a widespread mechanism supporting microbial survival. *ISME J.* **2019**, *13*, 2868–2881. [[CrossRef](#)]
10. Ji, M.; Greening, C.; VanWanterghem, I.; Carere, C.R.; Bay, S.K.; Steen, J.A.; Montgomery, K.; Lines, T.; Beardall, J.; Van Dorst, J.; et al. Atmospheric trace gases support primary production in Antarctic desert surface soil. *Nature* **2017**, *552*, 400–403. [[CrossRef](#)]
11. Greening, C.; Carere, C.R.; Rushton-Green, R.; Harold, L.K.; Hards, K.; Taylor, M.C.; Morales, S.E.; Stott, M.B.; Cook, G.M. Persistence of the dominant soil phylum Acidobacteria by trace gas scavenging. *Proc. Natl. Acad. Sci. USA* **2015**, *112*, 10497. [[CrossRef](#)]
12. Greening, C.; Berney, M.; Hards, K.; Cook, G.M.; Conrad, R. A soil actinobacterium scavenges atmospheric H<sub>2</sub> using two membrane-associated, oxygen-dependent [NiFe] hydrogenases. *Proc. Natl. Acad. Sci. USA* **2014**, *111*, 4257. [[CrossRef](#)] [[PubMed](#)]
13. Greening, C.; Biswas, A.; Carere, C.R.; Jackson, C.J.; Taylor, M.C.; Stott, M.B.; Cook, G.M.; Morales, S.E. Genomic and metagenomic surveys of hydrogenase distribution indicate H<sub>2</sub> is a widely utilised energy source for microbial growth and survival. *ISME J.* **2016**, *10*, 761–777. [[CrossRef](#)] [[PubMed](#)]
14. Ray, A.E.; Zhang, E.; Terauds, A.; Ji, M.; Kong, W.; Ferrari, B.C. Soil Microbiomes With the Genetic Capacity for Atmospheric Chemosynthesis Are Widespread Across the Poles and Are Associated With Moisture, Carbon, and Nitrogen Limitation. *Front. Microbiol.* **2020**, *11*. [[CrossRef](#)] [[PubMed](#)]
15. World Meteorological Organization. The State of Greenhouse Gases in the Atmosphere Using Global Observations through 2018. *WMO GHG Bullet.* **2019**, *15*, 1–8. ISSN 2078-0796.
16. Khalil, M.A.K.; Rasmussen, R.A. The global cycle of carbon monoxide: Trends and mass balance. *Chemosphere* **1990**, *20*, 227–242. [[CrossRef](#)]
17. Novelli, P.C.; Masarie, K.A.; Lang, P.M. Distributions and recent changes of carbon monoxide in the lower troposphere. *J. Geophys. Res. Atmos.* **1998**, *103*, 19015–19033. [[CrossRef](#)]
18. Chi, X.; Winderlich, J.; Mayer, J.-C.; Panov, A.V.; Heimann, M.; Birmili, W.; Heintzenberg, J.; Cheng, Y.; Andreae, M.O. Long-term measurements of aerosol and carbon monoxide at the ZOTTO tall tower to characterize polluted and pristine air in the Siberian taiga. *Atmos. Chem. Phys.* **2013**, *13*, 12271–12298. [[CrossRef](#)]
19. Petrenko, V.V.; Martinerie, P.; Novelli, P.; Etheridge, D.M.; Levin, I.; Wang, Z.; Blunier, T.; Chappellaz, J.; Kaiserli, J.; Lang, P.; et al. A 60 yr record of atmospheric carbon monoxide reconstructed from Greenland firn air. *Atmos. Chem. Phys.* **2013**, *13*, 7567–7585. [[CrossRef](#)]
20. Novelli, P.C.; Lang, P.M.; Masarie, K.A.; Hurst, D.F.; Myers, R.; Elkins, J.W. Molecular hydrogen in the troposphere: Global distribution and budget. *J. Geophys. Res. Atmos.* **1999**, *104*, 30427–30444. [[CrossRef](#)]
21. Schmitz, R.A.; Pol, A.; Mohammadi, S.S.; Hogendoorn, C.; Van Gelder, A.H.; Jetten, M.S.M.; Daumann, L.J.; Camp, H.J.M.O.D. The thermoacidophilic methanotroph *Methylacidiphilum fumariolicum* SolV oxidizes subatmospheric H<sub>2</sub> with a high-affinity, membrane-associated [NiFe] hydrogenase. *ISME J.* **2020**, *14*, 1223–1232. [[CrossRef](#)]
22. Hakobyan, A.; Zhu, J.; Glatter, T.; Paczia, N.; Liesack, W. Hydrogen utilization by *Methylocystis* sp. strain SC2 expands the known metabolic versatility of type IIa methanotrophs. *Metab. Eng.* **2020**, *61*, 181–196. [[CrossRef](#)] [[PubMed](#)]
23. R Development Core Team. *R: A Language and Environment for Statistical Computing*; R Foundation for Statistical Computing: Vienna, Austria, 2013. Available online: <http://www.R-project.org/> (accessed on 23 January 2020).
24. Wickham, H. *Ggplot2: Elegant Graphics for Data Analysis*; Springer: New York, NY, USA, 2016. Available online: <https://ggplot2.tidyverse.org> (accessed on 23 January 2020).
25. Pieja, A.J.; Sundstrom, E.R.; Criddle, C.S. Poly-3-Hydroxybutyrate Metabolism in the Type II Methanotroph *Methylocystis parvus* OBBP. *Appl. Environ. Microbiol.* **2011**, *77*, 6012–6019. [[CrossRef](#)] [[PubMed](#)]
26. Ratcliff, W.C.; Kadam, S.V.; Denison, R.F. Poly-3-hydroxybutyrate (PHB) supports survival and reproduction in starving rhizobia. *FEMS Microbiol. Ecol.* **2008**, *65*, 391–399. [[CrossRef](#)]
27. Lange, S.F.; Allaire, S.E.; van Bochove, E. Transfer of CO<sub>2</sub>, N<sub>2</sub>O and CH<sub>4</sub> to butyl rubber (polyisobutylene) septa during storage. *J. Environ. Monit.* **2008**, *10*, 775–777. [[CrossRef](#)] [[PubMed](#)]
28. Magnusson, T. A method for equilibration chamber sampling and gas chromatographic analysis of the soil atmosphere. *Plant Soil* **1989**, *120*, 39–47. [[CrossRef](#)]
29. Bonk, F.; Popp, D.; Weinrich, S.; Sträuber, H.; Becker, D.; Kleinstaub, S.; Harms, H.; Centler, F. Determination of Microbial Maintenance in Acetogenesis and Methanogenesis by Experimental and Modeling Techniques. *Front. Microbiol.* **2019**, *10*. [[CrossRef](#)]

## Paper 2

1 Physiological Basis for Atmospheric Methane Oxidation and  
2 Methanotrophic Growth on Air

3 Tilman Schmider<sup>a\*</sup>, Anne Grethe Hestnes<sup>a</sup>, Julia Brzykcy<sup>b</sup>, Hannes Schmidt<sup>c</sup>, Arno  
4 Schintlmeister<sup>d</sup>, Benjamin R. K. Roller<sup>d</sup>, Ezequiel Jesús Teran<sup>e,f</sup>, Andrea Söllinger<sup>a</sup>, Oliver  
5 Schmidt<sup>a</sup>, Martin F. Polz<sup>d</sup>, Andreas Richter<sup>c</sup>, Mette M. Svenning<sup>a</sup>, Alexander T. Tveit<sup>a\*</sup>

6 <sup>a</sup>Department of Arctic and Marine Biology, Faculty of Biosciences, Fisheries and Economics,  
7 UiT - The Arctic University of Norway, 9037 Tromsø, Norway;

8 <sup>b</sup>Department of Geomicrobiology, Institute of Microbiology, Faculty of Biology, University of  
9 Warsaw, 02-096 Warsaw, Poland

10 <sup>c</sup>Department of Microbiology and Environmental Systems Science, Division of Terrestrial  
11 Ecosystem Research, University of Vienna, 1030 Vienna, Austria;

12 <sup>d</sup>Department of Microbiology and Environmental Systems Science, Division of Microbial  
13 Ecology, University of Vienna, 1030 Vienna, Austria;

14 <sup>e</sup>Centro de Investigaciones en Física e Ingeniería del Centro de la Provincia de Buenos Aires  
15 (CIFICEN-UNCPBA-CONICET-CICPBA), Pinto 399, Tandil (7000), Argentina

16 <sup>f</sup>Universidad Nacional del Centro de la Provincia de Buenos Aires, Facultad de Ciencias Exactas,  
17 Instituto de Física Arroyo Seco (IFAS), Pinto 399, Tandil (7000), Argentina

18 \*Corresponding author. Email: [tilman.schmider@uit.no](mailto:tilman.schmider@uit.no); [alexander.t.tveit@uit.no](mailto:alexander.t.tveit@uit.no)

19

## 20 Abstract

21 Atmospheric methane oxidizing bacteria (atmMOB) constitute the sole biological sink for  
22 atmospheric methane and have been discovered worldwide over the past decades. Still, the  
23 physiological basis allowing atmMOB to grow “on air” is not understood. Here we assess the  
24 ability and strategies of seven methanotrophic species to grow with air as sole energy, carbon,  
25 and nitrogen source. Four species, including three outside the canonical atmMOB group USC $\alpha$ ,  
26 enduringly oxidized atmospheric methane, carbon monoxide, and hydrogen during 12 months  
27 of growth on air. These four species exhibited distinct substrate preferences implying the  
28 existence of multiple metabolic strategies to grow on air. Despite simultaneous oxidation of  
29 atmospheric methane, carbon monoxide, and hydrogen, the estimated energy yields of the  
30 atmMOB were substantially lower than previously assumed necessary for cellular  
31 maintenance in atmMOB and other aerobic microorganisms. Moreover, the atmMOB also  
32 covered their nitrogen requirements from air. During growth on air, the atmMOB allocated  
33 their proteome by decreasing investments in biosynthesis while increasing investments in  
34 trace gas oxidation. Additionally, we demonstrate high apparent affinities for methane by  
35 atmMOB in pure culture, similar to the affinities observed in upland soils more than two  
36 decades ago. Nevertheless, we show that the apparent specific affinity, rather than the  
37 apparent affinity, is the appropriate model to assess the efficiency of atmospheric methane  
38 utilization. Our work shows that atmMOB grow on the trace concentrations of methane,  
39 carbon monoxide, and hydrogen present in air and outlines the metabolic strategies that  
40 enable atmMOB to mitigate important greenhouse gases.

41

42

## 43 Introduction

44 During the first two decades after emission to the atmosphere, methane (CH<sub>4</sub>) is a greenhouse  
45 gas 80 times more potent than carbon dioxide (CO<sub>2</sub>)<sup>1,2</sup>. Since 2007, the atmospheric CH<sub>4</sub>  
46 concentration (1905 p.p.b.v. in July 2022 [https://gml.noaa.gov/ccgg/trends\\_ch4/](https://gml.noaa.gov/ccgg/trends_ch4/)), that is  
47 responsible for approximately 20% of the direct radiative forcing, has been increasing rapidly<sup>1</sup>.  
48 The CH<sub>4</sub> increase further accelerated in 2014 and is linked to several causes: A decline in the  
49 atmospheric concentration of hydroxyl radicals (OH) which is the main sink of atmospheric  
50 CH<sub>4</sub>, as OH oxidize CH<sub>4</sub> in the atmosphere<sup>3-5</sup>; anthropogenic emissions from fossil fuel,  
51 agricultural, and waste sources<sup>6</sup>; increased microbial CH<sub>4</sub> production in wetlands which  
52 suggests that current increases are also driven by feedback responses to global warming<sup>7</sup>.  
53 Atmospheric CH<sub>4</sub> oxidizing bacteria (atmMOB), a subgroup of aerobic methanotrophs, that  
54 oxidize CH<sub>4</sub> at its atmospheric trace concentration are the only known biological sink of  
55 atmospheric CH<sub>4</sub>. Compared to the OH sink (~500 Tg), the biological sink is rather small as it  
56 removes approximately 30 Tg (11 – 49 Tg) CH<sub>4</sub> from the atmosphere every year<sup>4</sup>. However,  
57 the biological sink has the potential to grow with increasing CH<sub>4</sub> concentrations. This is of  
58 particular importance as the decline of atmospheric OH, caused by reaction with atmospheric  
59 hydrogen (H<sub>2</sub>) and other gases, might accelerate due to increasing H<sub>2</sub> emissions from a  
60 hydrogen-based economy<sup>8,9</sup>. Additionally, the biological sink is within reach of management  
61 practices devised to maximize its natural potential and harness it for CH<sub>4</sub> removal<sup>10,11</sup>. Yet,  
62 substantial uncertainties concerning the size of the biological sink, and the ecology and  
63 metabolic basis for growth on atmospheric CH<sub>4</sub> by atmMOB, caused by a historical lack of  
64 atmMOB in pure culture, has impeded our ability to study, manage, and exploit the sink<sup>10</sup>. In

65 this study, by screening seven methanotrophic species, we have outlined the physiological  
66 basis that enables atmMOB to grow on atmospheric CH<sub>4</sub> and serve as an atmospheric CH<sub>4</sub> sink.

67 In 1992, ten years after Harriss *et al.* reported the first indications of atmospheric CH<sub>4</sub>  
68 oxidation by microorganisms<sup>12</sup>, Bender and Conrad concluded from biphasic CH<sub>4</sub> oxidation  
69 kinetics of soils that an unknown group of methanotrophs might be responsible for  
70 atmospheric CH<sub>4</sub> oxidation<sup>13</sup>. Since then, two major questions have remained partially  
71 unanswered: Which methanotrophs are responsible for oxidation of atmospheric CH<sub>4</sub>? How  
72 can these organisms survive and grow despite the apparent energetic limitations inherent to  
73 the oxidation of the low atmospheric CH<sub>4</sub> concentrations?

74 Isotopic labeling studies revealed that members of *Alpha-* and *Gammaproteobacteria*  
75 contributed to atmospheric CH<sub>4</sub> oxidation and assigned them to the upland soil clusters alpha  
76 and gamma (USC $\alpha$  and USC $\gamma$ )<sup>14–16</sup>. Several environmental and ecological studies have ascribed  
77 atmospheric CH<sub>4</sub> oxidation mainly to these two clusters<sup>17–20</sup>. However, over the years, studies  
78 targeting methanotrophs in upland soils have reported the presence of alphaproteobacterial  
79 methanotrophs outside the USC $\alpha$ <sup>14,21–24</sup>. These observations suggest that also “conventional”  
80 methanotrophs (methanotrophs assumed to grow only at high CH<sub>4</sub> concentrations), from  
81 genera like *Methylocapsa*, *Methylosinus* and *Methylocystis*, could contribute to the  
82 atmospheric CH<sub>4</sub> sink.

83 Dunfield<sup>25</sup> summarized three potential lifestyles of atmMOB that might enable cellular  
84 maintenance and growth at the low CH<sub>4</sub> concentrations in air and the associated energy  
85 limitation: (i) Flush feeding on high CH<sub>4</sub> concentrations generated periodically in deeper soil  
86 layers, in addition to atmospheric CH<sub>4</sub> oxidation; (ii) An oligotrophic lifestyle based on

87 atmospheric CH<sub>4</sub> as sole carbon and energy source; (iii) A mixotrophic lifestyle to utilize other  
88 substrates for energy conservation in addition to CH<sub>4</sub>.

89 Flush feeding (i) is supported by the declining potential of methanotrophs to oxidize  
90 atmospheric CH<sub>4</sub> after several months of CH<sub>4</sub> starvation<sup>25,26</sup>. A study on conventional  
91 methanotrophs in rice paddy soils showed that methanotrophs regained the ability to oxidize  
92 atmospheric CH<sub>4</sub> after exposure to high CH<sub>4</sub> concentrations<sup>27</sup>. A high specific affinity ( $a_A^0$ ) for  
93 CH<sub>4</sub> has been suggested as the key trait of oligotrophic atmMOB (ii) to enable growth with air  
94 as their only energy and carbon source<sup>25,28</sup>. This assumes that cellular energy requirements  
95 for maintenance are 4.5 kJ per carbon mole of biomass per hour (C-mol<sup>-1</sup> h<sup>-1</sup>) (at 25°C)<sup>29</sup>. Thus,  
96 to survive, oligotrophic atmMOB presumably need an atmospheric CH<sub>4</sub> oxidation rate high  
97 enough to meet these energy requirements. Such a rate can be achieved by the combination  
98 of a high affinity for CH<sub>4</sub>, reflected in a low half saturation constant ( $K_m$ ), and a high maximum  
99 CH<sub>4</sub> oxidation rate ( $V_{max}$ ), the fraction of  $V_{max}$  and  $K_m$  being referred to as  $a_A^0$ <sup>30</sup>. This theory is  
100 supported by low  $K_m$  values for CH<sub>4</sub> found in several soils<sup>13</sup>. However, in a later study the cell  
101 specific CH<sub>4</sub> oxidation of USCα members was estimated to be 2.9 to 40 times lower than the  
102 presumed rate needed for cellular maintenance<sup>31</sup>. Therefore, the authors considered that a  
103 mixotrophic lifestyle (iii) could be the basis for atmospheric CH<sub>4</sub> oxidation. In line with this, a  
104 recent study reported the simultaneous oxidation of atmospheric H<sub>2</sub>, carbon monoxide (CO),  
105 and CH<sub>4</sub> by *Methylocapsa gorgona* MG08, the first known methanotroph and USCα member  
106 in pure culture that can grow “on air” (with air as sole energy and carbon source)<sup>32,33</sup>. Despite  
107 its mixotrophic lifestyle, *M. gorgona* MG08 did not conserve enough energy (0.38 kJ C-mol<sup>-1</sup>  
108 h<sup>-1</sup>) to cover the 2.8 kJ C-mol<sup>-1</sup> h<sup>-1</sup> theoretically required to support maintenance at 20°C (2.8  
109 kJ C-mol<sup>-1</sup> h<sup>-1</sup> at 20°C correspond to 4.5 kJ C-mol<sup>-1</sup> h<sup>-1</sup> at 25°C)<sup>29,32</sup>, questioning whether this  
110 maintenance energy value and thus a high  $a_A^0$  is a relevant benchmark for the physiological

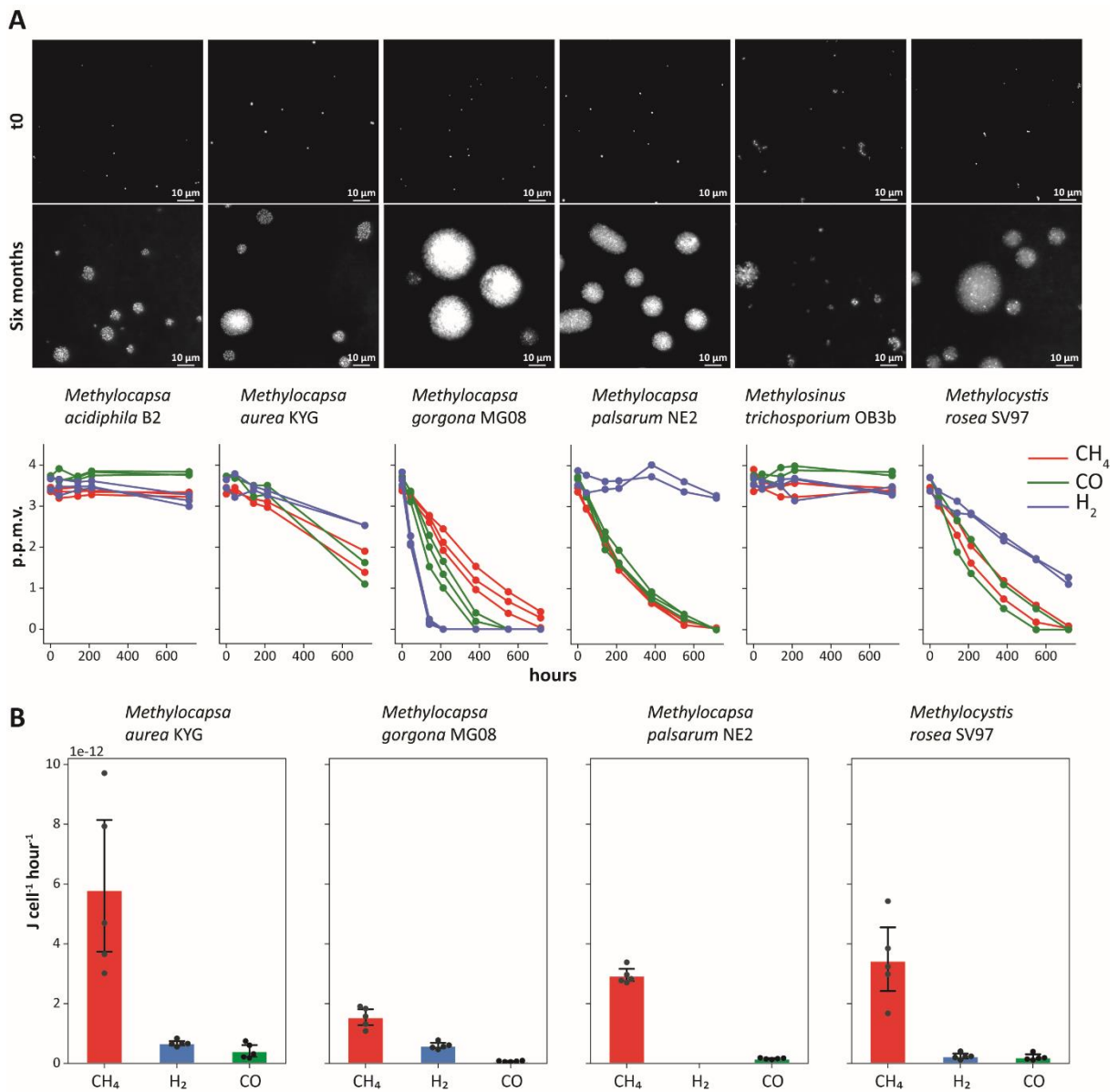
111 capabilities of trace gas oxidizing bacteria. While the initial isolation and study of *M. gorgona*  
112 MG08 led to important advancements in our understanding of atmMOB, our knowledge of  
113 the metabolic basis allowing atmMOB to grow on atmospheric CH<sub>4</sub> remained limited. Recent  
114 energy estimates relied on the untested assumptions that all cells remained active over time  
115 and could not grow on air without CH<sub>4</sub>, H<sub>2</sub> and CO. Furthermore, these methodologically  
116 limited of estimates had only been carried out on one strain, *M. gorgona* MG08, and had not  
117 been combined with other methods to reveal the metabolic strategies associated to the  
118 energy yields. On this background and to test if methanotrophs outside the USCα and USCγ  
119 can grow by oxidizing atmospheric CH<sub>4</sub>, H<sub>2</sub> and CO, we used filter cultivation to screen six  
120 alphaproteobacterial, methanotrophic strains and one gammaproteobacterial,  
121 methanotrophic strain for their ability to grow on air. We selected the six alphaproteobacterial  
122 strains *Methylocapsa gorgona* MG08, *Methylosinus trichosporium* OB3b, *Methylocystis rosea*  
123 SV97, *Methylocapsa aurea* KYG, *Methylocapsa acidiphila* B2, and *Methylocapsa palsarum*  
124 NE2<sup>33–38</sup> since members of *Methylocapsa*, *Methylosinus* and *Methylocystis* have been  
125 observed in net sinks for atmospheric CH<sub>4</sub> (upland soils). As representative methanotroph  
126 from the *Gammaproteobacteria* we included *Methylobacter tundripaludum* SV96. To outline  
127 the physiological basis for growth on air, we performed trace gas oxidation experiments,  
128 estimated energy yields from the oxidation of trace gases in air, used comparative proteomics  
129 to investigate proteome allocation, and determined the  $\alpha_A^0$  for CH<sub>4</sub> during growth on air. Based  
130 on the lack of knowledge about nitrogen limitation of atmMOB<sup>39</sup>, we also evaluated their  
131 ability to grow on the nitrogen sources available in air.

## 132 Results and Discussion

### 133 Colony formation, trace gas oxidation, and cellular energy yield during growth on air

134 To test the ability of the seven selected methanotrophs to grow on air, we incubated each  
135 strain on filters floating on carbon free medium with ambient air as the sole carbon and energy  
136 source, hereafter referred to as filter culture. Microscopy demonstrated that all strains except  
137 *Methylobacter tundripaludum* SV96, the gammaproteobacterial strain, formed colonies  
138 during six months of incubation (Fig. 1A). To test the metabolic activity of the six months old  
139 strains, we performed trace gas oxidation experiments (Fig. 1A, 1B). During these  
140 experiments, filter cultures were floating on mineral medium in bottles with trace  
141 concentrations of CH<sub>4</sub>, H<sub>2</sub>, and CO in the headspace. The strains, *M. aurea* KYG, *M. gorgona*  
142 MG08, *M. palsarum* NE2, and *M. rosea* SV97, hereafter referred to as atmMOB, oxidized CH<sub>4</sub>,  
143 CO, and H<sub>2</sub>, or CH<sub>4</sub> and CO to sub-atmospheric concentrations showing strain-specific  
144 oxidation patterns (Fig. 1A, Supplementary Fig. 1). *M. aurea* KYG oxidized CO at the highest  
145 rate, followed by CH<sub>4</sub> and H<sub>2</sub>. *M. gorgona* MG08 oxidized H<sub>2</sub> at the highest rate, followed by  
146 CO and CH<sub>4</sub>. *M. rosea* SV97 oxidized CO at the highest rate, followed by CH<sub>4</sub> and H<sub>2</sub>. *M.*  
147 *palsarum* NE2 oxidized CH<sub>4</sub> and CO at similar rates but did not oxidize H<sub>2</sub>. The gas oxidation  
148 patterns were similar after 12 months of incubation with air (Supplementary Fig. 1). To verify  
149 growth on the three trace gases in air, we incubated *M. gorgona* MG08 cells on filters under  
150 two different atmospheres: One of synthetic air without the trace gases CH<sub>4</sub>, CO, and H<sub>2</sub> (Gas  
151 composition: 400 p.p.m.v. CO<sub>2</sub> and 20.9% O<sub>2</sub> in N<sub>2</sub>) and another of ambient air. Growth by  
152 colony formation was only observed in the ambient air control, whereas no growth was  
153 observed in synthetic air (Supplementary Fig. 2). This and the repeated observations of trace  
154 gas oxidation confirm that these strains can live and grow with air as the sole energy and  
155 carbon source. The observed oxidation of at least one atmospheric trace gas in addition to

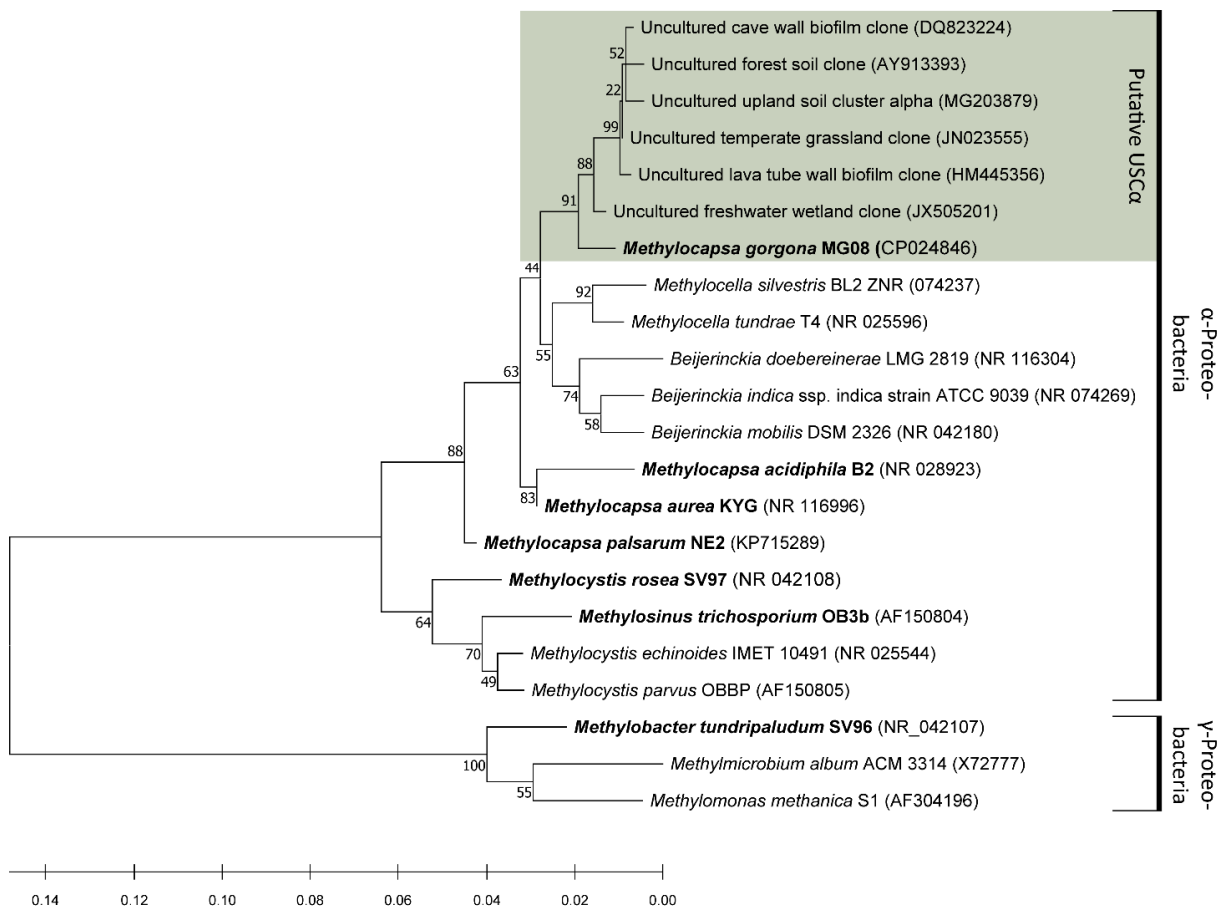
156 CH<sub>4</sub> demonstrates that all four strains are mixotrophic, matching the proposition by Dunfield  
 157 that mixotrophy could be a physiological basis for atmMOB<sup>25</sup>. Additionally, the strain-specific  
 158 trace gas uptake patterns demonstrate substantial metabolic differences between these four  
 159 strains, indicating that multiple metabolic strategies can support oxidation of atmospheric CH<sub>4</sub>  
 160 for growth. These results also demonstrated that the enduring oxidation of atmospheric CH<sub>4</sub>  
 161 after 12 months of growth on air is not restricted to members of the USCα and USCγ, but also  
 162 include members from the genera *Methylocystis* and *Methylocapsa*: *M. aurea* KYG, *M.*  
 163 *palsarum* NE2, and *M. rosea* SV97 (Fig. 2).



164

165 Figure 1. A) Images of SYBR green I stained cells and colonies formed by *M. acidiphila* B2, *aurea* KYG, *M. gorgona* MG08, *M.*  
 166 *palsarum* NE2, *M. trichosporium* OB3b, and *M. rosea* SV97 at incubation start (t0) and after six months of incubation on air  
 167 as sole energy and carbon source and the related CH<sub>4</sub>, H<sub>2</sub>, and CO oxidation at atmospheric pressure (Supplementary table  
 168 S1). B) Mean estimated energy yield per cell from the oxidation of atmospheric CH<sub>4</sub>, H<sub>2</sub>, and CO by *M. aurea* KYG, *M. gorgona*  
 169 MG08, *M. palsarum* NE2, and *M. rosea* SV97 (Supplementary table S3). Dots represent the energy yield of the respective  
 170 replicates and error bars the standard deviation (n = 5).

171 Despite formation of colonies when exposed to air only, *M. acidiphila* B2 and *M. trichosporium*  
 172 OB3b did not oxidize trace gases after six months of incubation (Fig. 1A). The ability of these  
 173 two strains to produce polyhydroxyalkanoates (PHA) as storage compounds<sup>36,40</sup> might serve  
 174 as an explanation for the initial colony formation. Possibly, the two strains accumulated PHA  
 175 during pre-cultivation at 20% CH<sub>4</sub>, and then sustained their growth on air by utilizing PHA and  
 176 atmospheric CH<sub>4</sub> as energy and carbon sources until the depletion of their storage  
 177 compounds. A study showing that both strains could not stay active at low CH<sub>4</sub>  
 178 concentrations<sup>21</sup> supports our observations, but further studies are needed to clarify whether  
 179 the initial colony formation is based on storage compounds.



180

181 Figure 2. Unrooted maximum-likelihood tree<sup>41,42</sup>. Full length 16S rRNA gene based phylogenetic relationship of the respective  
182 methanotrophs and the USC $\alpha$ . The species investigated in this study are indicated in bold print. The percentage of trees in  
183 which the associated taxa clustered together is shown next to the branches. NCBI accession numbers are given in brackets.

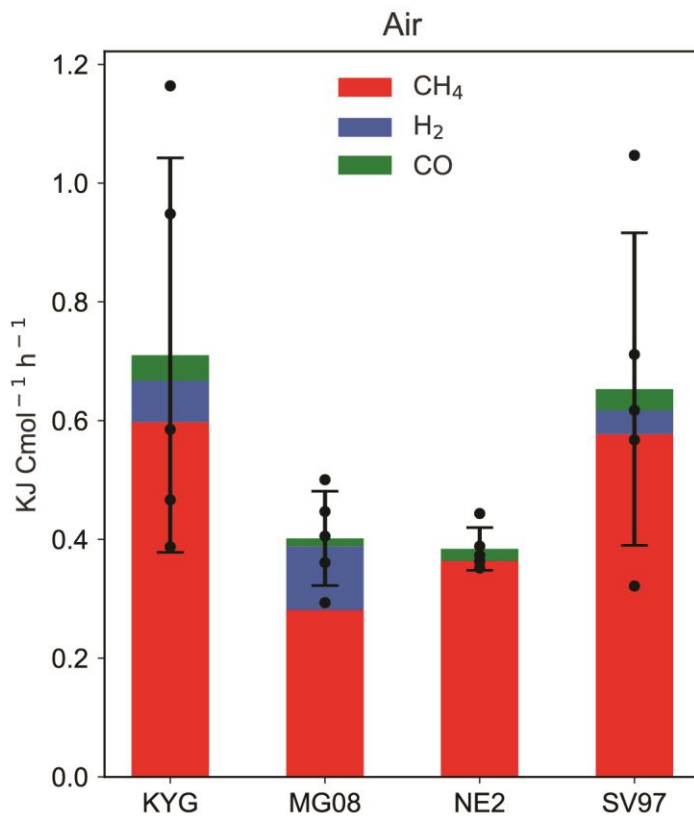
184

185 Next, we asked whether atmMOB can obtain enough energy from growth on air to meet the  
186 basic maintenance energy of 2.8 kJ C-mol<sup>-1</sup> h<sup>-1</sup> at 20°C postulated previously<sup>28</sup>. To calculate  
187 the strain-specific energy yields in C-mol, we first estimated the cellular energy yields based  
188 on the measured CH<sub>4</sub>, H<sub>2</sub>, and CO oxidation rates. *M. aurea* KYG yielded 6.89 x 10<sup>-12</sup> J cell<sup>-1</sup> h<sup>-1</sup>  
189 (n = 5, SD = 3.22 x 10<sup>-12</sup>), *M. gorgona* MG08 2.21 x 10<sup>-12</sup> J cell<sup>-1</sup> h<sup>-1</sup> (n = 5, SD = 4.36 x 10<sup>-13</sup>), *M.*  
190 *palsarum* NE2 3.09 x 10<sup>-12</sup> J cell<sup>-1</sup> h<sup>-1</sup> (n = 5, SD = 2.90 x 10<sup>-13</sup>), and *M. rosea* SV97 3.879 x 10<sup>-12</sup>  
191 J cell<sup>-1</sup> h<sup>-1</sup> (n = 5, SD = 1.57 x 10<sup>-12</sup>) by the oxidation of either two or three trace gases in air  
192 (Fig. 1B). Due to the higher free energy potential and atmospheric concentration of CH<sub>4</sub>  
193 compared to atmospheric H<sub>2</sub> and CO, the energy estimates predict CH<sub>4</sub> as the major energy  
194 source for all four strains. Our estimates derive from the Gibbs free energy change of the  
195 following reactions at atmospheric conditions:  $CH_4 + 2O_2 \rightarrow 2H_2O + CO_2$ ,  $2H_2 + O_2 \rightarrow$   
196  $2H_2O$ , and  $2CO + O_2 \rightarrow 2CO_2$  that amount to -797.4 kJ mol<sup>-1</sup>, -236.8 kJ mol<sup>-1</sup>, and -199.9 kJ  
197 mol<sup>-1</sup>, respectively. However, these numbers do not account for the energy required for  
198 activation of CH<sub>4</sub> by the pMMO or production cost of the enzymes involved in energy  
199 conservation from the gases. While the oxidation of H<sub>2</sub> and CO is catalyzed by one enzyme<sup>43</sup>,  
200 the oxidation of CH<sub>4</sub> to CO<sub>2</sub> by atmMOB involves at least seven enzymes (Fig. 4). Thus, due to  
201 the larger investments required for energy conservation from CH<sub>4</sub>, the gases CO and H<sub>2</sub> might  
202 play more important roles as energy sources for growth on trace gases in air than indicated  
203 by the energy calculations alone. Considering the cellular dry masses and carbon content  
204 (Supplementary table S3) of *M. gorgona* MG08, *M. aurea* KYG, *M. palsarum* NE2, and *M. rosea*  
205 SV97, the energy yields per cell and hour translates to 0.40 kJ C-mol<sup>-1</sup> h<sup>-1</sup> (SD = 0.08 kJ C-mol<sup>-1</sup>

206  $\text{h}^{-1}$ ), 0.71  $\text{kJ C-mol}^{-1} \text{h}^{-1}$  (SD = 0.33  $\text{kJ C-mol}^{-1} \text{h}^{-1}$ ), 0.38  $\text{kJ C-mol}^{-1} \text{h}^{-1}$  (SD = 0.04  $\text{kJ C-mol}^{-1} \text{h}^{-1}$ ),  
207 and 0.65  $\text{kJ C-mol}^{-1} \text{h}^{-1}$  (SD = 0.26  $\text{kJ C-mol}^{-1} \text{h}^{-1}$ ), at 20°C, respectively (Fig. 3). These estimated  
208 energy yields for *M. gorgona* MG08, *M. aurea* KYG, *M. palarum* NE2, and *M. rosea* SV97 are  
209 3.9 – 7.4 times lower than the reported average energy requirements for cellular maintenance  
210 in aerobic bacteria (2.8  $\text{kJ C-mol}^{-1} \text{h}^{-1}$  at 20°C correspond to 4.5  $\text{kJ C-mol}^{-1} \text{h}^{-1}$  at 25°C)<sup>29,32</sup>.

211 The energy estimation assumes that all cells of the filter cultures actively contributed to the  
212 observed oxidation rate. Thus, in case of inactive cells, the cellular oxidation rates and the  
213 energy yields might have been underestimated. However, while the applied cell quantification  
214 (see “Methods”) considers only intact cells without assessing cellular activity, Nanoscale  
215 secondary ion mass spectrometry (NanoSIMS) based <sup>15</sup>N incorporation confirmed activity of  
216 all measured cells (see section below: “Growth on nitrogen from air”), supporting our  
217 approach for energy yield estimations.

218 Thus, our observations contradict the basic energy premise for atmospheric CH<sub>4</sub> oxidizing  
219 bacteria<sup>28</sup>. Our energy estimations correspond to the similarly low energy estimates  
220 previously reported for *M. gorgona* MG08<sup>32</sup> and that of acetogenic and methanogenic  
221 microorganisms (0.2  $\text{kJ C-mol}^{-1} \text{h}^{-1}$  at 37°C)<sup>44</sup>.



222

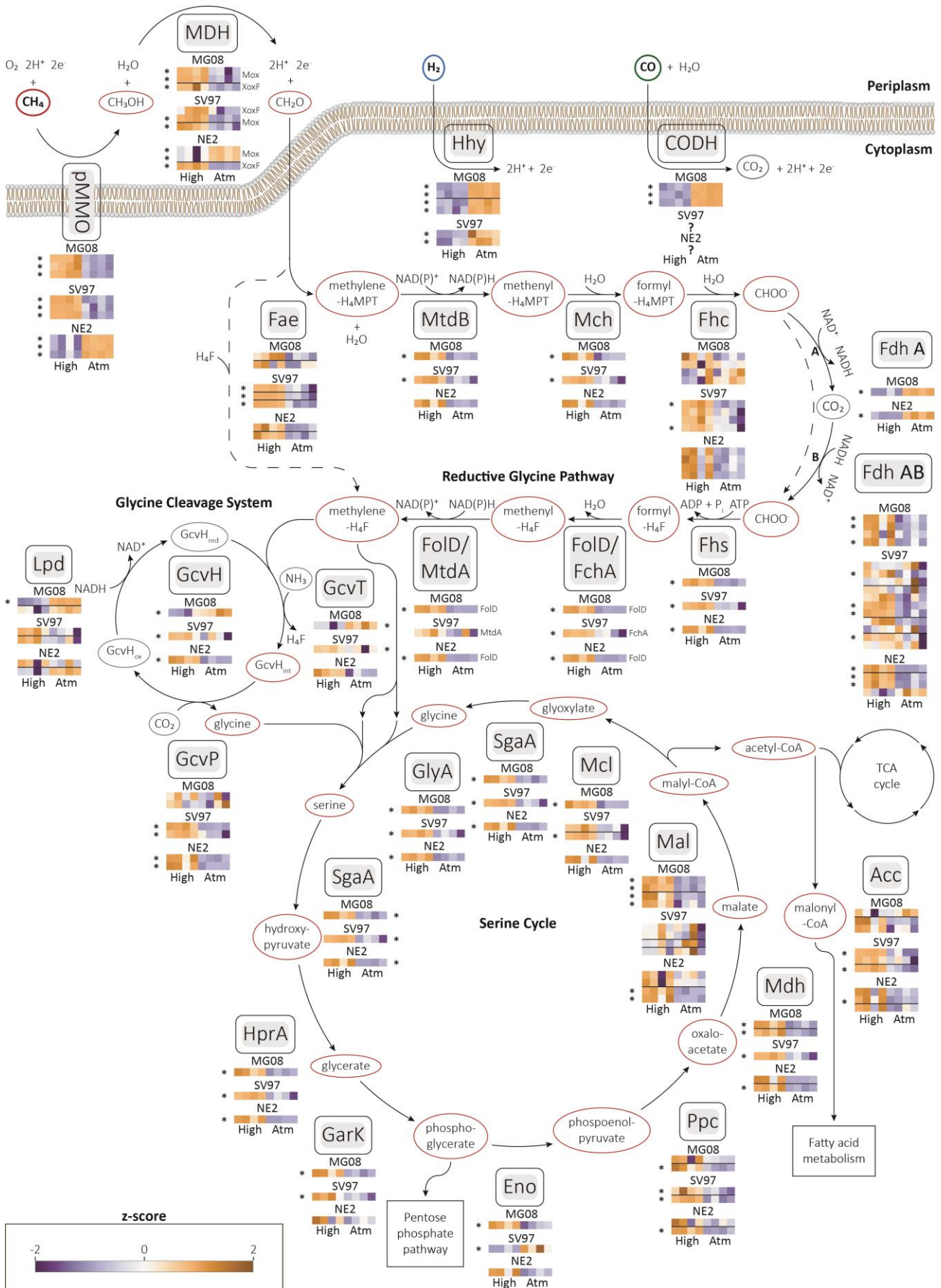
223 Figure 3. Total energy yield of *M. aurea* KYG, *M. gorgona* MG08, *M. palsarum* NE2, *M. rosea* SV97 from the oxidation of  
 224 atmospheric CH<sub>4</sub>, H<sub>2</sub>, and CO in kJ per mol cellular carbon (C-mol) and hour (Supplementary table S3). Colors indicate the  
 225 contribution of the individual trace gases to the total energy yield. Error bars represent the standard deviation (n = 5). Black  
 226 dots indicate the total energy yield from H<sub>2</sub>, CO, and CH<sub>4</sub> of the respective replicates.

227 Comparative proteomics

228 We further investigated the cellular adjustments required for life on air by *M. gorgona* MG08,  
 229 *M. rosea* SV97, and *M. palsarum* NE2 by comparing the proteomes of the three strains when  
 230 exposed to air (~1.9 p.p.m.v. CH<sub>4</sub>) and when exposed to high CH<sub>4</sub> concentrations (~1000  
 231 p.p.m.v. CH<sub>4</sub>) in air. Correspondence analyses (CA) of relative protein abundances at the two  
 232 CH<sub>4</sub> concentrations revealed a clear difference in proteome allocation. This is shown by the  
 233 separation of samples from the two conditions along the first CA dimension, which accounted  
 234 for 79.3%, 76.5%, and 69.6% of the total inertia for *M. gorgona* MG08, *palsarum* NE2, and *M.*  
 235 *rosea* SV97, respectively (Supplementary Fig. 3). Thus, the CA indicate that the largest shifts

236 in the proteomes occurred as responses to changes in CH<sub>4</sub> concentration. To identify which  
237 proteins contributed most to these shifts, we identified the proteins (top 10 %) with the  
238 largest contribution to the first-dimension inertias of the CA and plotted their abundances  
239 across the two conditions (Supplementary Fig. 4). We found major protein expression shifts  
240 within a variety of functional categories (based on hierarchical EggNOG<sup>45</sup> annotations), but for  
241 all three strains, a large proportion was related to core metabolisms, including transcription,  
242 translation, growth, energy metabolism, and amino acid and carbohydrate transport. A  
243 prominent trend observed for all three strains was that proteins associated with the  
244 categories "Cell cycle control, cell division, chromosome partitioning" and "Cell  
245 wall/membrane/envelope biogenesis" shifted towards lower relative abundances, hereafter  
246 referred to as "downregulation", at atmospheric CH<sub>4</sub> compared to the 1000 p.p.m.v. CH<sub>4</sub>  
247 treatment. This pattern suggests that atmMOB lower the allocation of resources for growth  
248 when CH<sub>4</sub> availability is low, which is in line with previously reported differences in colony  
249 growth over time when comparing incubations on atmospheric and 1000 p.p.m.v. CH<sub>4</sub>  
250 concentrations<sup>28</sup>. We also observed major shifts in protein abundances for the categories  
251 "Energy production and conversion" and "Carbohydrate transport and metabolism", including  
252 proteins involved in trace gas oxidation and carbon assimilation (Supplementary tables S12-  
253 14). Based on that and the differences in trace gas oxidation patterns between the strains (Fig.  
254 1), the relative abundances of proteins involved in trace gas oxidation, carbon assimilation via  
255 the serine cycle (Fig. 4), and the electron transport chain (Supplementary Fig. 5) were further  
256 investigated.

257



260 Figure 4. Comparative proteomics of *M. gorgona* MG08, *M. rosea* SV97, and *M. palsarum* NE2 exposed to 1000 p.p.m.v. CH<sub>4</sub>  
 261 (High) in air and 1.9 p.p.m.v. (Atm) CH<sub>4</sub> in air (Supplementary table S5). Normalized and standardized expression of enzymes  
 262 involved in the central carbon and energy metabolism is shown. High relative abundance = orange, low relative abundance  
 263 expression = blue. \* indicates significant difference in expression between treatments (two-sided t-test). Horizontal lines in  
 264 the heatmaps separate operons of enzymes catalyzing the same reaction. ? = unknown enzyme. Abbreviations: pMMO –  
 265 particulate methane monooxygenase, MDH – methanol dehydrogenase (Mox) and putative lanthanide-dependent methanol  
 266 dehydrogenase (XoxF), Hhy – [NiFe] group 1h hydrogenase, CODH – [MuCO] class I carbon monoxide dehydrogenase, Fae –  
 267 formaldehyde activating enzyme, MtdB – NAD(P)-dependent methylene-tetrahydromethanopterin dehydrogenase, Mch –  
 268 methenyl-tetrahydromethanopterin cyclohydrolase, Fhc – formyltransferase/hydrolase, Fdh A – NAD-dependent formate-  
 269 dehydrogenase, Fdh AB – molybdopterin binding reversible formate dehydrogenase/CO<sub>2</sub> reductase, Fhs – formate-  
 270 tetrahydrofolate ligase, FodD – bifunctional 5,10-methylene-tetrahydrofolate dehydrogenase/ 5,10-methenyl-  
 271 tetrahydrofolate cyclohydrolase, FchA – methenyltetrahydrofolate cyclohydrolase, MtdA – NADP-dependent  
 272 methylenetetrahydrofolate dehydrogenase, GcvH – glycine cleavage system H protein, GcvT – aminomethyltransferase, GcvP  
 273 - glycine dehydrogenase, Lpd – dihydrolipoyl dehydrogenase, GlyA – serine hydroxymethyltransferase, SgaA – Serine-  
 274 glyoxylate aminotransferase, HprA – glycerate dehydrogenase, GarK – 2-glycerate kinase, Eno – enolase, Ppc –  
 275 phosphoenolpyruvate carboxylase, Mdh – malate dehydrogenase, Mal – malate-CoA ligase, Mcl – L-malyl-CoA lyase, Acc –  
 276 Acetyl-CoA carboxylase, NAD<sup>+</sup> – nicotinamide adenine dinucleotide, NADP<sup>+</sup> – nicotinamide adenine dinucleotide phosphate,  
 277 ATP – adenosine triphosphate.

278 All three strains expressed a particulate methane monooxygenase (pMMO) that catalyzes the  
 279 hydroxylation of CH<sub>4</sub> to methanol (CH<sub>3</sub>OH). *M. gorgona* MG08 and *M. rosea* SV97 contained  
 280 higher relative abundances, hereafter referred to as “upregulation”, of pMMO at 1000  
 281 p.p.m.v. CH<sub>4</sub>, whereas *M. palsarum* NE2 upregulated pMMO at atmospheric CH<sub>4</sub>  
 282 concentrations. Furthermore, both *M. gorgona* MG08 and *M. rosea* SV97 upregulated a high  
 283 affinity [NiFe] hydrogenase (Hhy), and *M. gorgona* MG08 a molybdenum-dependent carbon  
 284 monoxide dehydrogenase (CODH), when exposed to air. These differences in enzyme  
 285 expression patterns demonstrate different metabolic strategies to grow on air: *M. rosea* SV97  
 286 and *M. gorgona* MG08 compensate for energy limitation by upregulating enzymes for energy  
 287 conservation from H<sub>2</sub> or H<sub>2</sub> and CO, while *M. palsarum* NE2 compensates for the limitation by  
 288 upregulating pMMO. The Hhy increase is similar to the Hhy increase in *Mycobacterium*  
 289 *smegmatis* enabling long-term persistence after carbon limitation<sup>46</sup>. The observed  
 290 upregulation of pMMO, Hhy, or CODH implies that the strains allocate resources to increase  
 291 their  $a_A^0$  (specific apparent affinity) for the respective trace gases as adaptations to growth on  
 292 air. Additionally, the distinct strategies to grow on air by the closely related strains *M. gorgona*  
 293 MG08 and *M. palsarum* NE2 suggest niche differentiation between atmMOB in nature.  
 294 Furthermore, our observations of the consumption of multiple trace gases by atmMOB and

295 adjusted resource allocation for trace gas uptake driven by changes in CH<sub>4</sub> concentration, are  
296 in line with earlier observations of a negative correlation between soil H<sub>2</sub> concentrations and  
297 the uptake of atmospheric CH<sub>4</sub><sup>47</sup>. Despite the ability of *M. rosea* SV97 and *M. palsarum* NE2  
298 to oxidize CO (Fig. 1A), we were not able to determine the responsible protein complex(es) or  
299 the corresponding gene expression responses. In *M. rosea* SV97, candidate genes for CODH  
300 were identified by blasting the genome sequences against a non-redundant CODH sequence  
301 database created by using the Identical Protein Groups resource<sup>48</sup> (Supplementary table S11).  
302 However, not all the potential CODH subunits necessary to form a functional CODH were  
303 detected in the proteomes. The same blast-based approach did not result in potential  
304 candidate genes that could encode a functioning CODH in *M. palsarum* NE2 (Supplementary  
305 table S10). Thus, our results indicate that distantly related or previously undiscovered  
306 enzymes catalyze atmospheric CO oxidation in *M. palsarum* NE2.

307 The expression of the methanol dehydrogenase (MDH), which catalyzes the second step in  
308 CH<sub>4</sub> oxidation, the oxidation of methanol (CH<sub>3</sub>OH) to formaldehyde (CH<sub>2</sub>O), matched the  
309 pMMO expression patterns for all three strains. This indicates a close interaction between  
310 these two enzymes as previously suggested for *Methylococcus capsulatus*<sup>49</sup>. MDHs were  
311 upregulated at high CH<sub>4</sub> concentrations by *M. gorgona* MG08 and *M. rosea* SV97, but not by  
312 *M. palsarum* NE2 (Fig. 4). Only the putative lanthanide-dependent methanol dehydrogenase  
313 (XoxF) of *M. palsarum* NE2 did not follow the pMMO pattern.

314 Formaldehyde is a key intermediate of both catabolism and anabolism in methanotrophs. The  
315 enzymes involved in the catabolic oxidation of formaldehyde via methylene-  
316 tetrahydromethanopterin (-H<sub>4</sub>MPT), methenyl-H<sub>4</sub>MPT, and formyl-H<sub>4</sub>MPT to formate (CHOO<sup>-</sup>  
317 ), were downregulated in the air treatment of the three strains (Fig. 4). The toxic and highly

318 reactive formaldehyde condenses spontaneously to methylene-H<sub>4</sub>MPT<sup>50</sup> and  
319 methylenetetrahydrofolate (H<sub>4</sub>F)<sup>51</sup> and thus, higher concentrations of formaldehyde  
320 activating enzymes (Fae) may not be required for the oxidation of formaldehyde during  
321 growth on air. This may explain why enzymes involved in formaldehyde oxidation, despite the  
322 upregulation of pMMO and MDH, were downregulated in *M. palsarum* NE2 at atmospheric  
323 CH<sub>4</sub> concentrations. At high CH<sub>4</sub> concentrations, the upregulation of Fae and downstream  
324 enzymes for further oxidation to formate could represent a cellular detoxification mechanism  
325 to avoid high cellular formaldehyde concentrations and to increase NADH synthesis<sup>52</sup>.

326 Two different formate dehydrogenases (Fdh A and Fdh AB) that catalyze the energy-  
327 conserving oxidation of formate to CO<sub>2</sub> were expressed by *M. gorgona* MG08 and *M. palsarum*  
328 NE2 (Fig. 4). The metal-free and potentially irreversible NAD<sup>+</sup>-dependent Fdh A<sup>33,53</sup> was  
329 upregulated at atmospheric CH<sub>4</sub> concentrations in *M. gorgona* MG08 and *M. palsarum* NE2.  
330 Possibly, the upregulation of a one-directional enzyme minimizes back-flow of CO<sub>2</sub> to formate  
331 at high CO<sub>2</sub> concentrations and thus prevents energy loss by CO<sub>2</sub> reduction. Fdh AB, which was  
332 expressed by all three strains, is molybdopterin-dependent and homologous to the reversible  
333 Fdh found in *Rhodobacter capsulatus*<sup>54</sup>. It catalyzes, in addition to formate oxidation, the  
334 reduction of CO<sub>2</sub> to formate<sup>54,55</sup>. The Fdh AB was upregulated in all three strains at high CH<sub>4</sub>  
335 concentration. Under these conditions, when excess reducing power is available, the Fdh AB  
336 might enable the reduction of CO<sub>2</sub> for carbon assimilation via the reductive glycine pathway  
337 and serine cycle, but further investigations are needed to test whether CO<sub>2</sub> reduction to  
338 formate truly occurs in atmMOB.

339 Comparative proteomics: Carbon assimilation

340 Carbon assimilation was downregulated in all three strains at atmospheric CH<sub>4</sub> concentrations.  
341 In the three strains, formaldehyde can condense with H<sub>4</sub>F to methylene-H<sub>4</sub>F and then be  
342 further assimilated through the glycine cleavage system and serine pathway. Additionally,  
343 formaldehyde can be first oxidized via the H<sub>4</sub>MPT-mediated pathway to formate and then  
344 enter, instead of being oxidized to CO<sub>2</sub>, the H<sub>4</sub>F-mediated reductive pathway to methylene-H<sub>4</sub>F  
345 (Fig. 4). The increased expression of enzymes involved in the reduction of formate via formyl-  
346 H<sub>4</sub>F and methenyl-H<sub>4</sub>F to methylene-H<sub>4</sub>F in the high CH<sub>4</sub> treatment indicates an enhanced  
347 investment into carbon assimilation. Since formaldehyde spontaneously condenses with H<sub>4</sub>F  
348 to methylene-H<sub>4</sub>F, the upregulated enzymes for H<sub>4</sub>F-mediated formaldehyde oxidation could  
349 also contribute to formate formation. However, experiments with *Methylobacterium*  
350 *extorquens* demonstrated that formaldehyde oxidation occurred through its H<sub>4</sub>MPT-mediated  
351 pathway while the reductive pathway via formate to methylene-H<sub>4</sub>F represented the major  
352 assimilatory flux<sup>52,56</sup>. Therefore, we consider this as the most likely explanation for the  
353 expression patterns in *M. gorgona* MG08, *M. rosea* SV97, and *M. palsarum* NE2.

354 The glycine cleavage/synthase system (GCS)<sup>57,58</sup> catalyzes the oxidative cleavage of glycine to  
355 NADH, NH<sub>3</sub>, CO<sub>2</sub>, and a methylene group. It also catalyzes the reverse reaction, the synthesis  
356 of glycine from NADH, NH<sub>3</sub>, CO<sub>2</sub>, and methylene-H<sub>4</sub>F. The upregulation of the GCS by *M. rosea*  
357 SV97 and *M. palsarum* NE2 at high CH<sub>4</sub> concentrations suggests an increased synthase activity  
358 and thus increased carbon assimilation, corresponding to the overall upregulation of the  
359 reductive glycine pathway (Fig. 4). However, we lack a plausible explanation for the increased  
360 expression of the GCS by *M. gorgona* MG08 at atmospheric CH<sub>4</sub> concentrations.

361 As the next step in carbon assimilation, the bidirectional serine hydroxymethyltransferase  
362 (GlyA) condenses glycine with methylene-H<sub>4</sub>F to serine, representing the first step of the  
363 serine cycle (Fig. 4). The enzymes involved in the serine cycle were upregulated by the strains  
364 when exposed to high CH<sub>4</sub> concentrations, indicating investment into carbon assimilation at  
365 this condition.

#### 366 Comparative proteomics: Electron transport chain

367 The relative abundances of protein complexes involved in the electron transport chain for ATP  
368 synthesis was lower in atmospheric CH<sub>4</sub> compared to the high CH<sub>4</sub> treatment (Supplementary  
369 Fig. 5). The NADH-quinone oxidoreductase, cytochrome c oxidase, and the ATP synthase were  
370 all highly expressed at high CH<sub>4</sub> concentrations indicating increased investment into energy  
371 conservation at high substrate supply. We propose that to overcome energy limitations when  
372 exposed to air, all three strains upregulate the expression of enzymes for the oxidation of at  
373 least one trace gas to maximize uptake rates and energy yield, while investments in energy  
374 conservation and energy-intensive carbon assimilation are reduced. This reduced investment  
375 in assimilation is in line with the low concentrations of the trace gases, low uptake rates, and  
376 overall slow growth of atmMOB when incubated with air as energy and carbon source<sup>33</sup>.

377

378 Specific affinity

379 The  $\alpha_A^0$  for CH<sub>4</sub>, expressed as the fraction of  $V_{\max(\text{app})}$  and  $K_{\text{m}(\text{app})}$ , directly represents the  
380 capacity to oxidize CH<sub>4</sub> at low concentrations. To test if the pMMO upregulation in *M.*  
381 *palsarum* NE2 and downregulation in *M. gorgona* MG08 at atmospheric CH<sub>4</sub> concentrations  
382 translate into a higher  $\alpha_A^0$  for CH<sub>4</sub> by *M. palsarum* NE2 compared to *M. gorgona* MG08, we  
383 measured the  $\alpha_A^0$  of the two strains when grown on air. To avoid increases in the apparent half  
384 saturation constant ( $K_{\text{m}(\text{app})}$ ) estimates at high CH<sub>4</sub> concentrations<sup>59</sup>, we pre-incubated the  
385 cultures on filters floating on carbon-free medium for five months with air as sole energy and  
386 carbon source.

387 By measuring the CH<sub>4</sub> oxidation per cell and hour at different CH<sub>4</sub> concentrations, we  
388 estimated a  $K_{\text{m}(\text{app})}$  of 48.54 nM CH<sub>4</sub> and a  $V_{\max(\text{app})}$  of  $4.91 \times 10^{-8}$  nmol cell<sup>-1</sup> h<sup>-1</sup> resulting in a  $\alpha_A^0$   
389 of  $1.01 \times 10^{-9}$  L cell<sup>-1</sup> h<sup>-1</sup> for *M. gorgona* MG08 (Supplementary Fig. 6). A  $K_{\text{m}(\text{app})}$  of 48.54 nM  
390 CH<sub>4</sub> is within the range of the  $K_{\text{m}(\text{app})}$  values measured for fresh oxic soils reported by Bender  
391 and Conrad (30 – 51 nM)<sup>13</sup>, which led to the theory that atmMOB are oligotrophs with a high  
392 affinity for CH<sub>4</sub>. This is the first observation of a methanotroph in pure culture showing a  $K_{\text{m}(\text{app})}$   
393 that is in the range of the low  $K_{\text{m}(\text{app})}$  values measured in upland soils<sup>25,60</sup>. Our  $\alpha_A^0$  estimate for  
394 *M. gorgona* MG08 ( $1.01 \times 10^{-9}$  L cell<sup>-1</sup> h<sup>-1</sup>) is approximately five times higher than the  $\alpha_A^0$   
395 reported by Tveit et al.  $1.95 \times 10^{-10}$  L cell<sup>-1</sup> h<sup>-1</sup><sup>33</sup>. However, the  $K_{\text{m}(\text{app})}$  and  $V_{\max(\text{app})}$  reported by  
396 Tveit et al. amount 4905 nM and  $95.4 \times 10^{-8}$  nmol cell<sup>-1</sup> h<sup>-1</sup>, respectively, values approximately  
397 100 and 20 times higher than in the current study. These differences might derive from the  
398 use of liquid cultures pre-incubated at 20% CH<sub>4</sub> by Tveit et al. Such a high CH<sub>4</sub> concentration  
399 could have influenced the cellular pMMO concentration, as indicated by the pMMO  
400 upregulation by *M. gorgona* MG08 at 1000 p.p.m.v. CH<sub>4</sub> described above (Fig. 4), and thus  
401 increased the  $K_{\text{m}(\text{app})}$  and  $V_{\max(\text{app})}$  estimates. Dunfield and Conrad reported a similar alteration

402 of  $K_{m(\text{app})}$  and  $V_{\text{max}(\text{app})}$  for *Methylocystis* strain LR1 after comparing starved cells to cells  
403 exposed to 10% CH<sub>4</sub> while the  $a_A^0$  was more constant<sup>59</sup>.

404 The  $K_{m(\text{app})}$  of *M. palsarum* NE2 was 402.08 nM CH<sub>4</sub>, which is approximately eight times higher  
405 than the  $K_{m(\text{app})}$  of *M. gorgona* MG08. Despite this higher  $K_{m(\text{app})}$ , the  $a_A^0$  of *M. palsarum* NE2  
406 was  $3.30 \times 10^{-9}$  L cell<sup>-1</sup> h<sup>-1</sup>, three times higher than estimated for *M. gorgona* MG08. This high  
407  $a_A^0$  derives from its substantially higher  $V_{\text{max}(\text{app})}$  of  $133 \times 10^{-8}$  nmol cell<sup>-1</sup> h<sup>-1</sup> (Supplementary  
408 Fig. 6) and aligns with the proteomic data. The upregulation of the pMMO at atmospheric CH<sub>4</sub>  
409 concentrations by *M. palsarum* NE2 seem to translate into higher a  $a_A^0$  for CH<sub>4</sub> compared to  
410 *M. gorgona* MG08 that downregulated its pMMO. This is also reflected in the CH<sub>4</sub> oxidation  
411 rate of *M. palsarum* NE2 at atmospheric concentrations, which surpassed the rate of *M.*  
412 *gorgona* MG08, despite having a lower apparent affinity for CH<sub>4</sub> (Supplementary Fig. 6).

413 An apparent affinity of 402.08 nM CH<sub>4</sub> is not considered as high affinity<sup>28,43</sup>. Thus, as both  
414 strains grow on air, a high apparent affinity for CH<sub>4</sub> cannot be considered a prerequisite for  
415 this lifestyle. The  $a_A^0$  of *M. gorgona* MG08 and *M. palsarum* NE2 are approximately equally  
416 high and three times higher, respectively, than the recently reported  $a_A^0$  of  
417 *Methylotuvimicrobium buryatense* 5GB1C<sup>61</sup> and 30 and 100 times higher, respectively, than  
418 the  $a_A^0$  of *Methylocystis* sp. SC2 ( $3.4 \times 10^{-11}$  L cell<sup>-1</sup> h<sup>-1</sup>)<sup>26</sup>, the MOB with the fourth highest  $a_A^0$   
419 for CH<sub>4</sub> known so far. However, the different experimental setups and CH<sub>4</sub> concentrations  
420 used to determine  $a_A^0$  might render the comparisons invalid<sup>26,61</sup>. Nevertheless, our results  
421 show that<sup>58</sup> the specific affinity ( $a_A^0$ ), rather than the affinity ( $K_{m(\text{app})}$ ), is the appropriate model  
422 to determine the efficiency of atmospheric CH<sub>4</sub> utilization by atmMOB. This is in line with the  
423 work on oligotrophic substrate uptake at low concentrations by Button<sup>62</sup>.

424

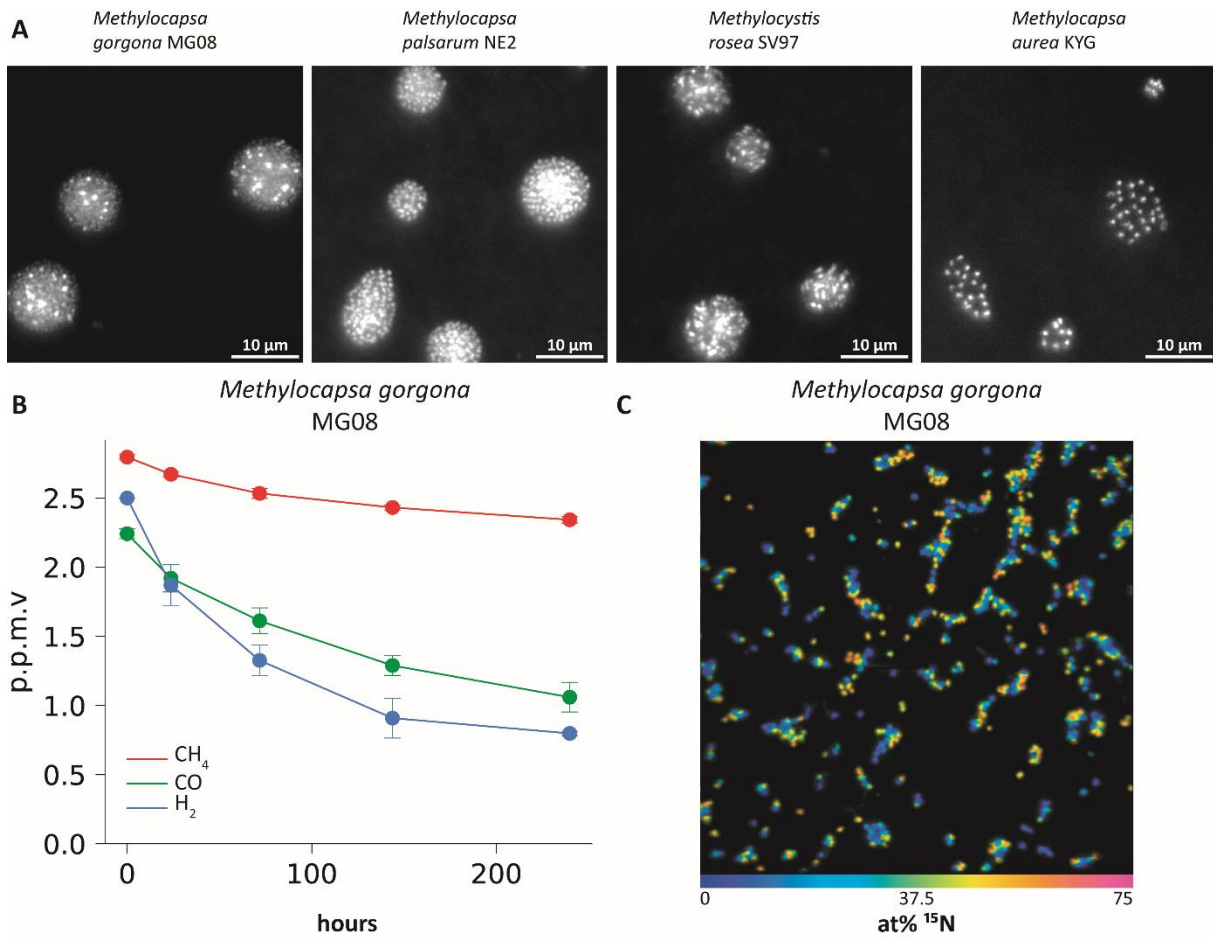
425 Growth on nitrogen from air

426 The four atmMOB, *M. gorgona* MG08, *M. palsarum* NE2, *M. rosea* SV97, and *M. aurea* KYG,  
427 encode all genes required for dinitrogen (N<sub>2</sub>) fixation<sup>33</sup> and grow in nitrogen-free medium at  
428 high CH<sub>4</sub> concentrations<sup>34,35,37,63</sup>. To test the potential for growth on nitrogen from air, we  
429 incubated filter cultures of these strains with air as the sole energy, carbon, and nitrogen  
430 source. The colony formation of all four strains after three months, and trace gas uptake by  
431 *M. gorgona* MG08 after one year, demonstrates growth in the absence of bioavailable  
432 nitrogen sources in the medium (Fig. 5A, 5B, and Supplementary Fig. 7). This suggests that all  
433 four strains can either cover their nitrogen requirements by the fixation of N<sub>2</sub>, by the  
434 utilization of atmospheric reactive nitrogen during growth on air, or both. While the N<sub>2</sub>  
435 concentration in air is approximately 78 %, ammonia concentrations, for example, have been  
436 observed to range between 0.2 and 24 p.p.b.v.<sup>64</sup>.

437 To test for N<sub>2</sub> fixation during growth on air by *M. gorgona* MG08, we incubated filter cultures  
438 in air enriched with <sup>15</sup>N-N<sub>2</sub> (~23 atom % (at%) of the total N<sub>2</sub>) and CH<sub>4</sub>, H<sub>2</sub>, and CO  
439 concentrations fluctuating between 0.03 and 3 p.p.m.v. for two months. Afterwards, we  
440 measured cellular <sup>15</sup>N<sub>2</sub> fixation using NanoSIMS (Fig. 5C). All cells (n = 379) measured during  
441 NanoSIMS incorporated <sup>15</sup>N (Table S15 and S16) indicating that all cells have been active  
442 during incubation. This supports the validity of our energy estimations (as mentioned above)  
443 and demonstrates growth on trace gases in air. The cellular <sup>15</sup>N ranged from 2.99 at% to 61.89  
444 at% with an average of 30.79 at% (SD = 7.82 at%) (Supplementary table S15) while the control  
445 without <sup>15</sup>N<sub>2</sub> enrichment averaged at 0.37 at% (SD = 0.04) (Supplementary table S16). Since  
446 the <sup>15</sup>N<sub>2</sub> in the headspace amounted to approximately 23 at% of the total N<sub>2</sub> during incubation,  
447 the <sup>15</sup>N average of the cells should not have amounted to more than 23 at%. The high values  
448 might issue from bioavailable <sup>15</sup>N-species in the <sup>15</sup>N<sub>2</sub> gas used for incubation<sup>65</sup>. Purity tests of

449 the  $^{15}\text{N}_2$  gas prior to the  $^{15}\text{N}_2$  fixation experiments revealed only a minor  $\text{NO}_x$  contamination  
450 of 101.59 ( $\text{nmol ml}^{-1}$ ) with a very low  $^{15}\text{N}$  fraction of 0.0014 at% and ammonia levels below  
451 detection limit ( $1 \text{ nmol ml}^{-1}$ ), and thus do not provide indications that contamination can  
452 explain our observations. However, even undetectable trace amounts of  $^{15}\text{N}$  ammonia  
453 contaminating the  $^{15}\text{N}_2$  might be sufficient to cause high cellular  $^{15}\text{N}$ -enrichments given the  
454 low amount of biomass of the filter cultures and the long incubation times. Thus, despite not  
455 being able to detect any  $^{15}\text{N}$ -contaminants, we cannot exclude contamination and thereby  
456 cannot confirm  $\text{N}_2$  fixation. However, considering the growth on nitrogen-free medium  
457 (Supplementary Fig. 7) and the NanoSIMS experiment, we can conclude that *M. gorgona*  
458 MG08 either fixes  $\text{N}_2$  or trace concentrations of reactive nitrogen species. This demonstrates  
459 that atmMOB can cover their nitrogen requirements for growth, in addition to energy and  
460 carbon, from air. Additionally, it suggests that atmMOB may not be nitrogen limited under  
461 most natural conditions, partially answering the question by Bodelier and Steenberg regarding  
462 conditions that can be nitrogen limiting to atmMOB<sup>39</sup>.

463



465

466 Figure 5. A) Images of SYBR green I stained colonies formed by *M. gorgona* MG08, *M. palarum* NE2, *M. rosea* SV97, and *M.*  
 467 *aurea* KYG after three months of incubation with air as sole energy, carbon, and nitrogen source B) Trace gas oxidation of  
 468 *Methylocapsa gorgona* MG08 filter cultures after 12 months of incubation with air as sole carbon, energy, and nitrogen  
 469 source. Error bars indicate standard deviation (n = 4) (Supplementary table S1). C) NanoSIMS visualization of <sup>15</sup>N incorporation  
 470 by *M. gorgona* MG08 after two months of incubation under a <sup>15</sup>N<sub>2</sub>-enriched atmosphere. Fraction values of <sup>15</sup>N/(<sup>14</sup>N + <sup>15</sup>N)  
 471 are given in at%.

472

473 Conclusion

474 Growth on air and enduring oxidation of atmospheric CH<sub>4</sub> is not restricted to members of the  
475 clades USC $\alpha$  and  $\gamma$ , but more widespread than previously assumed. Our data shows that  
476 former liquid culture-based cultivation approaches lead to an underestimation of the true  
477 potential of methanotrophic pure cultures to oxidize atmospheric CH<sub>4</sub>. The appearance of  
478 atmMOB outside the USC $\alpha$  and  $\gamma$  revises our understanding of the biological atmospheric CH<sub>4</sub>  
479 sink and should be considered in future studies. The strain specific oxidation patterns and the  
480 estimations of the  $a_A^0$  for CH<sub>4</sub> demonstrate that both the mixotrophic oxidation of atmospheric  
481 trace gases and a high  $a_A^0$  for CH<sub>4</sub> are key to obtain sufficient energy for growth on air. The  
482 estimated energy requirements for growth of the four atmMOB are substantially lower than  
483 the maintenance energy value used as basic premise for an oligotrophic lifestyle of MOB.  
484 Additionally, atmMOB seem to cover not only their energy and carbon but also their nitrogen  
485 requirements from the atmosphere. This opens a new perspective on physiological limitations  
486 of atmospheric trace gas oxidizers and suggests that atmMOB may carry an ideal set of  
487 properties needed for pioneering species to initiate primary succession in unfavorable  
488 environments. Additionally, the high  $a_A^0$  for CH<sub>4</sub> enables atmMOB to utilize trace  
489 concentrations of CH<sub>4</sub> as energy and carbon source for growth while being extremely  
490 oligotrophic. This bears the potential for cost-effective and efficient biofiltration of  
491 anthropogenic emissions containing CH<sub>4</sub> concentrations far below the lower explosive limit.  
492 The common metabolic strategy to grow on air seems to be the downregulation of enzymes  
493 involved in energy-intensive processes combined with the upregulation of enzymes for the  
494 oxidation of trace gases. However, the differing expression patterns of enzymes for trace gas  
495 oxidation and the strain-specific trace gas oxidation patterns indicate that a diverse metabolic  
496 repertoire has evolved to enable life on air.

497 Acknowledgements

498 We thank Alena Didriksen from the University of Tromsø for her involvement in cell  
499 quantification, Toril Anne Grønset and Jack-Ansgar Bruun from PRiME for their contributions  
500 to the comparative proteomics analysis and Cornelia Rottensteiner, Judith Prommer, and  
501 Margarete Watzka from the University of Vienna for the carbon content analysis and <sup>15</sup>N<sub>2</sub> gas  
502 purity test.

503 Funding: This study was supported by the Research Council of Norway FRIPRO Young  
504 Researcher Grant 315129, Living on Air, and Tromsø Research Foundation starting grant  
505 project Cells in the Cold 17\_SG\_ATT to ATT. Mass spectrometry-based proteomic analyses  
506 were performed by UiT Proteomics and Metabolomics Core Facility (PRiME). This facility is a  
507 member of the National Network of Advanced Proteomics Infrastructure (NAPI), which is  
508 funded by the Research Council of Norway INFRASTRUKTUR-program (project number:  
509 295910).

510 Authors contributions

511 T.S., M.M.S. and A.T.T. conceived the study. T.S., A.G.H., J.B., H.S., A.Sch., B.R., E.J.T, O.S., and  
512 A.T.T. performed experiments. T.S., H.S., A.Sch., A.S., A.R. and A.T.T. analyzed data. T.S. and  
513 A.T.T. created the figures. T.S., H.S., A.Sch., B.R., A.R., A.S., M.P, M.M.S, and A.T.T. contributed  
514 to methods. T.S. and A.T.T. wrote the manuscript with inputs from all authors.

515 Competing interests

516 The authors declare no conflict of interest.

517

518 Data availability

519 The proteomics data have been deposited to the ProteomeXchange Consortium via the  
520 PRIDE<sup>66</sup> partner repository with the dataset identifier PXD046190. The data used in this study  
521 are provided in the excel file “Supplementary tables”.

522

523 Methods

524 Filter-based cultivation with air as the sole carbon and energy source

525 The strains were pre-incubated in liquid cultures in 100 mL serum bottles containing 10 mL of  
526 10x diluted, EDTA-free NMS medium (DSMZ medium 921 with 10x the iron concentration and  
527 1  $\mu$ M lanthanum) and a headspace of 20% CH<sub>4</sub> in air. The Fe-EDTA stated in the original DSMZ  
528 recipe was substituted with FeSO<sub>4</sub>. Depending on the strain, the medium was adjusted to a  
529 pH of 6.8 (*Methylocapsa gorgona* MG08, *Methylosinus trichosporium* OB3b, *Methylocystis*  
530 *rosea* SV97, *Methylobacter tundripaludum* SV96) or 5.8 (*Methylocapsa aurea* KYG,  
531 *Methylocapsa acidiphila* B2, and *Methylocapsa palsarum* NE2). The serum bottles were sealed  
532 using butyl rubber stoppers (Chromacol 20-B3P, Thermo Fisher Scientific, Waltham,  
533 Massachusetts, USA) and crimp caps, and incubated at 20°C in dark, until the strains were in  
534 an exponential growth phase. Strain purity was controlled routinely via microscopy and by  
535 confirming the absence of heterotrophic growth on agar plates with a rich medium containing  
536 tryptone, yeast extract, and glucose<sup>32</sup>. After reaching exponential growth phase, the strains  
537 were diluted with the described medium and filtered on 25 mm polycarbonate (PC) filters  
538 (Whatman 10417006, Cytiva, Massachusetts, Marlborough, USA) using a filtration manifold  
539 (EQU-FM-10X20-SET, DHI, Hørsholm, Denmark)<sup>28</sup>. The final cell density on the filters  
540 amounted approximately 20 cells per photo area (630x magnification). The filters were

541 transferred into Petri dishes containing 10x diluted, EDTA-free NMS medium (DSMZ medium  
542 921 with 10x the iron concentration and 1  $\mu\text{M}$  lanthanum) and left floating on the medium  
543 with the cells facing upwards. The Petri dishes enable constant ventilation of the filter cultures  
544 with ambient air while keeping the cultures sterile. The cultures were incubated at 20°C in  
545 dark, with air as the sole energy and carbon source, for at least three months until initiation  
546 of experiments. All cultivation steps were carried out under sterile conditions. Before  
547 experiments, colony formation and microcolony morphology of the strains was routinely  
548 checked via microscopy as previously described<sup>33</sup>. To verify that atmMOB grow on the three  
549 trace gases CH<sub>4</sub>, CO, and H<sub>2</sub> in air, we incubated *M. gorgona* MG08 cells on filters floating on  
550 10x diluted EDTA-free NMS medium in glass bottles sealed with Safety-Caps (JR-S-11011, VICI  
551 AG International, Schenk, Switzerland) under two different atmospheres: One of synthetic  
552 air without the trace gases CH<sub>4</sub>, CO, and H<sub>2</sub> (Gas composition: 400 p.p.m.v. CO<sub>2</sub> and 20.9% O<sub>2</sub>  
553 in N<sub>2</sub>) and another of ambient air. After an incubation period of 15, 20, and 50 days at 20°C,  
554 the growth of cells in the different treatments was compared via microscopy<sup>33</sup> (Supplementary  
555 Fig. 2). To create the synthetic air atmosphere, the bottles were gassed as written in “Trace  
556 gas oxidation experiments”.

#### 557 Trace gas oxidation experiments

558 For all trace gas oxidation experiments, filter cultures of the respective strains, pre-incubated  
559 with air as the sole carbon and energy source, were transferred into 250 mL glass bottles  
560 containing 50 mL 10x diluted EDTA-free NMS medium (DSMZ medium 921 with 10x the iron  
561 concentration and 1  $\mu\text{M}$  lanthanum). The bottles were capped with Safety-Caps (JR-S-11011,  
562 VICI AG International). To create a defined atmosphere within the bottles, the headspace of  
563 each bottle was flushed for 10 minutes with high-purity synthetic air containing 400 p.p.m.v.  
564 CO<sub>2</sub> (HiQ, AGA, Sweden) using a gassing manifold. The headspace pressure was adjusted to

565 approximately 1.05 bar. Then, 1 mL 1000 p.p.m.v. CH<sub>4</sub> in N<sub>2</sub> (HiQ, AGA, Sweden), 1 mL 1000  
566 p.p.m.v. H<sub>2</sub> in N<sub>2</sub> (HiQ, AGA, Sweden), and 1 mL 1000 p.p.m.v. CO in N<sub>2</sub> (HiQ, AGA, Sweden)  
567 were added to the headspace using a gas tight syringe. To assess the oxidation rate of the  
568 respective strains, the cultures were incubated at 20°C and the change in CH<sub>4</sub>, H<sub>2</sub>, and CO  
569 concentrations within bottle headspaces were measured. For each measurement, 2 mL of the  
570 gas in the headspace were sampled using a gas tight syringe. The gas samples were analyzed  
571 with a gas chromatograph (ThermoScientific Trace 1300, Thermo Fisher Scientific) equipped  
572 with a sample loop, a Hayesep column (SU12875, RESTEK, Bellefonte, Pennsylvania, USA), a  
573 Molsieve 5A column (PKC17080, RESTEK), a pulsed discharge detector, and a flame ionization  
574 detector. A high-quality gas containing 2.5 p.p.m.v. CH<sub>4</sub>, 2.5 p.p.m.v. H<sub>2</sub>, and 2.5 p.p.m.v. CO  
575 in N<sub>2</sub> served as standard (HiQ, AGA, Sweden). To determine the gas concentrations in the  
576 bottle headspaces, standard curves were created every day of measurement. The headspace  
577 pressure was measured at the end of the experiment using a manometer (LEO1, Keller,  
578 Winterthur, Switzerland). The mass of each trace gas was calculated by applying the ideal gas  
579 law and adjusted for changes in pressure caused by gas removal during measurement.

#### 580 Cell quantification

581 For quantification, cells from filters were processed as follows: The filters were placed on 150  
582 µL 25x SYBR green I (10463252, Thermo Fisher Scientific) with cells facing upwards and  
583 incubated for 10 minutes in dark. Next, the cells were washed twice by letting the filters float  
584 on milliQ water for 5 minutes in dark. To remove the cells from the filters, the filters were  
585 transferred into 5 mL tubes (0030122321, Eppendorf, Hamburg, Germany) containing 2 mL  
586 10x diluted solution 1 (DSMZ medium 921), so that the filters stucked to the tube wall and the  
587 cells faced inwards<sup>67</sup>. The tubes were vortexed for 10 minutes at medium speed. After  
588 vortexing, remaining cells on the filters were washed off and collected by rinsing the filters

589 with 1 mL solution 1 (DSMZ medium 921). The washed filters were dried in dark, and the cell  
590 removal controlled via fluorescence microscopy. The 3 mL cell suspension resulting from the  
591 cell removal was spiked with 50  $\mu$ L absolute counting beads (Invitrogen<sup>tm</sup> CountBright<sup>tm</sup> Plus,  
592 Thermo Fisher Scientific). After, the cells in suspension were immediately counted using a flow  
593 cytometer (BD FACSAria III, BD Biosciences, Franklin Lakes, New Jersey, USA). The flow  
594 cytometer was set up to capture SYBR Green I (excitation = 498 nm, emission = 522 nm) in the  
595 green channel and the Invitrogen<sup>tm</sup> CountBright<sup>tm</sup> Plus Absolute Counting Beads (excitation =  
596 350 – 810 nm, emission = 385 – 860 nm) in the blue channel. Unstained cells of *M. gorgona*  
597 MG08, *M. palarum* NE2, *M. rosea* SV97, and *M. aurea* KYG were used to define the  
598 autofluorescence threshold in the different channels. Size beads (NPPS-4K, Spherotech, Lake  
599 Forest, Illinois, USA) were used to draw the forward scatter gate covering events between 0.58  
600 and 4  $\mu$ m (Supplementary Fig. 11). SYBR green I stained cells and absolute counting beads  
601 were counted to determine  
602 the cell number within filter cultures, using the following equation:

603 
$$x_{filter} = \frac{b_{abs}}{b_c} \times x_c$$

604 Where  $x_{filter}$  is the absolute cell number of the filter culture,  $b_{abs}$  the number of counting  
605 beads added,  $b_c$  the number of counting beads counted, and  $x_c$  the number of SYBR green I  
606 stained cells counted.

#### 607 Cell-specific oxidation rates and energy calculation

608 The gas-specific oxidation rates of the different strains at atmospheric CH<sub>4</sub>, H<sub>2</sub>, and CO  
609 concentrations and pseudo first order kinetics were calculated and tested as described by  
610 Tveit et al<sup>32</sup>. The oxidation rate per cell was calculated by dividing the oxidation rate of the  
611 filter culture by the corresponding cell number. The Gibbs free energy changes ( $\Delta_r G$ ) for the

612 following reactions:  $CH_4 + 2O_2 \rightarrow 2H_2O + CO_2$ ,  $2H_2 + O_2 \rightarrow 2H_2O$ ,  $2CO + O_2 \rightarrow 2CO_2$ , at  
613 20°C, 1.013 bar absolute, and atmospheric concentrations of  $CH_4$  (1.87 p.p.m.v.),  $H_2$  (0.5  
614 p.p.m.v.), and  $CO$  (0.2 p.p.m.v.) amount to  $-797.4 \text{ kJ mol}^{-1}$ ,  $-236.8 \text{ kJ mol}^{-1}$ , and  $-199.9 \text{ kJ mol}^{-1}$   
615 respectively. The values are based on the values for Gibbs free energy of formation  
616 found in literature<sup>32,68</sup> and the following equation:

$$622 \quad \Delta_r G = \Delta_r G^\circ + RT \ln Q_r$$

617 where  $\Delta_r G^\circ$  is the Gibbs free energy change at standard conditions,  $R$  the gas constant,  $T$  the  
618 temperature,  $\ln$  the natural logarithm, and  $Q_r$  the reaction quotient. The estimates of energy  
619 yield per cell were obtained from the trace gas oxidation per cell and the  $\Delta_r G$ . The energy  
620 yield from trace gas oxidation per carbon mol of biomass and hour ( $\text{kJ C-mol}^{-1} \text{ hour}^{-1}$ ) was  
621 estimated including the strain specific carbon content and dry weight as previously shown<sup>26</sup>.

#### 623 Cellular dry mass and carbon content estimations

624 The strain-specific cellular dry mass was determined by measuring single-cell buoyant mass  
625 distributions of the strains in  $H_2O$ -based and deuterium oxide ( $D_2O$ )-based solutions of  
626 phosphate saline buffer (PBS) using a suspended microchannel resonator (SMR)<sup>69,70</sup>. To do so,  
627 filter cultures of *M. gorgona* MG08, *M. rosea* SV97, *M. palarum* NE2, and *M. aurea* KYG were  
628 incubated on 10x diluted, EDTA-free NMS medium (DSMZ medium 921 with 10x the iron  
629 concentration and 1  $\mu\text{M}$  lanthanum) under an atmosphere of 1000 p.p.m.v.  $CH_4$  in air for three  
630 weeks. After, cells of filter cultures were fixed by incubating the filters on 150  $\mu\text{l}$  formaldehyde  
631 in 1xPBS (4% w/v) for an hour at room temperature. The cells were washed twice by letting  
632 the filters float on water for 5 minutes. The fixed cells were harvested as described in "Cell  
633 quantification". The resulting cell suspension was stored at 4°C until measurements of the  
634 buoyant cell mass. For the measurements, two aliquots with the same volume of each cell  
635 suspension were created. The water of the aliquots was replaced by  $H_2O$ -based (1x PBS in  $H_2O$ )

636 and D<sub>2</sub>O-based (1x PBS in 9:1 D<sub>2</sub>O:H<sub>2</sub>O) solutions of known density (1.0043 g cm<sup>-3</sup> and 1.1033  
637 g cm<sup>-3</sup> at 20°C, respectively). To do so the aliquots were dried in a vacuum concentrator at  
638 37°C. After, the cells of one of the two aliquots were resuspended in 50 µl of the H<sub>2</sub>O-based  
639 solution. The cells of the second aliquot were resuspended in 50 µl of the D<sub>2</sub>O-based solution.  
640 The buoyant mass of the cells in the aliquots were measured with a SMR (LifeScale, Affinity  
641 Biosensors, Santa Barbara, California, USA). The precision and accuracy of the SMR was  
642 verified by creating calibration curves using NIST-certified polystyrene beads (ThermoFisher  
643 Scientific) as performed previously<sup>71</sup>.

644 The buoyant mass data were exported from the LifeScale instrument and further analyzed  
645 using the Python 3<sup>72</sup> packages Pandas<sup>73</sup>, Matplotlib<sup>74</sup>, and Seaborn<sup>72,75</sup> (Supplementary Fig.  
646 10). The dry mass of the strains was calculated as described<sup>69</sup> using the median of the single-  
647 cell buoyant mass distributions in H<sub>2</sub>O-based and D<sub>2</sub>O-based solutions and the following  
648 equation:

$$649 \quad m_{dry} = \frac{\rho_{D_2O} \times m_{b,H_2O} - \rho_{H_2O} \times m_{b,d_2O}}{\rho_{D_2O} - \rho_{H_2O}}$$

650 Where  $m_{dry}$  is the dry mass,  $\rho_{D_2O}$  the density of the D<sub>2</sub>O-based solution,  $m_{b,H_2O}$  the cell's  
651 buoyant mass in the H<sub>2</sub>O-based solution,  $\rho_{H_2O}$  the density of the H<sub>2</sub>O-based solution, and  
652  $m_{b,d_2O}$  the cell's buoyant mass in the D<sub>2</sub>O-based solution.

653 The cellular carbon contents of the atmMOB were analyzed using an elemental analyzer  
654 coupled to an isotope ratio mass spectrometer (EA-IRMS; EA1110 coupled via a ConFlo III  
655 interface to a DeltaPLUS IRMS, Thermo Fisher Scientific). Biomass for the carbon content  
656 analysis was derived from stirred-tank bioreactor (DASbox<sup>®</sup> Mini Bioreactor System,  
657 Eppendorf) cultures. The cultures were grown in 10x diluted, EDTA-free NMS medium (DSMZ

658 medium 921 with 10x the iron concentration and 1  $\mu$ M lanthanum) at 80 rpm (marine  
659 impeller), 20°C, pH 6.8 (CO<sub>2</sub> controlled) and a gassing rate of 0.24 vessel volumes per minute  
660 (6000 p.p.m.v. CH<sub>4</sub> in air) using a microsparger (78530205, Eppendorf). After harvest, cultures  
661 were washed three times with milliQ water and lyophilized.

## 662 Comparative proteomics

663 For the atmospheric CH<sub>4</sub> treatment, filter-cultures of *M. gorgona* MG08, *M. rosea* SV97 and  
664 *M. palsarum* NE2 were incubated with air as the only carbon and energy source for seven  
665 months. After, the cells on filters were harvested as described in “Cell quantification”,  
666 lyophilized, and stored at -80°C until further processing. The 1000 p.p.m.v. CH<sub>4</sub> treatment of  
667 the respective strains was processed the same way as the atmospheric CH<sub>4</sub> treatment with  
668 the difference that filter cultures had been exposed to approximately 1000 p.p.m.v. CH<sub>4</sub> in air  
669 for two weeks before harvest. Samples of lyophilized cells were lysed by sonication in 20  $\mu$ L  
670 buffer containing 4 M urea, 2.5 % sodium deoxycholate (SDC) and 100 mM triethylammonium  
671 bicarbonate (TEAB). Samples were sonicated for 25 cycles (1 min on, 30 sec off) with maximum  
672 amplitude in a cup horn sonicator with a recirculating chiller (Cup horn: model 413C2, Qsonica,  
673 Newtown, Connecticut, USA; Sonicator: Fisherbrandtm FB705, Thermo Fisher Scientific;  
674 Recirculating chiller: model 4905 Qsonica). Then, disulfide bridges were reduced with 1,4-  
675 dithiothreitol (DTT) at a final concentration of 5 mM and incubation at 54°C for 30 min.  
676 Cysteines were alkylated with 15 mM iodoacetamide (IAA) and incubated for 30 min at room  
677 temperature in dark. To remove excess IAA, DTT solution corresponding to a final  
678 concentration of 5 mM was added. Calcium chloride solution (final concentration of 1 mM)  
679 and 1  $\mu$ g Lysyl Endopeptidase (125-05061, FUJIFILM Wako Chemicals Europe, Neuss,  
680 Germany) were added to the samples and incubated for 5 hours under gentle agitation at 37°C  
681 for enzymatic digestion. After, samples were diluted with a buffer containing 100 mM

682 triethylammonium bicarbonate (TEAB) and 1 mM CaCl<sub>2</sub> to lower the urea and sodium  
683 deoxycholate (SDC) concentration to 1 M and 0.65 % v/v, respectively, resulting in a final  
684 sample volume of 80 µL. For digestion, 2 µg trypsin (V511A, Promega, Wisconsin, USA) were  
685 added and the samples incubated on a gently agitated shaker at 37°C for 16 hours. After  
686 digestion, SDC was precipitated by adding 50% formic acid to the sample (final concentration  
687 of 2.5% v/v). Samples were then incubated for 10 min and centrifuged at 16200 rcf for 15 min.  
688 Supernatants containing peptides were transferred to low-protein-binding tubes. The  
689 peptides were concentrated and cleaned up using DPX C18 pipette tips (DPX Technologies,  
690 XTR tips 10 mg C18AQ 300Å) on a Tecan Fluent pipetting robot (Tecan Group Ltd., Männedorf,  
691 Switzerland). Purified peptide samples were dried in a vacuum concentrator and dissolved in  
692 12 µL 0.1% formic acid. Peptide concentrations were measured on a spectrophotometer  
693 (Nanodrop ONE, Thermo Fisher Scientific) at 205 nm. 0.25 µg peptides per sample were loaded  
694 onto a liquid chromatograph (EASY-nLC1200, Thermo Fisher Scientific) equipped with an  
695 EASY-Spray column (C18, 2µm, 100 Å, 50µm, 50 cm). Peptides were fractionated using a 5 –  
696 80% acetonitrile gradient in 0.1 % formic acid over 120 min at a flow rate of 300 nL min<sup>-1</sup>. The  
697 separated peptides were analyzed using a mass spectrometer (Orbitrap Exploris 480, Thermo  
698 Fisher Scientific). Data was collected in data dependent mode using a Top40 method.  
699 Annotated genomes of the three strains downloaded from MicroScope<sup>76</sup> served as databases  
700 for the CHIMERYS-based data search using Proteome Discoverer 3.0. Normalized abundances  
701 (scaling mode: On All Average) of proteins were further processed via Perseus<sup>77</sup>. Normal  
702 distribution of Log<sub>2</sub> fold transformed data was visually screened using histograms. Proteins  
703 were filtered using a threshold of at least three valid values in at least one treatment (n = 4  
704 per treatment). Proteins that passed the filtering were included in downstream analyses.  
705 Missing values were imputed from normal distribution using default settings (width = 0.3,

706 down shift = 1.8). The Pearson correlation coefficient ranged from  $\rho = 0.918$  to  $\rho = 0.989$   
707 between replicates and from 0.68 to 0.799 between replicates of the different treatments.  
708 Imputed protein abundance results of the 1.9 p.p.m.v. and 1000 p.p.m.v. treatments were  
709 used for correspondence analysis (CA). CA was conducted in R<sup>78</sup> using the “ca” function of R  
710 package “ca”<sup>79</sup>. The top 10% of proteins that contributed most to the inertia of the CA’s first  
711 dimension were extracted using the function “get\_ca\_row” of the R package “factoextra”<sup>80</sup>.  
712 To map the abundances and the hierarchical EggNOG<sup>45</sup> annotations of the top 10% proteins,  
713 the EggNOG annotations of the three strains were downloaded from MicroScope. For the in-  
714 depth analysis of trace gas oxidation, carbon assimilation, and the electron transport chain,  
715 the differences between treatments were tested using a two-sided t-test ( $s_0 = 2$ ) and  
716 permutation-based false discovery rate (FDR = 0.01). From the z-score normalized results, the  
717 proteins involved in trace gas oxidation, carbon assimilation via the serine cycle, and the  
718 electron transport chain were selected for further analysis using Python 3<sup>72</sup>. The core carbon  
719 and energy metabolism of *M. rosea* SV97 and *M. palsarum* NE2 were reconstructed manually  
720 using MicroScope annotations, the published metabolism entries of *M. gorgona* MG08<sup>33</sup>,  
721 KEGG<sup>81</sup>, and protein BLAST searches<sup>82</sup>. To conduct a thorough screening for putative carbon  
722 monoxide dehydrogenase subunits a blast-searchable database was constructed out of all  
723 sequences retrieved from the NCBI Identical Protein Groups resource<sup>48</sup> (accessed May, 30<sup>th</sup>  
724 2023) using the search term “carbon monoxide dehydrogenase” (54076 amino acid sequence  
725 entries). Entries with an amino acid sequence length <30 were removed from the database  
726 prior to the blastp search. The annotated genomes of *M. rosea* SV97 and *M. palsarum* NE2,  
727 downloaded from MicroScope, were used as blastp queries (default settings, -outfmt 6  
728 including slen). After a pre-filtering removing hits with an E-value >1 and an alignment length

729 <50% of the aligned database entry, the blastp output tables were manually evaluated  
730 (Supplementary table S10-11).

### 731 Specific affinity

732 Filter cultures of *M. gorgona* MG08 and *M. palsarum* NE2 were pre-incubated on 10x diluted,  
733 EDTA-free NMS medium (DSMZ medium 921 with 10x the iron concentration and 1  $\mu$ M  
734 lanthanum) for five months with air as sole energy and carbon source. The filter cultures were  
735 transferred into 250 mL glass bottles containing 250 mL of the mentioned medium. The glass  
736 bottles were capped with Safety-Caps (JR-S-11011, VICI AG International). For each strain, the  
737 CH<sub>4</sub> concentrations in the 50 mL headspace were adjusted to approximately 1.9, 14, 30, 70,  
738 and 175 p.p.m.v. by adding 0 – 2.5 mL 1000 or 5000 p.p.m.v. CH<sub>4</sub> in N<sub>2</sub> (HiQ, Linde, Sweden).  
739 The headspace pressure of all bottles was adjusted to approximately 1.1 bar using air. After,  
740 the strains were incubated for 48 hours at 20°C. The change in CH<sub>4</sub> was measured at  
741 incubation start, after 24 hours and 48 hours as described above. Standard curves were  
742 created using 2.5 and 50 p.p.m.v. CH<sub>4</sub> in N<sub>2</sub> (HiQ, AGA, Sweden). At the end of the oxidation  
743 experiment, cells in filter cultures were quantified as described above. The change in mass of  
744 CH<sub>4</sub> in the headspace was calculated by applying the ideal gas law and adjusted for changes in  
745 pressure caused by gas removal during measurement. The mass of dissolved CH<sub>4</sub> at different  
746 CH<sub>4</sub> partial pressures in the headspace was calculated by applying the Henry's law solubility  
747 constant for CH<sub>4</sub> at 20°C. The Michaelis-Menten CH<sub>4</sub> oxidation kinetics were modelled using  
748 the "nls" function of the "nlstools" R package<sup>83</sup>, specifying the "michaelis" model and  
749 providing start values for  $K_{m(\text{app})}$  and  $V_{\text{max}(\text{app})}$ . The  $\alpha_A^0$  was calculated by dividing  $V_{\text{max}}$  by  $K_m$ .

750 Growth on nitrogen from air

751 Filter cultures of *M. gorgona* MG08, *M. palsarum* NE2, *M. rosea* SV97, and *M. aurea* KYG were  
752 pre-incubated on 10x diluted, EDTA-free, and potassium nitrate (KNO<sub>3</sub>)-free NMS medium  
753 (DSMZ medium 921 with 10x the iron concentration and 1 μM lanthanum) with air as sole  
754 energy, carbon, and nitrogen source. After three months, colony formation was checked via  
755 microscopy<sup>33</sup>. After 12 months, the activity of *M. gorgona* MG08 was measured as described  
756 in the section “Trace gas oxidation experiments” with the only difference that the KNO<sub>3</sub>-free  
757 medium was used.

758 For the detection of <sup>15</sup>N<sub>2</sub> fixation via NanoSIMS, filter cultures were pre-incubated on 10x  
759 diluted, EDTA-free, and potassium nitrate (KNO<sub>3</sub>)-free NMS medium with air as sole energy,  
760 carbon source, and nitrogen source. After three months, the filters were transferred into 250  
761 ml glass bottles containing 50ml of the KNO<sub>3</sub>-free NMS medium. The bottles were capped with  
762 Safety-Caps (JR-S-11011, VICI AG International) and the headspace of each bottle was flushed  
763 for five minutes with compressed air using a gassing manifold. Afterwards, 50 ml of 98+ at%  
764 <sup>15</sup>N<sub>2</sub> gas (NLM-363-1-LB, Cambridge Isotopes Laboratories, Twerksbury, Massachusetts, USA)  
765 were added using a gas syringe so that the <sup>15</sup>N-N<sub>2</sub> in headspace atmosphere amounted  
766 approximately 23 at% of the total N<sub>2</sub>. The headspace pressure was adjusted to 1.05 bar and  
767 0.5 mL 1000 p.p.m.v. CH<sub>4</sub> in N<sub>2</sub> (HiQ, AGA, Sweden), 1 mL 1000 p.p.m.v. H<sub>2</sub> in N<sub>2</sub> (HiQ, AGA,  
768 Sweden), and 1 mL 1000 p.p.m.v. CO in N<sub>2</sub> (HiQ, AGA, Sweden) were added to the headspace  
769 using a gas syringe. To account for the natural abundance of <sup>15</sup>N-N<sub>2</sub>, a control without the  
770 addition of <sup>15</sup>N<sub>2</sub> gas was prepared accordingly. The filter cultures were incubated at 20°C for  
771 two months. The headspace concentration of CH<sub>4</sub>, H<sub>2</sub>, and CO during incubation was  
772 measured once a week as mentioned in the “Trace gas oxidation experiments” section and

773 replenished if the concentration of CH<sub>4</sub>, H<sub>2</sub>, and CO dropped below 1.9 p.p.m.v., 0.5 p.p.m.v.,  
774 0.2 p.p.m.v., respectively.

775 After two months, the cells of the filter cultures were fixed by incubating the filters on 150 µl  
776 formaldehyde in 1×PBS (4% w/v) for an hour at room temperature. The cells were washed  
777 twice by letting the filters float on water for 5 minutes. The fixed cells were harvested as  
778 described in “Cell quantification”, lyophilized, and stored at -80°C until further processing. For  
779 NanoSIMS analysis the lyophilized cells were resuspended in 20 µl MilliQ water. 10 µl of the  
780 cell suspensions were deposited on antimony-doped silicon wafer platelets (7.1 × 7.1 × 0.75  
781 mm, Active Business Company, Germany) and dried in air. The following two samples were  
782 prepared accordingly for NanoSIMS analysis: i) The unlabeled *M. gorgona* MG08 cells, serving  
783 as control for the natural abundance of <sup>15</sup>N<sub>2</sub>; and ii) the *M. gorgona* MG08 cells incubated with  
784 <sup>15</sup>N<sub>2</sub> gas and trace concentrations of CH<sub>4</sub>, H<sub>2</sub>, and CO that were analyzed to see whether the  
785 strain is capable of fixing atmospheric nitrogen during growth with air as sole energy and  
786 carbon source.

787 The NanoSIMS measurements were performed on a NanoSIMS 50 I (Cameca, Gennevilliers,  
788 France) at the Large-Instrument Facility for Advanced Isotope Research at the University of  
789 Vienna. Before the data acquisition, analysis areas were preconditioned *in situ* by rastering of  
790 a high-intensity, defocused Cs<sup>+</sup> ion beam in the following sequence of high and extreme low  
791 ion impact energies (HE/16 keV and EXLIE/50 eV, respectively): HE at 25 pA beam current to a  
792 Cs<sup>+</sup> fluence of 5.0E14 ions cm<sup>-2</sup>; EXLIE at 400 pA beam current to a fluence of 5.0E16 ions cm<sup>-2</sup>;  
793 and HE at 25 pA to a fluence of 5.0E14 ions cm<sup>-2</sup>. Data were acquired as multilayer image  
794 stacks by repeated scanning of a finely focused Cs<sup>+</sup> primary ion beam (c. 80 nm probe size at

795 approx. 2 pA beam current) over areas between  $34 \times 34$  and  $72 \times 72 \mu\text{m}^2$  at  $512 \times 512$ -pixel  
796 image resolution and a primary ion beam dwell time of  $5 \text{ ms pixel}^{-1}$ .

797 NanoSIMS images were generated and analyzed with the OpenMIMS plugin<sup>84</sup> in the image  
798 processing package Fiji<sup>85</sup>. All images were auto-tracked for compensation of primary ion beam  
799 and/or sample stage drift, and secondary ion signal intensities were corrected for detector  
800 dead-time and quasi-simultaneous arrival (QSA) of secondary ions, utilizing sensitivity factors  
801 ('beta' values) of 1.06, and 1.05 for  $\text{C}_2^-$ , and  $\text{CN}^-$  ions, respectively. Regions of interest (ROIs)  
802 were defined in the  $^{12}\text{C}^-$ -ion image where each ROI corresponded to an individual cell. Cells  
803 touching the border of the image were omitted from the selection.

804 Acquisition cycles of all three analysis areas were reduced to 27 each to improve comparability  
805 among the measurements. Regions of interest were analyzed for their  $^{15}\text{N}$  content by  
806 calculating the average value across acquisition cycles per analysis area, referred to by the  
807  $^{15}\text{N}/(^{14}\text{N} + ^{15}\text{N})$  isotope fraction designated as at%  $^{15}\text{N}$ , which was calculated from the  $^{12}\text{CN}^-$   
808 signal intensities via:

809 
$$\text{at}\% ^{15}\text{N} = \frac{^{12}\text{C}^{15}\text{N}^-}{^{12}\text{C}^{15}\text{N}^- + ^{12}\text{C}^{14}\text{N}^-}$$

810 The natural abundance of  $^{15}\text{N}$  in cellular biomass was inferred from unlabeled cells yielding  
811  $0.369 \pm 0.043$  at% (mean  $\pm 1$  SD).

812

### 813 Plotting

814 Plots were created using the Python 3<sup>72</sup> packages Pandas<sup>73</sup>, Matplotlib<sup>74</sup>, and Seaborn<sup>75</sup> and  
815 R packages ggplot2<sup>86</sup>. Figures were finalized using Adobe Illustrator 2023.

816 References

- 817 1. Intergovernmental Panel on Climate Change. The Earth's Energy Budget, Climate  
818 Feedbacks and Climate Sensitivity. In: *Climate Change 2021 – The Physical Science Basis*.  
819 Cambridge University Press; 2023:923-1054. doi:10.1017/9781009157896.009
- 820 2. Mar KA, Unger C, Walderdorff L, Butler T. Beyond CO2 equivalence: The impacts of  
821 methane on climate, ecosystems, and health. *Environ Sci Policy*. 2022;134:127-136.  
822 doi:10.1016/j.envsci.2022.03.027
- 823 3. Ehhalt DH. The atmospheric cycle of methane. *Tellus*. 1974;26(1-2):58-70.  
824 doi:10.1111/j.2153-3490.1974.tb01952.x
- 825 4. Saunio M, Stavert AR, Poulter B, et al. The Global Methane Budget 2000–2017. *Earth*  
826 *Syst Sci Data*. 2020;12(3):1561-1623. doi:10.5194/essd-12-1561-2020
- 827 5. Rigby M, Montzka SA, Prinn RG, et al. Role of atmospheric oxidation in recent methane  
828 growth. *Proceedings of the National Academy of Sciences*. 2017;114(21):5373-5377.  
829 doi:10.1073/pnas.1616426114
- 830 6. Jackson RB, Saunio M, Bousquet P, et al. Increasing anthropogenic methane emissions  
831 arise equally from agricultural and fossil fuel sources. *Environmental Research Letters*.  
832 2020;15(7):071002. doi:10.1088/1748-9326/ab9ed2
- 833 7. Peng S, Lin X, Thompson RL, et al. Wetland emission and atmospheric sink changes  
834 explain methane growth in 2020. *Nature*. 2022;612(7940):477-482.  
835 doi:10.1038/s41586-022-05447-w
- 836 8. Ocko IB, Hamburg SP. Climate consequences of hydrogen emissions. *Atmos Chem Phys*.  
837 2022;22(14):9349-9368. doi:10.5194/acp-22-9349-2022
- 838 9. Dincer I. Hydrogen 1.0: A new age. *Int J Hydrogen Energy*. 2023;48(43):16143-16147.  
839 doi:10.1016/j.ijhydene.2023.01.124
- 840 10. Tate KR. Soil methane oxidation and land-use change – from process to mitigation. *Soil*  
841 *Biol Biochem*. 2015;80:260-272. doi:10.1016/j.soilbio.2014.10.010
- 842 11. La H, Hettiaratchi JPA, Achari G, Dunfield PF. Biofiltration of methane. *Bioresour*  
843 *Technol*. 2018;268:759-772. doi:10.1016/j.biortech.2018.07.043
- 844 12. Harriss RC, Sebacher DI, Day FP. Methane flux in the Great Dismal Swamp. *Nature*.  
845 1982;297(5868):673-674. doi:10.1038/297673a0
- 846 13. Bender M, Conrad R. Kinetics of CH<sub>4</sub> oxidation in oxic soils exposed to ambient air or  
847 high CH<sub>4</sub> mixing ratios. *FEMS Microbiol Ecol*. 1992;10(4):261-269. doi:10.1111/j.1574-  
848 6941.1992.tb01663.x
- 849 14. Knief C, Lipski A, Dunfield PF. Diversity and Activity of Methanotrophic Bacteria in  
850 Different Upland Soils. *Appl Environ Microbiol*. 2003;69(11):6703-6714.  
851 doi:10.1128/AEM.69.11.6703-6714.2003
- 852 15. Holmes AJ, Roslev P, McDonald IR, Iversen N, Henriksen K, Murrell JC. Characterization  
853 of Methanotrophic Bacterial Populations in Soils Showing Atmospheric Methane

- 854 Uptake. *Appl Environ Microbiol.* 1999;65(8):3312-3318. doi:10.1128/AEM.65.8.3312-  
855 3318.1999
- 856 16. Roslev P, Iversen N. Radioactive Fingerprinting of Microorganisms That Oxidize  
857 Atmospheric Methane in Different Soils. *Appl Environ Microbiol.* 1999;65(9):4064-4070.  
858 doi:10.1128/AEM.65.9.4064-4070.1999
- 859 17. Täumer J, Kolb S, Boeddinghaus RS, et al. Divergent drivers of the microbial methane  
860 sink in temperate forest and grassland soils. *Glob Chang Biol.* 2021;27(4):929-940.  
861 doi:10.1111/gcb.15430
- 862 18. Zhao R, Wang H, Cheng X, Yun Y, Qiu X. Upland soil cluster  $\gamma$  dominates the  
863 methanotroph communities in the karst Heshang Cave. *FEMS Microbiol Ecol.*  
864 2018;94(12):192. doi:10.1093/FEMSEC/FIY192
- 865 19. Cai Y, Zhou X, Shi L, Jia Z. Atmospheric Methane Oxidizers Are Dominated by Upland  
866 Soil Cluster Alpha in 20 Forest Soils of China. *Microb Ecol.* 2020;80(4):859-871.  
867 doi:10.1007/s00248-020-01570-1
- 868 20. Pratscher J, Vollmers J, Wiegand S, Dumont MG, Kaster A. Unravelling the Identity,  
869 Metabolic Potential and Global Biogeography of the Atmospheric Methane-Oxidizing  
870 Upland Soil Cluster  $\alpha$ . *Environ Microbiol.* 2018;20(3):1016-1029. doi:10.1111/1462-  
871 2920.14036
- 872 21. Täumer J, Marhan S, Groß V, et al. Linking transcriptional dynamics of CH<sub>4</sub>-cycling  
873 grassland soil microbiomes to seasonal gas fluxes. *ISME J.* 2022;16(7):1788-1797.  
874 doi:10.1038/s41396-022-01229-4
- 875 22. Deng Y, Che R, Wang F, et al. Upland Soil Cluster Gamma dominates methanotrophic  
876 communities in upland grassland soils. *Science of The Total Environment.* 2019;670:826-  
877 836. doi:10.1016/j.scitotenv.2019.03.299
- 878 23. Knief C. Diversity and Habitat Preferences of Cultivated and Uncultivated Aerobic  
879 Methanotrophic Bacteria Evaluated Based on pmoA as Molecular Marker. *Front*  
880 *Microbiol.* 2015;6(DEC). doi:10.3389/fmicb.2015.01346
- 881 24. Dunfield PF, Liesack W, Henckel T, Knowles R, Conrad R. High-Affinity Methane  
882 Oxidation by a Soil Enrichment Culture Containing a Type II Methanotroph. *Appl Environ*  
883 *Microbiol.* 1999;65(3):1009-1014. doi:10.1128/AEM.65.3.1009-1014.1999
- 884 25. Dunfield PF. The soil methane sink. In: *Greenhouse Gas Sinks.* CABI; 2007:152-170.  
885 doi:10.1079/9781845931896.0152
- 886 26. Knief C, Dunfield PF. Response and adaptation of different methanotrophic bacteria to  
887 low methane mixing ratios. *Environ Microbiol.* 2005;7(9):1307-1317.  
888 doi:10.1111/j.1462-2920.2005.00814.x
- 889 27. Cai Y, Zheng Y, Bodelier PLE, Conrad R, Jia Z. Conventional methanotrophs are  
890 responsible for atmospheric methane oxidation in paddy soils. *Nat Commun.*  
891 2016;7(1):11728. doi:10.1038/ncomms11728
- 892 28. Conrad R. Soil microorganisms oxidizing atmospheric trace gases (CH<sub>4</sub>, CO, H<sub>2</sub>, NO).  
893 *Indian J Microbiol.* 1999;39:193-203.

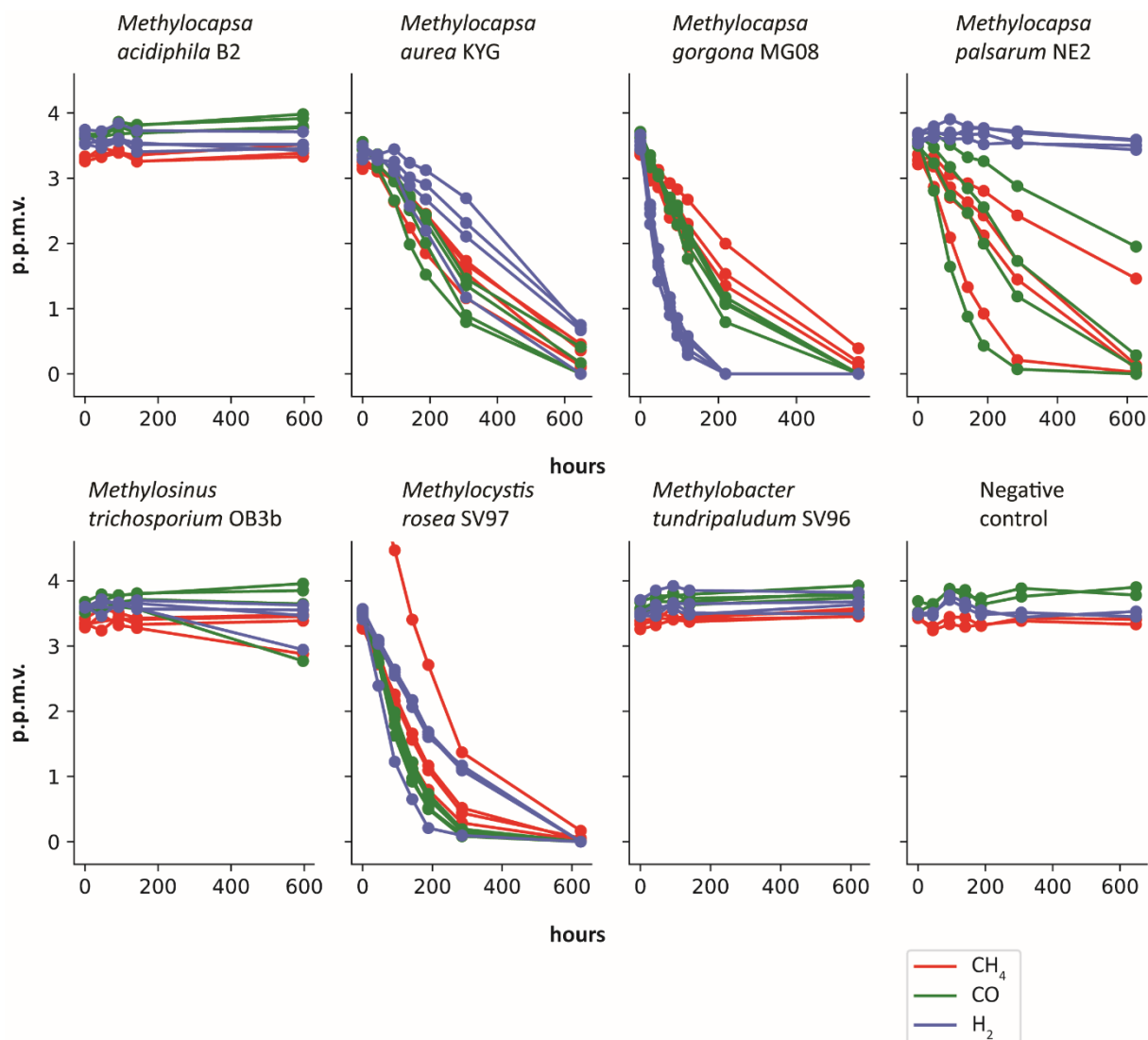
- 894 29. Tijhuis L, Van Loosdrecht MCM, Heijnen JJ. A thermodynamically based correlation for  
895 maintenance gibbs energy requirements in aerobic and anaerobic chemotrophic  
896 growth. *Biotechnol Bioeng.* 1993;42(4):509-519. doi:10.1002/bit.260420415
- 897 30. Button DK. Differences between the kinetics of nutrient uptake by micro-organisms,  
898 growth and enzyme kinetics. *Trends Biochem Sci.* 1983;8(4):121-124.  
899 doi:10.1016/0968-0004(83)90232-3
- 900 31. Degelmann DM, Borken W, Drake HL, Kolb S. Different Atmospheric Methane-Oxidizing  
901 Communities in European Beech and Norway Spruce Soils. *Appl Environ Microbiol.*  
902 2010;76(10):3228-3235. doi:10.1128/AEM.02730-09
- 903 32. Tveit AT, Schmider T, Hestnes AG, Lindgren M, Didriksen A, Svenning MM. Simultaneous  
904 Oxidation of Atmospheric Methane, Carbon Monoxide and Hydrogen for Bacterial  
905 Growth. *Microorganisms.* 2021;9(1):153. doi:10.3390/microorganisms9010153
- 906 33. Tveit AT, Hestnes AG, Robinson SL, et al. Widespread soil bacterium that oxidizes  
907 atmospheric methane. *Proceedings of the National Academy of Sciences.*  
908 2019;116(17):8515-8524. doi:10.1073/pnas.1817812116
- 909 34. Warttinen I, Hestnes AG, McDonald IR, Svenning MM. *Methylocystis rosea* sp. nov., a  
910 novel methanotrophic bacterium from Arctic wetland soil, Svalbard, Norway (78° N).  
911 *Int J Syst Evol Microbiol.* 2006;56(3):541-547. doi:10.1099/ijs.0.63912-0
- 912 35. Dunfield PF, Belova SE, Vorob'ev A V., Cornish SL, Dedysh SN. *Methylocapsa aurea* sp.  
913 nov., a facultative methanotroph possessing a particulate methane monooxygenase,  
914 and emended description of the genus *Methylocapsa*. *Int J Syst Evol Microbiol.*  
915 2010;60(11):2659-2664. doi:10.1099/ijs.0.020149-0
- 916 36. Dedysh SN, Khmelenina VN, Suzina NE, et al. *Methylocapsa acidiphila* gen. nov., sp.  
917 nov., a novel methane-oxidizing and dinitrogen-fixing acidophilic bacterium from  
918 Sphagnum bog. *Int J Syst Evol Microbiol.* 2002;52(1):251-261. doi:10.1099/00207713-  
919 52-1-251
- 920 37. Dedysh SN, Didriksen A, Danilova O V., Belova SE, Liebner S, Svenning MM.  
921 *Methylocapsa palsarum* sp. nov., a methanotroph isolated from a subArctic  
922 discontinuous permafrost ecosystem. *Int J Syst Evol Microbiol.* 2015;65(Pt\_10):3618-  
923 3624. doi:10.1099/ijsem.0.000465
- 924 38. Whittenbury R, Phillips KC, Wilkinson JF. Enrichment, Isolation and Some Properties of  
925 Methane-utilizing Bacteria. *J Gen Microbiol.* 1970;61(2):205-218.  
926 doi:10.1099/00221287-61-2-205
- 927 39. Bodelier PLE, Steenbergh AK. Interactions between methane and the nitrogen cycle in  
928 light of climate change. *Curr Opin Environ Sustain.* 2014;9-10:26-36.  
929 doi:10.1016/j.cosust.2014.07.004
- 930 40. Zhang T, Zhou J, Wang X, Zhang Y. Poly- $\beta$ -hydroxybutyrate Production by *Methylosinus*  
931 *trichosporium* OB3b at Different Gas-phase Conditions. *Iran J Biotechnol.*  
932 2019;17(1):10-16. doi:10.21859/IJB.1866

- 933 41. Tamura K, Nei M. Estimation of the number of nucleotide substitutions in the control  
934 region of mitochondrial DNA in humans and chimpanzees. *Mol Biol Evol.*  
935 1993;10(3):512-526. doi:10.1093/oxfordjournals.molbev.a040023
- 936 42. Tamura K, Stecher G, Kumar S. MEGA11: Molecular Evolutionary Genetics Analysis  
937 Version 11. Battistuzzi FU, ed. *Mol Biol Evol.* 2021;38(7):3022-3027.  
938 doi:10.1093/molbev/msab120
- 939 43. Greening C, Grinter R. Microbial oxidation of atmospheric trace gases. *Nat Rev*  
940 *Microbiol.* 2022;20(9):513-528. doi:10.1038/s41579-022-00724-x
- 941 44. Bonk F, Popp D, Weinrich S, et al. Determination of Microbial Maintenance in  
942 Acetogenesis and Methanogenesis by Experimental and Modeling Techniques. *Front*  
943 *Microbiol.* 2019;10(FEB). doi:10.3389/fmicb.2019.00166
- 944 45. Cantalapiedra CP, Hernández-Plaza A, Letunic I, Bork P, Huerta-Cepas J. eggNOG-  
945 mapper v2: Functional Annotation, Orthology Assignments, and Domain Prediction at  
946 the Metagenomic Scale. Tamura K, ed. *Mol Biol Evol.* 2021;38(12):5825-5829.  
947 doi:10.1093/molbev/msab293
- 948 46. Cordero PRF, Grinter R, Hards K, et al. Two uptake hydrogenases differentially interact  
949 with the aerobic respiratory chain during mycobacterial growth and persistence.  
950 *Journal of Biological Chemistry.* 2019;294(50):18980-18991.  
951 doi:10.1074/jbc.RA119.011076
- 952 47. Piché-Choquette S, Khdhiri M, Constant P. Dose-response relationships between  
953 environmentally-relevant H<sub>2</sub> concentrations and the biological sinks of H<sub>2</sub>, CH<sub>4</sub> and CO  
954 in soil. *Soil Biol Biochem.* 2018;123:190-199. doi:10.1016/J.SOILBIO.2018.05.008
- 955 48. Agarwala R, Barrett T, Beck J, et al. Database resources of the National Center for  
956 Biotechnology Information. *Nucleic Acids Res.* 2018;46(D1):D8-D13.  
957 doi:10.1093/nar/gkx1095
- 958 49. Culpepper MA, Rosenzweig AC. Structure and protein-protein interactions of methanol  
959 dehydrogenase from *Methylococcus capsulatus* (Bath). *Biochemistry.*  
960 2014;53(39):6211-6219. doi:org/10.1021/bi500850j
- 961 50. Escalante-Semerena JC, Wolfe RS. Tetrahydromethanopterin-dependent  
962 methanogenesis from non-physiological C<sub>1</sub> donors in *Methanobacterium*  
963 *thermoautotrophicum*. *J Bacteriol.* 1985;161(2):696-701. doi:10.1128/jb.161.2.696-  
964 701.1985
- 965 51. Kallen RG, Jencks WP. The Mechanism of the Condensation of Formaldehyde with  
966 Tetrahydrofolic Acid. *Journal of Biological Chemistry.* 1966;241(24):5851-5863.  
967 doi:10.1016/S0021-9258(18)96350-7
- 968 52. Marx CJ, Chistoserdova L, Lidstrom ME. Formaldehyde-detoxifying role of the  
969 tetrahydromethanopterin-linked pathway in *Methylobacterium extorquens* AM1. *J*  
970 *Bacteriol.* 2003;185(24):7160-7168. doi:10.1128/JB.185.23.7160-7168.2003
- 971 53. Moon M, Park GW, Lee J pyo, Lee JS, Min K. Recent progress in formate dehydrogenase  
972 (FDH) as a non-photosynthetic CO<sub>2</sub> utilizing enzyme: A short review. *Journal of CO2*  
973 *Utilization.* 2020;42:101353. doi:10.1016/j.jcou.2020.101353

- 974 54. Hartmann T, Leimkühler S. The oxygen-tolerant and NAD<sup>+</sup>-dependent formate  
975 dehydrogenase from *Rhodobacter capsulatus* is able to catalyze the reduction of CO<sub>2</sub>  
976 to formate. *FEBS J.* 2013;280(23):6083-6096. doi:10.1111/febs.12528
- 977 55. Yu X, Niks D, Mulchandani A, Hille R. Efficient reduction of CO<sub>2</sub> by the molybdenum-  
978 containing formate dehydrogenase from *Cupriavidus necator* (*Ralstonia eutropha*).  
979 *Journal of Biological Chemistry.* 2017;292(41):16872-16879.  
980 doi:10.1074/jbc.M117.785576
- 981 56. Crowther GJ, Kosály G, Lidstrom ME. Formate as the Main Branch Point for  
982 Methylophilic Metabolism in *Methylobacterium extorquens* AM1. *J Bacteriol.*  
983 2008;190(14):5057-5062. doi:10.1128/JB.00228-08
- 984 57. Kikuchi G, Motokawa Y, Yoshida T, Hiraga K. Glycine cleavage system: reaction  
985 mechanism, physiological significance, and hyperglycinemia. *Proceedings of the Japan*  
986 *Academy, Series B.* 2008;84(7):246-263. doi:10.2183/pjab.84.246
- 987 58. Claassens NJ, Satanowski A, Bysani VR, et al. Engineering the Reductive Glycine  
988 Pathway: A Promising Synthetic Metabolism Approach for C<sub>1</sub>-Assimilation. In: *Advances*  
989 *in Biochemical Engineering/Biotechnology.* Vol 180. Adv Biochem Eng Biotechnol;  
990 2022:299-350. doi:10.1007/10\_2021\_181
- 991 59. Dunfield PF, Conrad R. Starvation Alters the Apparent Half-Saturation Constant for  
992 Methane in the Type II Methanotroph *Methylocystis* Strain LR1. *Appl Environ Microbiol.*  
993 2000;66(9):4136-4138. doi:10.1128/AEM.66.9.4136-4138.2000
- 994 60. Knief C, Kolb S, Bodelier PLE, Lipski A, Dunfield PF. The active methanotrophic  
995 community in hydromorphic soils changes in response to changing methane  
996 concentration. *Environ Microbiol.* 2006;8(2):321-333. doi:10.1111/j.1462-  
997 2920.2005.00898.x
- 998 61. He L, Groom JD, Wilson EH, et al. A methanotrophic bacterium to enable methane  
999 removal for climate mitigation. *Proceedings of the National Academy of Sciences.*  
1000 2023;120(35). doi:10.1073/pnas.2310046120
- 1001 62. Button DK. Nutrient-limited microbial growth kinetics: overview and recent advances.  
1002 *Antonie Van Leeuwenhoek.* 1993;63(3-4):225-235. doi:10.1007/BF00871220
- 1003 63. Murrell JC, Dalton H. Nitrogen Fixation in Obligate Methanotrophs. *Microbiology (N Y).*  
1004 1983;129(11):3481-3486. doi:10.1099/00221287-129-11-3481
- 1005 64. Nair AA, Yu F. Quantification of Atmospheric Ammonia Concentrations: A Review of Its  
1006 Measurement and Modeling. *Atmosphere (Basel).* 2020;11(10):1092.  
1007 doi:10.3390/atmos11101092
- 1008 65. Dabundo R, Lehmann MF, Treibergs L, et al. The Contamination of Commercial 15N<sub>2</sub>  
1009 Gas Stocks with 15N-Labeled Nitrate and Ammonium and Consequences for Nitrogen  
1010 Fixation Measurements. Love JB, ed. *PLoS One.* 2014;9(10):e110335.  
1011 doi:10.1371/journal.pone.0110335
- 1012 66. Perez-Riverol Y, Bai J, Bandla C, et al. The PRIDE database resources in 2022: A hub for  
1013 mass spectrometry-based proteomics evidences. *Nucleic Acids Res.* 2022;50(D1).  
1014 doi:10.1093/nar/gkab1038

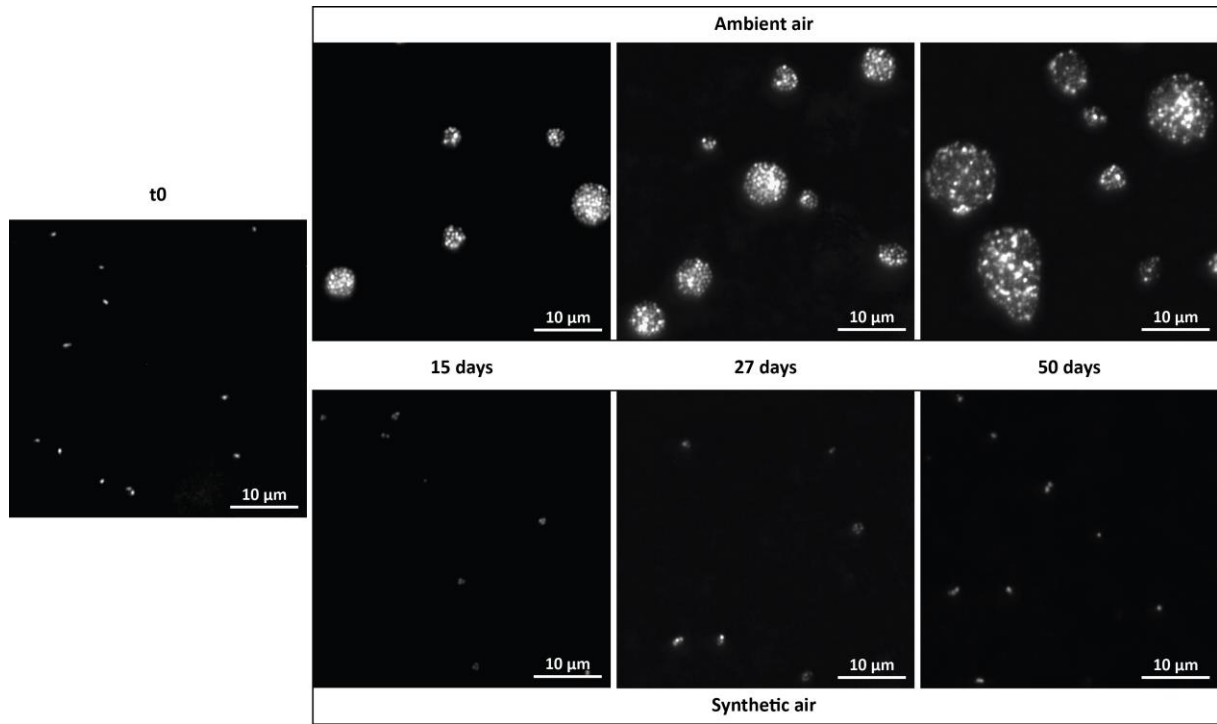
- 1015 67. Couradeau E, Sasse J, Goudeau D, et al. Probing the active fraction of soil microbiomes  
1016 using BONCAT-FACS. *Nat Commun.* 2019;10(1):2770. doi:10.1038/s41467-019-10542-  
1017 0
- 1018 68. Dean JA. LANGE'S HANDBOOK OF CHEMISTRY. *Materials and Manufacturing Processes.*  
1019 1990;5(4):687-688. doi:10.1080/10426919008953291
- 1020 69. Feijó Delgado F, Cermak N, Hecht VC, et al. Intracellular Water Exchange for Measuring  
1021 the Dry Mass, Water Mass and Changes in Chemical Composition of Living Cells.  
1022 Polymenis M, ed. *PLoS One.* 2013;8(7):e67590. doi:10.1371/journal.pone.0067590
- 1023 70. Cermak N, Becker JW, Knudsen SM, Chisholm SW, Manalis SR, Polz MF. Direct single-  
1024 cell biomass estimates for marine bacteria via Archimedes' principle. *ISME J.*  
1025 2017;11(3):825-828. doi:10.1038/ismej.2016.161
- 1026 71. Roller BRK, Hellerschmied C, Wu Y, et al. Single-cell mass distributions reveal simple  
1027 rules for achieving steady-state growth. Ruby EG, ed. *mBio.* Published online September  
1028 6, 2023. doi:10.1128/mbio.01585-23
- 1029 72. Van Rossum G, Drake FL. *Python 3 Reference Manual.* CreateSpace; 2009.
- 1030 73. The Pandas Development T, eam. pandas-dev/pandas: Pandas. Published online  
1031 February 2020. doi:org/10.5281/zenodo.3509134
- 1032 74. Hunter JD. Matplotlib: A 2D Graphics Environment. *Comput Sci Eng.* 2007;9(3):90-95.  
1033 doi:10.1109/MCSE.2007.55
- 1034 75. Waskom M. Seaborn: Statistical Data Visualization. *J Open Source Softw.*  
1035 2021;6(60):3021. doi:10.21105/joss.03021
- 1036 76. Vallenet D, Calteau A, Dubois M, et al. MicroScope: An integrated platform for the  
1037 annotation and exploration of microbial gene functions through genomic, pangenomic  
1038 and metabolic comparative analysis. *Nucleic Acids Res.* 2019;48(D1):D579-D589.  
1039 doi:10.1093/nar/gkz926
- 1040 77. Tyanova S, Temu T, Sinitcyn P, et al. The Perseus computational platform for  
1041 comprehensive analysis of (prote)omics data. *Nat Methods.* 2016;13(9):731-740.  
1042 doi:10.1038/nmeth.3901
- 1043 78. R Core Team. R: A Language and Environment for Statistical Computing. Published  
1044 online 2022. <https://www.R-project.org/>
- 1045 79. c ON, Greenacre M. Correspondence Analysis in R, with Two- and Three-dimensional  
1046 Graphics: The ca Package. *J Stat Softw.* 2007;20(3). doi:10.18637/jss.v020.i03
- 1047 80. Kassambara A, Mundt F. factoextra: Extract and Visualize the Results of Multivariate  
1048 Data Analyses. Published online April 1, 2020. Accessed October 13, 2023.  
1049 <http://www.sthda.com/english/rpkgs/factoextra>
- 1050 81. Kanehisa M. KEGG: Kyoto Encyclopedia of Genes and Genomes. *Nucleic Acids Res.*  
1051 2000;28(1):27-30. doi:10.1093/nar/28.1.27
- 1052 82. Altschul S. Gapped BLAST and PSI-BLAST: a new generation of protein database search  
1053 programs. *Nucleic Acids Res.* 1997;25(17):3389-3402. doi:10.1093/nar/25.17.3389

- 1054 83. Baty F, Ritz C, Charles S, Brutsche M, Flandrois JP, Delignette-Muller ML. A Toolbox for  
1055 Nonlinear Regression in *R*: The Package **nlstools**. *J Stat Softw*. 2015;66(5).  
1056 doi:10.18637/jss.v066.i05
- 1057 84. Gormanns P, Reckow S, Poczatek JC, Turck CW, Lechene C. Segmentation of Multi-  
1058 Isotope Imaging Mass Spectrometry Data for Semi-Automatic Detection of Regions of  
1059 Interest. Rogers S, ed. *PLoS One*. 2012;7(2):e30576. doi:10.1371/journal.pone.0030576
- 1060 85. Schindelin J, Arganda-Carreras I, Frise E, et al. Fiji: an open-source platform for  
1061 biological-image analysis. *Nat Methods*. 2012;9(7):676-682. doi:10.1038/nmeth.2019
- 1062 86. Wickham H. *Ggplot2*. Springer International Publishing; 2016. doi:10.1007/978-3-319-  
1063 24277-4
- 1064
- 1065



1067

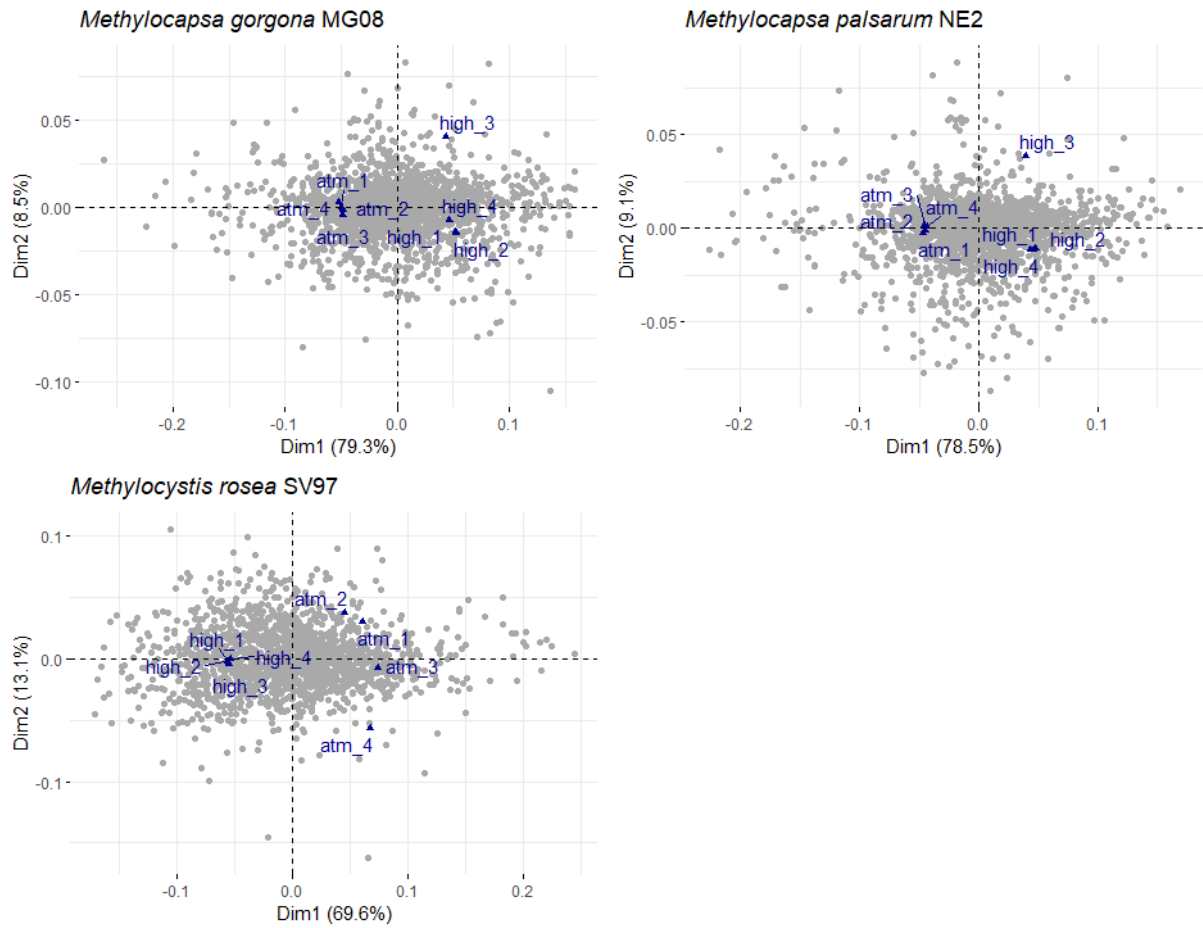
1068 Supplementary Figure 1. CH<sub>4</sub>, H<sub>2</sub>, and CO oxidation at atmospheric pressure by *M. acidiphila* B2, *M. aurea* KYG, *M. gorgona*  
 1069 MG08, *M. palsarum* NE2, *M. trichosporium* OB3b, *M. rosea* SV97, and *M. tundripaludum* SV96 after 12 months of incubation  
 1070 with air as sole carbon and energy source (Supplementary table S1).



1071

1072  
1073

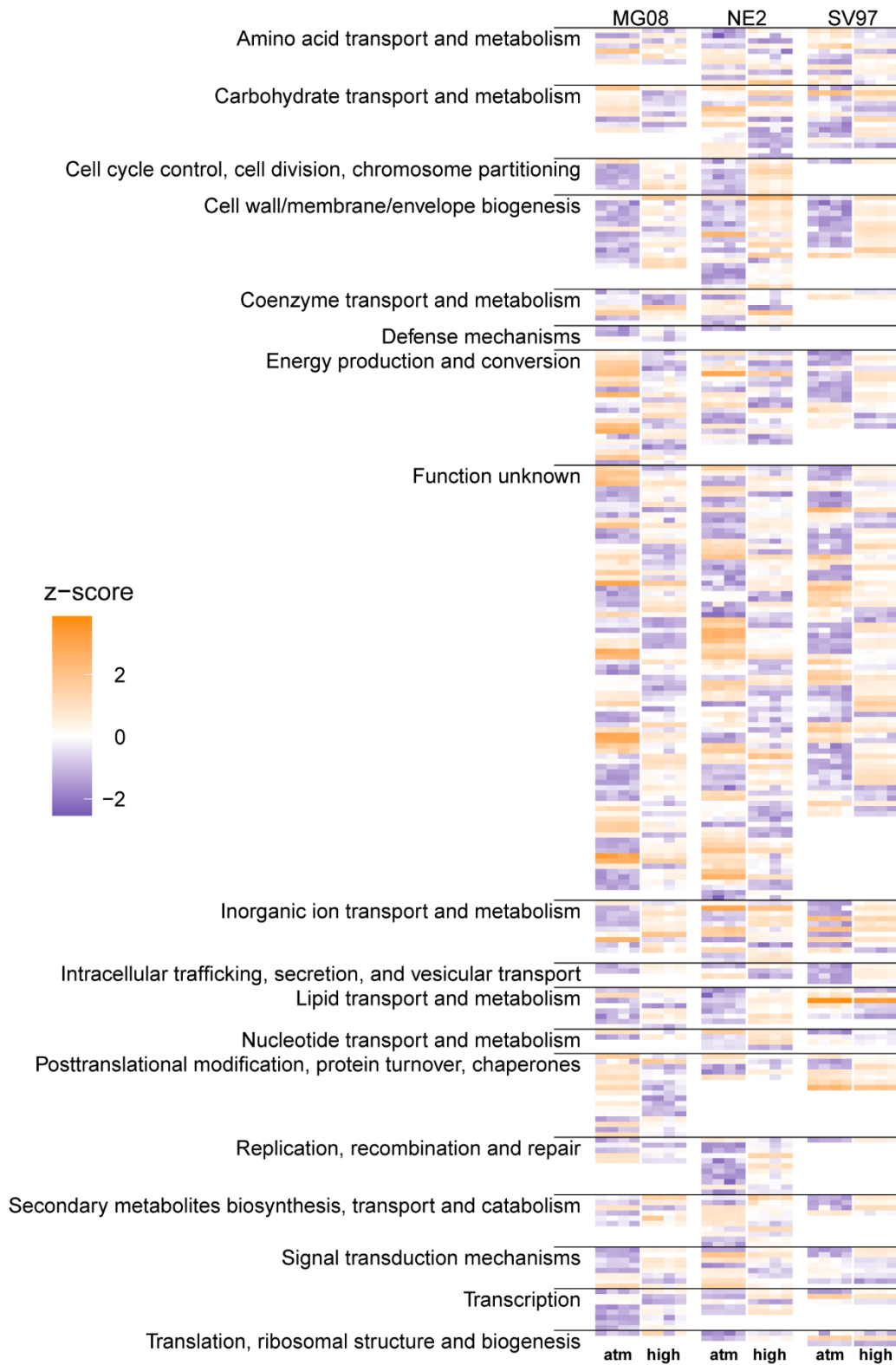
Supplementary Figure 2. SYBR green I stained cells of *M. gorgona* MG08 incubated for 15, 27, and 50 days under an atmosphere of ambient air and an atmosphere of synthetic air without the atmospheric trace gases CH<sub>4</sub>, CO, and H<sub>2</sub>.



1074

1075  
1076  
1077

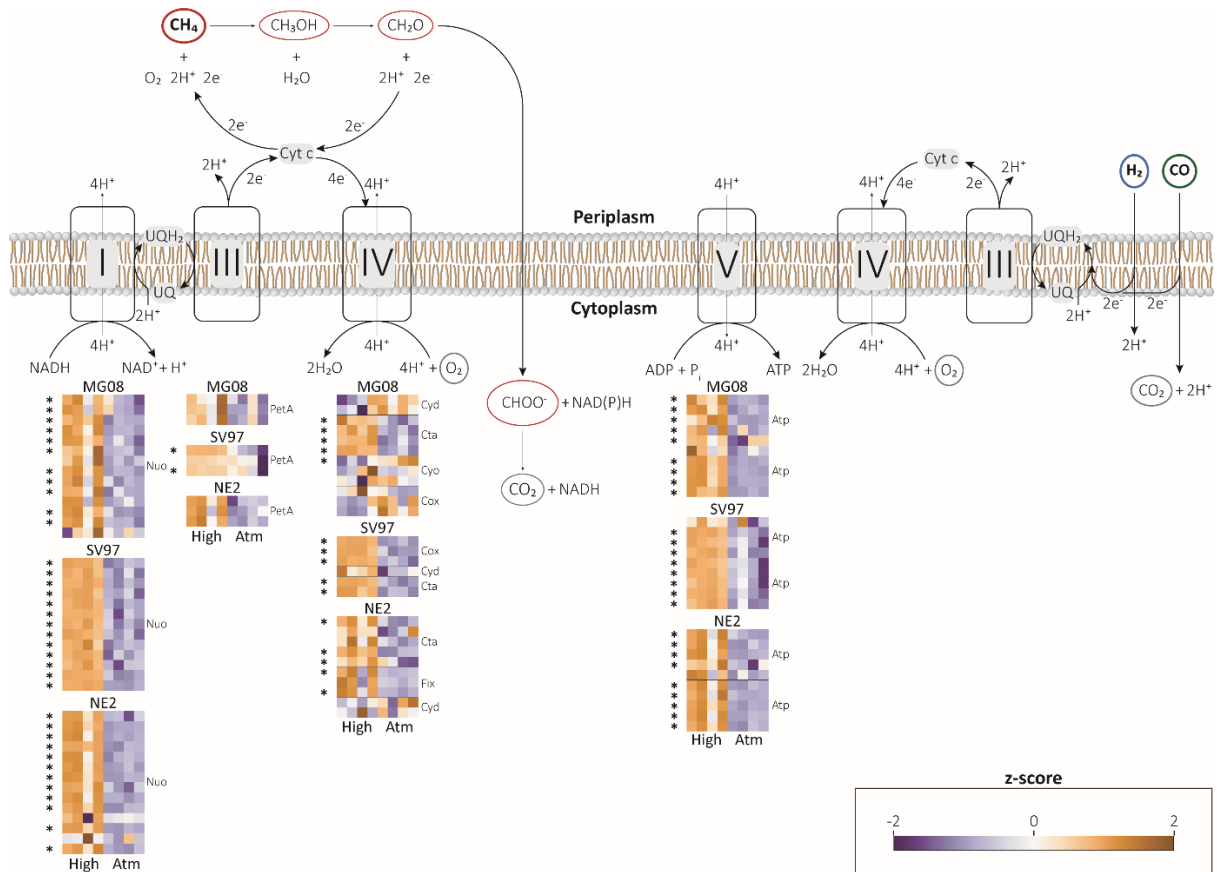
Supplementary Figure 3. Correspondence analysis biplot of protein abundances of *M. gorgona* MG08, *M. palsarum* NE2, and *M. rosea* SV97 at 1.9 p.p.m.v. (atm) and 1000 p.p.m.v. (high) methane in air (Supplementary table S6-8). Replicates (n = 4) incubated at the two CH<sub>4</sub> concentrations are shown in blue. Proteins are shown in grey. Dim – dimension.



1078

1079  
1080  
1081  
1082  
1083

Supplementary Figure 4. Comparative proteomics of *M. gorgona* MG08, *M. rosea* SV97, and *M. palmarum* NE2 exposed to 1000 p.p.m.v. CH<sub>4</sub> (high) in air and 1.9 p.p.m.v. CH<sub>4</sub> (atm) in air (Supplementary table S12-14). Normalized and standardized expression of top 10% proteins contributing most to the inertia of the correspondence analyses (Supplementary Figure 3). High relative abundance = orange, low relative abundance expression = blue. The proteins are grouped by the hierarchical EggNOG categories.

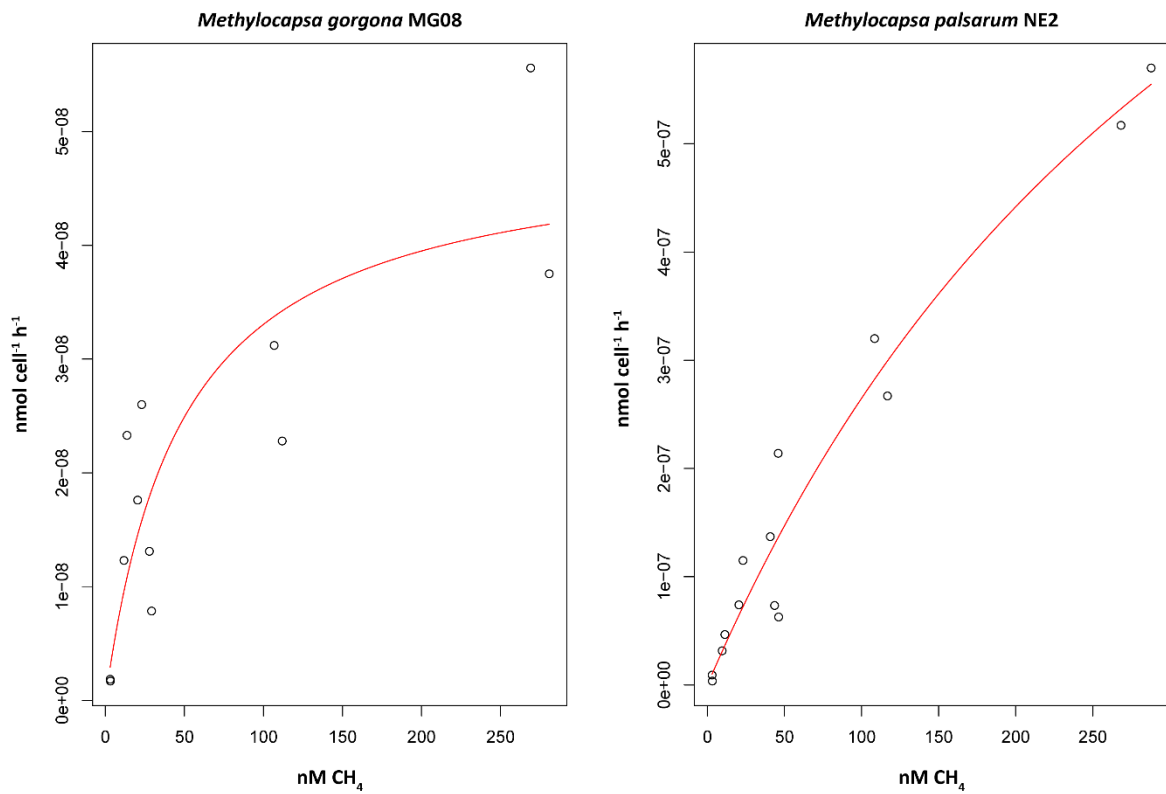


1084

1085 Supplementary Figure 5. Comparative proteomics of *M. gorgona* MG08, *M. rosea* SV97, and *M. parsarum* NE2 exposed to  
 1086 1000 p.p.m.v.  $\text{CH}_4$  (High) in air and 1.9 p.p.m.v. (Atm)  $\text{CH}_4$  in air (Supplementary table S5). Normalized and standardized  
 1087 expression of enzymes involved in the electron transport chain. High relative abundance = orange, low relative abundance  
 1088 expression = blue. \* indicates significant difference in expression between treatments (two sided t-test). Horizontal lines in  
 1089 the heatmaps separate operons of enzymes catalyzing the same reaction. I – NADH ubiquinone oxidoreductase, III –  
 1090 ubiquinol-cytochrome c reductase, IV – cytochrome c oxidase, V – ATP synthase.

1091

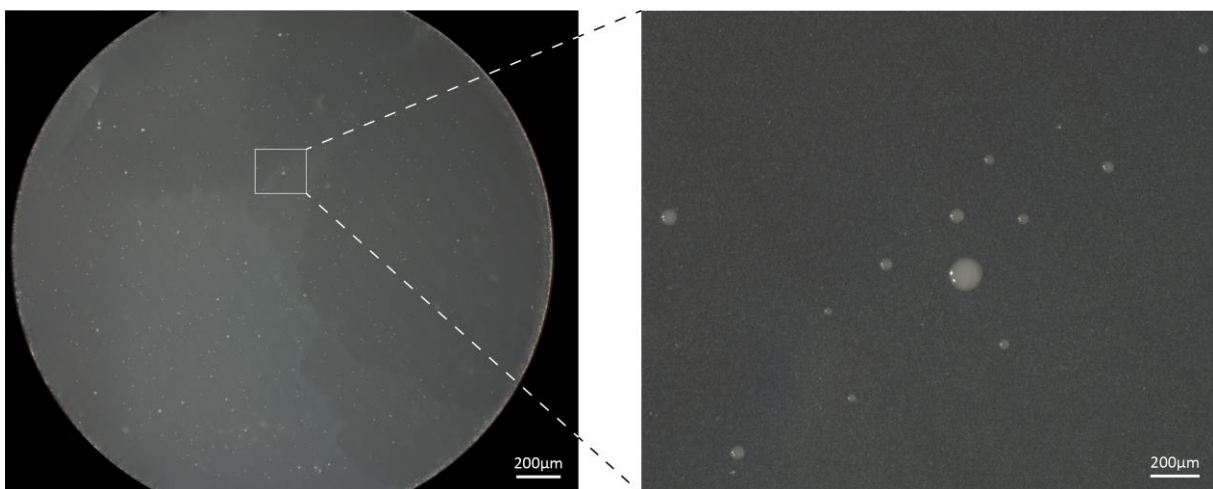
1092



1093

1094 Supplementary Figure 6. Michaelis-Menten hyperbolic curve fitted to the oxidation rate per cell of *M. gorgona* MG08 and *M.*  
 1095 *palsarum* NE2 at CH<sub>4</sub> concentrations ranging between 3 nM and 287 nM (Supplementary table S9). The nM CH<sub>4</sub> display CH<sub>4</sub>  
 1096 concentrations dissolved in water and correlate with the partial pressure of CH<sub>4</sub> above the water. At 20°C and atmospheric  
 1097 pressure (1.013 bar), 2.98, 50, 100, and 250 nM CH<sub>4</sub> dissolved in water correspond to 1.9, 31.9, 63.7, and 159.3 p.p.m.v. in  
 1098 air.

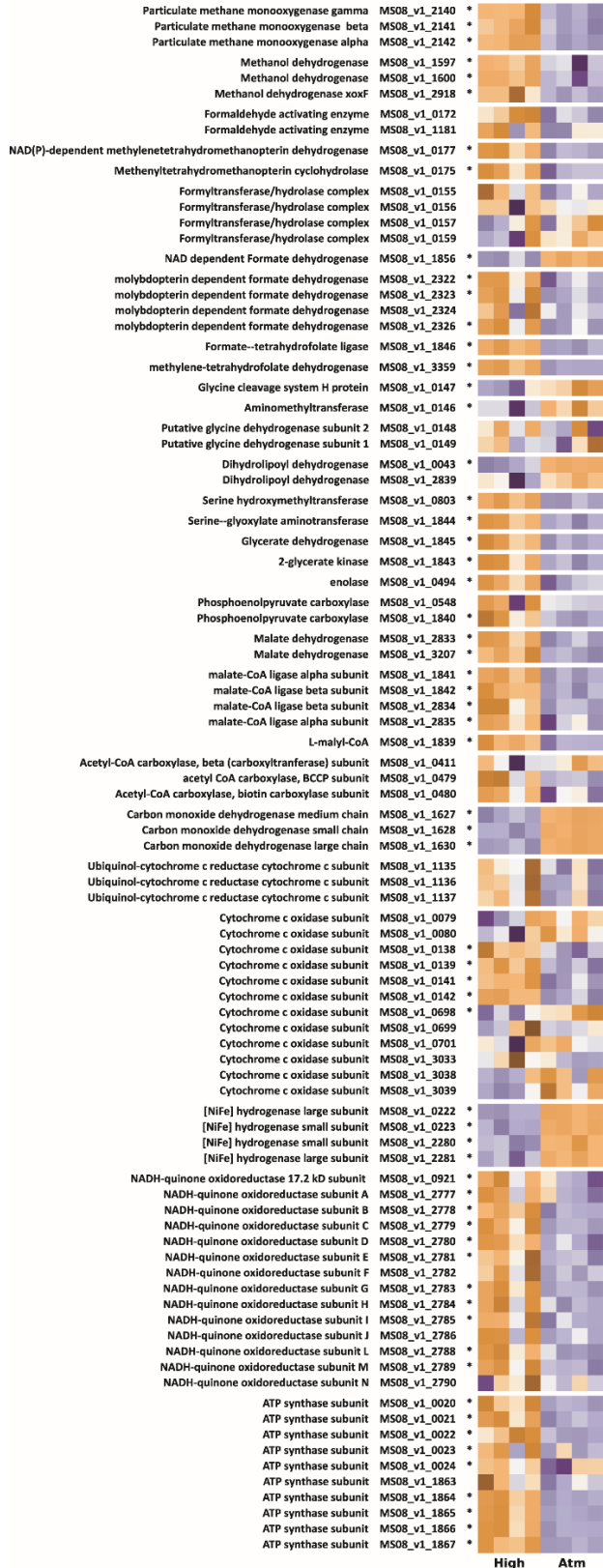
1099



1100

1101 Supplementary Figure 7. Light microscopic image of a *Methylocapsa gorgona* MG08 culture on a polycarbonate filter after 12  
 1102 months incubation period on a carbon- and nitrogen-free growth medium

*Methylocapsa gorgona* MG08



*Methylocystis rosea* SV97

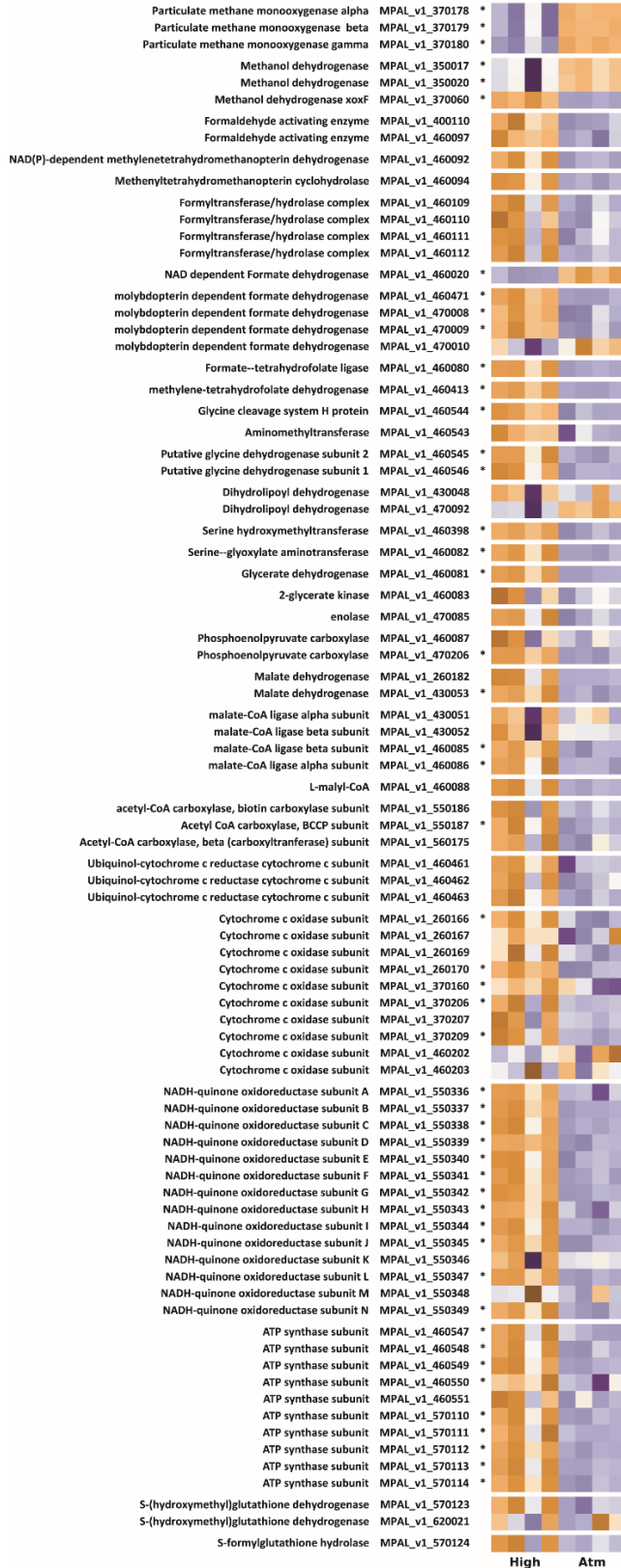


1103

1104  
1105  
1106  
1107  
1108

Supplementary Figure 8. Comparative proteomics of *M. gorgona* MG08, *M. rosea* SV97 exposed to 1000 p.p.m.v CH<sub>4</sub> (High) in air and 1.9 p.p.m.v. (Atm) CH<sub>4</sub> in air (Supplementary table S5). Normalized and standardized expression of enzymes involved in the central carbon and energy metabolism is shown. Same heatmaps as in Figure 4 and Supplementary Figure 5 but with protein name and MicroScope accession number. \* indicates significant difference in expression between treatments (two sided t-test).

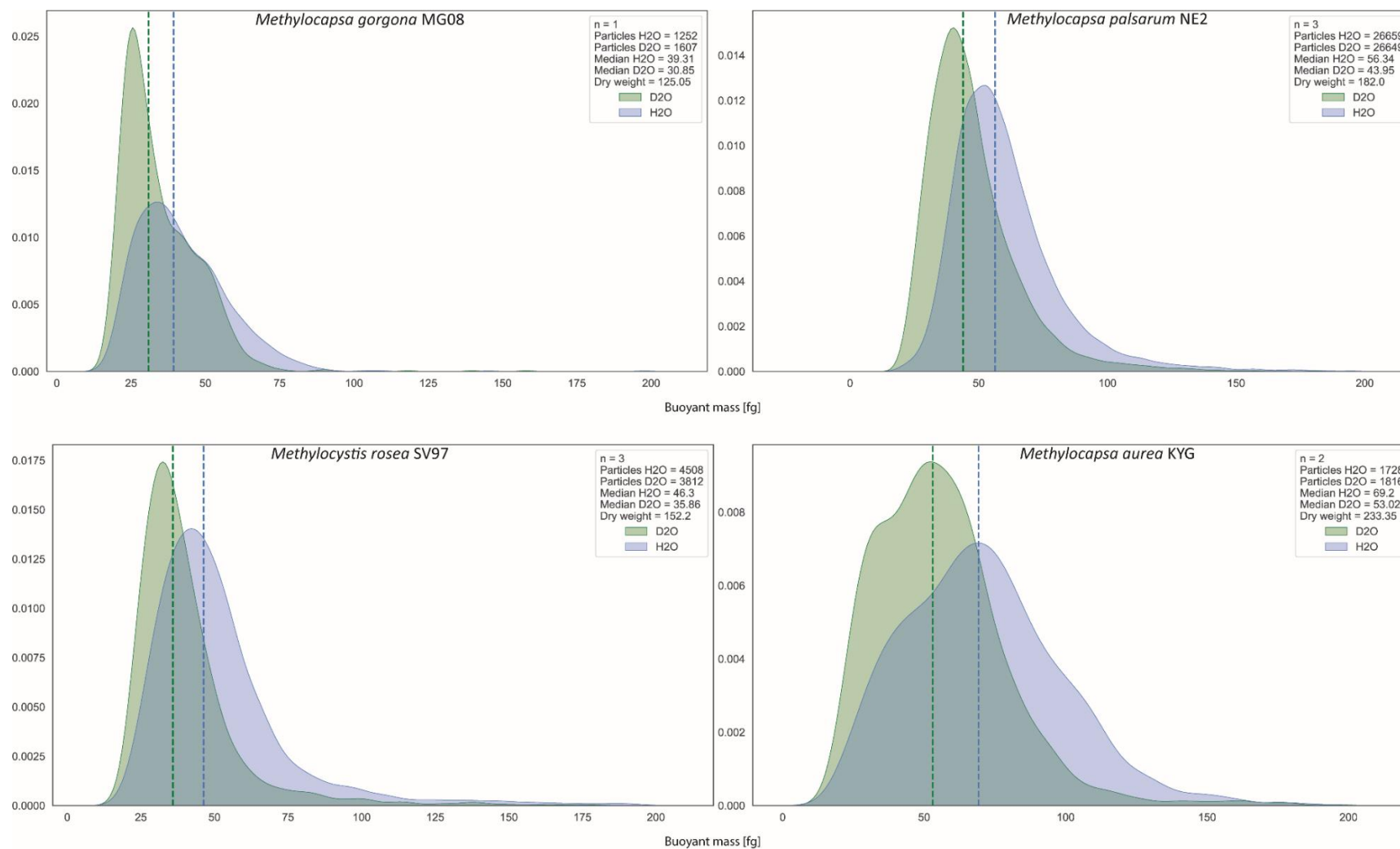
*Methylocapsa palsarum* NE2



1109

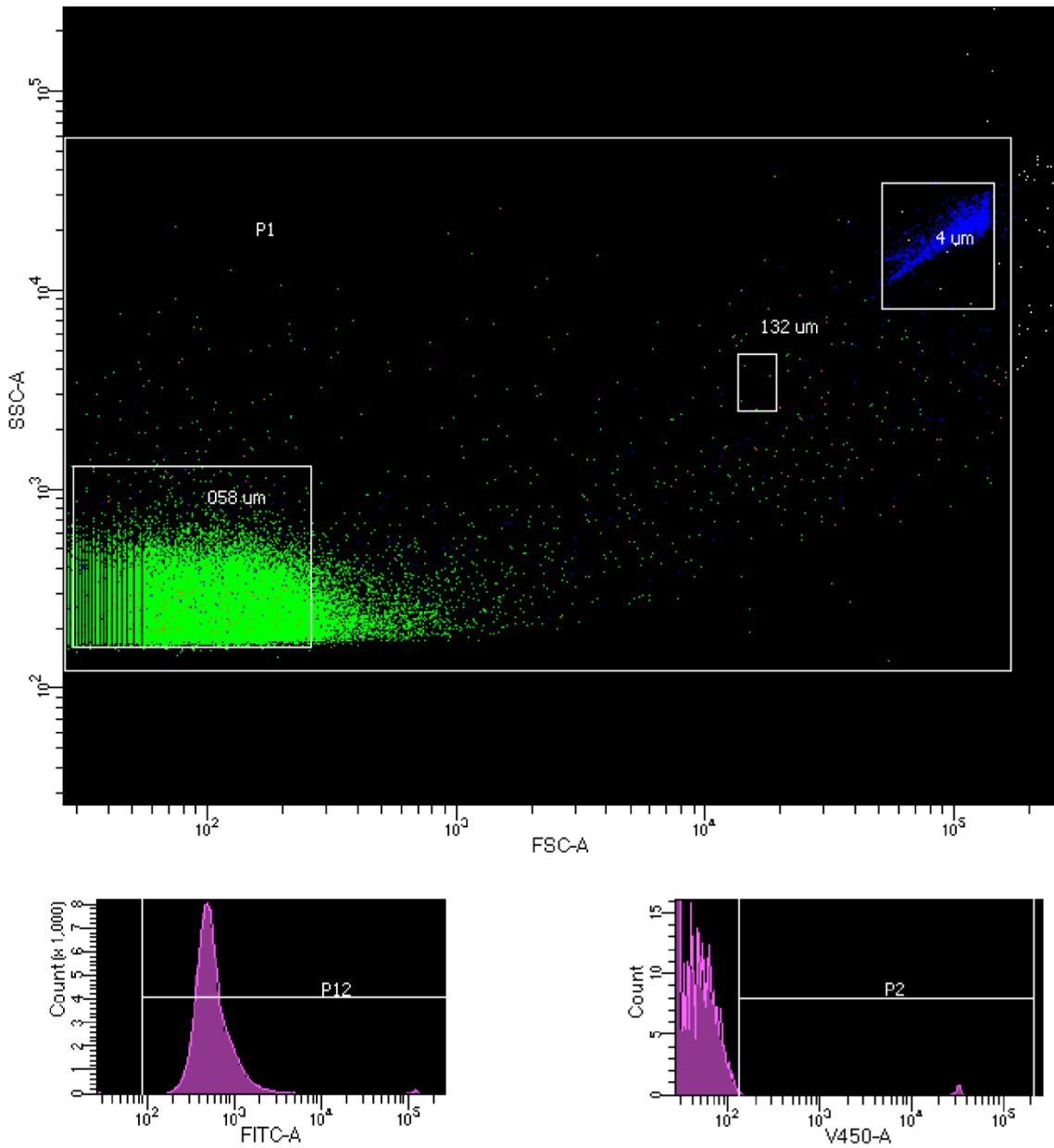
1110  
1111  
1112  
1113  
1114

Supplementary Figure 9. Comparative proteomics of *M. palsarum* NE2 exposed to 1000 p.p.m.v. CH<sub>4</sub> (High) in air and 1.9 p.p.m.v. (Atm) CH<sub>4</sub> in air (Supplementary table S5). Normalized and standardized expression of enzymes involved in the central carbon and energy metabolism is shown. Same heatmaps as in Figure 4 and Supplementary Figure 5 but with protein name and MicroScope accession number. \* indicates significant difference in expression between treatments (two sided t-test).



1115

1116 Supplementary Figure 10. Median and buoyant mass distribution of cells of the respective strains in the D<sub>2</sub>O-based (green) and H<sub>2</sub>O-based (blue) solution. n - number of biological replicates  
 1117 pooled for analysis, Particles H<sub>2</sub>O - Number of cells measured in H<sub>2</sub>O-based solution contributing to the median and distribution, Particles D<sub>2</sub>O - Number of cells measured in D<sub>2</sub>O-based solution  
 1118 contributing to the median and distribution. Median H<sub>2</sub>O – median of buoyant mass in H<sub>2</sub>O-based solution in femtogram, Median D<sub>2</sub>O – median of buoyant mass in D<sub>2</sub>O-based solution in  
 1119 femtogram, Dry weight – estimated cellular dry weight derived from the median of buoyant mass in H<sub>2</sub>O-based and D<sub>2</sub>O-based solutions in femtogram.



1120

1121 Supplementary Figure 11. Flow cytometry gating strategy example for the cell quantification of filter cultures. SYBR green I  
 1122 stained *M. gorgona* MG08 cells in green. 4  $\mu$ m counting beads in blue. "058  $\mu$ m" – gate defined using 0.58  $\mu$ m size beads.  
 1123 "132  $\mu$ m" – gate defined using 1.32  $\mu$ m size beads. "4  $\mu$ m" - gate defined using 4  $\mu$ m counting beads. P1 – events of interest  
 1124 for the quantification of cells. SSC-A – side scatter. FSC- A – forward scatter. FITC-A – signal intensity of events detected in  
 1125 the green channel (*M. gorgona* MG08 cells + counting beads). V450-A – signal intensity of events detected in the blue channel  
 1126 (counting beads).

1127

